EXPERIMENTAL STUDY OF THE MECHANICS OF THE INTRA-AORTIC BALLOON

A thesis submitted for the degree of Doctor of Philosophy

by

Giovanni Biglino

Brunel Institute for Bioengineering

Brunel University

May 2010

DECLARATION OF AUTHENTICITY

I hereby declare that the work presented in this thesis is my own.

Giovanni Biglino

ABSTRACT

This thesis deals with the mechanics of the Intra-Aortic Balloon Pump (IABP), the most widely used temporary cardiac assist device, whose beneficial action is based on the principle of counterpulsation.

The investigation is carried out *in vitro* in increasingly more realistic setups, including a mock circulatory system with physiological distribution of peripheral resistance and compliance in which IABP counterpulsation was simulated.

Pressure and flow measurements show the effect of variables such as intra-luminal pressure, angle and aortic compliance on balloon hemodynamics. These data are complemented by results on the duration of balloon inflation and deflation obtained by means of high-speed camera visualisation. Furthermore, wave intensity analysis is carried out and it is identified as a possible alternative method for the assessment of IABP performance.

This work includes two prototypes of intra-aortic balloons of novel shape with the balloon chamber tapering both from and toward the balloon tip.

In clinical terms, with reference to the semi-recumbent position in which patients assisted with the IABP are nursed in the intensive care unit, the results presented in this thesis indicate that operating the balloon at an angle compromises the benefit of counterpulsation when assessed *in vitro*.

ACKNOWLEDGEMENTS

I would like to thank those people who helped me during the course of my PhD and to whom I owe the completion of this thesis.

First of all, my supervisor, Dr Ashraf Khir, and my second supervisor, Prof Ian Sutherland.
Everyone at the Brunel Institute for Bioengineering, for being so welcoming and friendly.
Margaret, Jenny and Caroline, for all their support and kindness.
Roger Paton, for the help with the electrical equipment.
Dr Graham Hassell of Dantec Dynamics, for an interesting introduction to PIV.
Tony Hunt and Dr Olive Murphy of Imperial College.
Prof Pascal Verdonck, Dr Kris Dumont and the Hydraulics lab of the University of Ghent, where I first came into contact with a mock circulatory system.
Dr Christopher Bowles of Harefield Hospital, for the precious advice and the pleasant discussions.
Prof Kim Parker of Imperial College, for introducing me to fluid mechanics when I was a student at Imperial and for being so inspiring.
Prof Colin Clark, for the generous help and the invaluable suggestions.
Jiling, Chloe and Marcel, for sharing this journey together.
Christina: I will be forever thankful for a list of reasons too long to be reported here. You have been incredibly supportive and infinitely kind.
All my wonderful friends, for being such creative individuals, providing a mix of distraction, laughs and encouragement.
Last but certainly not least, everyone in my amazing family, a constant source of inspiration.

This thesis is dedicated
to the memory of my grandfather, Prof Giuseppe Biglino
and to the memory of Prof John Lever of Imperial College.

LIST OF CONTENTS

LIST OF TABLES

LIST OF FIGURES

GLOSSARY

BCW = backward compression wave

BEW = backward expansion wave

c = wave speed (m/s)

C = compliance (ml/mmHg)

C_d = distal compliance

C_{prox} = proximal compliance

dI = wave intensity (W/m^2)

DPA = diastolic pressure augmentation

E = Young's modulus (MPa)

EDPR = end-diastolic pressure reduction

F = force

FCW = forward compression wave

h = thickness

I = wave energy (J/m^2)

IABP = intra-aortic balloon pump

L = length

LV = left ventricle

LVAD = left ventricular assist device

MCS = mock circulatory system

μ = viscosity (mPa·s)

P = pressure (mmHg or Pa)

P_b = balloon pressure

P_{head} = head pressure

P_i = intra-luminal pressure

PIV = particle image velocimetry

P_{max} = peak pressure

$P_{shuttle}$ = shuttle gas pressure (balloon catheter pressure)

P_t = transmural pressure

Q = flow (l/min)

r = radius

ρ = density (kg/m^3)

R = resistance (mmHg/l/min)

R_c = capillary resistance

R_{prox} = proximal resistance

R_t = terminal resistance

S = hoop stress

TDD = tapered decreasing diameter (balloon prototype)

TID = tapered increasing diameter (balloon prototype)

TPC = transmural pressure curve

U = velocity (m/s)

V = volume

V_b = balloon volume

V_{down} = antegrade volume

V_{up} = retrograde volume

WIA = wave intensity analysis

CHAPTER 1

BACKGROUND

1.1. The field of Ventricular Assist Devices (VADs)

In his opus *Exercitatio anatomica de motu cordis et sanguinis in animalibus* (The movement of the heart and blood in animals: an anatomical essay, 1628) William Harvey, Physician to Charles I and historically one of the most important investigators of the cardiovascular system, concluded: “Just as the king has the first and highest authority in the state, so the heart governs the whole body. It is, one might say, the source and root from which in the animal all power derives, and on which all power depends” [1].

Impairment of the heart’s function in fact results in one of the major causes of death, despite the clinical and research efforts that have been and are dedicated to this organ. According to statistics from the World Health Organization, it was recognised that in the year 2005 cardiovascular disease accounted for 30% of global deaths and it was further predicted that by 2015 about 20 million people will die from cardiovascular disease [2]. Also, the American Heart Association pointed out that in 2006 one in three American adults was affected by cardiovascular disease (80 million people) and the estimated economic costs (direct and indirect) related to cardiovascular disease for the year 2008 is above $ 475 billion [3].

In the process of treating and assisting patients and tackling the issues related to cardiovascular disease, mechanical circulatory support has been adopted over the years in a variety of forms. Historically, the introduction of mechanical support to the failing heart is dated in the year 1953, when Gibbon

performed a surgical intervention involving the first cardiopulmonary bypass [4]. Since then the study, design and evaluation of mechanical devices able to aid and promote heart recovery has never stopped.

There are several definitions available in the literature for Ventricular Assist Devices (VADs), but, as Walter Welkowitz points out in *Engineering hemodynamics: application to cardiac assist devices*, all devices share some characteristics, in his words: “Many methods of mechanical assistance to aid the failing heart have been, and are being, extensively investigated. The hemodynamic goals of the different methods being studied vary depending upon the specific patient problems; however, they all fit into three general categories: decreasing the work of the failing myocardium by reducing the load on the left ventricle; increasing blood flow through the coronary circulation, and consequently increasing the oxygen supply to the hypoxic tissue; and increasing cardiac output, and thus increasing the blood supply to the peripheral organs” [5].

Nevertheless it is possible to classify VADs according to different parameters. One possible distinction is based on the duration of time for which the VAD is applied to the patient [6-8] as follows:

(a) short-term support, e.g. Impella (Cardiotechnik AG, Aachen, Germany), TandemHeart Pump (Cardiodynamics, Pittsburgh, PA, USA), Intra-Aortic Balloon Pump (IABP)

(b) medium-term support, e.g. Abiomed BVS 5000 (Abiomed Inc, Danvers, MA, USA), BerlinHeart (Mediport, Berlin, Germany), Thoratec VAD (Thoratec Corporation, Pleasaton, CA, USA)

(c) long-term support, e.g. Novacor (World Heart Corporation, Ottawa, Canada), HeartMate XVE (Thoratec Corporation, Pleasaton, CA, USA), Jarvik 2000 (Jarvik Heart Inc, New York, USA).

Another distinction is based on mobility, distinguishing between bedside, portable and wearable devices [7]. Also, VADs can be classified in terms of "technology" [9]:

- Centrifugal pumps, e.g. Rotodynamic (Cleveland Clinic Foundation, OH, USA), Gyro pump (Baylor College of Medicine, Houston, TX, USA), Vienna centrifugal (Vienna University, Vienna, Austria)
- Axial pumps, e.g. Jarvik 2000 (Jarvik Heart Inc), Impella (Cardiotechnik AG), DeBakey VAD (MicroMed Technology Inc, TX, USA)
- Pusher plate, e.g. BCM 3.5 (Biomed S.A., Madrid, Spain)
- Diagonal, e.g. Ventrassist (Micromedical Ltd, Sydney University, Australia), Deltastream (HIA/Medos, GmbH, Aachen, Germany)
- Pulsatile, e.g. PUCA pump, IABP
- Total Artificial Heart (TAH), e.g. PennState TAH (Hershey, PA; Minnesota Mining and Manufacturing, Minneapolis, MN, USA), Jarvik 7 (Jarvik Heart Inc)

Another distinction [10, 11] takes into account the position of the device. In this regard the most commonly used VADs can be grouped as (a) extracorporeal (including devices such as: Abiomed BVS 5000, Thoratec CentriMag, BerlinHeart EXCOR, ExtraCorporeal Membrane Oxygenation or ECMO) and (b) intracorporeal (including devices such as: the IABP, Thoratec HeartMate, Novacor LVAD, MicroMed DeBakey, BerlinHeart INCOR, Jarvik 2000).

Goldstein and Oz [10] also suggest another category, which they denominate as "future devices", in which are included devices such as:

DeBakey VAD, epicardial compression mechanical devices, PennState University totally implantable LVAD and Total Artificial Heart (TAH), Heartsaver VAD (fully implantable for long-term support).

Another possible distinction can be drawn by creating an electrical circuit equivalent to the cardiovascular system. The electrical equivalent allows us to distinguish between in-series and in-parallel arrangement. The frequent mode of operation of long-term VADs is to work in-parallel with the heart. This is achieved by pumping blood from the left atrium directly to the ascending aorta and in such a way the mechanical device is responsible for a varying percentage of the pumping work [12]. On the other hand, temporary devices are driven in-series with the heart. In parallel assistance provides larger cardiac output augmentation than in series, but in series assistance has the benefits of reliability and documented long-term clinical efficacy [13].

In this context, the IABP is recognised as one of the most widely used and most effective VADs worldwide [14, 15]. The IABP is a VAD for intracorporeal use that, using the electrical analogy, works in-series with the heart [16]. Traditionally employed for short-term patient support, recent work focused on the possibility of using the IABP as a permanent implantable VAD [17]. This will be explained further in the following sections, in which the history, the functioning, the benefits and the complications associated with IABP will be presented.

1.2. The introduction of IABP

In 1951, Adrian Kantrowitz conceived the idea that the augmentation of arterial diastolic pressure by means of an external force could be a solution to support an ischemic heart [18] and this can be regarded as the birth of the

IABP. Such an increase of arterial diastolic pressure is obtainable using what now is known as a counterpulsating device, such as that employed in 1958 by Birtwell and Harken and reported three years later in the study *The arterial counterpulsator* by Clauss et al. [19]. The IABP is the prototypical example of counterpulsating device and the principle of counterpulsation will be described in section 1.3.

Regarding the clinical introduction of IABP, in 1962 Moulopoulos and coworkers were the first to use an intra-aortic balloon to apply the concept of counterpulsation and in this regard their work is now considered as pioneering in the field [20]. A few years later, in 1968, three papers by Kantrowitz et al. presented the first clinical data about the application of IABP [21-23]. These cases referred to patients with cardiogenic shock, the condition provoked by impairment of cardiac function by myocardial infarction, myocarditis or arrhythmia [24].

Already in the early stages of its introduction, the IABP underwent some drastic modifications: from the original device consisting of a latex balloon inflated with carbon dioxide – as Adrian Kantrowitz recalls in his 1990 paper *Origins of Intraaortic Balloon Pumping* – "by early 1967, we had enough experience in the experimental animal to show clearly the advantages of a non-distensible polyurethane balloon" and further "the use of helium as the shuttle gas gave us sufficiently transit speed to assure appropriate timing" [19]. Helium is mostly used as shuttle gas. In 1988 Walter Welkowitz referred to helium (He), nitrogen (N_2) and carbon dioxide (CO_2) as the three primary driving gases [12] although nowadays helium is the common choice, because of its low density and, in case of balloon rupture, it would not be as harmful for the patient as CO_2.

Kantrowitz interestingly pointed out that, at the origins of IABP therapy, despite the low rate of survival of patients in cardiogenic shock, the counterpulsator was inducing clear hemodynamic benefits in the patients and this encouraged researchers in the field to apply this technique in other acute low-output left ventricular problems. In fact, a vast number of both *in vivo* and *in vitro* studies as well as clinical trails followed. From patients with cardiogenic shock, the use of IABP has evolved over the years and it was reported that in the year 2001, in the US alone, 150,000 patients were assisted by means of IABP [25]. The components of the balloon are shown in Figure 1.1 and an example of modern IABP is provided in Figure 1.2.

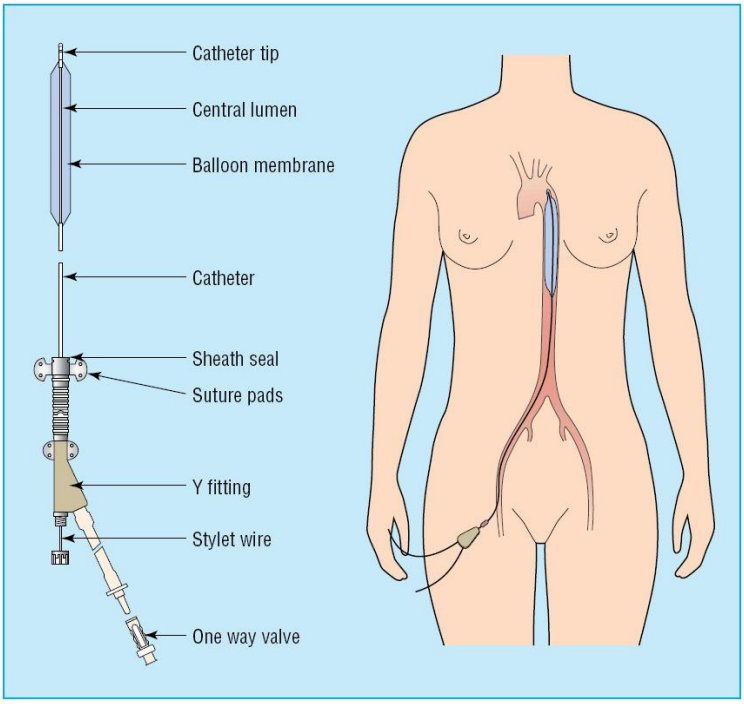

Figure 1.1: Components of the balloon catheter and position in the aorta. The schematic drawing shows the balloon chamber, identifying the tip of the balloon, the lumen and the membrane. The catheter is shown together with the characteristic Y connection and the "one way valve" represents the point at which the balloon is connected to the IABP. Image from [26].

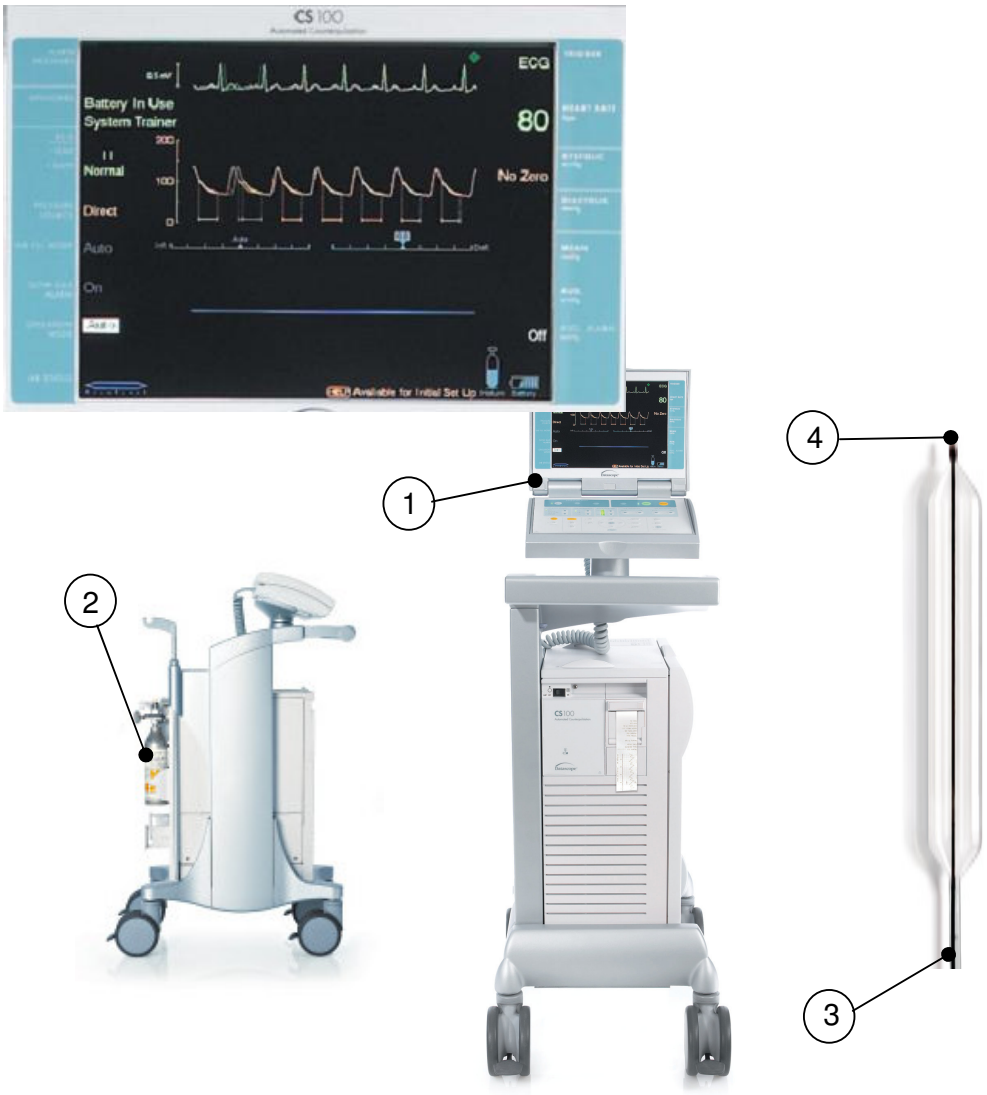

Figure 1.2: Overview of modern IABP from leading manufacturer Datascope (Fairfield, NJ, USA), showing: (1) the monitor of the IABP, also magnified, where the aortic pressure signal and the ECG are shown, (2) the helium gas storage, (3) the catheter of the balloon and (4) the tip of the balloon. The size of the balloon is out of scale. Images from [27, 28].

1.3. IABP guidelines

1.3.1. Choice and insertion

IABP therapy is suited for a variety of conditions, including: cardiogenic shock; pre-shock syndrome; myocardial infarction; unstable angina; as prophylactic support for coronary angiography, coronary angioplasty, thrombolysis and high risk interventional procedures (stenting); post-surgical myocardial infarction [29, 30]. Nowadays the IABP is employed pre-, intra- and post-operatively [15, 31-37] and as a bridge to transplantation [38-40].

The balloon is usually inserted via the femoral artery. Instead of a surgical approach, the balloon is inserted percutaneously. The surgical approach consisted in performing an incision in the groin area, sewing a vascular graft to the common femoral artery and inserting the balloon into the artery via the graft [41]. The benefits of percutaneous insertion are the rapidity of the operation and the minimization of hemorrhagic complications [42]. Percutaneous insertion has been used since 1979 using a modified Seldinger technique [43, 44]. Named after the Swedish radiologist Sven-Ivar Seldinger, this is a technique to access a vessel by: puncturing the vessel, advancing a guidewire in the vessel and inserting a sheath or cannula which is then removed once insertion is completed [45]. Sheathless insertion has contributed to further reduce complications [46].

An alternative approach is known as the “subclavian approach” and consists in introducing the balloon via the subclavian artery [47]. Alternative access routes also involved the axillary and iliac arteries and the ascending aorta or the aortic arch [48-50] but percutaneous insertion can be indicated as the commonly used technique.

Balloons of different volumes are available and they are chosen with respect to patient's size. In the case of intra-aortic balloons produced by market leader Datascope (Fairfield, NJ, USA), the range of balloon volumes and the corresponding patient size are reported in Table 1.1. Other manufacturers follow similar guidelines.

Balloon membrane volume (cc)	*Balloon membrane dimensions*		*Patient height (cm)*
	Length (mm)	*Diameter (mm)*	
25 (paediatric)	174	14.7	< 152
34	219	14.7	152 – 162
40	263	15	162 – 183
50	269	16.3	≥ 183

Table 1.1: Balloon membrane sizing table. Different balloon volume is chosen according to patient's height, as indicated by the manufacturer, in this case Datascope [51].

1.3.2. Position

Once inserted through the femoral artery, the balloon is positioned in the descending aorta, typically between the aortic arch and the renal bifurcation, and proper position of the IAB catheter tip is considered at about 2 cm from the left subclavian artery [51]. Correct position of the balloon is an important parameter, as malposition results in complications for the patient:

(a) if the balloon is too close to the aortic valve, it may obstruct the left subclavian artery or the carotids

(b) if the balloon is too low, it may obstruct the renal and mesenteric arteries [29].

Position of the balloon is shown in Figure 1.1 and 1.3. In the modern clinical setting, fluoroscopy visualisation can be used to check the correct positioning of the tip of the balloon [52].

1.3.3. Removal

As said, the IABP is used for short-term assistance. A study on 103 patients reported the average duration of counterpulsation assistance to be 3.4 ± 1.6 days [53]. The range of IABP assistance has been reported to be from 5 minutes to 89 days [32].

Once specific hemodynamic criteria are satisfied – namely mean blood pressure above 70 mmHg, systolic pressure or diastolic augmentation above 90 mmHg, pulmonary capillary wedge pressure below 18 mmHg, cardiac index above 2.2 l/min/m^2 – a patient can be considered ready for weaning from IABP. This is done either by reducing assisting frequency (e.g. from 1:1 to 1:2, from every heart beat to every other beat assisted) or by reducing balloon volume [54].

Removal of the percutaneously inserted balloon does not involve a surgical operation. There is no need to aspire the balloon by means of a syringe because the balloon is collapsed by the patient's own blood pressure [29]. In the case of unexpected resistance during the withdrawal, surgical removal can be considered [29].

1.4. The benefits of IABP support

1.4.1. Benefits of balloon inflation

At the onset of diastole, as judged by the dicrotic notch on the aortic pressure waveform, the balloon chamber is inflated with helium. The choice of timing is related to the fact that maximum volume availability is registered at the beginning of diastole, while in late diastole a high proportion of the blood has moved to the periphery. If inflation is correctly timed as such, the following hemodynamic benefits are achieved:

(a) Augmentation of coronary perfusion pressure results in a potential increase of coronary collateral circulation.

(b) Increased diastolic pressure

(c) Increased systemic pressure

with point (c) relating to a higher perfusion of distal organs, resulting in effects such as increased urine output and increased cerebral perfusion [5].

The most apparent effect of a correctly timed inflation will show on the arterial pressure waveform as an increase of peak diastolic pressure. Balloon inflation is shown in Figure 1.3a and 1.4.

1.4.2. Benefits of balloon deflation

IABP support produces hemodynamic benefits equally during inflation phase as well as during deflation phase. Balloon deflation occurs mainly during the isovolumic contraction phase, preceding blood ejection from the left ventricle through the aortic valve. The fact that the balloon is deflated before left ventricular ejection generates a drop in pressure that results in the left ventricle having to build less pressure in order to initiate ejection.

Correct timing of balloon deflation will result in:

(a) reduction of left ventricular afterload

(b) shortening of the isovolumic contraction phase

(c) increase in stroke volume: the reduction of afterload (a) results in more effective emptying of the left ventricle

(d) enhanced forward cardiac output also decreases the amount of blood shunted from left to right in case of intraventricular septal defects and incompetent mitral valve. [29]

A sign of correctly timed deflation on the arterial pressure waveform is the reduction of peak systolic pressure in the assisted beat compared to that of the non-assisted beat. Balloon deflation is shown in Figure 1.3b and 1.4.

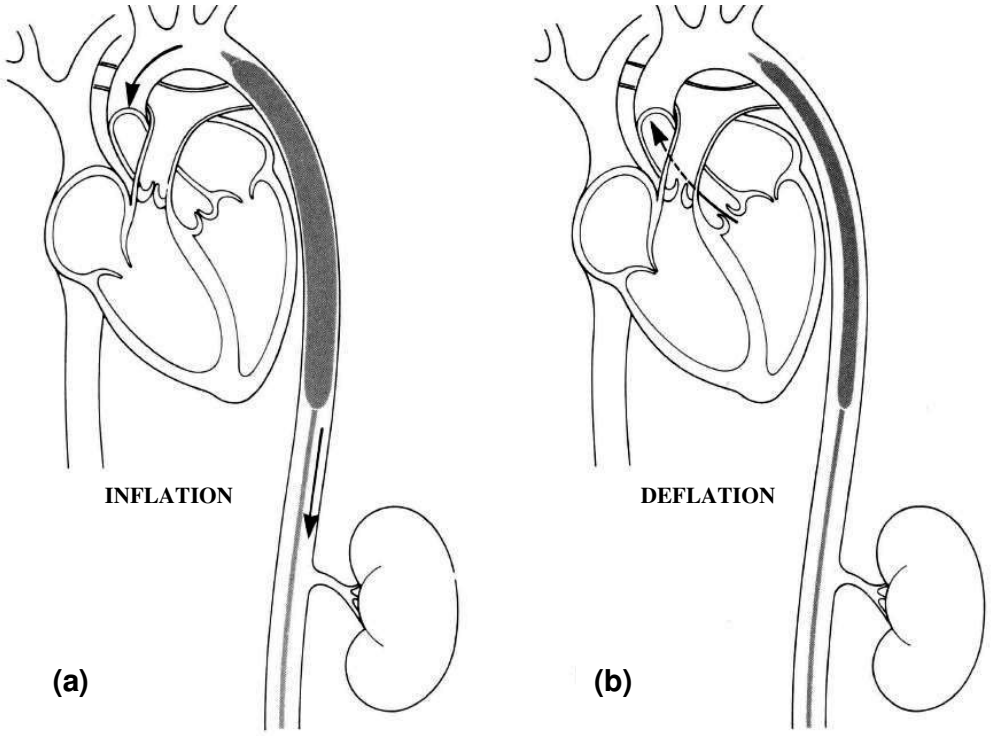

Figure 1.3: Schematic representation of balloon inflation (a) and deflation (b). It is inflated during the diastolic phase, with the onset of inflation coinciding with the onset of diastole (dicrotic notch). It is deflated before the systolic phase or, according to a different school of thought, deflation can extend during the following systole. Image from [30].

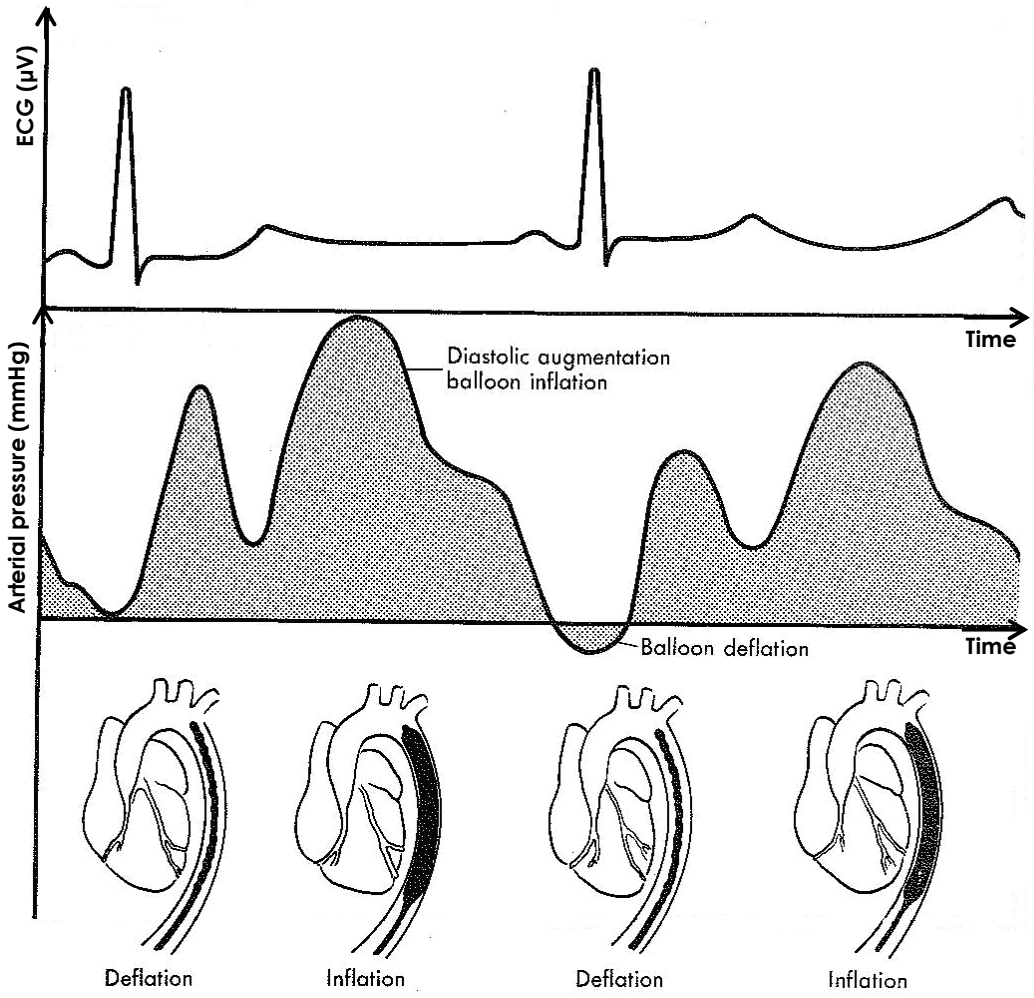

Figure 1.4: Inflation of the balloon results in augmentation of early diastolic aortic pressure, while deflation of the balloon results in reduction of end-diastolic pressure. This is visible on the arterial pressure trace (lower trace). ECG is also provided as a time reference (upper trace). Image redrawn from [30].

1.4.3. Impact of IABP on cardiac energy

The work of the myocardium is dependent on oxidative reactions. This implies that a crucial factor to establish the capacity of the heart to work (or recover) depends on the balance between the availability of oxygen and the level of oxygen consumption. The given definitions of oxygen availability and consumption are, respectively, the maximum amount of oxygen that can be extracted from coronary blood supply and the amount of oxygen needed to sustain myocardial work and heat loss.

The benefits of IABP inflation and deflation can be summarised into two main points: increased coronary perfusion during inflation and decreased left ventricular afterload during deflation. In other words, in-series cardiac support tries to re-establish the balance between oxygen availability and consuption in the failing myocardium, by increasing oxygen availability during balloon inflation and decreasing oxygen consumption during balloon deflation, as described by Barnea et al. in 1990 [55]. Oxygen availability is defined as:

$$V_{Oa} = \frac{(A-V)O_2}{100}\int_{beat} Q_{cor}(\tau)d\tau \qquad \textbf{Eq.1}$$

where Q_{cor} is coronary flow and $(A\text{-}V)O_2$ is the maximum physiological arteriovenous oxygen difference expressed in volume percent, with maximum $(A\text{-}V)O_2$ corresponding to maximum oxygen extraction and τ is the viscoelastic time constant.

Oxygen consumption is defined as:

$$V_{Oc} = A \cdot PVA + B \cdot E_{\max} + C \qquad \textbf{Eq.2}$$

therefore depending on LV pressure-volume area (*PVA*), which is used in the literature to correlate with oxygen consumption rate per beat [56-58], and on the elastance function (E_{max}), which represents contractility, with B and C indicated as constants.

Barnea et al. concluded that "the major direct effect of intra-aortic balloon pumping is augmentation of oxygen availability".

Instead, Williams et al. [59] have highlighted that the reduction of oxygen consumption is the principal mechanism by which IABP therapy alleviates myocardial ischemia in patients affected by unstable angina pectoris.

A schematic representation of the effect of IABP on cardiac energy is shown in Figure 1.5.

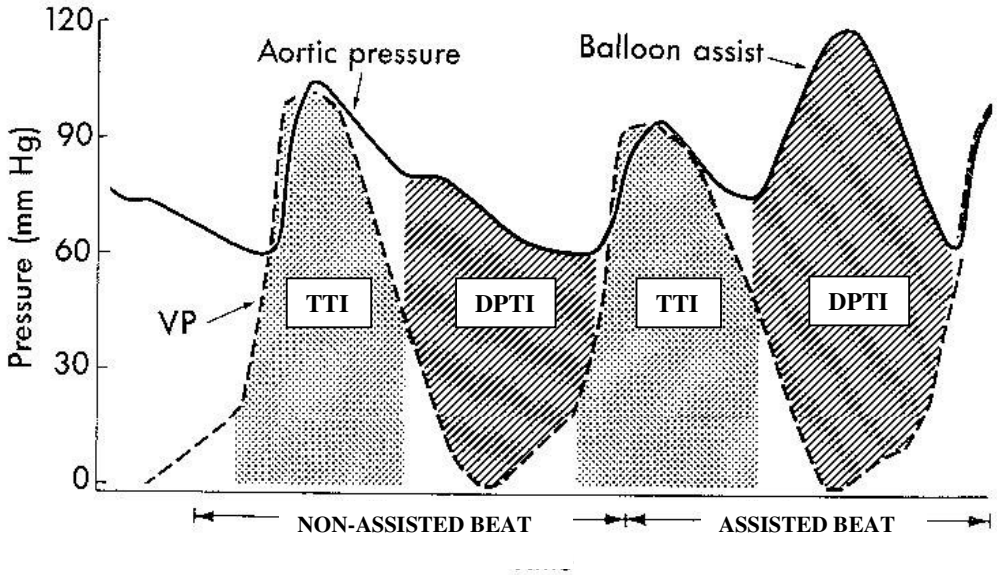

Figure 1.5: The area beneath the systolic portion of the pressure waveform (time tension index, TTI) represents myocardial oxygen consumption, while the area beneath the diastolic portion of the pressure waveform (diastolic pressure time index, DPTI) relates to oxygen supply. During IABP assistance, TTI is lowered and DPTI is increased, as shown on the plot redrawn from [30].

1.5. Counterpulsation

1.5.1. The principle

In general, the definition of counterpulsation arises from the fact that the assist device is pumping during diastole, against (counter) the normal activity of the heart [60].

The benefits of IABP therapy, described in section 1.4, are obtained by displacement of blood flow-volume and imposing blood pressure changes at precise time intervals during the heart cycle. The onset of balloon inflation is timed with the onset of diastole and the dicrotic notch is taken as a reference point on the arterial pressure waveform. Inflation should begin at this point. At this instant the helium is displaced into the balloon chamber and the balloon is inflated. The balloon then remains inflated during diastole. The exact timing of balloon deflation, on the other hand, does not rely on a landmark point on the pressure trace. Deflation occurs during the isovolumic contraction phase of systole and, more specifically, the rapid deflation of the balloon chamber is timed just before the onset of left ventricular ejection. Some studies have indicated that deflation timing during counterpulsation can be considered optimal when the volume of the balloon is halved before the end of left ventricular diastole and then the deflation process extends into the following systole [15, 55, 61]. However, in the course of the study of the literature relative to IABP counterpulsation, a certain degree of disagreement relative to deflation timing has emerged. It is reported that deflation should be completed before the onset of the following systole [62, 63].

1.5.2. The importance of correct timing

In order for IABP therapy to be beneficial for the patient, the timing of inflation and deflation of the counterpulsating balloon need to be carefully controlled with respect to the heart cycle. As said, the balloon is inflated at the dicrotic notch at the onset of diastole and is deflated before the following systole without a marker on the aortic pressure signal. Any change imposed to this timing principle, by inflating/deflating the balloon either too early or too late, reduces the effectiveness of IABP therapy.

1. Early inflation: the balloon is inflated before the aortic valve is closed and induces premature closure of the valve at the end of systole. Early inflation results in a loss of forward cardiac output.
2. Late inflation: after aortic valve closure, the balloon can displace a lower volume of blood. Late inflation results in lower pressure increase.
3. Early deflation: the balloon is deflated before isovolumic contraction. At the onset of the following systole, the beneficial unloading effect of balloon deflation is lost.
4. Late deflation: the balloon is still partially inflated at the onset of the following systole, resulting in an impediment during ejection. Late deflation results in increased impedance and increased workload for the myocardium.

In terms of the effect of IABP therapy on cardiac energy balance, described in section 1.4.3, the level of oxygen consumption is not greatly affected by the timing of inflation and deflation of the balloon, unless inflation is triggered too early or deflation too late: “in the case of inflation beginning before the end of systole or deflation beginning too late in the systole of the following beat, an increase of oxygen consumption was observed” [55].

1.6. Complications associated with the IABP

Despite its beneficial action and its widespread use, the IABP is prone to several complications, although in the literature the estimate of complications related to IABP therapy varies from 3%, as reported by Underwood et al. [64], to 47%, as reported by Eltchaninoff et al. [65] and Funk et al. [66].

The major complication associated with the IABP is limb ischemia and insertion technique, insertion site and catheter choice are linked with limb ischemia incidence [67, 68]. Other complications observed in an *in vivo* study by Elahi et al. [69] alongside limb ischemia include groin haematoma, femoral artery trauma and infection, respectively occurring in 3.22%, 3.76% and 0.5% of the cases of their clinical study.

Another possible complication is balloon rupture, involving a leak of shuttle gas into the circulation. Because of increasing patient age, Wolvek observes that a calcified aorta represents a hostile environment for IABP therapy [70]. The problem is double-sided: on the one hand repetitive abrasion due to the presence of atherosclerotic plaques may result in balloon membrane rupture, and on the other hand repetitive contact during balloon inflation may result in plaque dislodgment and consequent thrombosis.

An obstacle associated with balloon removal is defined “balloon entrapment”. The difficulty in removal experienced in the case of entrapment is related to the presence of a blood clot within the balloon [67, 71, 72]. The formation of such a clot is due to the presence of a small tear or perforation in the membrane of the balloon through which blood enters the balloon chamber and dries in contact with helium.

1.7. Variables affecting IABP performance

1.7.1. Arterial compliance (and relation with patient age)

Arterial compliance has been identified as one of the major variables affecting IABP counterpulsation. In their 2002 study, Papaioannou et al. built a hydraulic model to investigate the independent effect of arterial compliance on IABP counterpulsation simulating a wide range of compliance values (1.05-2.62 ml/mmHg) [25]. The same authors observed that "arterial compliance is a main and independent biological factor affecting the performance" of balloon counterpulsation and linked their remark with clinical data [73] "indicating that patients with post-infarction, cardiogenic shock showed a better hemodynamic response to [counterpulsation] when their arterial compliance was low, independently of the arterial pressure and vice versa".

A summary of their results [25] is shown in Figure 1.6, where the effect of compliance is evaluated in terms of diastolic pressure augmentation (ΔAUG), reduction of systolic aortic pressure (ΔSAP) and reduction of end-diastolic pressure (ΔEDAP) as markers of counterpulsation benefits at three levels of aortic pressure (55, 75 and 95 mmHg) and three different heart rates (80, 100 and 120 bpm).

In clinical terms, arterial compliance should also be taken into account in relation with patient age. A 1999 review reported that the majority of patients undergoing IABP placement are in the range of 61 to 70 years of age [41] and advanced age is commonly linked with stiffening of the aorta. On the other hand, observations about the paediatric use of IABP have indicated that the high compliance of the aorta (together with high heart rate) renders IABP therapy ineffective in children [74-76].

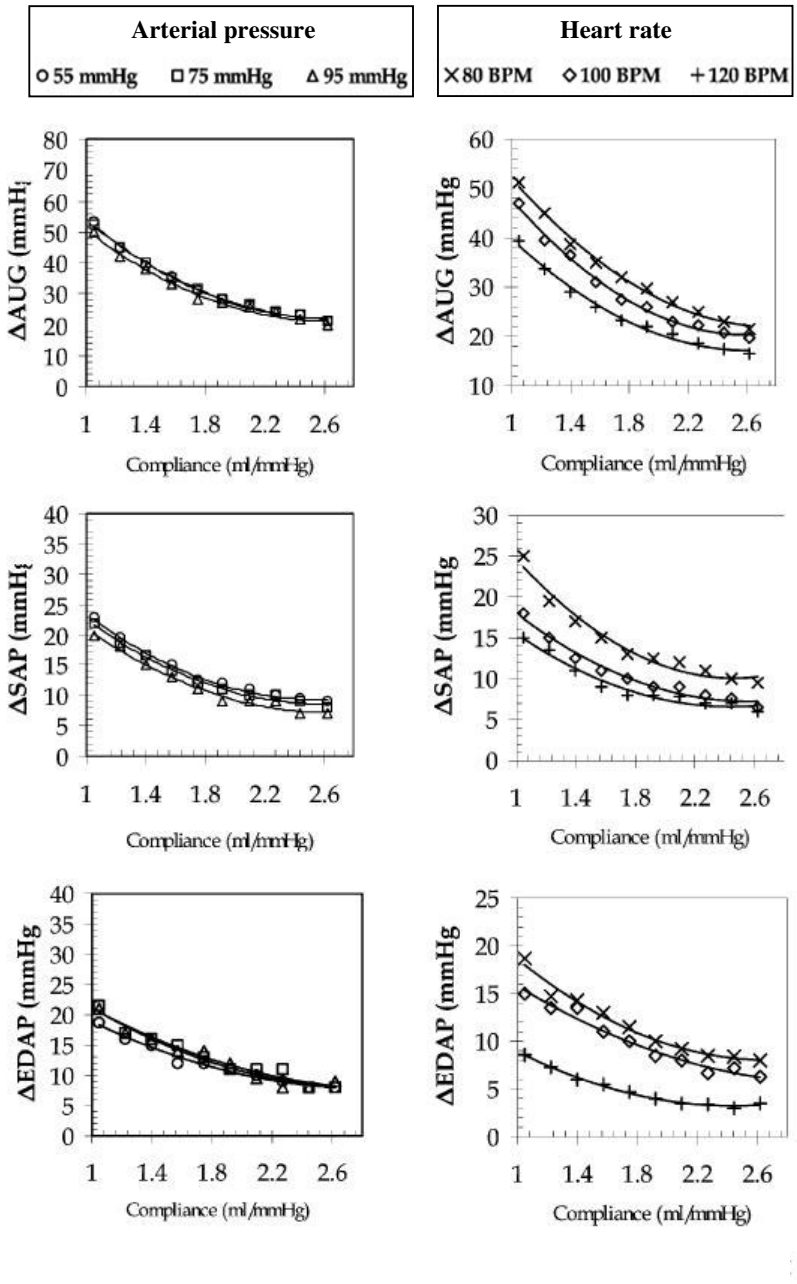

Figure 1.6: The effect of arterial compliance on IABP counterpulsation evaluated in terms of diastolic pressure augmentation (ΔAUG), systolic arterial pressure reduction (ΔSAP) and end-diastolic pressure reduction (ΔEDAP) at three levels of arterial pressure and three heart rates [25]. These parameters are taken as markers of counterpulsation benefits.

1.7.2. Heart rate

Another variable influencing the performance of the IAB is heart rate. Kao and Ohley indicated heart rate, along with left ventricular pressure and peripheral resistance, as the most significant vascular parameter in their non-linear arterial/IABP model [77]. Furthermore, Papaioannou et al. specifically addressed the effect of heart rate in their 2002 study *Heart rate effect on hemodynamics during mechanical assistance by the intra-aortic balloon pump* [78]. Their work established that acute effects of IABP therapy are significantly related to variations in heart rate, according to a non-linear, quadratic relationship, and an optimal range of heart rates in which intra-aortic balloon performance is enhanced was identified. Such range was found between 80 and 110 bpm.

1.7.3. Balloon volume

The volume of the balloon itself is also indicated as a variable affecting balloon counterpulsation and contrasting views can be found in the literature in this regard. In 2002 Cohen et al. studied the effect of different counterpulsating volumes on echocardiographic and invasive hemodynamic measurements of cardiac output [79]. They underline that such *in vivo* study involved a group of patients large enough that would avoid beta error and a false negative result [79]. Different volumes were achieved by means of a volume-limiter disk in the IABP console. Their results showed that there were no substantial differences in cardiac output or other hemodynamic parameters during IABP assistance with either balloon volumes of 32 or 40 cc and consequently it was assumed that the smaller volume would result in a better choice since it would reduce vascular complications during catheter insertion.

On the other hand, an earlier study conducted by Stamatelopoulos et al. concerning large counterpulsating volumes evaluated the hemodynamic effects of counterpulsation therapy and also variables of cardiogenic shock, such as urine output and renal artery flow [80]. In this case the authors concluded that "the effectiveness of intraaortic balloon pumping in severe cardiogenic shock may be improved by increasing the volume of the balloon" and also remarked that "a counterpulsation volume much larger than the one provided by the commonly used balloons might be applied as a bridge to implantation of a leftventricular assist device for patients in severe cardiogenic shock".

1.7.4. Shape and arrangement

In the history of the IABP, different configurations have been tested aiming to optimize the benefits deriving from counterpulsation support. The two examples discussed in this section show that the shape of the balloon and its arrangement influence IABP performance.

1.7.4.1. Multi-chamber balloon

The proposal of a multi-chamber configuration for intra-aortic balloon therapy was raised by Bai et al. in 1994 [81]. Referring to earlier work from the 1970s [82, 83] Bai and co-workers developed the concept of a balloon composed by three successive chambers (Figure 1.7) and they compared one-, two- and three-chambered balloons keeping the balloon volume constant (13 ml). They performed both computer simulations and physical tests and the parameters chosen to quantify the effectiveness of IABP were: mean aortic systolic pressure (MSP), mean aortic diastolic pressure (MDP), the ratio MDP/MSP, total coronary flow per beat (TCF), end aortic diastolic pressure

(EDPR). In the case of a three-chambered balloon, the chambers were inflated from the catheter to the tip in sequence. From the results of the simulation the authors observed: "mean diastolic pressure can be maximised and mean systolic pressure and end diastolic pressure can be minimised when the sum of the volume of the middle and rear chambers is about 40% of the total balloon's volume" for the case of a three-chambered balloon. Further, the ratio MDP/MSP was an indicator of effectiveness, since maximum MDP/MSP can be obtained by increasing MDP (increasing oxygen supply) or minimizing MSP (reducing oxygen consumption), and "MDP/MSP increased about 23% compared with the single chamber balloon by using a three chamber balloon of the same volume; the coronary flow increased 16%, and the afterload decreased about 8%".

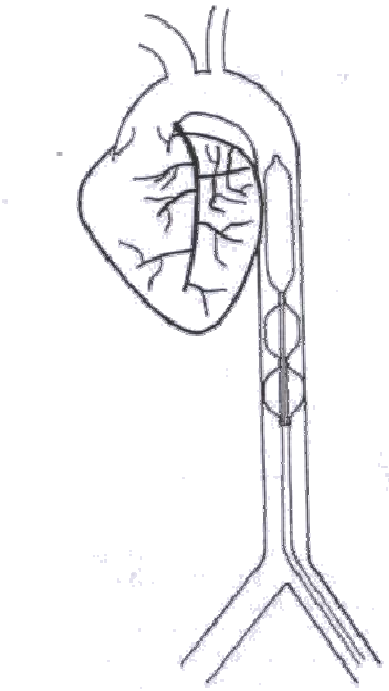

Figure 1.7: Multi-chamber intra-aortic balloon, as proposed by Bai et al. [81]. The three chambers are inflated in succession, from the catheter to the tip.

1.7.4.2. Enhanced IABP (EIABP)

Another arrangement for IABP counterpulsation was described in 2002 by Bian and Downey [84] presenting their results from a canine study involving a so-called enhanced IABP (EIABP). Compared to a traditional counterpulsating balloon, the EIABP operates according to the same timing principle but also involves an additional external chamber which provides additional pumping capacity, as shown in Figure 1.8. Results of this study showed that, in the presence of global LV disfunction, "only EIABP could significantly augment diastolic aortic pressure, and this effect was pronounced, from 32 mmHg to 87 mmHg". Also, a "significant increase in coronary and carotid artery blood flows produced only by EAIBP" was observed.

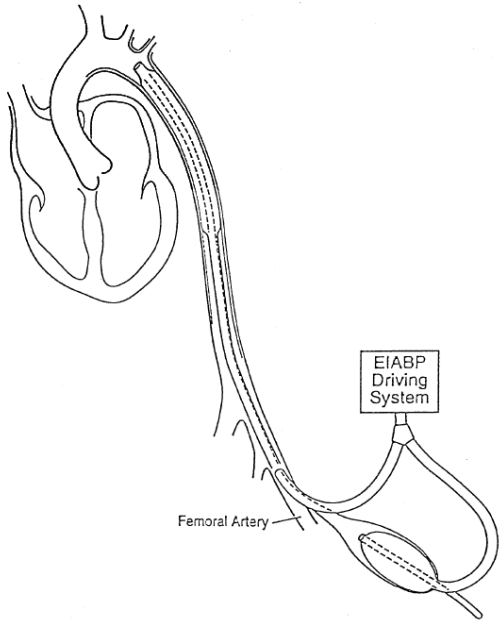

Figure 1.8: Enhanced IABP, or EIABP, as proposed by Bian and Downey [84]. The external chamber provides additional pumping capacity.

1.7.4.3. Ascending aorta balloon

A comparison between 'ascending' and 'descending' aortic balloon pumping was carried out by Meyns et al. [85] comparing a specifically designed ascending aorta balloon catheter suitable for introduction via the groin (Figure 1.9) with traditional IABP. The new device was an 'Intraarterial Cardiac Support system' or ICS-Supracor (Abiomed, Danvers, MA) and had a volume of 45 cc and maximum diameter of 35 mm. The characteristic of this design was that the catheter of the ICS-Supracor was preshaped to fit in the curvature of the aortic arch (Figure 1.9). The authors compared the ICS-Supracor with a traditional 40 cc balloon (St Jude Medical, Chelmsford, MA). Hemodynamic results showed an increment in myocardial blood flow with the 'ascending' IABP design with respect to the traditional 'descending' design, with no unfavourable effect on cerebral perfusion. However, "the degree of complications caused by vascular access and dislodged plaques in the ascending aorta ha[d] to await the results of clinical trials".

Figure 1.9: Abiomed ICS-Supracor balloon has a preshaped catheter to fit the curvature of the aortic arch. Image from [85].

1.7.5. Patient's posture

IABP therapy is commonly used with patients in the intensive care unit (ICU), where they are usually nursed in an inclined position, or semi-recumbent position. The main reason for this setting is that patients in the ICU are usually mechanically ventilated and it has been advocated that the semi-recumbent position helps in preventing the common complication of ventilator-associated pneumonia (VAP) [86, 87]. In the case of semi-recumbent position, the backrest angle has been indicated as 30-45° [88]. According to National Health Service guidelines [89] VAP "accounts for up to half of all infections in the intensive care unit" and in order to reduce this risk "patients should have a minimum resting height of 30° […] established in whatever resting position the patient is placed".

Initial observations about the effect of patient's posture (angle) on balloon counterpulsation were made by Khir et al. in 2005 [90]. The authors tested the IAB *in vitro* at a range of angles from 0 to 90° and *in vivo* at the horizontal and semi-recumbent (30°) positions. The authors concluded that "unless patients using IABP are required to be semi-recumbent, it may be best to position them horizontally to gain the full benefits of balloon counter pulsation to the coronary circulation".

1.8. *In vivo* perspective

Clinical data about the balloon effectiveness is widely available in literature. The largest clinical study is the Benchmark Counterpulsation Outcomes Registry, a "comprehensive, prospective, multicenter computerized database program" that involved 16,909 patients between 1996 and 2000 [32]. This broad study showed that modern IABP therapy has a low incidence of complications (2.8%) and low mortality rate (5 patients in 10,000 due to balloon

failure or insertion). It also identified female gender, high age, small body surface area and peripheral vascular disease as independent predictors of IABP complications.

The beneficial effect of balloon inflation resulting in augmentation of coronary perfusion has been questioned, especially in the presence of coronary stenosis. Akyurekli et al. in their study on the effectiveness of IABP counterpulsation concluded that "the therapeutic action of IABP must result from increases in coronary blood flow by diastolic augmentation" and that the unloading action of IABP therapy was ineffective in hypotensive states [91], while other authors identified with myocardial unloading the major benefit of IABP therapy. A 1982 animal study in the awake pig showed that coronary blood flow to the ischemic myocardium is not always increased by the action of counterpulsation [92]. A 1996 animal study in dogs reinforced this observation, concluding that IABP "failed to increase diastolic inflow in the myocardium and did not enhance systolic retrograde flow from the myocardium to the extramural coronary artery" [93]. Observations in patients performed by Williams et al. showed that "relief of angina during IABP cannot be ascribed to an absolute increase in coronary blood flow" but instead the authors noted that myocardial oxygen consumption, measured as the product of great cardiac vein flow and the difference in oxygen content of the paired arterial and great cardiac vein samples, was consistently reduced and therefore ascribed the benefit of IABP counterpulsation to the reduction of myocardial oxygen demand [59].

In the light of these clinical observations, and bearing in mind the differences between *in vivo* and *in vitro* studies, this project will investigate both pressure and flow changes induced by the IAB. Flow measurements in the direction opposite to the balloon tip, henceforth defined as "retrograde flow",

and diastolic pressure augmentation will be mainly referred to when analysing the effect of balloon inflation. End-diastolic pressure reduction will be taken as the principal index of the effect of balloon deflation and the suction generated during this phase.

1.9. Aims of the study

In the light of the characteristics of the IABP described in this chapter and of the extensive literature available on the subject and here summarized, the aims of this project are:

- To quantify the pressure and flow changes induced by the IAB (with emphasis on the retrograde direction) at different levels of intra-luminal pressure
- To establish the effect of angle on the mechanics of the IAB by means of experimental and visualisation studies, resembling patient's posture as described in section 1.7.5.
- To build a mock circulatory system suitable for IABP testing
- To assess the potential of wave intensity analysis (described in Chapter 2, section 2.4) as an alternative descriptor of IAB performance
- To include in the study two novel balloons of conical shape, alongside commercially available cylindrical balloons, in order to assess the possible benefit of a new balloon design.

1.10. Thesis outline

The work performed in order to achieve the aforementioned aims has been performed in progressively more physiological setups and has been structured in this thesis according to the following outline:

- **Chapter 2** (Methodology) describes the IABP operation, the measuring equipment used for the experiments, the calibration techniques and the reproducibility of the recorded signals. This chapter also includes a short description of wave intensity analysis.
- **Chapter 3** (Preliminary assessment of balloon volume displacement in a straight compliant tube) refers to measurements in a single latex tube. Balloons of different shape and size are tested at the horizontal position and at an angle.
- **Chapter 4** (The effect of changes in transmural pressure on balloon mechanics) includes measurements in an artificial aorta in the absence of counterpulsation. The effect of intra-luminal pressure on balloon volume displacement and end-diastolic pressure reduction is studied. Preliminary wave intensity analysis results are also presented.
- **Chapter 5** (Duration of inflation and deflation: visualisation study) describes the results of a visualisation study that provided knowledge of the duration of balloon inflation and deflation and the effect of intra-luminal pressure and angle on these parameters. Also, since for visualisation purposes the balloon was operated in a glass tube, the effect of the compliance of the tube housing the balloon is tested by measuring balloon internal pressure.
- **Chapter 6** (Designing a mock circulatory system for IABP testing) describes a mock circulatory system built for IABP testing, the main characteristic of the mock loop being the physiological distribution of terminal resistance and compliance.
- **Chapter 7** (The effect of angle on IABP mechanics: measurements in the mock circulatory system) establishes the effect of posture on IABP

counterpulsation, testing the balloon in the mock circulatory system while simulating counterpulsation with a synchronised LVAD.

- **Chapter 8** (Conclusions and future outlook)

CHAPTER 2

METHODOLOGY

This chapter will discuss the experimental procedures, instrumentation, calibration methods and analytical tools that were adopted in the course of this thesis. Specific experimental setups will be separately described in detail in the relevant chapters.

2.1. Instrumentation and measurements

- The IABP: two different models of IABP were used during this project, a Datascope CS 100 model and a Datascope 98 model. Both models operate according to the same principles.

The IABP can be controlled from the main panel and an overview of the Datascope 98 IABP control panel is provided in Figure 2.1.

Balloon augmentation volume can be regulated and was set on “maximal augmentation” throughout the experiments presented in this thesis.

Different assisting frequencies can be selected: every beat assisted (or 1:1), every other beat assisted (or 1:2) and every third beat assisted (or 1:3). Different frequencies have been used and compared, mainly 1:1 and 1:3 (Chapter 3, 4, 5 and 7).

The IABP can be triggered with either an ECG signal or an aortic pressure signal. In this thesis the ECG always used and was provided either by a patient simulator (Datascope) or, in the case of the Datascope 98 IABP, fed externally in the form of a spike signal. A spike signal was extracted from a stepper motor driver and fed to the IABP in the form of a short square wave, as

will be further explained in Chapter 6. It was in fact shown that the IABP does not read features of the ECG signal which is input, such as the P and T waves, but instead it calculates heart rate from the distance between R-peaks. This was tested by triggering the IABP with different ECG signals whose features had been purposefully modified but with same R-to-R distance and as a result the IABP was reading the same heart rate.

Different balloon cycles are selected automatically depending on heart rate and the timing of balloon inflation and deflation is pre-set in the IABP. However, if necessary these times can be separately anticipated or delayed by ± 80 ms by means of two slides control on the IABP front panel.

In terms of triggering, modern IABPs can adjust the timing of balloon cycle according to sophisticated algorithms, such as the intrabeat dicrotic notch prediction algorithm described in 2005 by Schreuder et al., a timing algorithm that works efficiently both for regular beats and during arrhythmia [94]. Datascope CS 100 IABP is equipped with an automated arrhythmia tracking and timing algorithm [95].

In practical terms, following from the description provided by Quaal [30], when balloon inflation is initiated, the pneumatics of the IABP are filled with helium. A transducer, positioned between the helium tank and the balloon, senses the filling pressure. Then helium is propelled into the catheter, resulting in a rapid upstroke. An overshoot pressure artifact is seen at peak inflation resulting from the gas pressure in the pneumatic line. The balloon is kept inflated and then deflation is represented by a rapid pressure drop, with an undershoot artifact as helium is sucked back to the IABP.

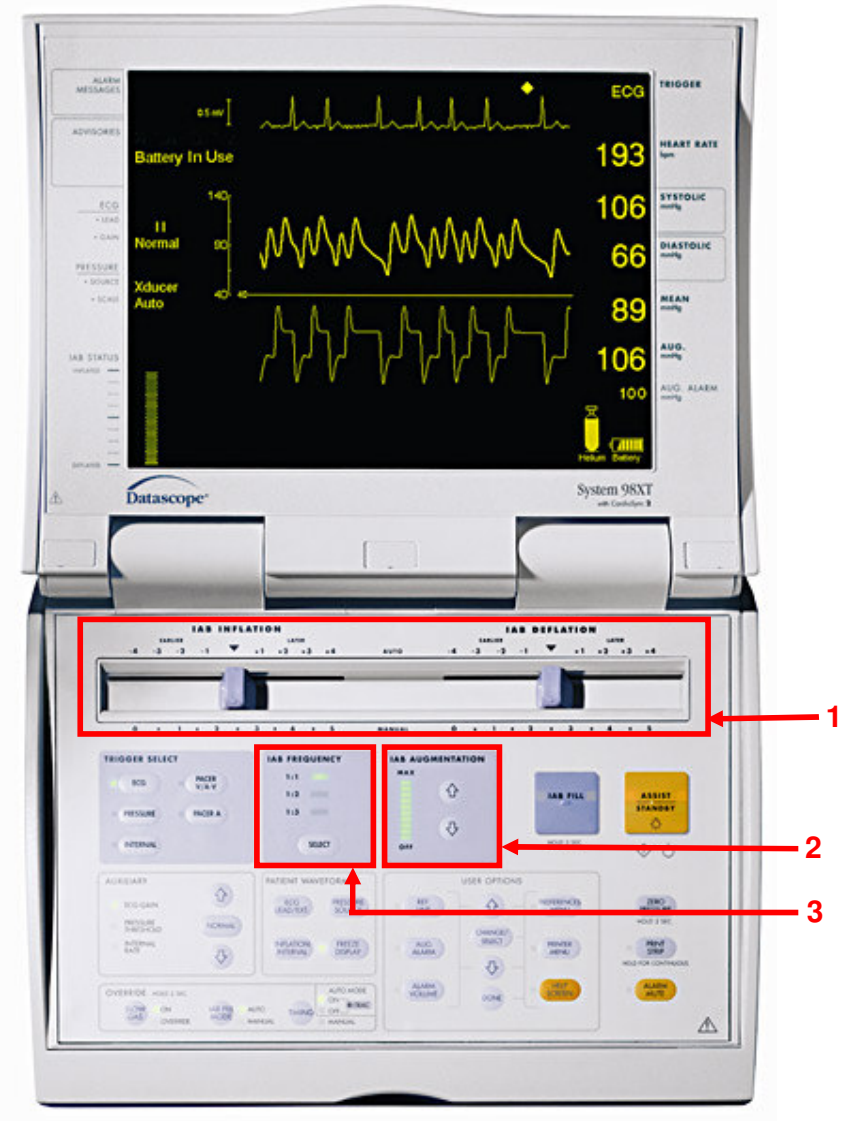

Figure 2.1: Overview of the front control panel of the Datascope 98 IABP. Commands for modification of inflation/deflation timing (1), balloon volume augmentation (2) and assisting frequency (3) are highlighted. Image from [96].

- Balloons: different balloons were used in the course of this study. Traditional cylindrical balloons (Datascope) were tested. Balloons of different sizes were used (25, 34, 40 and 50 cc in volume). Dimensions of these IABs are provided in Table 1.1 in the Background, where they are related to patient's height.

Alongside traditional balloons, two novel balloons of conical shape were included in this study. These tapered balloons were of opposite shape, one having tapered increasing diameter from catheter to tip ("TID balloon") and the other having tapered decreasing diameter from catheter to tip ("TDD balloon"). The tapered balloons were manufactured by Datascope specifically for Brunel University. A schematic representation of the TID and TDD designs is provided in Figure 2.2. The volume of the tapered balloons is 36 cc and they are 38 cm long. Wall thickness of the balloon chamber membrane was measured by means of calliper and compared with that of the commercially available and clinically used cylindrical balloons: the thickness of the membrane of the TID and TDD balloons was approximately 0.275 mm whereas for the other balloons it was approximately 0.128 mm. During the course of an experiment the balloons were inflated/deflated with the same IABP with constant settings, in order to highlight the effect of the new shape on the measured parameters.

This change in shape was based on the rationale that in one case the change in tapering would enhance the benefit associated with balloon inflation (diastolic pressure augmentation and coronary perfusion augmentation) while in the other it would enhance the benefit associated with balloon deflation (myocardial unloading). Such rationale is presented in the patent application no 0900638.8GB. The idea of a balloon with tapering diameter was originally suggested in 1996 by Stamatelopoulos et al. [80].

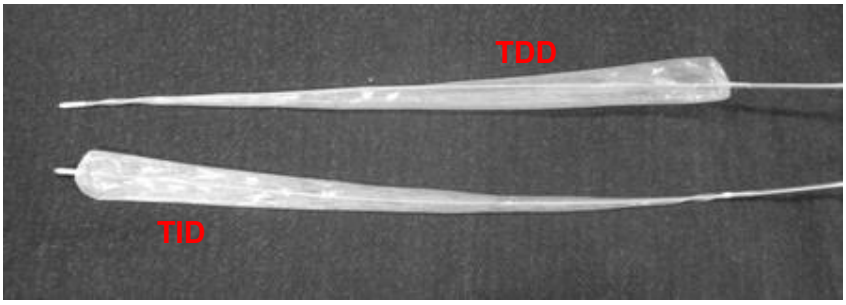

Figure 2.2: The tapered balloon, with decreasing diameter from catheter to tip (TDD) and with increasing diameter from catheter to tip (TID).

- Artificial aorta: different experimental setups have been used in this project and will be described in the relevant sections. In the experiments which required a more physiological environment, an artificial aorta was utilized. The aorta was manufactured by Ranier (Cambridge, UK) and it was made of a polyurethane compound. The aorta itself was tapered towards the iliac bifurcation (maximum diameter of 29.4 mm and minimum diameter of 10.4 mm). It accounted for 14 main branches: left and right coronary, left and right carotid arteries, left and right subclavian arteries, mesenteric, splenic, left and right renal, left and right iliac arteries bifurcating into left and right femoral and deep femoral arteries. The artificial aorta provided adequate geometry and physiological compliance, although the curvature of the aortic arch was not included in the model.

The aorta was used as an item for the generation of the mock circulatory system that will be presented and discussed in Chapter 6.

- Stepper motor: Another piece of equipment that was used in the course of this work, specifically for the construction and operation of the mock

circulatory system (Chapter 6 and 7), is a personal computer-controlled stepper motor (Placepower, Norfolk, UK). The stepper motor is coupled via a timing belt and low backlash lead-screw to a piston (6.28 cm bore) of a water-filled stainless steel cylinder. The forward and backward movement of the stepper motor can be independently controlled via the software (EasiTools Interface, Version 1.5, Parker Hannifin Automation, Dorset, UK). For both phases, motor acceleration ($rev \cdot s^{-2}$), motor deceleration ($rev \cdot s^{-2}$), number of forward steps (proportional to stroke volume) and maximum velocity ($rev \cdot s^{-1}$) can be adjusted. By varying these parameters, different pumping frequencies and duty cycle are achieved. For this reason the stepper motor was used, in conjunction with a BVS 5000 ventricular assist device (Abiomed Inc, MA, USA), providing accurate control over heart rate, systole/diastole ratio and stroke volume in the mock circulatory system.

- Data acquisition system: A rack-mount BNC accessory (BNC 2090) was used for connecting analogue and digital signals to the data acquisition device (NI-DAQ 7, National Instruments, Austin, TX, USA). The BNC 2090 can use 8 differential or 16 single-ended analogue input channels and 8 differential channels were used throughout the experiments, with 16 bits ADC resolution and minimum interchannel delay of 4 μs.

- Pressure-measuring equipment: pressure was measured with transducer-tipped pressure catheters. Different catheters were used during the course of the experiments: 5F single-transducer catheters (Gaeltec, Isle of Skye, UK), a 5F catheter with two sensors 5 cm apart (PCU 2000 pressure control unit, Millar Instruments Inc, Houston, TX, USA) and a 7F catheter with

seven sensors equally spaced 5 cm apart (Gaeltec). Further, a 0.014-inch pressure wire (Radi Medical Systems AB, Uppsala, Sweden) was used in order to gain access to the balloon chamber and measure balloon internal pressure, since data on balloon internal pressure has not been reported previously. The frequency response of the Millar catheter according to manufacturer specifications is: DC to 1000 Hz (-3 dB), minimum [97]. Pressure data was acquired at 500 Hz with Labview (National Instruments, Austin, TX, USA) and later processed in Matlab (The Mathworks, Natick, MA, USA).

- Flow-measuring equipment: flow was measured with ultrasonic perivascular flow probes (Transonic, Ithaca, NY, USA). Different probe sizes have been used according to the different setups, including: 3, 8, 10, 20, 24 and 28 mm. The smaller probes (3 and 8 mm) operate according to the principle of V-beam illumination, with one pair of transducers on the same side of the vessel transmitting alternately in upstream and downstream directions, while larger probes (10-28 mm) operate according to the principle of X-beam illumination, with two pairs of transducers on opposites sides of the vessel transmit alternately in upstream and downstream directions [98], as shown in Figure 2.3. The probes were attached to Transonic flowmeters (T206 model and HT323 model). The sampling rate of Transonic flow probes, according to manufacturer instructions, ranges from 3.6 KHz (smallest probes) to 225 Hz (largest probes) allowing full resolution of pulsatile flow [99].

Similarly to pressure measurements, flow data was recorded with Labview and later processed in Matlab.

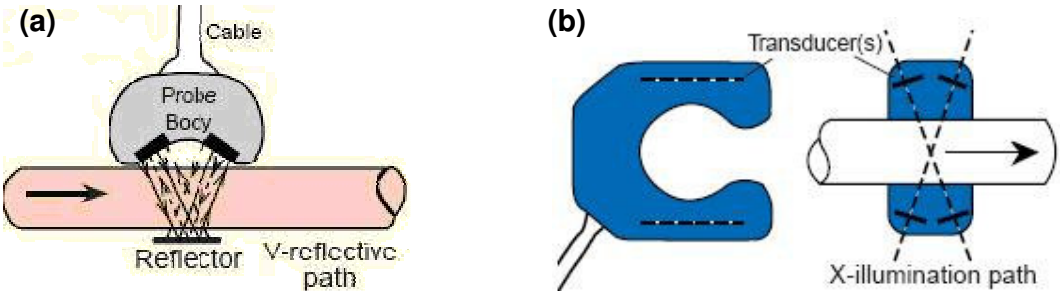

Figure 2.3: Transonic flow probes with V-shape (a) and X-shaped (b) pattern of ultrasonic illumination. Image from [98].

2.2. Calibrations

2.2.1. Pressure calibrations

Pressure calibrations were performed with the method of the column of water. Pressure in volts was recorded advancing the pressure sensor in the water-column in steps of 10 cm up to a height of either 100 cm or 180 cm, depending on the range of pressures expected during the individual experiments. The pressure due to the water-column was converted into mmHg (or Pa). Pressure in volts and pressure in mmHg (or Pa) were plotted and the equation of the regression line relating these values was used to converted the pressure measured in volts into mmHg (or Pa).

Conversion lines for the Gaeltec 7sd tip sensor and the Millar tip sensor are shown as examples in Figure 2.4a and 2.4b respectively.

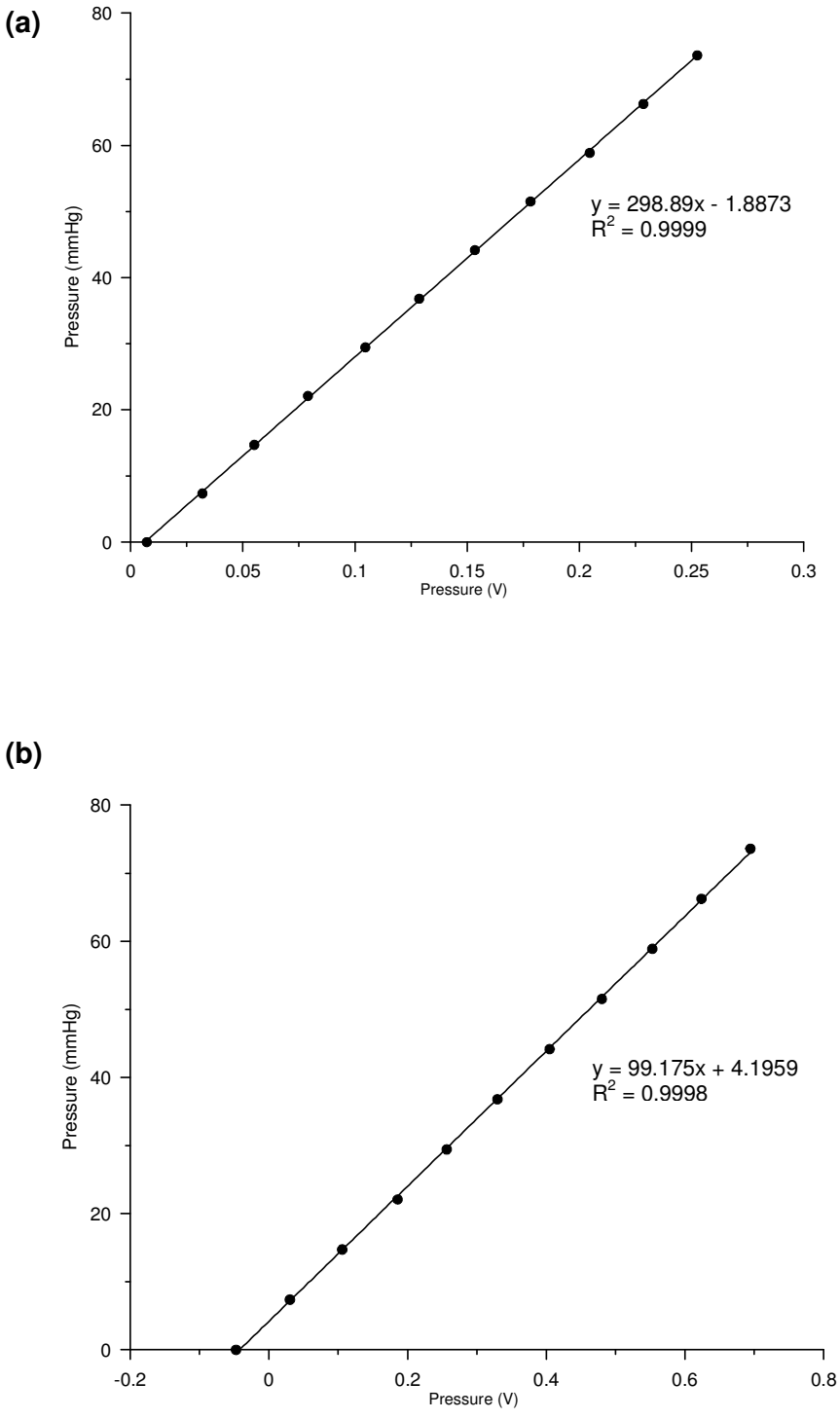

Figure 2.4: Pressure conversion lines for the Galetec 7sd tip sensor (a) and Millar tip sensor (b), showing the relationship between measured pressure in volts (V) and pressure in mmHg.

2.2.2. Flow calibrations

Transonic flow probes are pre-calibrated by the manufacturer [100] and conversion values from volts to l/min are provided for different probe sizes. Probes with diameter > 6 mm are calibrated in latex [100]. Since the experimental setups in this thesis involve tubing of different materials (latex, but also silicone and polyurethane) manufacturer calibration values were used only in the case of measurements in latex tubes, but calibrations were repeated for probes of different sizes in silicone tubes.

For the calibration procedure, a continuous flow pump was used to generate flow. Once constant flow in the system was ensured, flow was regulated by means of a tap in order to generate different flow-rates. Flow was measured with the Transonic probes of interest fitted around the silicone tube, which was submerged in a water bath. At the same time, output flow was also collected for 30 seconds with a measuring cylinder.

Measured flow in l/min was plotted versus flow in V as measured by the flow probe being calibrated and conversion lines were thus obtained. Examples of conversion lines for different probe sizes (28 mm, 20 mm and two 8 mm probes) are shown in Figure 2.5.

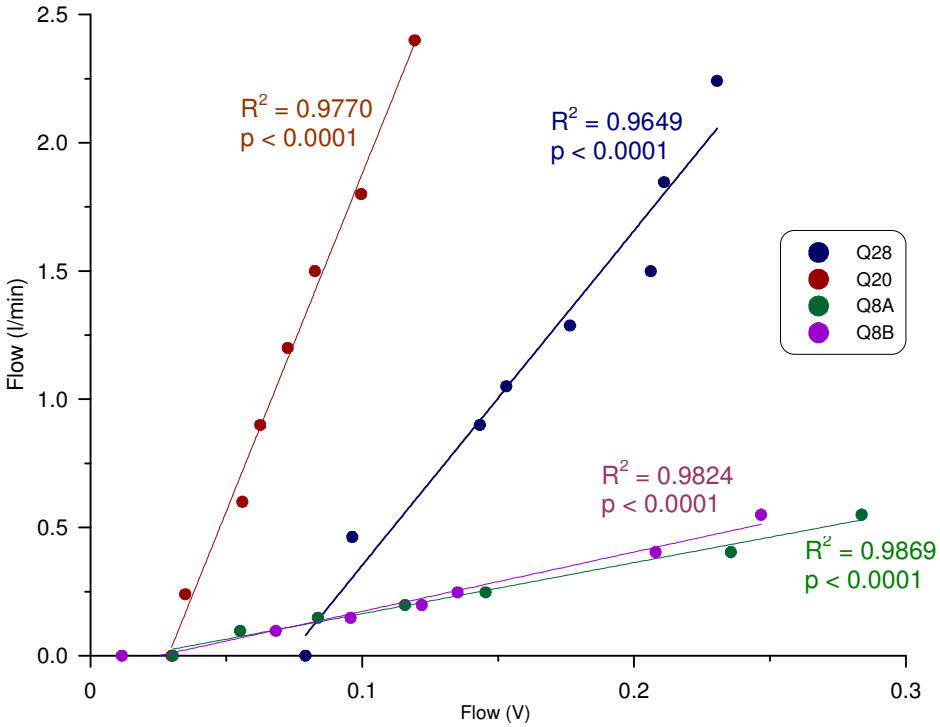

Figure 2.5: Conversion lines for flow measured in l/min and flow in volts measured by different Transonic flow probes: 28 mm (Q28), 20 mm (Q20) and two 8 mm probes (Q8A and Q8B).

2.3. Reproducibility

In order to ensure the reproducibility of the balloon behaviour, pressure in the balloon catheter ($P_{shuttle}$) was repeatedly measured with a transducer-tipped pressure catheter, with the balloon pulsating inside a straight silicone tube. Twelve recordings were compared (Figure 2.6) and it was shown that the behaviour of the balloon is highly reproducible.

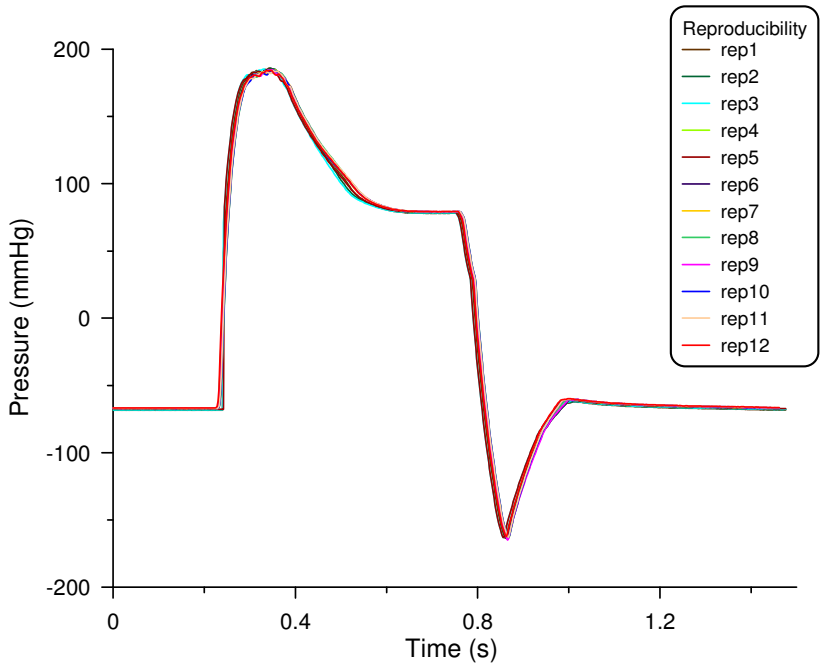

Figure 2.6: Comparison of twelve individual not consecutive measurements of shuttle gas pressure, showing that the balloon behaviour is highly reproducible.

2.4. Analytical methods: wave intensity analysis

Wave Intensity Analysis (WIA) was introduced in 1990 by Parker and Jones [101] and it has lately been described by Avolio et al. as "the most recent and probably most important impetus to the interpretation of arterial hemodynamics and as an alternative to arterial input impedance analysis" [102].

WIA is a time-domain technique, as opposed to impedance analysis, which is a frequency-domain technique [103]. It is based on Riemann's method of characteristics [104] and considers pressure and velocity waveforms as successive wavefronts rather than a summation of sinusoidal wavetrains [103].

Wave intensity (*dI*, in W/m^2) is defined as the product of the differentials of simultaneously measured pressure (*P*) and velocity (*U*) [101], or:

$$dI = dPdU \qquad \textbf{Eq.3}$$

and an example is provided in Figure 2.7. Flow velocity U was derived experimentally dividing the measured flow rate by the cross-sectional area of the corresponding flow probe.

It is possible to separate *dI* into forward and backward wave intensity, $dI_{\pm}$, as follows:

$$dI_{\pm} = \pm\frac{1}{4\rho c}(dP \pm \rho c dU)^2 \qquad \textbf{Eq.4}$$

where ρ = density of the fluid, c = wave speed and +/- indicate the forward/backward direction with respect to flow. Forward waves have positive values of *dI* and backward waves have negative values of *dI*. Knowledge of c is necessary to calculate separated *dI*.

The definition of c of a wave travelling in an elastic tube according to Moens [105] and Korteweg [106] is as follows:

$$c = \sqrt{\frac{Eh}{2\rho r}} \qquad \textbf{Eq.5}$$

where E = Young's modulus of tube's material, h = wall thickness and r = radius of the tube.

Methods for calculation of c include (i) the foot-to-foot method [107], (ii) the sum of squares method [108] and (iii) the PU loop method. In this study c was calculated with the PU loop method, introduced by Khir et al. [109]. According to this technique, measured P and U are plotted together and the linear slope of the initial portion of the obtained loop yields a value equal to ρc, according to the waterhammer equation [110] which relates dP and dU as follows:

$$dP_{\pm} = \pm\rho c dU_{\pm} \qquad \textbf{Eq.6}$$

The first published example of a PU loop is provided in Figure 2.8. [109]. It has been shown that calculation of c with the PU loop method is sensitive to

the choice of the linear part [109] and to the properties of the vessel's wall [111]. In the course of data analysis the linearity of the linear part was ensured by aligning the P and U signals using a different number of shifts, hence producing a series of PU loops for each measurement and identifying the one with the most linear part. This method, used to guard against erroneous selection of the linear part of the loop, has also been automated [112].

In relation to WIA clinical relevance, Sugawara et al., in describing a non-invasive Doppler technique for *dI* acquisition, refer to *dI* as "a hemodynamic index, which can evaluate the working condition of the heart interacting with the arterial system" [113]. WIA has been previously applied in the aorta [114], the coronary circulation [115], the left ventricle [116], the pulmonary circulation [117], the carotid artery [118] and the peripheral circulation [119].

The reason for applying WIA in this study was to investigate the waves associated with balloon inflation and deflation. Further, given that the energy carried by a wave (*I*) can be calculated by integrating *dI* in the time span of interest as:

$$I = \int_{t_0}^{t_1} dIdt \qquad \textbf{Eq.7}$$

with t_0 and t_1 being the onset and the end of inflation/deflation it would thus be possible to estimate the energy carried by the inflation and deflation wave.

Wave intensity analysis has not been applied in the context of counterpulsation. It is here hypothesised that this time-domain technique that allows for determining the energy carried by the waves traversing the arterial system can be used to describe the behaviour of the IAB. In fact, isolating the waves generated during balloon inflation and deflation, it is possible to calculate the energy associated with either phase. Changes in wave energy may describe

the operation of the balloon in addition to the established parameters of diastolic pressure augmentation, end-diastolic pressure reduction and coronary perfusion augmentation.

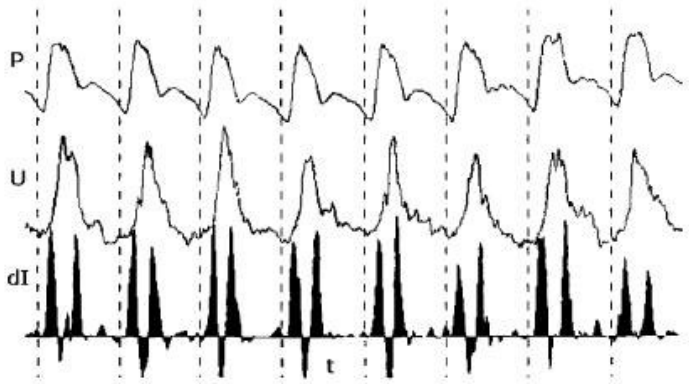

Figure 2.7: Example of wave intensity analysis, representing the first measurement of wave intensity in man, measured in the human ascending aorta in the original wave intensity study by Parker and Jones in 1990 [101]. P = measured pressure, U = measured velocity and dI = calculated net wave intensity.

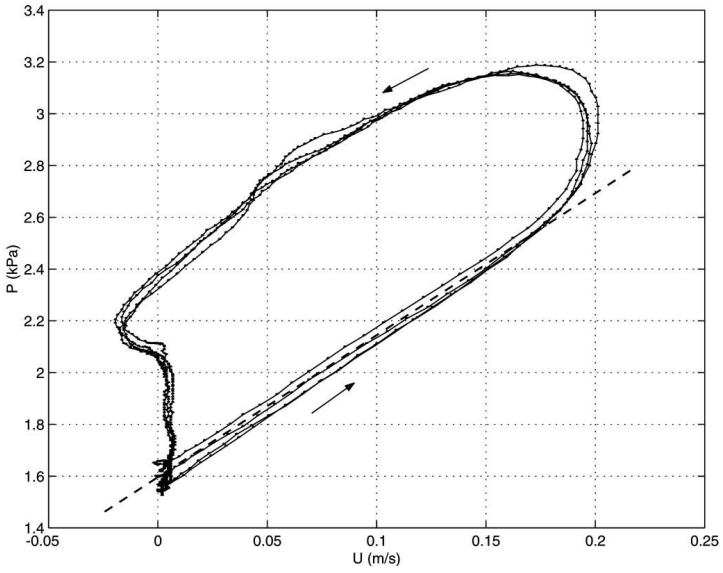

Figure 2.8: PU loop method as measured in the main pulmonary artery by Khir et al. in 2001 [109]. The slope of the dashed line indicates wave speed, $c = \frac{1}{\rho}\frac{dP}{dU}$*, with P = pressure, U = velocity and ρ = fluid density.*

CHAPTER 3

PRELIMINARY ASSESSMENT OF BALLOON VOLUME DISPLACEMENT IN A STRAIGHT COMPLIANT TUBE*

3.1. Introduction

Current knowledge about the IABP and balloon mechanics does not include information about the amount of fluid volume which is displaced at the extremities of the balloon during inflation. The importance of quantifying volume displacement lies in its relation to the hemodynamic benefit achieved during inflation (augmentation of coronary perfusion due to additional volume displaced in the retrograde direction).

One benefit of an *in vitro* study is the possibility of reducing the complexity of a setup in order to get insight into the question – what is the amount of volume displaced by the balloon in the retrograde direction? – before moving into more complex and more anatomically relevant settings, such as an artificial aortic model (Chapter 4, 6 and 7).

In the light of this consideration, preliminary measurements have been carried out in a single straight tube, aiming to quantify the volume displaced by the inflating balloon for different balloon sizes both at the horizontal and angled positions. Also, the following hypothesis was put forward in relation to volume displacement: considering that the IAB displaces fluid on both sides when inflating and that a pressure gradient is required in order to drive the flow, a

* *Partly published in: G Biglino, M Whitehorne, JR Pepper and AW Khir, Pressure and flow-volume distribution associated with intra-aortic balloon inflation: an* in vitro *study, Artif Organs 2008; 32(1):19-27*

pressure locus (indicating maximum pressure) should be located along the IAB length. The measurements aim to verify this hypothesis.

Finally, this experiment also allows the investigation of the effect of balloon shape on volume displacement and pressure locus distribution, by including both cylindrical and tapered balloons. The tapered balloons are characterised by either decreasing or increasing diameter from the catheter to the tip (TDD and TID respectively, see Chapter 2, Figure 2.2).

3.2. Materials and methods

3.2.1. The setup

A schematic representation of the complete setup and an image of the same setup are shown in Figure 3.1. Measurements were carried out using four sized cylindrical balloons: 25, 34, 40 and 50 cc (Datascope). Tapered diameter balloons (TID and TDD) were also tested. All balloons were inflated once from standstill with the IABP (CS 100, Datascope) set at 1:3 assisting frequency, in order to isolate one balloon cycle and studying a single beat. Heart rate was set at 80 bpm. Heart rate settings and triggering of the IABP were provided by a patient simulator (System trainer 90 series, Datascope) with the ECG set at sinus rhythm.

The balloons were inserted into a straight latex tube (2.4 cm ID, 82 cm long). A latex tube was chosen because latex is commonly used to mimic the elastic properties of blood vessels[†]. All balloons were positioned so that the centre of the IAB chamber and the centre of the latex tube coincided.

The tube was submerged into a water-filled Perspex tank (room temperature 20°C). It was positioned both horizontally and diagonally (at 19°

[†] Unpublished results from a tensile strength experiment carried out within the Biofluid Mechanics group of Brunel University has shown that Young's modulus (E) for a latex tube of ID = 2.4 cm is E = 0.82 MPa and that of an aortic specimen is E = 0.72 MPa.

hinged at the catheter, the maximum angle achievable due to the dimensions of the water tank). The ends of the latex tube were attached to the rigid plastic connectors of the water tank and these were in turn connected to two lateral rubber tubes linking to two upper reservoirs providing head pressure (P_{head}). Because of the thin-walled latex tube, P_{head} could not be in a physiological range and was kept constant throughout the measurements at 24 mmHg.

The setup was built as symmetrical as possible, to avoid the balloon working against different impedance either at the tip or the catheter side, using lateral tubes of same size and length.

Simultaneous pressure and flow rate measurements were taken at regular spatial intervals along the latex tube. The intervals were 5 cm apart for a total of 13 measurement sites, with site 7 coinciding with the centre of the balloon and the centre of the latex tube for all the balloons tested. Pressure was measured with a transducer-tipped catheter (Gaeltec, Isle of Skye, UK) which was always calibrated before the measurements. Flow was measured with a snugly fitting 24 mm ultrasound flow probe (Transonic, Ithaca, NY, USA) and calibration of the probe was based on the flow meter (T206, Transonic) internal calibration factor, fixed at 1 V = 20 l/min. In order to avoid interference between the ultrasound flow probe and the pressure catheter, the latter was always positioned just outside the region occupied by the probe at the same measuring site.

In order to ensure the reproducibility of the data, 5 measurements were repeated at each measurement site for all balloons tested. Also, as demonstrated in the following section (3.2.2), the direction of balloon insertion did not affect the recorded signals.

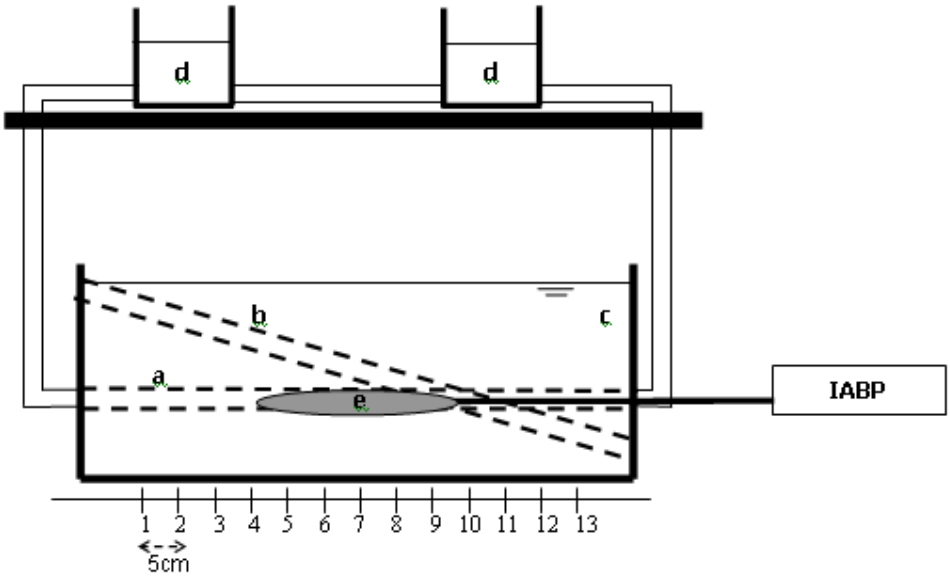

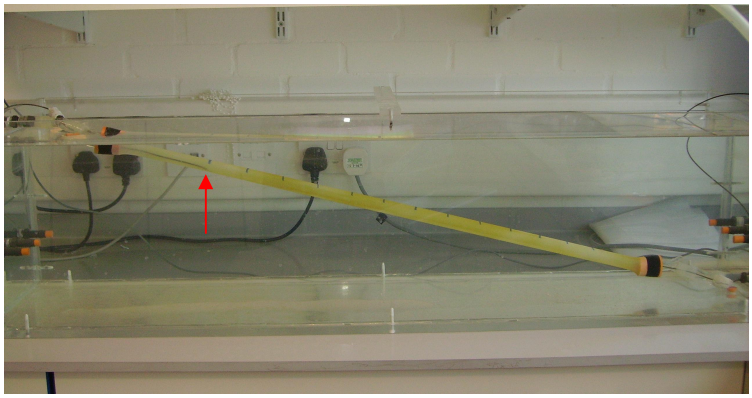

Figure 3.1: Schematic representation of the experimental setup (above). The latex tube is shown in the horizontal (a) and angled (b) position, submerged in the water tank (c). The upper reservoirs (d) provide head pressure. The balloon (e), inflated by the external IABP, is inserted in the latex tube. Measurement sites (1-13) are equally spaced 5 cm apart and site 7 corresponds to the centre of the balloon and of the latex tube. In the picture (below) the latex tube, submerged in the water tank, is shown in the angled position. The marks indicating the 13 measurement sites are visible on the tube. The pressure catheter is at site 1, as indicated by the red arrow.

3.2.2. Insertion of the balloon catheter

In order to confirm that the direction of insertion of the balloon catheter does not have an effect on the measured signals, a simple test was performed. A 40 cc cylindrical balloon (Datascope) was positioned into the latex tube of the setup described in Figure 3.1, with the centre of the balloon coinciding with the centre of the tube. Flow measurements were taken at two symmetrical points 15 cm away from the extremities of the tube with a 24 mm ultrasound flow probe (Transonic) and were repeated with the balloon inserted both from the right- and from the left-hand side (Figure 3.2). Measurements showed that similar flow patterns occur at the location distal from the balloon tip (retrograde) as well as at the location where the catheter is present (antegrade), whether the balloon is inserted from the right- or the left-hand side. This is shown in Figure 3.3.

Based on these measurements, it was thus concluded that the direction of insertion would not have an effect in this study, provided that the setup was symmetrical. All balloons in the described experimental setup were inserted from the same side.

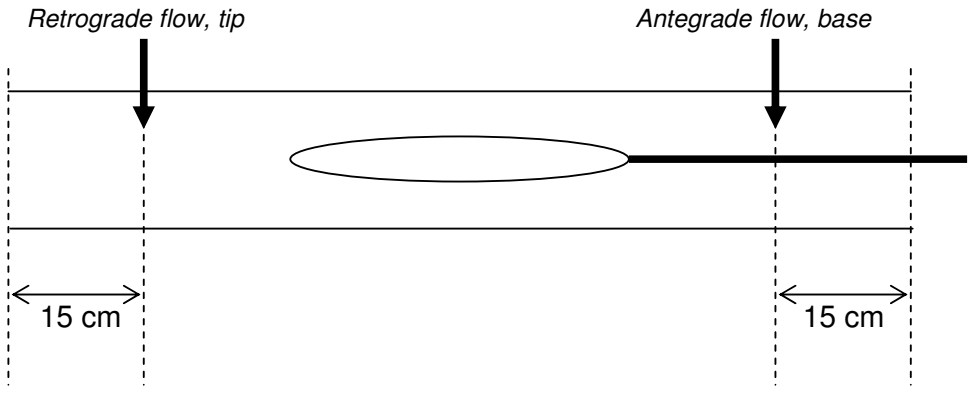

Figure 3.2: Arrangement for testing the effect of the direction of insertion of the IAB catheter. Tip flow and base flow were measured at symmetrical points, as indicated by the arrows. Measurements were repeated with the balloon inserted from the right- and the left-hand side.

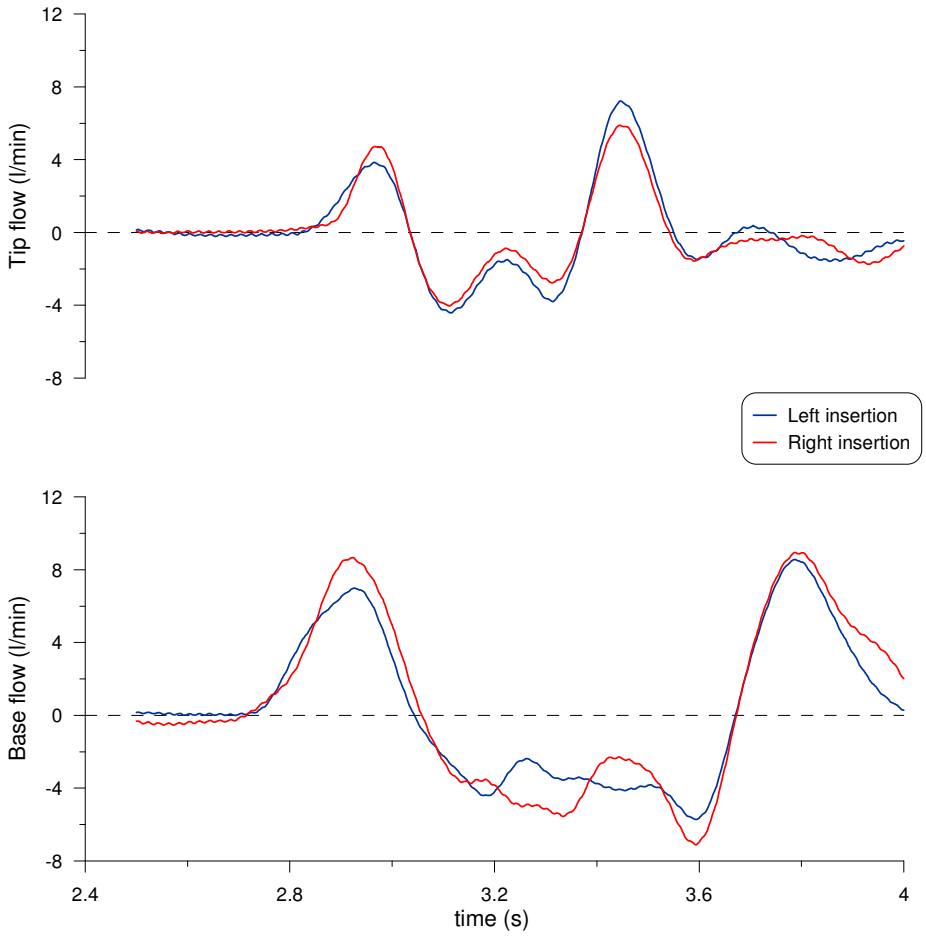

Figure 3.3: Measurements of tip flow (top) and base flow (bottom) indicated that very similar flow is measured whether the balloon is inserted from the right- (red line) or left-hand side (blue line) in the setup shown in Figure 3.2, demonstrating that the direction of insertion of the catheter did not affect the measurements.

3.2.3. Data analysis

Data were sampled at 500 Hz using in-house software written in LabView (National Instruments, Austin, TX, USA) and data analysis was later carried out using MatLab (Math Works, Natick, MA, USA). From the pressure signal, values of peak pressure during inflation (P_{max}) were obtained at each of the thirteen measurement sites. Flow velocity (U) was determined dividing the measured flow rate (Q) by the cross-sectional area (A) of the probe, U = Q/A.

Knowledge of inflation and deflation timing of the balloon was gained from the balloon shuttle gas pressure waveform (Figure 3.4) as obtained from

the IABP diagnostic output, a port on the back of the IABP allowing extraction of signals including shuttle gas pressure. Three phases were distinguished: 1) rapid inflation of the balloon, 2) the balloon is fully inflated, 3) deflation of the balloon. Combining information about balloon timing with the Q signal it became evident that even before the deflation phase starts there is a significant amount of negative Q. Since from the clinical point of view coronary perfusion augmentation during inflation is achieved by the net fluid volume displaced in the retrograde direction, in the present study only positive Q peak was integrated for quantifying volume displacement due to inflation. This quantity represents the retrograde contribution or "retrograde push" of the balloon. Retrograde volume displacement is defined V_{up} and volume displacement in the antegrade direction is defined V_{down}.

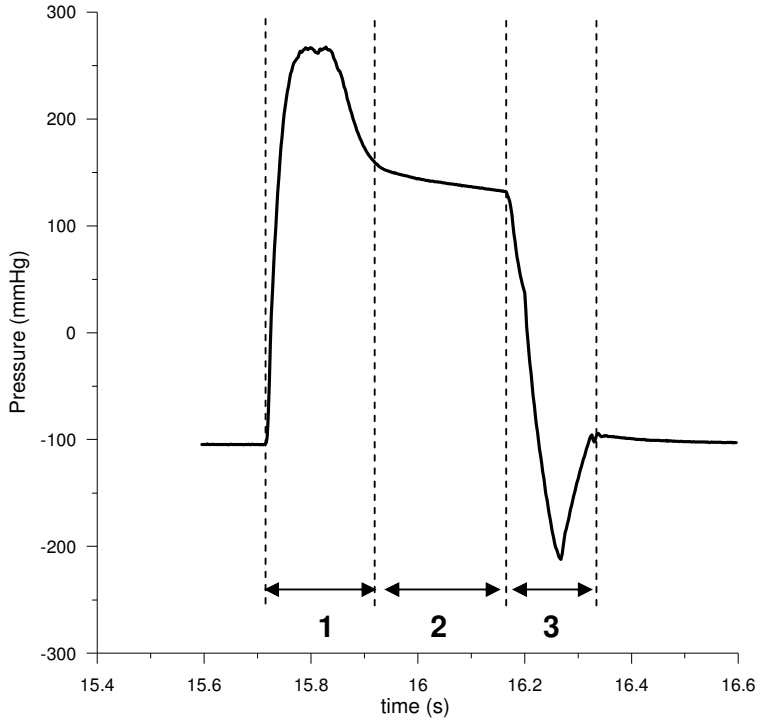

Figure 3.4: Example of balloon shuttle gas pressure as obtained via the diagnostic output of the IABP, showing (phase 1) the balloon being inflated, (phase 2) the balloon fully inflated and (phase 3) the balloon being deflated.

However, preliminary analysis of the Q signal showed that still during the inflation phase a varying amount of negative Q. This is shown in Figure 3.5. Effectively the correct value of V_{up}, representing the retrograde contribution or "retrograde push" of the balloon, is represented by the integration of the positive peak on the Q signal during the inflation phase.

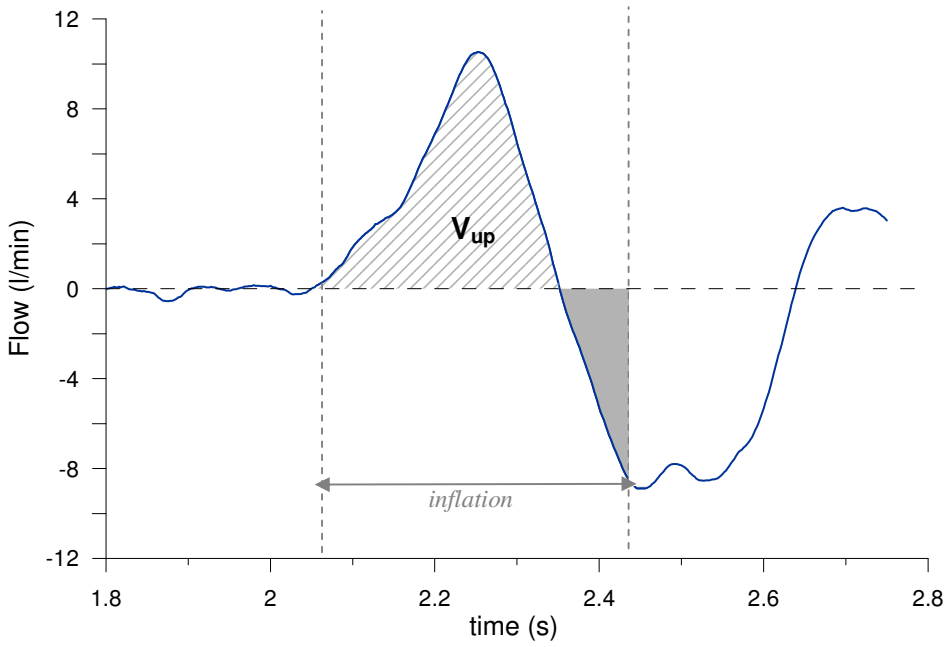

Figure 3.5: Example of a flow measurement in a site along the latex tube away from the balloon, showing negative flow before the onset of deflation (solid grey area). The amount of retrograde volume (V_{up}) is obtained from integration of the positive peak during inflation.

Having thus defined V_{up}, the same principle can be applied for the definition of V_{down}, only in the antegrade direction. Also, in order to allow immediate comparison between the horizontal and angled positions for balloons of different size and shape, the quantify of "volume split" is defined, where $VolumeSplit = \frac{V_{up}}{V_{down}}$.

3.3. Results

The presence of a pressure locus along the balloon was confirmed by P_{max} results and, for all horizontal cylindrical balloons, it was located at the centre of the balloon (measurement site 7), as shown in Figure 3.6a. When the balloons were tilted, the effect of hydrostatic pressure was subtracted from the P_{max} results by taking into consideration the pulse amplitude with respect to P_{head}, hence (P_{max}-P_{head}). Again, for all cylindrical balloons the locus was at site 7, as shown in Figure 3.7a. Interestingly, for the tapered balloons the locus corresponded to the area of maximum balloon diameter, both for the horizontal and angled case, as shown in Figure 3.6b and 3.7b.

Flow results indicated that, in the horizontal case, the inflating balloon displaces more volume in the retrograde direction, as demonstrated by the volume split > 1 across all balloon sizes and shapes. All volume results are reported in Table 3.1.

When the balloon was tilted, a reduction in V_{up} was measured across the range of tested balloons. Consequently, the volume split yielded smaller values with respect to the horizontal case. To illustrate graphically the reduction in retrograde volume displacement associated with the increase in angle, the case of the 50 cc balloon is shown in Figure 3.8.

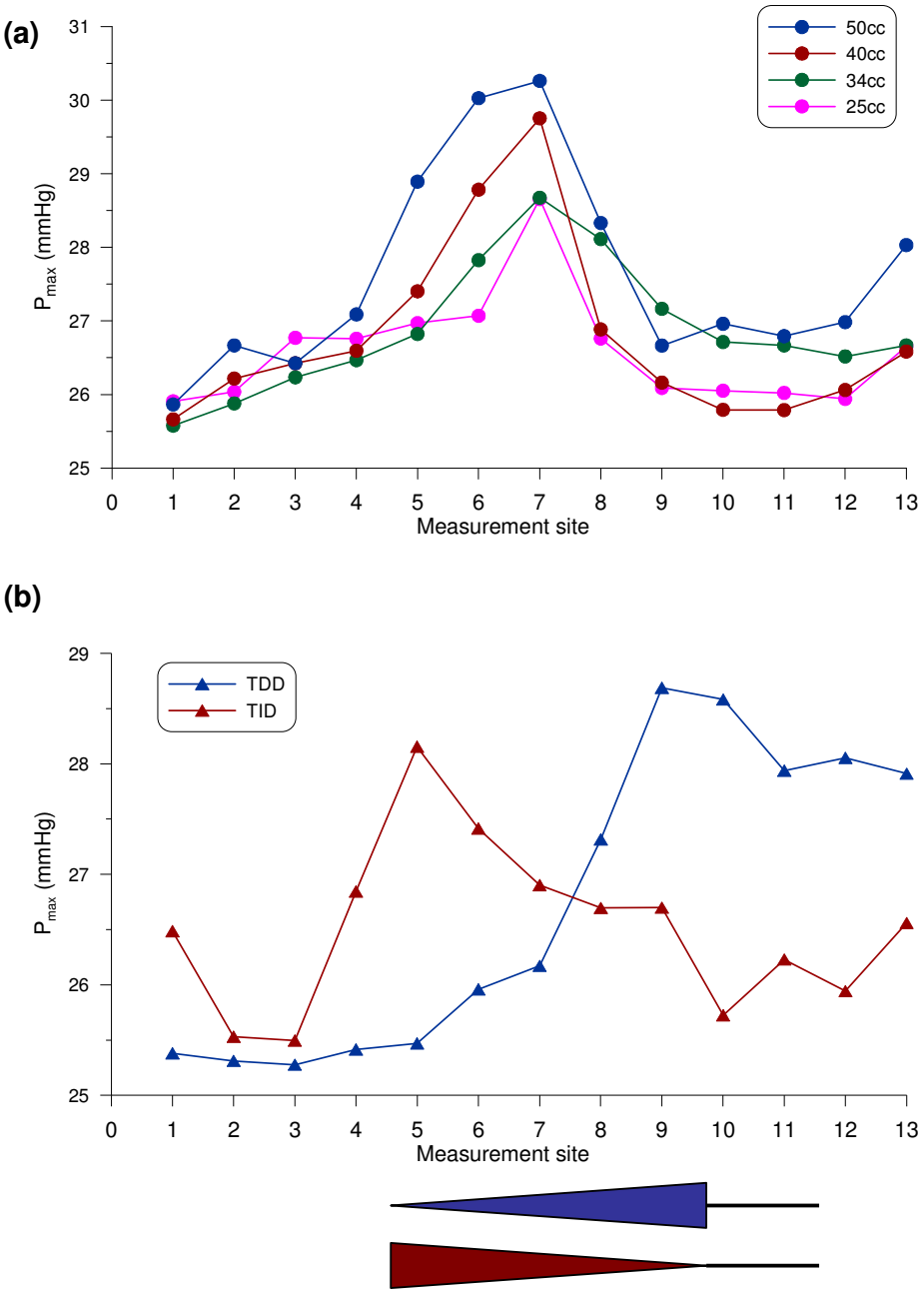

Figure 3.6: P_{max} measurements for horizontal cylindrical balloons (a) of different size (25, 34, 40 and 50 cc). The position of the pressure locus was established at the centre of the balloon, site 7. P_{max} results for the tapered balloons in the horizontal position (b) showed that both for the TDD and TID shapes the pressure locus moved from the centre to the region of larger diameter, site 9 for the TDD and site 5 for the TID.

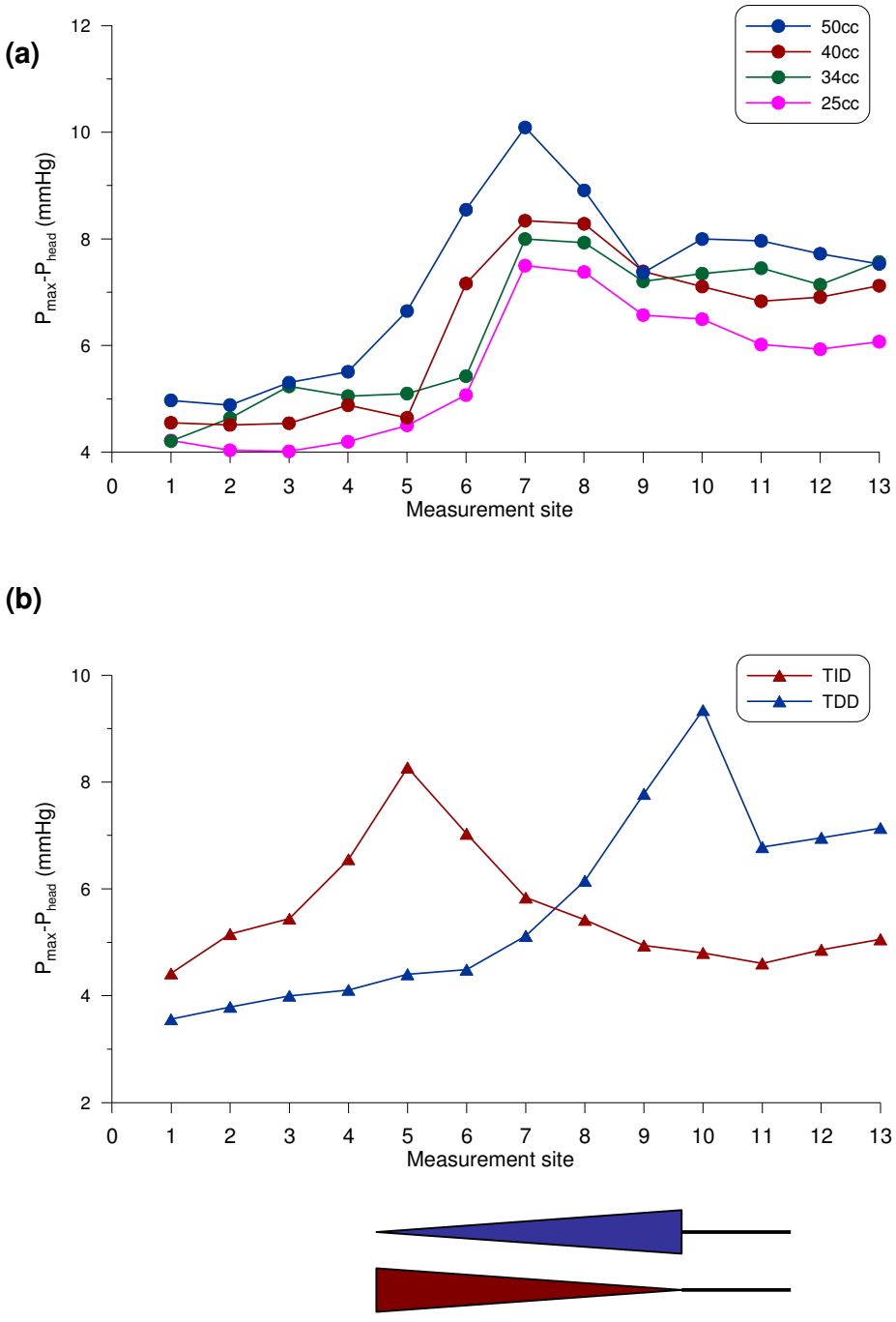

Figure 3.7: At an angle, pulse pressure (P_{max}–P_{head}) indicated that, despite the effect of hydrostatic pressure, the pressure locus for the cylindrical balloons (a) was still located at site 7. Similarly, (P_{max}–P_{head}) for the TDD and TID shapes (b) confirmed the presence of the pressure locus at the region of larger diameter, site 9 for the TDD and site 5 for the TID.

Balloon	*Sites*	Horizontal			Angled		
		V_{up} (ml)	*V_{down} (ml)*	*Split*	*V_{up} (ml)*	*V_{down} (ml)*	*Split*
25 cc	1 and 13	14.3±0.8	10.5±1.5	1.4	11.1±1.9	9.0±1.5	1.2
	2 and 12	15.5±1.2	11.1±1.3	1.4	12.8±1.3	12.2±1.1	1.1
	3 and 11	17.0±1.3	12.3±0.9	1.4	14.6±0.8	12.0±1.6	1.2
	4 and 10	15.1±0.9	11.9±1.2	1.3	13.4±0.9	12.8±2.0	1.0
	5 and 9	16.7±1.8	11.2±1.6	1.5	13.3±2.0	15.8±1.1	0.8
34 cc	1 and 13	13.9±2.6	8.7±1.5	1.6	12.5±1.3	14.7±1.1	0.8
	2 and 12	20.3±1.2	14.6±2.2	1.4	15.1±0.9	16.3±0.9	0.9
	3 and 11	18.3±1.0	15.3±1.0	1.2	16.9±0.9	17.9±1.8	0.9
	4 and 10	20.8±2.3	13.2±1.4	1.6	14.5±1.5	14.3±1.6	1.0
	5 and 9	24.2±0.8	13.8±1.5	1.8	16.2±1.7	15.2±1.0	1.1
40 cc	1 and 13	20.8±1.6	10.9±2.1	1.9	16.6±1.0	14.0±1.4	1.2
	2 and 12	22.1±1.6	12.3±0.9	1.8	18.4±1.6	16.1±2.1	1.1
	3 and 11	22.4±0.9	14.3±1.7	1.6	19.1±0.8	17.9±1.3	1.1
	4 and 10	20.8±2.1	14.8±1.5	1.4	17.9±1.5	18.9±1.3	0.9
50 cc	1 and 13	22.0±1.2	12.7±1.0	1.7	15.2±1.5	15.3±1.3	1.0
	2 and 12	25.7±0.7	14.5±0.8	1.8	18.2±1.8	17.9±0.7	1.0
	3 and 11	28.2±1.5	10.8±1.7	2.6	22.5±0.7	18.5±2.0	1.2
	4 and 10	26.1±0.8	18.2±1.6	1.4	23.8±0.6	19.8±1.7	1.2
TDD	1 and 13	16.2±2.0	10.3±2.0	1.6	12.7±2.3	13.0±0.8	1.0
	2 and 12	17.9±1.3	13.1±0.9	1.4	15.0±1.7	14.0±1.0	1.1
	3 and 11	21.0±1.4	16.4±1.7	1.3	17.5±1.8	13.1±1.7	1.3
TID	1 and 13	16.2±0.8	8.5±1.9	1.9	13.5±1.9	10.1±1.1	1.3
	2 and 12	14.9±1.8	9.7±1.8	1.5	15.2±0.9	13.8±1.4	1.1
	3 and 11	17.0±1.6	12.3±1.1	1.4	17.5±1.4	14.6±1.2	1.2

Table 3.1: Volume displacement in the retrograde (V_{up}) and antegrade (V_{down}) directions reported for all balloons both at the horizontal and at an angle (19°). The volume split is defined as (V_{up}/V_{down}).

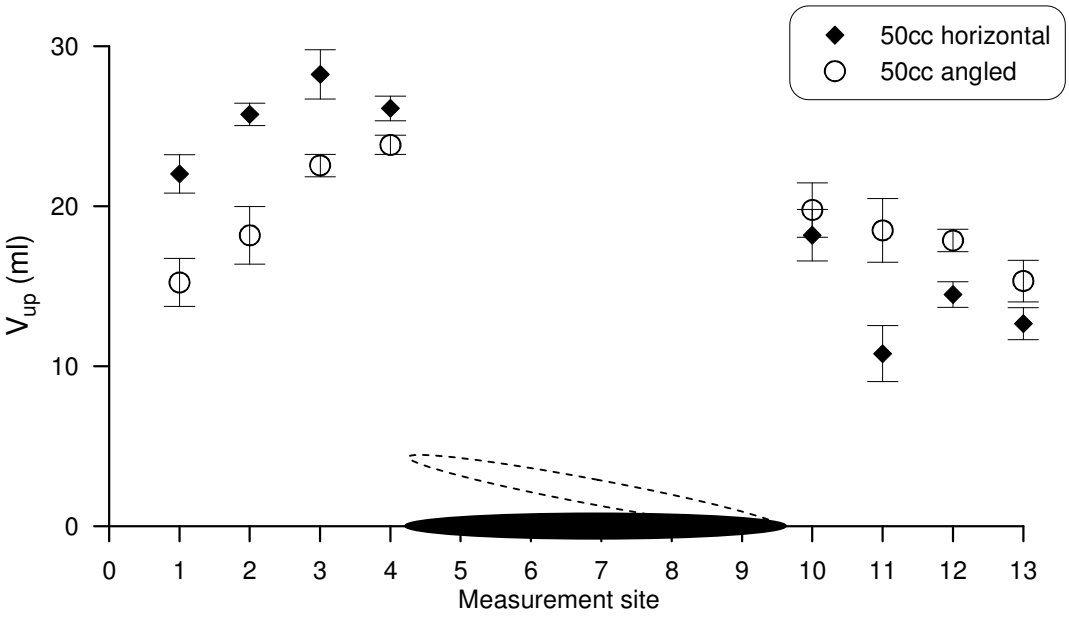

Figure 3.8: A reduction in retrograde volume was measured at an angle (19°, circles) compared to the horizontal (diamonds). This figure shows the example of the 50 cc balloon. Each point is the average of 5 measurements.

3.4. Discussion

In this study the retrograde volume displaced by inflating balloons of different sizes and shapes was quantified and the results indicated that (1) a horizontal balloon displaces a larger proportion of its nominal volume in the retrograde than in the antegrade direction, and (2) this amount is reduced if the balloon is inclined. The second point is particularly clinically relevant, because it suggests that the benefit of inflation (augmentation of coronary perfusion) may be reduced for patients nursed in the semi-recumbent position, in agreement with previous observations [90].

Looking at the volume results in Table 3.1 it is worth noting that, for a same balloon, V_{up} and V_{down} are not constant at adjacent measurement sites, with a tendency for both to decrease towards the extremities of the latex tube

(sites 1 and 13). Despite the fact that, according to the law of conservation of mass, constant V_{up} and V_{down} would be expected at subsequent sites, this variation can be attributed to the highly compliant wall of the latex tube which can accommodate part of the volume displaced by the inflating balloon. It is likely that, when measuring at the extremities, a larger proportion of balloon volume would be stored in the compliant wall between the balloon tip/base and the measuring site, hence resulting in the ostensibly observed reduced values of V_{up} and V_{down}.

A methodological observation arising from this experiment concerns the quantification of V_{up} which should not be based on integration over the duration of balloon inflation, but rather considering only the "retrograde push" of the inflating balloon. As shown in Figure 3.5, an amount of negative flow is detected before the onset of deflation, this observation being applicable to different balloon sizes and shapes. This observation has been further validated by means of an ad hoc Particle Image Velocimetry (PIV) study, whose results are reported in Appendix A. This consideration will be taken into account for flow quantification in more physiological setups described in following chapters.

The newly shaped tapered balloons exhibited a different pressure locus, representing the point of separation of V_{up} and V_{down}, which in this case was associated with the region of maximum diameter of the balloon chamber. Despite this difference, volume results do not suggest that a substantial augmentation in V_{up} may be achieved by either of the tapered balloons.

The low level of head pressure was a limitation in this experiment, since physiological levels of "intra-aortic" pressures could not be simulated. This was due to the inability of the thin walls of the latex tube to withstand higher pressures.

Another limitation of this experiment is related to the uniform cross-sectional area of the single tube that was used. Tapering of the aorta and branching were not simulated.

On the other hand, the flow distribution during balloon inflation and the concept of the pressure locus were established. On the basis of these initial observations, more physiological setups are used in further studies of this thesis, both in terms of physiological head pressure and in terms of geometry.

Overall this chapter focused on the inflation phase, from the point of view of both the pressure locus and the volume split. The importance of the deflation phase (clinically, the unloading action on the recovering myocardium) is however acknowledged and deflation will be studied in the following chapters.

3.5. Conclusion

This experiment provided the primary understanding of the flow distribution around the balloon during inflation. Experiments with more physiological pressure are presented in Chapters 4 and 5.

CHAPTER 4

THE EFFECT OF CHANGES IN TRANSMURAL PRESSURE ON BALLOON MECHANICS[‡]

In this chapter pressure and flow measurements are carried out in a more anatomically correct setup to investigate the effect of varying intra-luminal pressure, resulting in varying transmural pressure, on balloon mechanics. It is also attempted to observe these changes on the wave intensity pattern.

4.1. Introduction

Studies in the literature regarding the IABP have highlighted that the effectiveness of intra-aortic counterpulsation is dependent on the level of aortic pressure. Specifically, Charitos et al. conducted a study on the effectiveness of counterpulsation on fourteen dogs with severe cardiogenic shock, dividing the results in three groups: (1) with systolic aortic pressure less than 30 mmHg, (2) with systolic aortic pressure more than 30 mmHg and less than 56 mmHg, and (3) with systolic aortic pressure more than 56 mmHg. Assistance was considered adequate when mean aortic pressure was at least 50 mmHg during support. The authors concluded that low level of aortic pressure is the major factor preventing sufficient assistance by counterpulsation [120]. Before this study, Moulopoulos, assessing the limits of counterpulsation, already identified aortic pressure < 60-70 mmHg as an impediment to adequate counterpulsation support [121].

[‡] *Partly in: G Biglino, C Kolyva, M Whitehorne, JR Pepper and AW Khir, Variations in aortic pressure affect the mechanics of the intra-aortic balloon, Artif Organs (in press)*

Following from these observations, the importance of investigating the effect of changes in intra-luminal pressure (P_i) on balloon hemodynamics is clinically related to the case of non-normotensive patients. In addition, in the case of patients nursed in the semi-recumbent position, the change in posture implies non-uniform distribution of P_i along the balloon. The aim of this chapter is to investigate the effect of variations in P_i on IABP mechanics. The balloon will be tested in a more physiological setup allowing measurements at a range of angles to the horizontal, as described in section 4.2. As part of this investigation, wave intensity analysis will be performed and so an additional aim is to identify the wave intensity pattern associated with the intra-aortic balloon cycle *in vitro* quantifying the IABP-waves under different P_i conditions.

4.2. Materials and methods

A schematic representation and a picture of the setup are shown in Figure 4.1. A 40 cc balloon (Datascope) was inserted into an artificial real-size silicone aorta[§]. The aorta was a simplified model, consisting of ten main branches: right and left coronary, right and left carotid, right and left subclavian, mesenteric, renal, right and left iliac. The balloon was inserted via the right iliac branch. The aorta provided an anatomically correct environment, including aortic tapering, and silicone ensured adequate elastic properties. However, the artificial aorta accounted for only ten branches and the aortic arch was straightened.

[§] This artificial aortic model was manufactured by the Hydraulics Laboratory of the University of Ghent (Belgium). This is a silicone model. The compliance of a similar silicone rubber arterial tree from the same Laboratory was described as physiological in a study by Vandenberghe et al. [138].

The system was filled with water and both the inlet of the aorta and the collection of all the branches were connected to an overhead reservoir providing head pressure. The aorta was positioned on a hinged wooden platform which was constructed so that measurements could be performed at a range of angles. With reference to the semi-recumbent position in the ICU [88, 89], angles of 0, 10, 20, 30 and 45º were tested in the study.

The balloon was driven by the external IABP (System 98, Datascope). Settings of the pump were constant throughout the experiments and were controlled via the IABP panel and with a patient simulator (System Trainer 90 Series, Datascope). The pump was triggered with the ECG signal provided by the patient simulator, set at sinus rhythm. Heart rate was set at 60 bpm and assisting frequency was set at 1:3. The balloon was inflated and deflated once and each measurement was repeated three times.

Both P_i and flow (Q) were measured simultaneously 5 cm retrograde from the tip of the balloon. Measurements of P_i were taken with a 5F transducer-tipped catheter (Gaeltec) inserted via the left iliac branch. Measurements of Q were taken with a 28 mm ultrasonic flow probe (Transonic) snugly fitted at the straightened aortic arch. Shuttle gas pressure ($P_{shuttle}$) was also measured as a reference of the balloon cycle and another 5F transducer-tipped catheter (Gaeltec) was used for this purpose.

Measurements were first taken at the horizontal position increasing P_i from 45 to 115 mmHg. Then measurements were repeated both at low P_i (45 mmHg) and at high P_i (115 mmHg) over the range of angles up to 45º. Data were collected at 500 Hz with Labview (National Instruments) and later analysed in Matlab (The Mathworks). Results are shown as the average of three measurements ± SD.

A sample of the P_i and Q signals is provided in Figure 4.2.

In order to assess the operation of the balloon, two main parameters were quantified:

(a) retrograde volume displacement in the direction of the coronary circulation (V_{up}), calculated by integrating the positive peak of the Q signal and regarded as an indicator of the augmentation in coronary perfusion associated with balloon inflation, and

(b) end-diastolic pressure reduction (EDPR), defined as the negative pulse with respect to the undisturbed initial P_i and considered an indicator of the unloading action of balloon deflation.

Both V_{up} and EDPR are shown in Figure 4.2, together with $P_{shuttle}$.

As part of the analysis, wave intensity, dI = dPdU, was also calculated. As already mentioned in section 2.4., the pressure and velocity differentials are related by the waterhammer equation (Eq. 6) and in this study knowledge of wave speed c was obtained with the PU loop method [109]. An example of PU loop computed from the data collected during this experiment is shown in Figure 4.3, highlighting the slope of the loop which is equal to ρc.

By integrating the dI signal it is possible to calculate the energy carried by a wave (Eq. 7). Once the waves associated with balloon inflation and deflation *in vitro* had been identified, their energy was calculated for the different experimental cases.

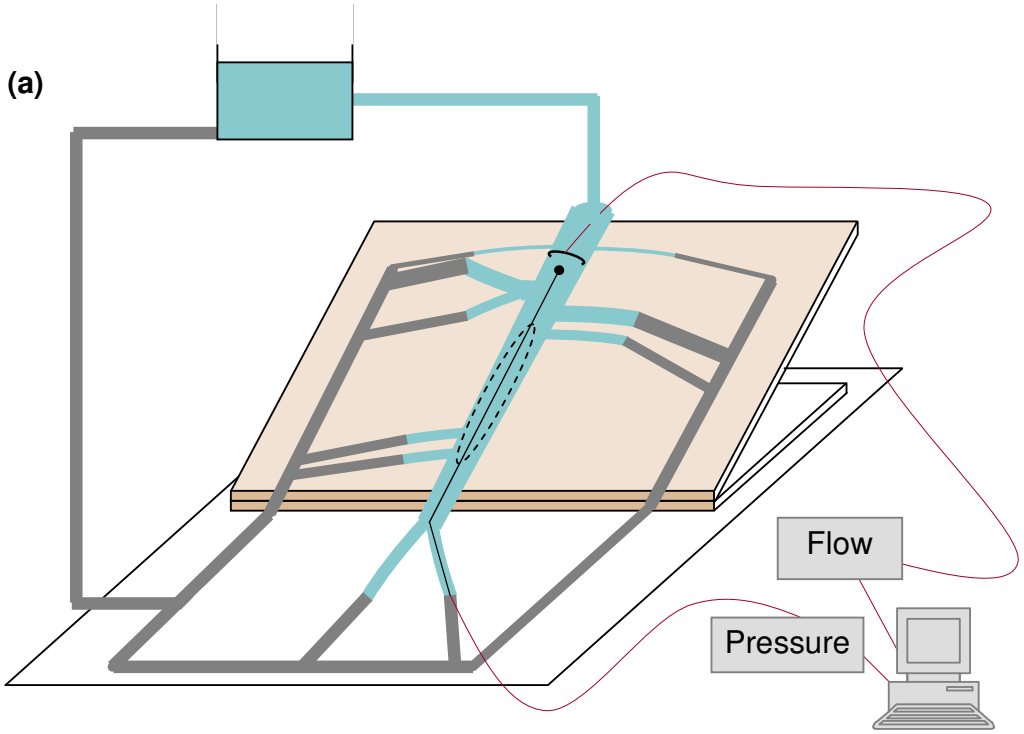

Figure 4.1: Schematic representation (a) of the artificial aorta (blue), positioned on the inclined platform to simulate the semi-recumbent position. All branches of the aorta were collected in one common output (grey) and, together with the inlet of the aorta, were connected to the overhead reservoir providing head pressure. In the picture (b) the IABP (1), the overhead reservoir (2) and the flow and pressure measuring consoles (3) are indicated.

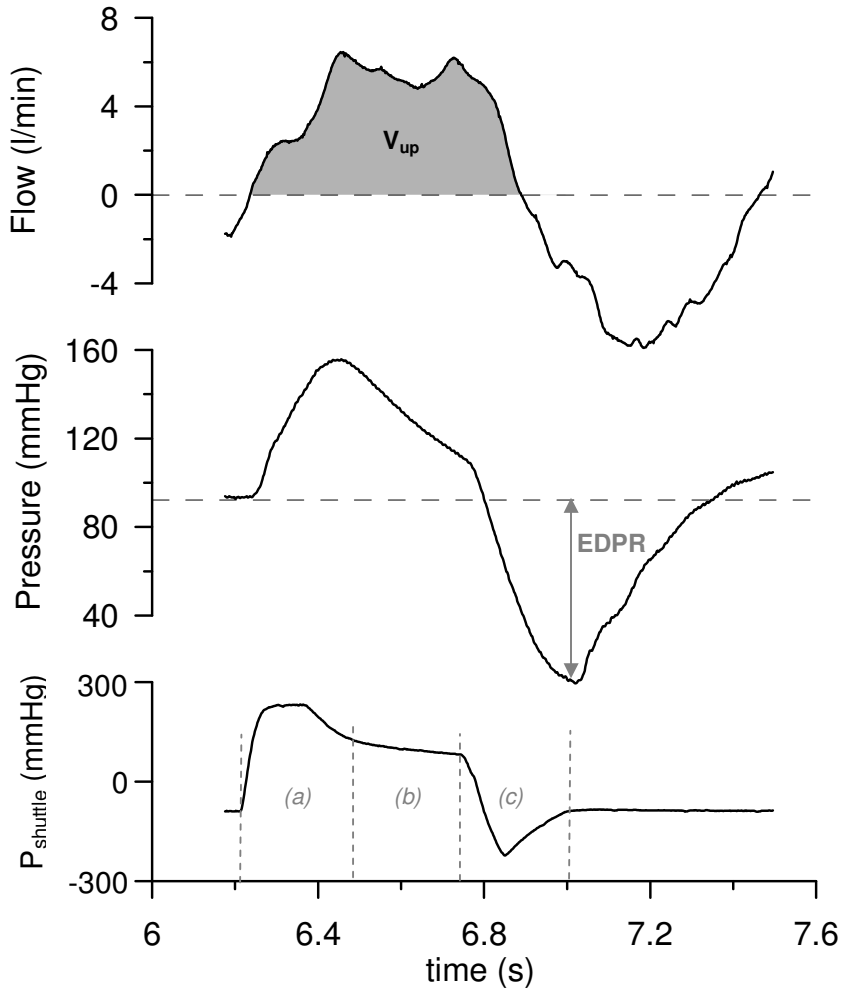

Figure 4.2: Representative measurements of flow (top) and pressure (middle) in the artificial aorta, with the shuttle gas pressure tracing ($P_{shuttle}$, bottom) as reference of the balloon cycle. Volume towards the coronary circulation (Q_{up}) is shown on the flow tracing and end-diastolic pressure reduction (EDPR) on the pressure tracing. On $P_{shuttle}$ it is possible to distinguish the three phases of the balloon cycle: (a) the balloon being inflated, (b) the balloon remaining inflated, (c) the balloon being deflated.

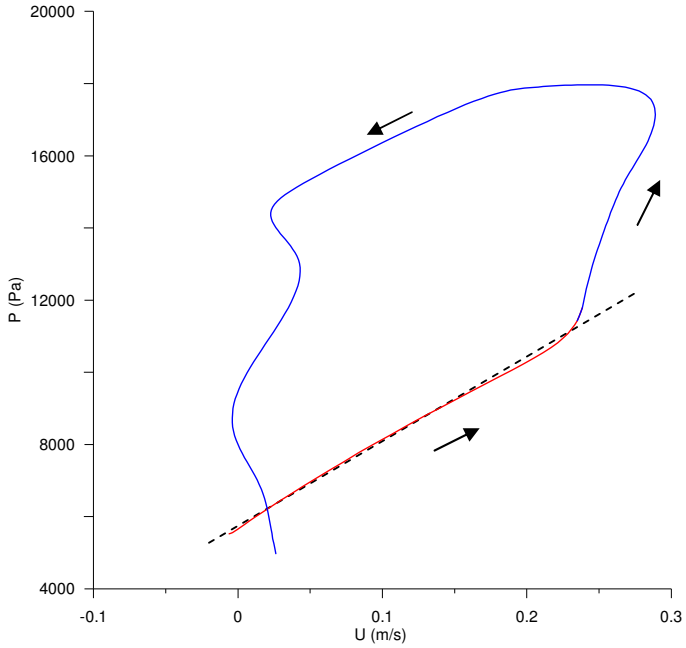

Figure 4.3: A sample of a PU loop, calculated with P and U data from the artificial aorta. The slope of the initial linear part of the PU loop (highlighted in red) is equal to ρc, where ρ is fluid density and c is wave speed. The arrows indicate the direction of the loop. This method requires pressure to be plotted in Pascals (Pa) and velocity in m/s.

4.3. Results

4.3.1. The horizontal case

Measurements of P_i in the horizontal artificial aorta showed that increasing P_i from 42.5 to 114.9 mmHg resulted in a 149% increase of EDPR (44.6 ± 0.9 vs 111.2 ± 1.9 mmHg). This is shown in Figure 4.4. The corresponding Q measurements showed that increasing P_i over the same range resulted in an 18% reduction of V_{up} (30.4 ± 1.9 vs 25.0 ± 1.0 ml). This is shown in Figure 4.5.

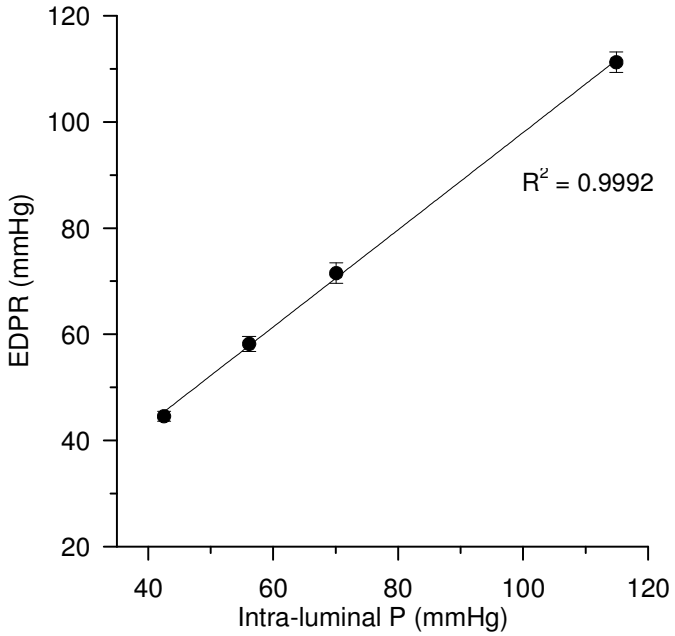

Figure 4.4: End-diastolic pressure reduction (EDPR) is increasing with increasing intra-luminal pressure. Results are shown as the average of three measurements ± SD. Error bars are scarcely visible because SD < 2 mmHg.

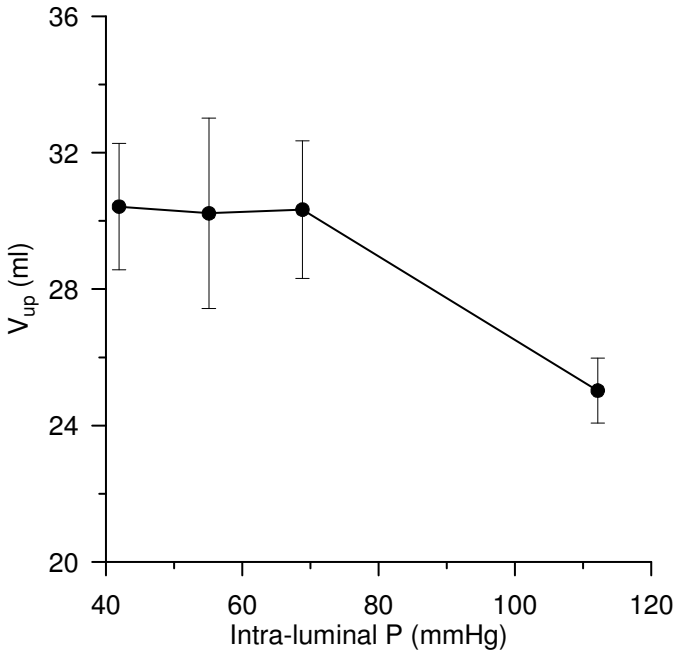

Figure 4.5: Measurements of V_{up} with increasing intra-luminal pressure, showing that an increase of 70 mmHg in P_i results in an 18% reduction of V_{up} (30.4 ± 1.9 vs 25.0 ± 1.0 ml). Results are shown as the average of three measurements ± SD.

4.3.2. The angled case

Measurements in the inclined artificial aorta at low P_i (45 mmHg) and high P_i (115 mmHg) showed a statistically significant correlation ($R^2 = 0.98$, $p < 0.005$, both at low and high P_i) between EDPR and angle. This is shown in Figure 4.6. At the low P_i case, EDPR was reduced by 66% (48.9 ± 0.6 vs 16.5 ± 0.1 mmHg) with increasing angle from 0 to 45°. At the high P_i case and the same range of angles, EDPR was reduced by 24% (106.4 ± 0.3 vs 80.6 ± 0.8 mmHg).

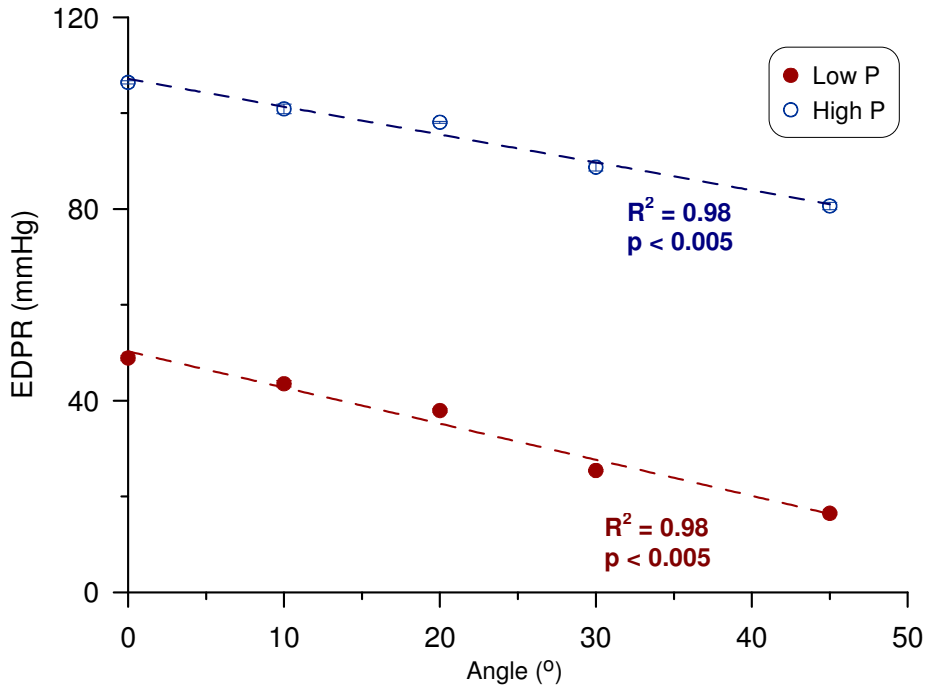

Figure 4.6: EDPR reduction with increasing angle, both at low P_i (45 mmHg, "●") and high P_i (115 mmHg, "o"). Results are presented as the average of three measurements ± SD, but error bars are not visible since all SD values are small (< 1mmHg).

Flow measurements in the inclined aorta at low P_i (45 mmHg) and at high P_i (115 mmHg) showed that it was differently affected by increasing angle depending on the level of P_i. In fact, V_{up} progressively reduced with increasing angle at low P_i, as shown in Figure 4.7, resulting in a 30% reduction in V_{up} at 45° (28.3 ± 1.7 vs 19.8 ± 2.3 ml). Instead, V_{up} was overall lower and it remained unchanged with increasing angle at high P_i, as also shown in Figure 4.7, with an average value of 20.0 ± 1.0 ml.

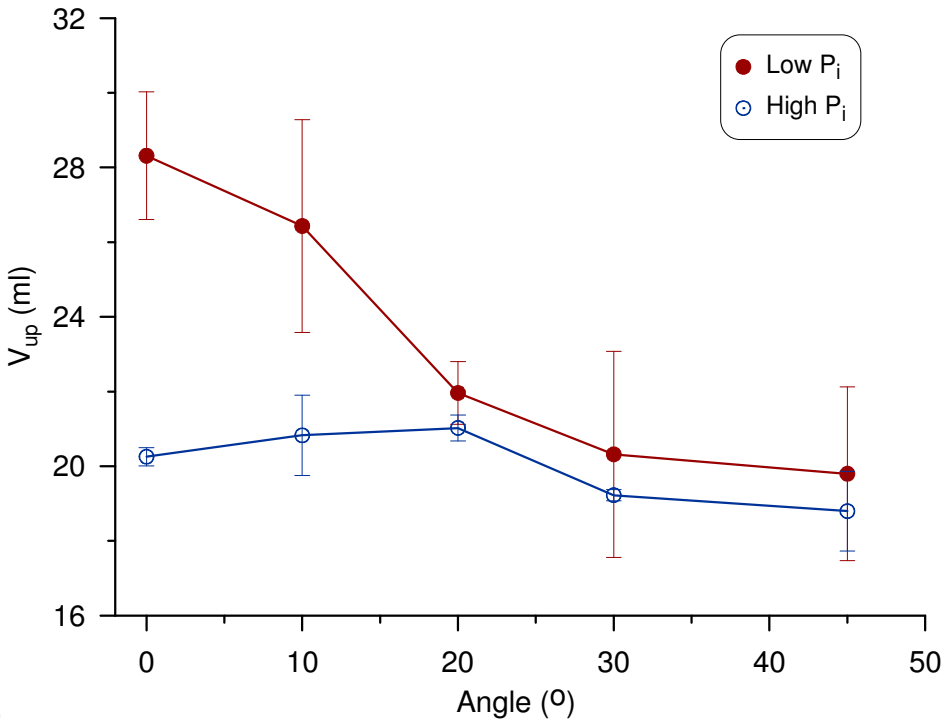

.

Figure 4.7: Variations of Q_{up} in the inclined artificial aorta were affected by the level of intra-luminal pressure: at low P_i (45 mmHg) Q_{up} is reduced with increasing angle ("●") while at high P_i (115 mmHg) Q_{up} is constant and overall lower ("o"). Error bars represent SD and each point is the average of 3 measurements.

4.3.3. Wave intensity analysis

Applying wave intensity analysis, it was possible to identify the wave pattern associated with balloon inflation and deflation. Balloon inflation generated a compression wave, while balloon deflation generated an expansion wave. These waves, and their reflections, are shown in Figure 4.8. These waves travel in the backward direction and hence they are named 'backward compression wave' (BCW), for the inflation wave, and 'backward expansion wave' (BEW), for the deflation wave.

From integration of the dI signal, it was possible to calculate the energy carried by the waves associated with inflation and deflation. Integration of the BCW showed that, when the aorta was horizontal, increasing P_i resulted in a substantial reduction in BCW energy. Increasing P_i from 42.7 to 114.7 mmHg corresponded to a 38% reduction in BCW energy (0.128 ± 0.009 vs 0.079 ± 0.002 J/m^2). This is shown in Figure 4.9.

Integration of the BEW showed that, when the aorta was horizontal, increasing P_i resulted in a substantial increment in BEW energy. Increasing P_i from 42.7 to 114.7 mmHg corresponded to a fifteen-fold increase in BEW energy (0.0093 ± 0.007 vs 0.1475 ± 0.003 J/m^2). This is shown in Figure 4.10.

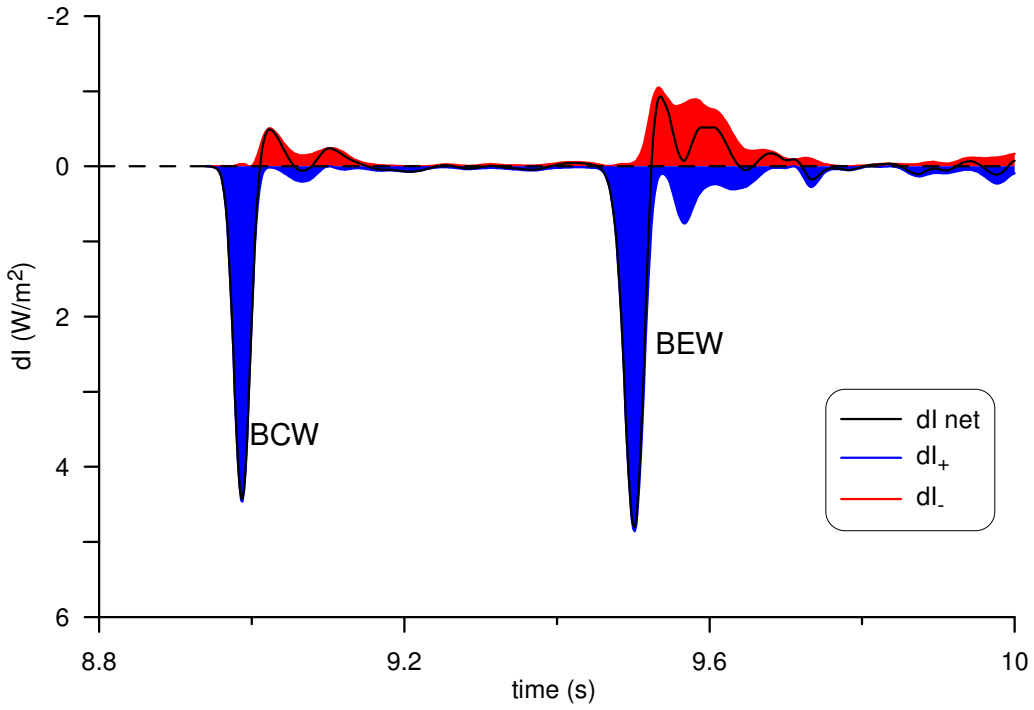

Figure 4.8: Wave intensity (dI) pattern associated with the balloon cycle. The backward compression wave (BCW) associated with balloon inflation and the backward expansion wave (BEW) associated with balloon deflation are highlighted on the plot. Net dI, dI+ and dI- can be distinguished on the plot.

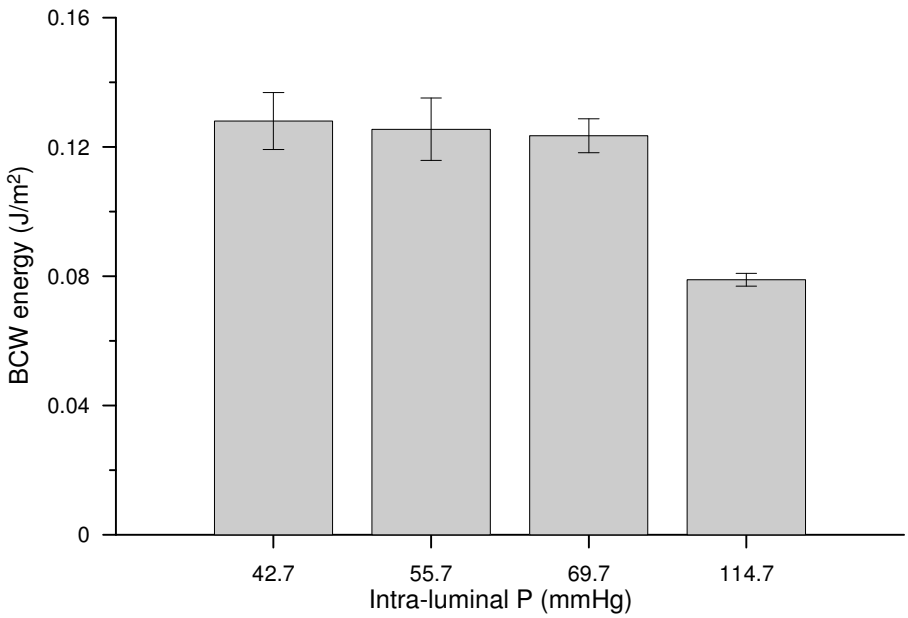

Figure 4.9: The energy carried by the compression wave associated with balloon inflation (BCW), as quantified by integrating the dI signal over the duration of inflation, decreased with increasing P_i. Results are shown as the average of three measurements ± SD.

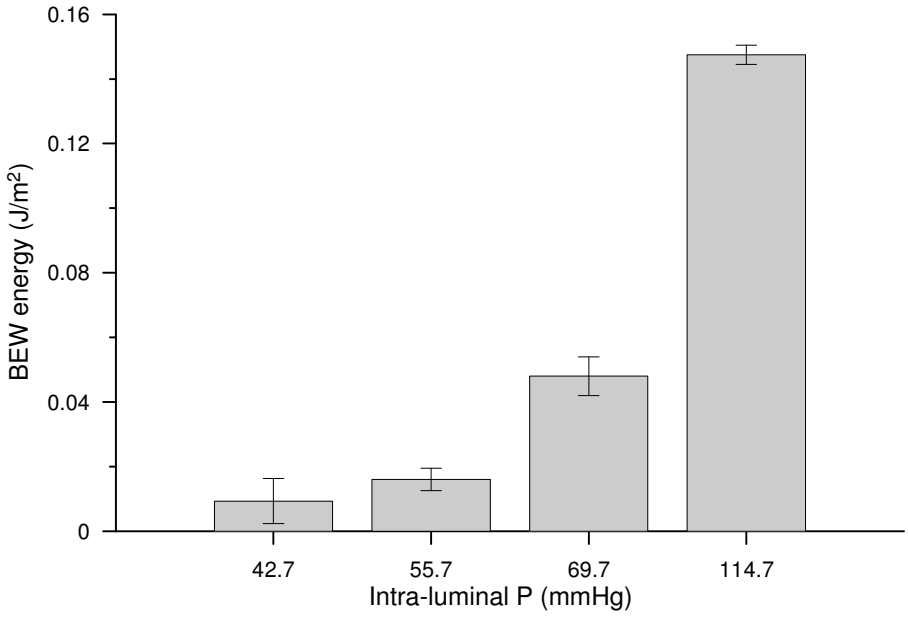

Figure 4.10: The energy carried by the expansion wave associated with balloon inflation (BEW), as quantified by integrating the dI signal over the duration of deflation, increased with increasing P_i. Results are shown as the average of three measurements ± SD.

4.4. Discussion

Balloon mechanics are affected by changes in intra-luminal pressure, P_i, both in the case of a horizontal balloon, with uniform P_i acting on it, and in the case of a tilted balloon, with varying P_i along its length. The effect of P_i was on pressure and flow data as well as on wave intensity.

4.4.1. Volume displacement

In terms of volume displacement, the effect of increasing P_i was that of reducing retrograde volume V_{up}. This is shown in Figure 4.5.

It was also found that not only does increasing P_i correspond to reduced V_{up}, but also that V_{up} correlated significantly with duration of inflation ($R^2 = 0.52$, $p < 0.005$). The inverse correlation between V_{up} and duration of inflation, shown in Figure 4.11, signifies that a considerable increase in P_i around a horizontal balloon results in a smaller amount of V_{up} being displaced in longer time. In this thesis, knowledge of duration of inflation was obtained by means of the high-speed visualisation study presented in Chapter 5, which also highlighted that the effect of increasing P_i on duration of inflation. As direct comparison of data from Chapter 4 and 5 will be affected by the different experimental setups that were used, in the context of this experiment an indication of the duration of inflation was however derived from the $P_{shuttle}$ signal for the corresponding measurement. An example of $P_{shuttle}$ signal is provided in Figure 4.2. As previously described (Figure 3.4) the phases of "balloon being rapidly inflated" and "balloon remaining inflated prior to onset of deflation" can be distinguished on the $P_{shuttle}$ signal. The phase of "balloon being inflated" was used in this case.

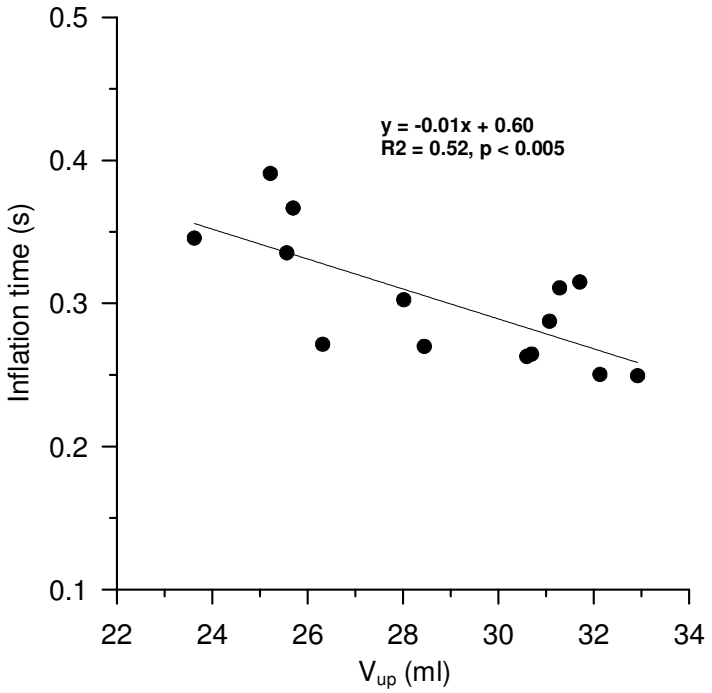

Figure 4.11: Inverse correlation between retrograde volume (V_{up}) and the duration of inflation. The correlation is based in measurements in the horizontal artificial aorta.

In order to explain the effect of increasing P_i on V_{up}, the effect of varying transmural pressure on the volume displaced by the balloon during inflation was investigated. This was done by submerging the same balloon (40 cc) in a water bath with minimal water height above the balloon. Transmural pressure (P_t) was then varied in steps by keeping P_i constant and manually inflating the balloon using gradually higher pressures. The volume (V) displaced by the balloon was collected for each measurement with a measuring cylinder. A relationship was thus obtained, between P_t and V, resulting in the curve shown in Figure 4.12.

The transmural pressure curve (TPC) exhibits two regions: (a) a linear region at low P_t, with V increasing with increasing P and (b) a near-plateau region at high P_t (> 50 mmHg), with constant V for increasing P_t. In the plateau

region the balloon can displace its total nominal volume and, for very high P_t, even more than its total nominal volume (for example, 45.5 ml at P_t = 185 mmHg displaced by the 40 cc balloon).

The shape of the TPC relates in fact to the mechanical properties of the balloon flexible membrane. Adopting the terminology used by Pedley [122] and Shapiro [123] in the field of collapsible tube theory, in the case of low P_t the partial collapse of the wall is balanced by the bending stiffness of the balloon membrane. On the other hand, at high P_t, stretching is supported by hoop tension. As a result of this, the changes in balloon cross-sectional area resulting by bending or stretching explain the ability of the balloon to displace either more or less than its total nominal volume, depending on the level of P_t. Bending and stretching for a flexible membrane segment are visually represented in Figure 4.13.

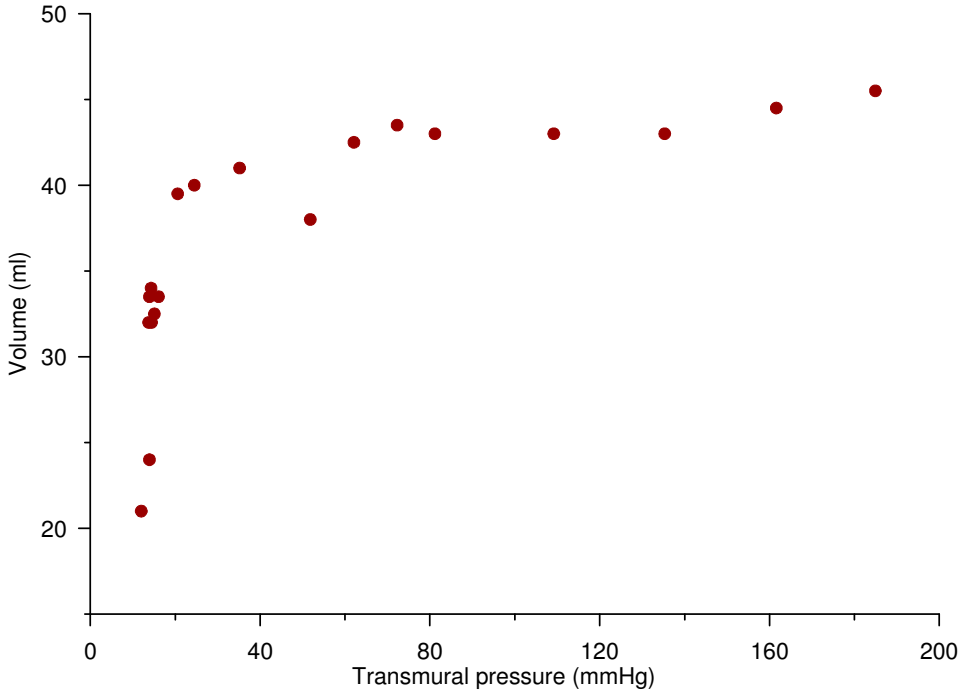

Figure 4.12: Relationship between increasing transmural pressure (P_t) and balloon volume (V). The curve can be divided into two regions: (a) linearly increasing region, at low P_t, and (b) near-plateau region, at high P_t.

(a) Bending

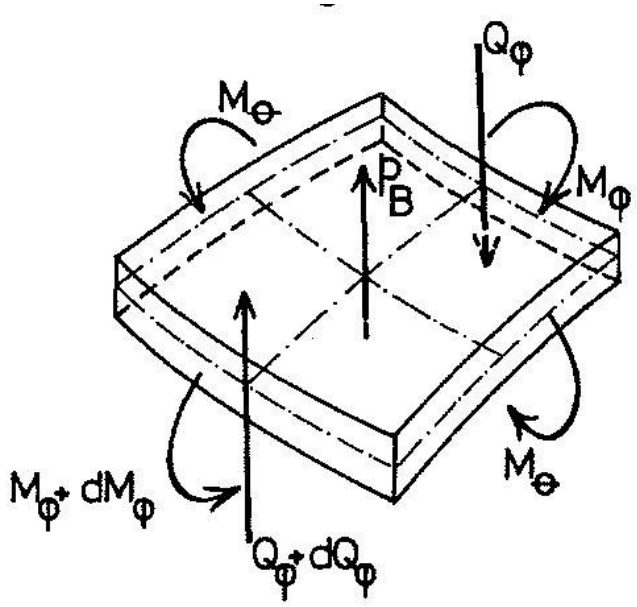

(b) Stretching

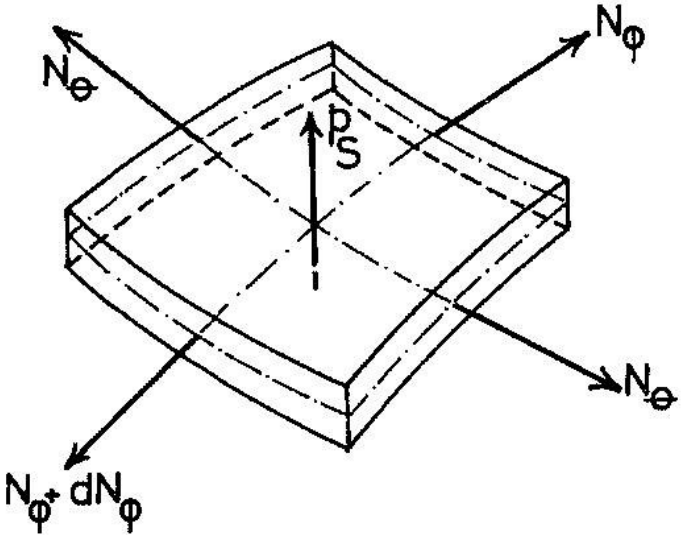

Figure 4.13: Bending (a) and stretching (b) of a thin shell, with, in the (a) case, M_φ and M_θ = meridional and hoop moments, Q_φ = out-of-plane shear force and p_b = externally applied normal force per unit surface area of the shell during bending, and, in the (b) case, N_φ and N_θ = meridional and hoop stresses and p_s = externally applied normal force per unit surface area of the shell during stretching. Image from [124].

Having also obtained the curve for different balloons confirming its reproducibility (as reported in Appendix B), it is worth noting that the TPC does not intend to mimic or model the clinical setting but rather to isolate the mechanical properties of the balloon, reducing the number of variables acting on it.

The TPC was a useful tool for understanding the effect of P_t on volume displacement. The TPC can also be read in terms of P_i, since the same variations in P_t across the IAB membrane can be induced by either changing pressure inside the balloon and keeping P_i constant or by keeping pressure inside the balloon constant and varying P_i. In fact, the latter case is a more accurate approximation of the way changes in P_t are induced across the membrane when the balloon is operated with the IABP.

The way the TPC can be read in terms of P_i is demonstrated in Figure 4.5, showing V_{up} for the 40 cc balloon: for points at low P_i (high P_t) V_{up} remained constant (~30 ml) corresponding to the TPC plateau phase, followed by a drop in V_{up} at high P_i (low P_t), corresponding to the linear part of the TPC. These observations on V_{up} refer to the horizontal case, but results showed that, when the artificial aorta was inclined, V_{up} also varied differently depending on the level of P_i. The link between changes in V_{up} and increasing P_i lies in the fact that when the balloon membrane is operating in the linear part of the TPC (bending mode) the cross-sectional area decreases at each increment in P_i, eventually reaching a point at which P_i would be so high that the P_t acting on the balloon membrane would be too low to allow its expansion (= no inflation). This relationship showing the gradual increase in balloon cross-sectional area with increasing P_t (decreasing P_i) is depicted in Figure 4.14.

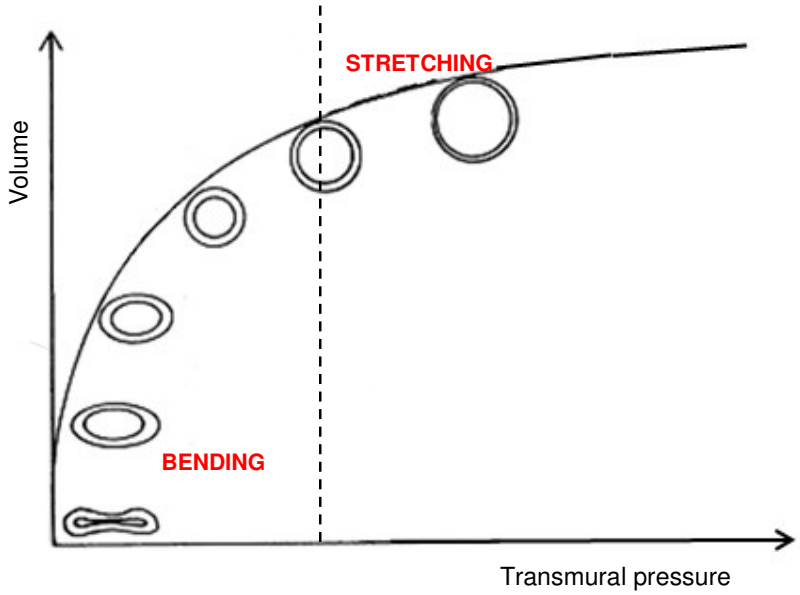

Figure 4.14: Relationship between increasing transmural pressure (P_t) and balloon volume highlighting the changes in cross-sectional area of the balloon with varying P_t. The changes in balloon cross-sectional area deriving from the balloon membrane bending (at low P_t) or stretching (at high P_t) explain the ability of the balloon to displace more or less than its total nominal volume. Image redrawn from [125].

The TPC can be further exploited to further investigate the behaviour of the balloon with varying P_t if translated in terms of stress and strain. In a typical stress-strain plot, the phase of elastic deformation corresponds to the linear part of the curve, the slope of which yields Young's modulus E. In the case of the TPC, a quantity corresponding to strain can be found in the parameter $(V-V_0)/V_0$, where V is the measured volume at any given P_t and V_0 is the initial volume of the deflated balloon. Assuming that in the experimental setting used for obtaining the TPC 10% of the nominal balloon volume remained in the folds of the membrane of a totally deflated balloon, for a 40 cc balloon V_0 = 4ml. Transmural pressure can be directly corresponded to stress. The TPC re-plotted as a stress-strain plot is shown in Figure 4.15 and two regions are clearly distinct. For the whole range of P_t shown in the 'stress-strain TPC', the

balloon membrane is expected to exhibit elastic behaviour only, since the balloon is designed for use without the need to be replaced mid-treatment due to degeneration or failure of the material. This suggests that in this case it is possible to calculate two distinct values of 'volumetric' E, above and below the knee visible in Figure 4.15. In the low P_t region E = 1.7 x 10^{-4} MPa, while in the high P_t region E = 105 x 10^{-4} MPa. The two substantially different values of E indicate that at low P_t the membrane of the balloon is much more easily deformable than at high P_t. Therefore for the same rate of change in P_t, a faster increase in volume during inflation can be expected when the balloon membrane is operating at low P_t.

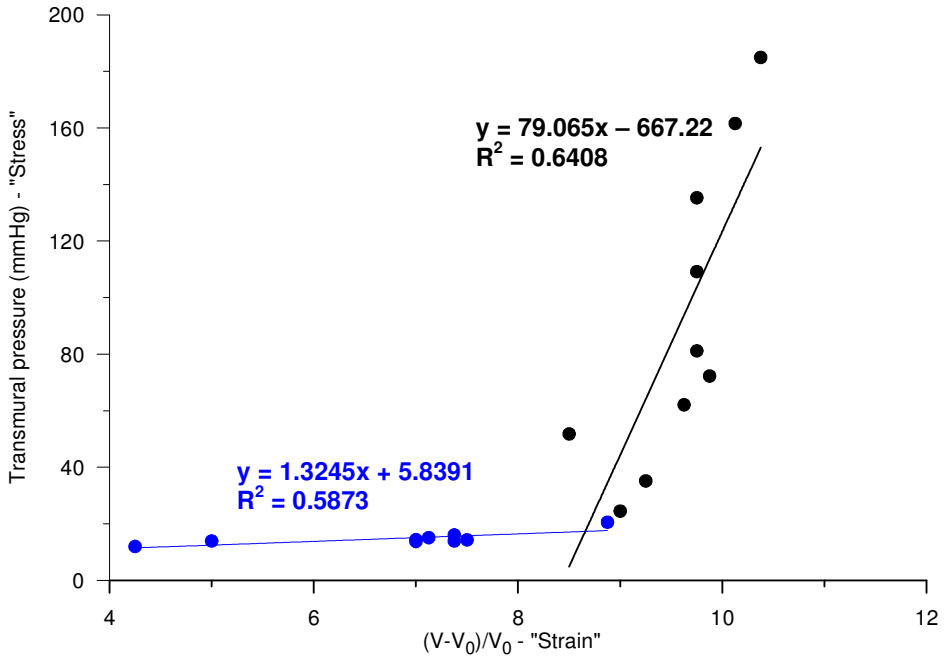

Figure 4.15: Transmural pressure (P_t) is equivalent to stress while a parameter $(V-V_0)/V_0$ is equivalent to strain, where V is balloon volume at a corresponding value of P_t and V_0 is the volume of the deflated balloon. The TPC is re-plotted in terms of stress and strain and Young's modulus (E) is calculated below and above the knee in the diagram as the slope of the stress-strain curve.

4.4.2. Dimensional analysis

The effect of increasing angle on the flow generated by the IAB can also be investigated by means of dimensional analysis. The pressure differentials required for the local acceleration, $\partial u/\partial t$, and convection, $u \cdot \partial u/\partial x$, of the fluid around the IAB in order to compensate for inertia and for the tapering of the aorta, respectively, follow from the conservation of momentum equation:

$$\frac{\partial p}{\partial x} = -\rho\left(\frac{\partial u}{\partial t} + u\frac{\partial u}{\partial x}\right) \qquad \textbf{Eq.8}$$

where ∂p = pressure difference, x = position along the axis of the IAB, ρ = fluid density, ∂u = velocity differential and t = time, assuming non-viscous flow parallel to the balloon axis.

The pressure differential needed for counterbalancing the effect of gravity induced by the angled position is:

$$\frac{\partial p}{\partial x} = -\rho g \sin\beta \qquad \textbf{Eq.9}$$

where g is the gravitational acceleration and β is the angle of the balloon with respect to the horizontal plane.

Non-dimensional ratios were calculated in order to evaluate the relative importance of each term with respect to the others, using representative values obtained from the measurements in the artificial aorta and for x = l_b = IAB length, u = u_b = IAB velocity pulse during inflation and t = t_{infl} = IAB inflation time. Thus:

$$\frac{LocalAcceleration}{Convection} \approx \frac{l_b}{t_{\inf}} \cdot \frac{1}{u_b}$$

and

$$\frac{LocalAcceleration}{Gravitational} \approx \frac{u_b}{t_{\inf}(g \sin\beta)}$$

Finally, the ratio of convection component over gravitational component can be derived as the ratio of the previous two ratios.

For example, considering the 10° position of the low P_i scenario shown earlier in Figure 4.7, given l_b = 0.26 m, in this case u_b = 0.408 m/s and t_{infl} = 0.246 s yielding:

$$\frac{LocalAcceleration}{Convection} \approx \frac{l_b}{t_{\inf}} \cdot \frac{1}{u_b} = \frac{0.26}{0.246} \cdot \frac{1}{0.408} = 2.59$$

and

$$\frac{LocalAcceleration}{Gravitational} \approx \frac{u_b}{t_{\inf}(g \sin \beta)} = \frac{0.408}{0.246 \cdot (9.81 \cdot 0.173)} = 0.98$$

which are combined:

$$\frac{LocalAcceleration}{Gravitational} \cdot \frac{1}{\frac{LocalAcceleration}{Convection}} = \frac{Convection}{Gravitational} = 0.38$$

The Local acceleration / Gravitational and Convection / Gravitational ratios are presented in Figure 4.16a and 4.16b respectively, including the examples from above.

The dominance of the gravitational element, both over the local acceleration component and the convective component, was especially pronounced at high P_i of 115 mmHg, with Local acceleration / Gravitational = 0.18 and Convection / Gravitational = 0.07 at 45°, whereas at P_i of 45 mmHg Local acceleration / Gravitational = 0.34 and Convection / Gravitational = 0.17 at 45°.

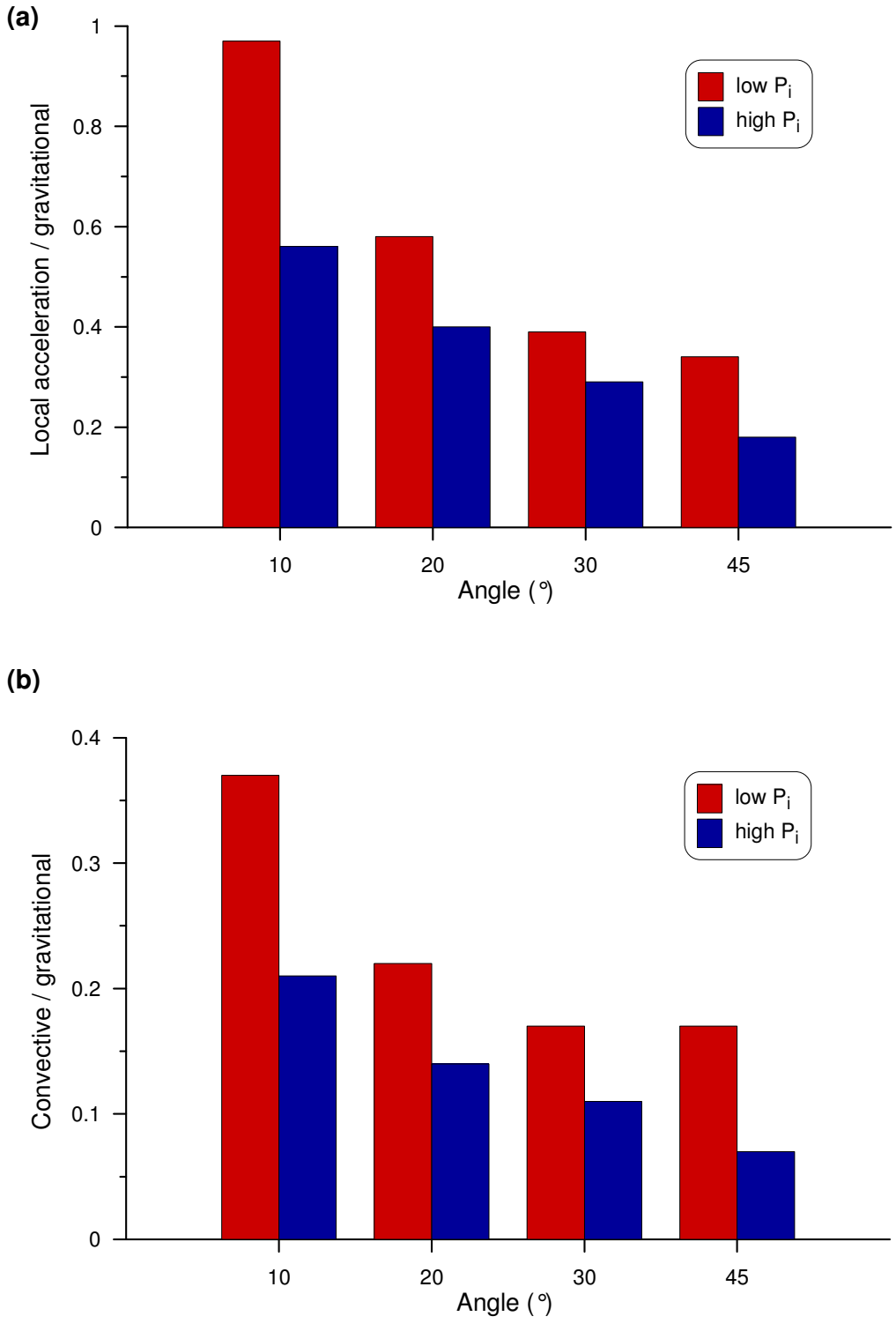

Figure 4.16: Non-dimensional ratios showing the dominance of the gravitational element in the system both over the local acceleration element (a) and over the convective acceleration element (b). In both cases, the dominance of the gravitational element is enhanced by higher intra-luminal pressure.

4.4.3. End-diastolic pressure reduction

In this study, the effect of varying P_i and of the change in P_i resulting from a change in posture was also evaluated in terms of end-diastolic pressure reduction (EDPR). In the horizontal position higher EDPR was evident at increased P_i (44.6 mmHg at P_i = 42.5 mmHg vs 111.2 mmHg at P_i = 114.9 mmHg). When increasing the angle at which the balloon is operated, EDPR was reduced, as shown in Figure 4.6. This result suggests that at least one of the major hemodynamic benefits of IAB deflation, namely the unloading action of IABP during deflation, is compromised by inclination.

Measurements in the artificial aorta were performed with the IAB pumping with no systolic flow. Therefore end-diastolic pressure reduction could not be defined with respect to the end-diastolic pressure of a non-assisted heart beat, as done in clinical studies, but only with respect to the mean pressure of the standstill conditions (Figure 4.2). This negative pulse in P_i was decreased with increasing angle. The reduction accounted for 32 mmHg at P_i = 45 mmHg and for 26 mmHg at P_i = 115 mmHg.

In this study the operation of the balloon was investigated in isolation and not simulating counterpulsation. However, it can be expected that IABP deflation would be less efficient in reducing end-diastolic pressure at an angle also when counterpulsating with a heart. This case will be simulated (and confirmed) in Chapter 7.

4.4.4. Considerations on the wave intensity results

Another significant result of this study was the identification of the waves associated with balloon inflation and deflation *in vitro* by means of wave intensity analysis. Wave intensity analysis was applied to *in vitro*

counterpulsation and the dI pattern was characterized by a compression wave (inflation wave) and an expansion wave (deflation wave). Compression waves increase the pressure in the fluid in which they propagate, while expansion waves decrease it [101, 126]. It is reasonable therefore to attribute the compression wave to the push of balloon inflation and the expansion wave to the suction generated by balloon deflation, as observed.

Regarding the direction in which such waves travel, the waves are named 'backward compression wave' (BCW) and 'backward expansion wave' (BEW) since, were a heart present, both these waves would be traveling toward the heart, in the opposite direction of blood flow from the heart.

In order to further underline the effect of varying P_i, it is important to note that the calculation of energy carried by the BCW showed a marked reduction with increasing P_i. An increment of P_i from 42.7 to 114.7 mmHg resulted in a 38% reduction in the energy carried by the BCW. At high P_i inflation of the balloon is slower, resulting in smaller changes in pressure and velocity, dP and dU. Smaller dP and dU consequently result in smaller dI from the definition of wave intensity, and as a result the energy (I) carried by the waves is also smaller. More interestingly, the change in BCW energy was remarkably similar to the drop in V_{up} observed over the same range of P_i, with a significant reduction measured at about P_i = 115 mmHg. Likewise, the calculation of the energy carried by the BEW showed an increase with increasing P_i, exhibiting a behaviour similar to that of EDPR. An increment of P_i from 42.7 to 114.7 mmHg resulted in a fifteen-fold increase in the energy carried by the BEW.

In the light of this remark, it is possible to affirm that at high P_i the balloon not only displaces less volume in a longer time, as explained with the TPC and with the negative correlation between V_{up} and duration of inflation, but also that

the BCW generated during inflation carries less energy. Furthermore, it is evident that the effect on increasing P_i is equally visible on V_{up} and BCW energy for inflation and on EDPR and BEW for deflation. The potential of WIA to assess changes during IABP counterpulsation will be further examined in Chapter 7, where the counterpulsation principle is simulated.

4.4.5. Clinical relevance

The measurements in the artificial aorta suggest that diastolic retrograde volume augmentation and end-diastolic pressure reduction might both be compromised when patients are nursed in the semi-recumbent position, as indicated by the changes in V_{up} and EDPR observed with angle. A backrest angle of 30-45^o [88, 89] can induce a reduction in both V_{up} and EDPR compared to the horizontal position, as shown in Figures 4.6 and 4.7.

The effect of P_i on IAB hemodynamic benefits can be relevant in the treatment of non-normotensive patients. Assessing the IABP benefit in terms of pressure and the unloading action associated with balloon deflation, results suggest that the benefit will be greater at higher aortic pressure, in agreement with previous studies [120, 121]. On the other hand, patient studies during counterpulsation have indicated that mean aortic pressure can be as low as 40-50 mmHg [127]. Flow results showed that, for this level of P_i, V_{up} is larger. This would suggest a degree of disagreement with the literature. However, to state this with more certainty it would be at least necessary to establish if this larger amount of V_{up} corresponds to an actual increase in coronary perfusion. Given that this data is not available, it is not accurate to state that, in disagreement with the literature, lower P_i can be beneficial in terms of coronary perfusion.

4.4.6. Methodological considerations

Pressure and flow measurements were performed at angles of 0, 10, 20, 30 and 45º. The range of operating angles up to 45º is of clinical relevance, according to the guidelines regarding nursing patients in the semi-recumbent position [88, 89]. Measurements were not performed at angles of 65 and 75º, whereas the visualisation study presented in Chapter 4 was carried out up to 75º. The results presented in Figure 5.6 and 5.7 could not be expanded to 65 and 75º because, due to the low P_i retrograde from the IAB tip, the ascending and descending aortic wall collapsed during deflation, inducing noise that affected the quality of the signals.

The aforementioned TPC (Figure 5.12) was an important tool for the understanding of the effect of variations in pressure across the balloon membrane on volume displacement. The experiment conducted for the acquisition of the TPC was not performed with the IABP, for the specific purpose of deriving results that would characterize solely the IAB. If the experiments had been conducted with the IABP, it would have been necessary to vary P_i around the balloon (hence P_t) by increasing head pressure modifying the height of a lateral water column. This would have resulted in the IABP working against a varying impedance. Also, the ease with which the balloon can inflate and deflate might act as a varying load for the IABP. Therefore, had the experiment been conducted with the IABP, it would have been difficult to deconvolute a change in displaced volume because of the change in P across the balloon membrane from a change in displaced volume because the IABP pumped less efficiently. Furthermore, varying head pressure also affects the duration of balloon inflation and deflation, as will be shown by the visualisation

study in Chapter 5 (with considerably longer inflation time corresponding to higher head). As shown in Figure 4.11, longer inflation time correlates significantly with reduced volume displaced by the balloon, hence affecting the whole purpose of the TPC.

It was not regarded as necessary to repeat the acquisition of the TPC at different angles. The same curve recorded at the horizontal position can be used when the IAB is tilted, but different membrane segments along the IAB will be having a different working point along the TPC.

4.5. Conclusion

It has been shown that variations in intra-luminal pressure affect the hemodynamics of the IAB both in terms of volume displacement in the direction of the coronary circulation and of end-diastolic pressure reduction. For a horizontal balloon, higher P_i resulted in reduced V_{up} and increased EDPR.

The changes in balloon volume displacement have been explained in the light of the relationship between changes in transmural pressure across the balloon membrane and balloon volume.

It was also shown that a change in angle, clinically corresponding to the semi-recumbent position, affects the benefits of balloon inflation and deflation. This was deduced by the reduction in V_{up} and in EDPR recorded over the range of angles 0-45º.

The dominance of the gravitational element on the flow field generated by the balloon was confirmed by dimensional analysis. The dominance of the gravitational element was further reinforced at high P_i, as indicated by the non-dimensional ratios.

Wave intensity analysis was performed and it was thus possible to identify the compression wave and the expansion wave associated with balloon inflation and deflation respectively. These pilot results will be expanded in a more complete physiological setup (Chapter 7) by simulating the principle of counterpulsation *in vitro* and obtaining a more complete wave intensity pattern. In our analysis of the effect of P_i on balloon mechanics, it was shown that the energy carried by the compression wave associated with inflation was reduced at high P_i, exhibiting a behaviour much similar to V_{up}, and the energy carried by the expansion wave associated with deflation was increased at high P_i, as in the case of EDPR.

Finally, the current results showed that high P_i may reduce coronary perfusion augmentation, but on the other hand enhance the unloading action of the balloon. Taking into account the limitations of an *in vitro* study, in order to infer the effect of P_i in clinical terms, it would be first necessary to establish whether the changes in retrograde volume displacement correspond to changes in actual coronary perfusion. On the other hand, it was shown that a balloon tilted from the horizontal with an initial intra-luminal pressure of 45 mmHg experiences a substantial reduction in retrograde volume displacement and, since such a level of mean aortic pressure has been reported for patients assisted with IABP [127], it can be suggested that in those cases a reduction in coronary perfusion augmentation could be expected.

CHAPTER 5

DURATION OF INFLATION AND DEFLATION: VISUALISATION STUDY[**]

Following from the observations on pressure and flow distribution in a latex tube (Chapter 3) further understanding on how the intra-aortic balloon works is here gained by means of a visualisation study. Variations in the duration of inflation and deflation are measured for different angles and varying initial intra-luminal pressure. Since the balloon was inserted in a glass tube for visualisation purposes, the effect of varying the compliance of the tube housing the balloon was also studied by measurements of balloon internal pressure.

5.1. Introduction

In order to investigate the mechanical behaviour of the intra-aortic balloon, distinguishing it from its hemodynamic benefit, high-speed visualisation was considered a suitable option.

Previous studies involving visualisation in the context of balloon counterpulsation mainly include:

i) Bleifeld et al. (1972): the experiments were carried out using the technique of cineroentgenographic filming in a Perspex case. Inflation and deflation of a 28 ml balloon were recorded at 80 frames/s. Results showed that balloon dynamics are dependent on pressure outside the balloon, with inflation and deflation

[**] *Partly in: G Biglino, C Kolyva, M Whitehorne, JR Pepper and AW Khir, Variations in aortic pressure affect the mechanics of the intra-aortic balloon, Artif Organs (in press)*

beginning in the part with lowest and highest hydrostatic pressure respectively [128]

ii) Khir et al. (2005): balloon inflation and deflation were filmed at 125 frames/s with a high-speed camera (Kodak, HG2000) at the horizontal and vertical positions and three intermediate angles. Results showed that inflation and deflation were uniform in the horizontal position, while at higher angles the top of the balloon inflated first and the bottom of the balloon deflated first [90].

In the light of these studies, the aim of this chapter is to gain further knowledge on the duration of balloon inflation and deflation, both in the horizontal and angled positions, using high-speed visualisation. Three different balloon shapes are included in the experiments (traditional cylindrical and novel TID and TDD designs). The focus of the visualisations study will be on the duration and pattern of inflation and deflation. It is also aimed to identify and distinguish the effect of intra-luminal pressure and angle on these parameters.

5.2. High-speed camera movies: an isolated pulse

In order to understand balloon dynamics both during the inflation and deflation phases, isolating one balloon cycle was considered the best first step. It is acknowledged that the IABP is operated continuously *in vivo* and in fact filming of the IABP running continuously was also performed (section 5.3.), however the study of one pulse is regarded as a useful for two main reasons. Firstly, this mode would allow to study deflation in full, since the deflation period would not be affected by the onset of the following inflation. Secondly, the isolated beat mode would also allow to inflate the balloon from standstill, without the "inheritance" of the previous beat and the flow perturbations resulting from

it. For these reasons, as described in the following section (4.2.1.), the assisting frequency settings of the IABP was set at 1:3, allowing sufficient time to isolate one pulsation.

5.2.1. Materials and methods

Three balloons were studied: cylindrical 40 cc in volume (Datascope), TDD design and TID design (both 36 cc in volume). All balloons were inserted in a glass tube (4 cm ID, 84 cm long) for visualisation purposes, with the centre of the balloon coinciding with the centre of the tube. The glass tube was mounted on a hinged platform allowing angle variations (0-75°) to simulate the semi-recumbent position. When angled, the balloon was hinged at the catheter side. Both extremities of the glass tube were connected via tygon lateral tubes to an overhead reservoir, providing head pressure. Three different levels of head pressure were used: low (45 mmHg), medium (80 mmHg) and high (122 mmHg).

Each balloon was inflated and deflated once from standstill. Balloons were driven by the IABP (System 98, Datascope). With the appropriate patient simulator (System trainer 90 series, Datascope) IABP settings were fixed on: assisting frequency at 1:3, maximal volume augmentation and heart rate at 60 and 100 bpm.

Visualisation was performed with a high-speed camera (X-pri, AOS Technologies, Switzerland) at 500 frames/s. Images were recorded at 600x800 pixels, with shutter time of 1675 µs. In order to increase the quality of the resolution, DC lights were used to illuminate the glass tube and the water inside the tube was frequently recycled to prevent bubble accumulation and consequent increased light reflection. All recording were stored on a PC and

later analysed frame by frame with image processing software (AOS Imaging studio, version 2.5.4.1) to determine the onset and the end of inflation and deflation. Duration of inflation and deflation was thus calculated: the duration of inflation was measured from the moment the shuttle gas enters the balloon chamber unfolding the balloon membrane with a consequent increase in diameter until the balloon is fully filled with shuttle gas, while deflation was measured from the moment the balloon starts to shrink because the shuttle gas exists the chamber with a consequent reduction in diameter until the balloon chamber is completely empty.

5.2.2. Results

5.2.2.1. Pattern of inflation

Results showed that in the case of a horizontal IAB inflation and deflation occur fairly uniformly while at an angle inflation proceeds from tip to base and deflation proceeds from base to tip. This change in pattern is in agreement with previous observations [90, 128]. Both cylindrical and tapered balloons demonstrated to the same change in pattern of inflation. The case of the 40 cc cylindrical balloon is represented in Figure 5.1, showing inflation starting in the region of lower hydrostatic pressure and moving toward the region of higher hydrostatic pressure.

t = 102 ms

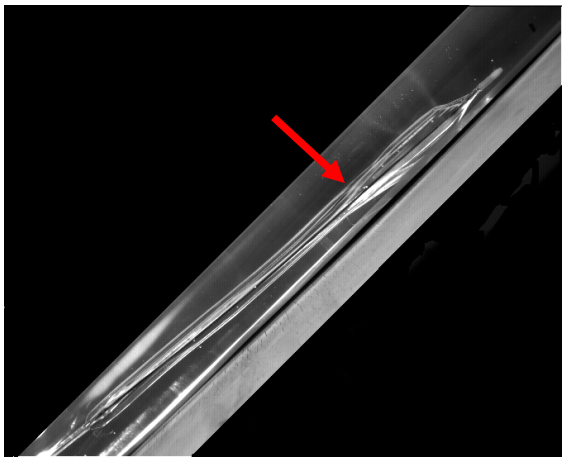

t = 158 ms

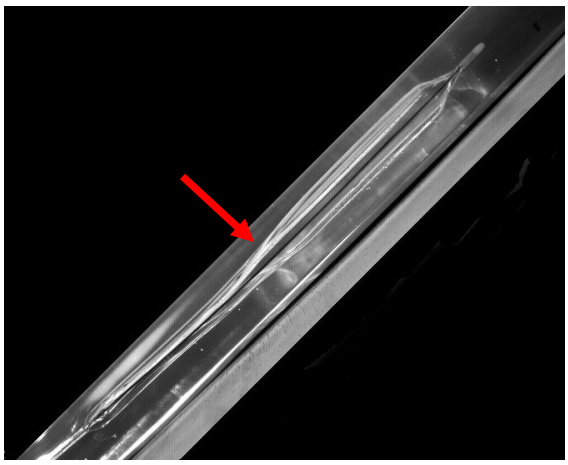

t = 230 ms

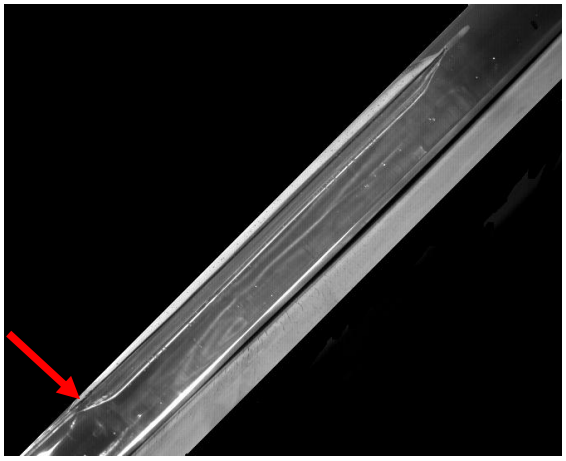

Figure 5.1: The pattern of balloon inflation from tip to base (as indicated by the red arrows) at an angle of 45°. The images illustrate the case of the cylindrical 40 cc balloon; similar pattern was observed for the TID and TDD balloons. Time from the onset of inflation (t = 0) is shown next to the corresponding frame.

5.2.2.2. The effect of angle

In the case of a horizontal balloon, results showed that increasing intra-luminal pressure (P_i) corresponds to longer duration of inflation and shorter duration of deflation. An increment in P_i of 77 mmHg corresponded to increasing the duration of inflation by 52 % (0.222 vs 0.338 s) and decreasing the duration of deflation by 12 % (0.398 vs 0.348 s). The duration of inflation for the tapered balloons exhibited similar behaviour as the cylindrical 40 cc, with increasing duration of inflation due to increased P_i. However, for the duration of deflation it was not possible to observe a common pattern between the different shapes. It appeared that increasing Pi resulted in longer duration of deflation both for the TDD and the TID shape.

A change in angle effectively also results in a change in hydrostatic pressure acting along the length of the balloon, so the effect of these two parameters on duration of inflation and deflation is entwined. The effect of angle on the duration of inflation calculated from the movies varied depending on the level of P_i (Figure 5.2a). For a 40 cc balloon, at low P_i (45 mmHg) inflation time was significantly ($p < 0.05$) extended with increasing angle, the increase accounting for 29% (0.222 at 0° vs 0.286 s at 75°), while at high P_i (122 mmHg) inflation was significantly ($p < 0.001$) decreased with increasing angle, the decrease accounting for 10% (0.338 at 0° vs 0.304 s at 65°). For the same balloon, increasing angle overall resulted in longer deflation time, more significantly so for higher P_i (Figure 5.2b). At low P_i deflation was not significantly affected by increasing angle. At medium P_i deflation was significantly ($p < 0.05$) prolonged with increasing angle by 17% (0.400 at 0° vs 0.468 s at 75°) and at high P_i (122 mmHg) by 35% (0.348 at 0° vs 0.472 s at 65°, $p < 0.01$).

(a)

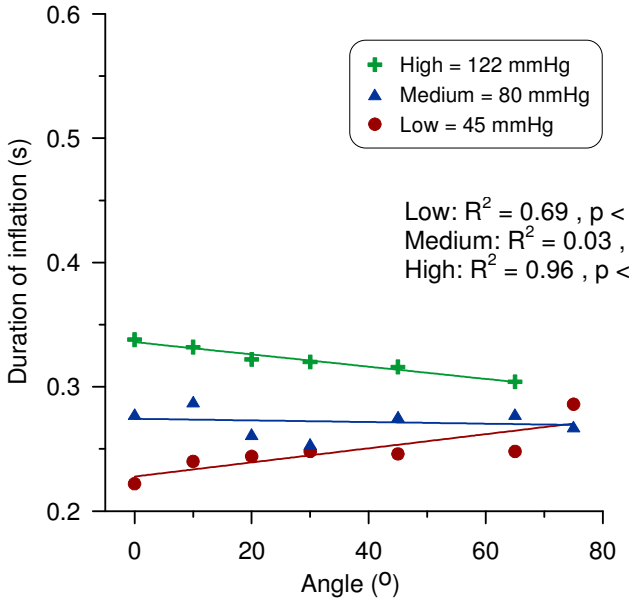

(b)

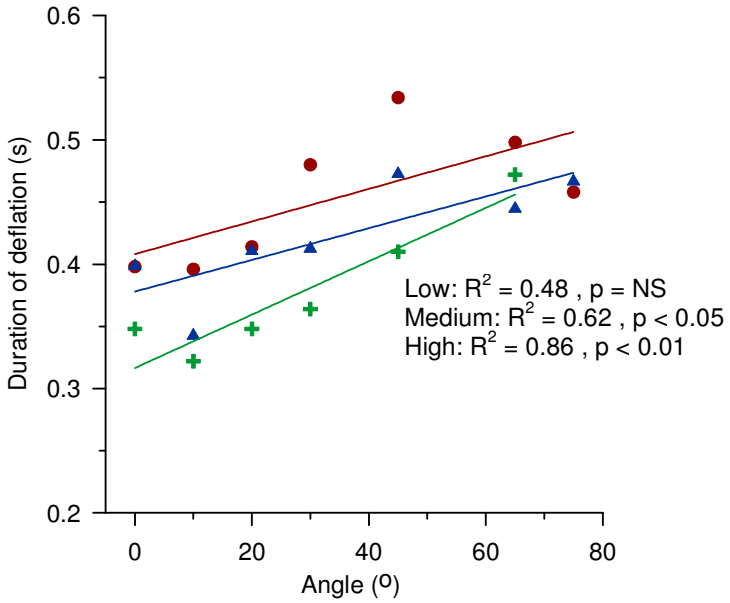

Figure 5.2: Duration of inflation (a) and deflation (b) is reported for the case of the 40 cc cylindrical balloon for low (45 mmHg, "●"), medium (80 mmHg, "▲") and high (122 mmHg, "+") levels of intra-luminal pressure, over the range of operating angles 0-75º.

Compared to the 40 cc balloon, the tapered balloons were affected differently by the change in angle, especially during inflation. An increase in angle for both the TID and the TDD result in duration of inflation either varying by a small amount or not statistically significantly affected ($p > 0.05$). Values of the duration of inflation are reported in Figure 5.3a (TID) and Figure 5.4a (TDD).

Because of corrupted quality of some recordings, duration of deflation of the tapered balloons is not reported for the case of P_i = 80 mmHg, for both the TID and TDD. The other cases are summarized in Figure 5.3b (TID) and 5.4b (TDD), showing that, especially in the case of the TID, duration of deflation was significantly increased with increasing angle.

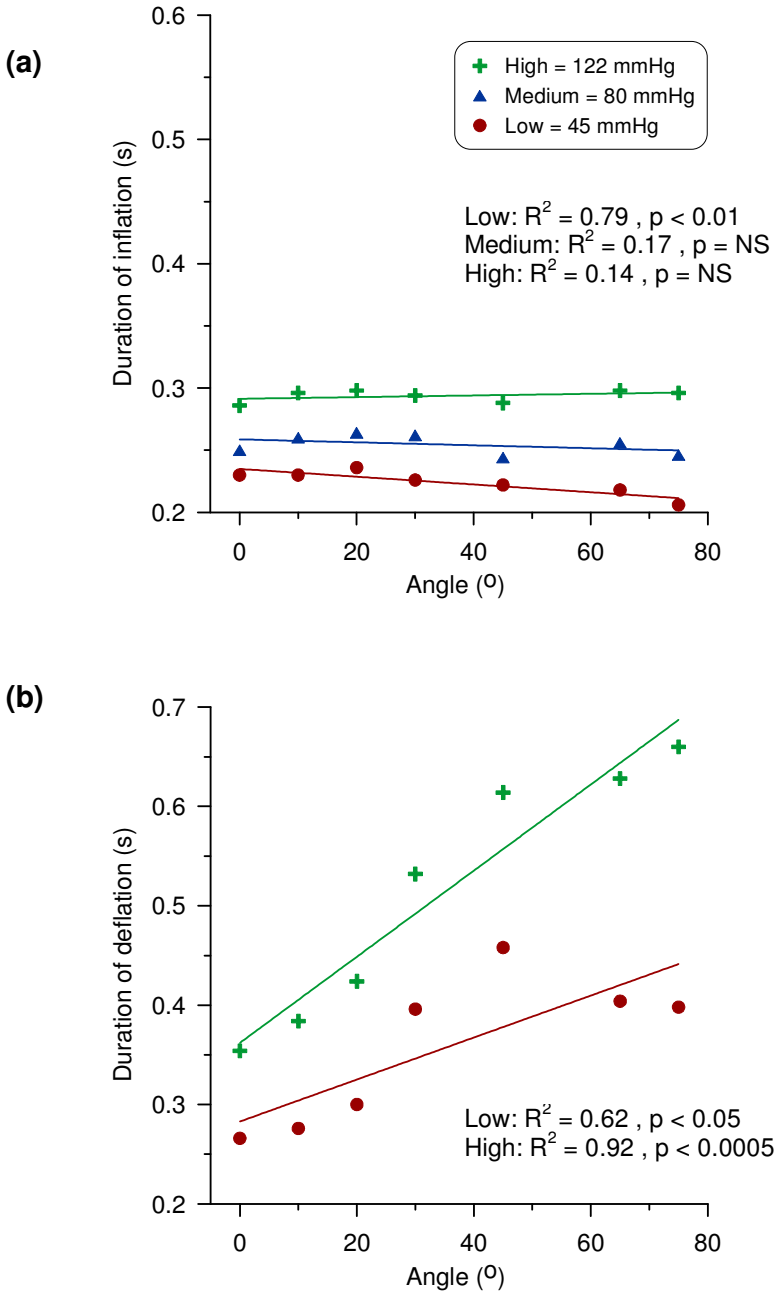

Figure 5.3: Duration of inflation (a) and deflation (b) is reported for the case of the TID balloon for low (45 mmHg, "●"), medium (80 mmHg, "▲") and high (122 mmHg, "+") levels of intra-luminal pressure, over the range of operating angles 0-75º.

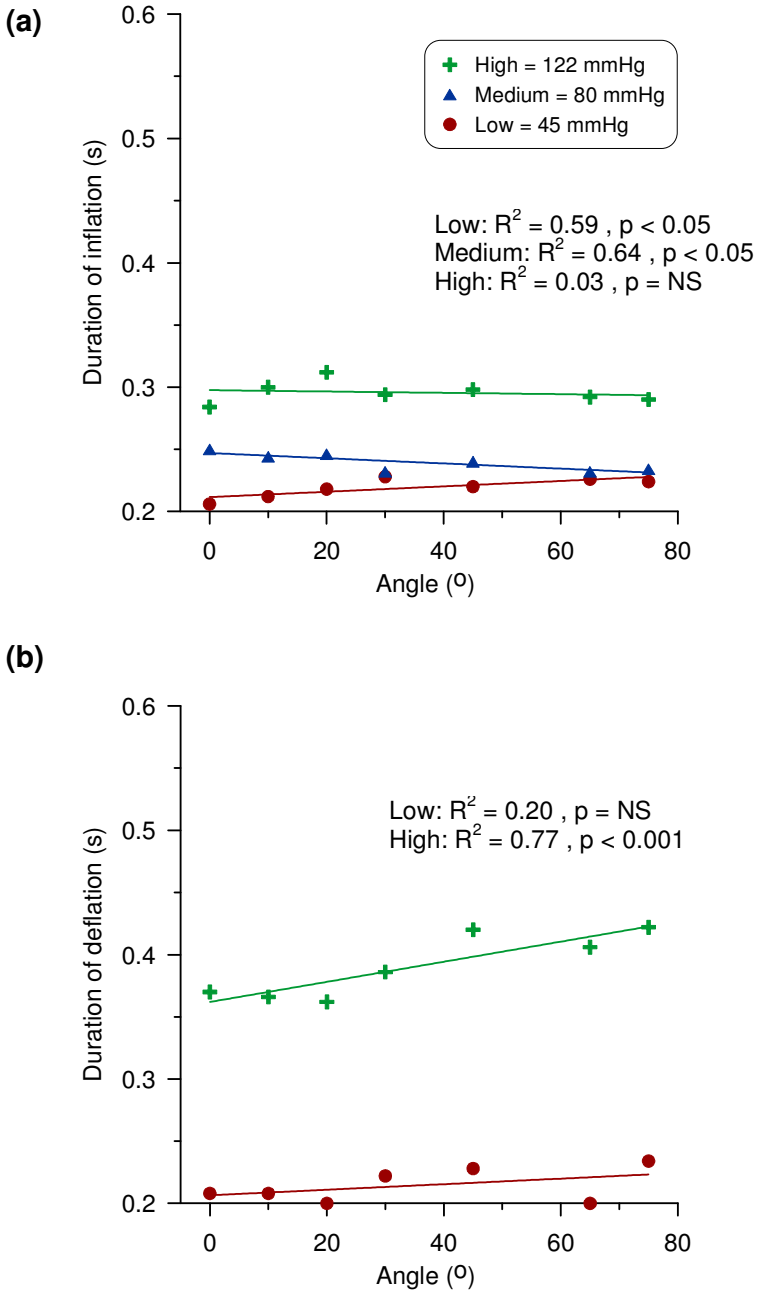

Figure 5.4: Duration of inflation (a) and deflation (b) is reported for the case of the TDD balloon for low (45 mmHg, "●"), medium (80 mmHg, "▲") and high (122 mmHg, "+") levels of intra-luminal pressure, over the range of operating angles 0-75º.

5.2.3. Discussion

It was shown that, for the case of the horizontal balloon, higher intra-luminal pressure resulted in longer duration of inflation and shorter duration of deflation. Irrespective of balloon shape, a possible qualitative explanation for this behaviour may be related to the compliance of the balloon membrane. At high P_i, it is more difficult for the balloon membrane to expand and thus for the shuttle gas to enter the balloon chamber, eventually resulting in partial or even unfeasible inflation at very high P_i levels. Visualisation has confirmed this phenomenon. The opposite is likely to be the case for the deflation phase; in fact, at high P_i, the balloon chamber is already subjected to increased surrounding pressure and hence will tend to deflate faster.

Once the balloon is tilted, in order to understand the effect of a change in angle on the pattern and duration of balloon inflation/deflation it is necessary to consider that a change in angle is intertwined with a change in P_i (hence P_t). A possible explanation of the different pattern of inflation between a horizontal and angled balloon follows.

Considering the setup used during visualisation, the balloon is placed at the centre of a rigid tube with connections of equal length to the overhead pressure reservoir (Figure 5.5):

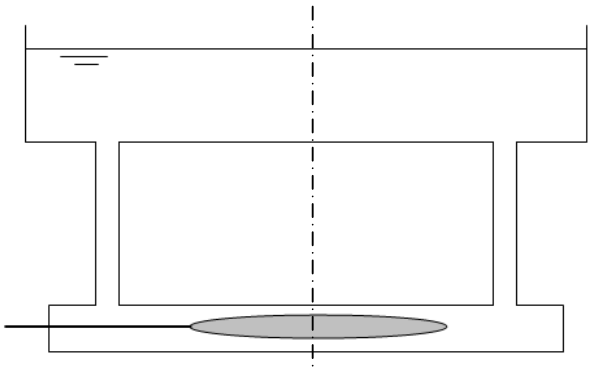

Figure 5.5: Schematic model of the setup used for visualisation.

The model can be simplified assuming one-dimensional flow and solving the problem for only half of the tube, since the system is symmetrical along the vertical axis. It is further assumed that no fluid volume can travel from the left half to the right half of the tube and vice versa. As half the setup is assumed, the balloon of the simplified model has half the volume of the original balloon. The simplified model is shown below (Figure 5.6):

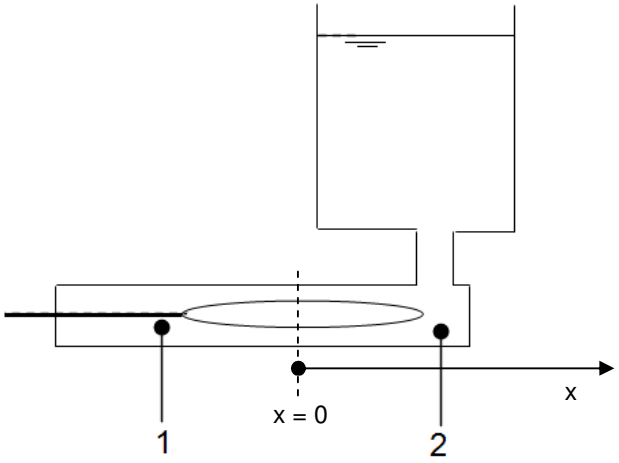

Figure 5.6: Schematic model of the simplified setup used for qualitative assessment of inflation pattern (horizontal).

Let us assume that at time t = 0 the balloon is fully deflated and therefore contains negligible. Let us also assume that the x axis coincides with the central line of the balloon, with x = 0 located in the middle of the balloon. The balloon internal pressure is P_b and it is assumed that $P_b = P_b(t)$ only, therefore P_b changes instantaneously along the length of the balloon and at any time instant it will be uniform at any x. P_b can be simplistically depicted as follows (Figure 5.7):

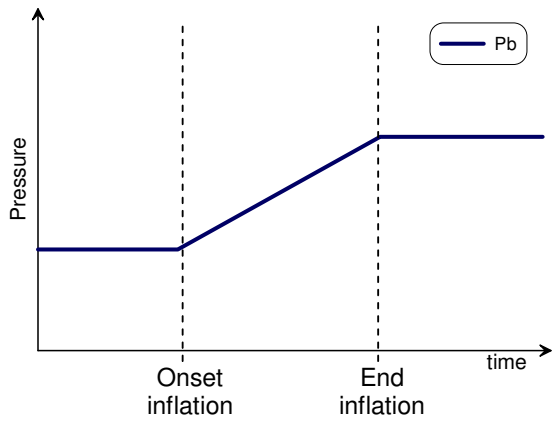

Figure 5.7: Schematic of the variation in balloon internal pressure (P_b) over the course of inflation.

Once the balloon starts inflating, its volume V_b will change with time roughly in the same way as P_b, as illustrated with the red trace in Figure 5.8. The figure also includes a schematic representation of the corresponding rate of change of balloon volume in grey $\dot{V}_b = \frac{dV_b}{dt}$.

Because the left end of the tube is closed the fluid volume displaced by the balloon during inflation has to pass through point 2. So, volumetric flow rate at this point will be $\dot{V}_2 = \dot{V}_b$. If k is the cross-sectional area of the tube at position 2, we then have $\dot{V}_2 = ku_2$ with u_2 = flow velocity at position 2. Flow velocity of the fluid at any location along the tube will be u = u(x,t).

From the equation of conservation of momentum and assuming negligible viscous effects, we have $-\frac{1}{\rho}\frac{\partial P}{\partial x} = \frac{\partial u}{\partial t} + u\frac{\partial u}{\partial x}$, where ρ is fluid density, $\frac{\partial u}{\partial t}$ is the element representing local acceleration and $u\frac{\partial u}{\partial x}$ is the element representing convective acceleration. If we assume that, in the absence of

tapering, the $\frac{\partial u}{\partial t}$ element dominates, hence $\frac{\partial u}{\partial t} >> u\frac{\partial u}{\partial x}$, then the equation of conservation of momentum can be reduced to $-\frac{\partial P}{\partial x} \approx \frac{\partial u}{\partial t}$.

Fluid pressure at position 1 (P_1) and pressure at position 2 (P_2) along the tube are represented in Figure 5.8 in a schematic way, indicative only, not based on computation, but used rather as part of the framework to understand the inflation pattern qualitatively.

In order for fluid to start moving toward position 2, high enough pressure needs to be built up at position 1, so that $P_1 > P_2$ and therefore $\frac{\partial u}{\partial t} > 0$ according to the equation above. When $\frac{\partial u}{\partial t} < 0$, i.e. flow volume will still be moving toward position 2 during inflation but at a decelerating rate, it will be $\frac{\partial P}{\partial x} < 0$, or $P_2 > P_1$. This change in sign occurs at time instant t_R, named "cross-over time", shown below.

Given that balloon inflation essentially depends on transmural pressure ($P_t = P_b - P_{liquid}$) across the balloon membrane, it is useful for the mechanistic understanding of balloon inflation pattern to consider transmural pressure at points 1 and 2, (P_b-P_1) and (P_b-P_2), respectively. As shown in Figure 5.9, before t_R, (P_b-P_2) > (P_b-P_1), while after t_R, (P_b-P_1) > (P_b-P_2).

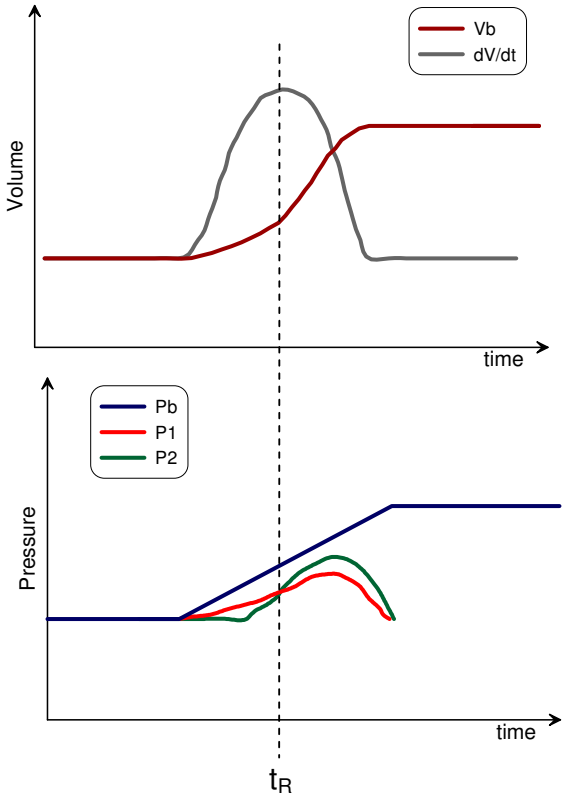

Figure 5.8: Change in balloon volume (V_b) and the corresponding dV_b/dt (top). Schematic representation of balloon internal pressure (P_b) and fluid pressure at sites 1 and site 2 as a function of time (bottom). Cross-over time (t_R) coincides with maximum dV_b/dt.

In order for fluid to start moving toward position 2, high enough pressure needs to be built up at position 1, so that $P_1 > P_2$ and therefore $\frac{\partial u}{\partial t} > 0$ according to the equation above. When $\frac{\partial u}{\partial t} < 0$, i.e. flow volume will still be moving toward position 2 during inflation but at a decelerating rate, it will be $\frac{\partial P}{\partial x} < 0$, or $P_2 > P_1$. This change in sign occurs at time instant t_R, named "cross-over time" (Figures 5.8 and 5.9).

Given that balloon inflation essentially depends on transmural pressure ($P_t = P_b - P_{liquid}$) across the balloon membrane, it is useful for the mechanistic understanding of balloon inflation pattern to consider transmural pressure at

points 1 and 2, (P_b-P_1) and (P_b-P_2), respectively. As shown in Figure 5.9, before t_R, (P_b-P_2) > (P_b-P_1), while after t_R, (P_b-P_1) > (P_b-P_2).

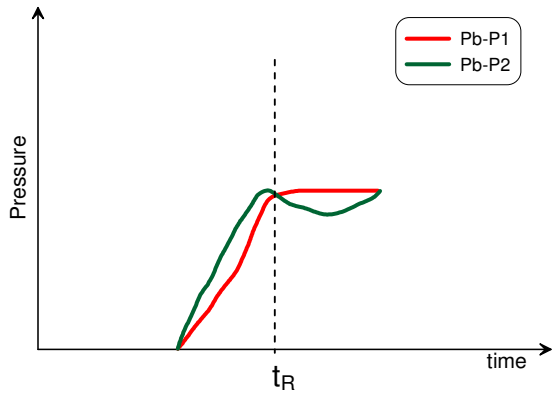

Figure 5.9: Schematic representation of balloon transmural pressure (P_b – P_{liquid}) with time, at positions 1 and 2.

When transmural pressure is higher at the position 2 , i.e. (P_b-P_2) > (P_b-P_1), the balloon will start to inflate from the right-hand side. But at t = t_R the transmural pressure at position 1 becomes larger, so there will be a second inflation wave that will travel in the other direction (from the left- toward the right-hand side). From this qualitative explanation it is possible to conclude that, even in a simple horizontal setup, the balloon does not inflate uniformly. Furthermore, it is also possible to comment on the fact that, although the balloon starts to inflate at one end and the first inflation wave travels toward position 1, it does not imply that flow is moving in that direction, since it cannot. Therefore it is not possible to infer the direction of flow in the tube simply observing the balloon.

When taking into account the case of the same setup but at an angle, it is necessary to include the hydrostatic pressure difference along the balloon in the analysis (Figure 5.10).

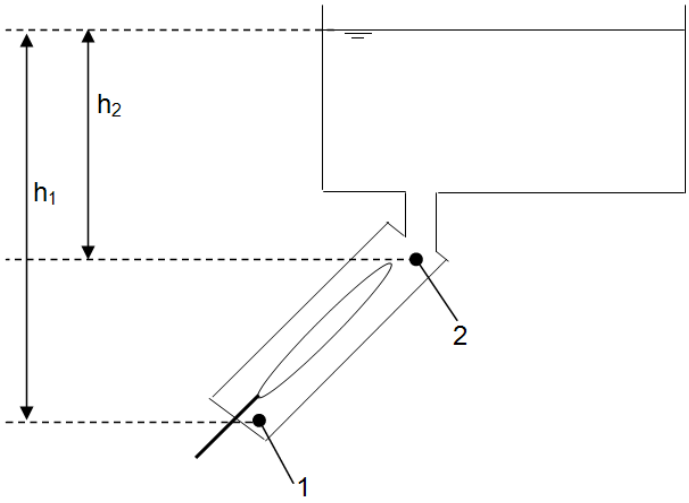

Figure 5.10: Schematic model of the simplified setup used for qualitative assessment of inflation pattern (angled).

Considering the same half of the setup as in the horizontal case, the same behaviour of P_b and of $\dot{V}_b = \dot{V}_2$ is assumed as in Figure 5.7 and 5.8. However, in the angled case the equation of conservation of momentum will take the form $-\frac{1}{\rho}\frac{\partial P}{\partial x} = \frac{\partial u}{\partial t} + u\frac{\partial u}{\partial x} + g\sin\vartheta$ and, based on the same assumptions as for the horizontal case, it can be reduced to $-\frac{\partial P}{\partial x} \approx \frac{\partial u}{\partial t} + g\sin\vartheta$. When the hydrostatic pressure difference ($\rho g h_1 - \rho g h_2$) is high enough, then, as opposed to the horizontal case, there will be no cross-over between P_1 and P_2, and consequently between (P_b-P_1) and (P_b-P_2), as shown in Figure 5.11.

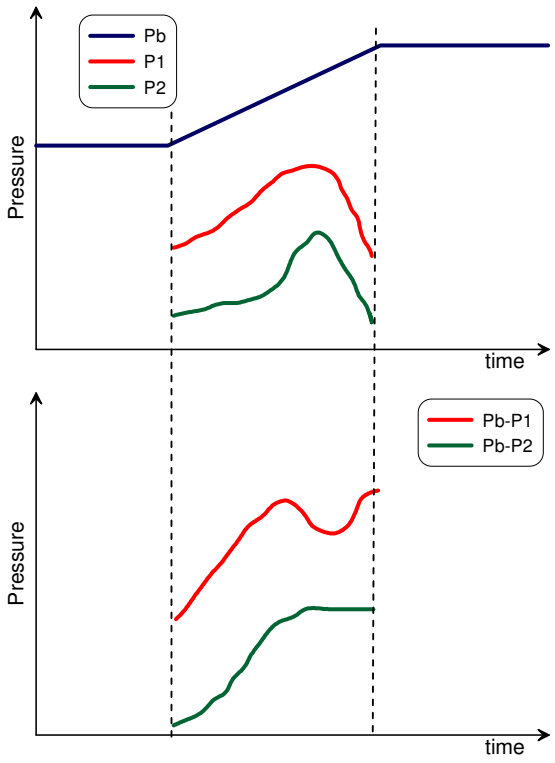

Figure 5.11: Schematic representation of balloon internal pressure (P_b), liquid pressure P in positions 1 and 2 and transmural pressure (P_b – P_{liquid}) in positions 1 and 2.).In the angled case, no cross-over time will be detected.

The absence of the cross-over implies that inflation will proceed uniformly from tip to base, confirming the observation from the high-speed visualisation experiment. In order for a cross-over to occur, there should be an inversion in the sign of pressure gradient (P_2-P_1) from negative to positive. We will investigate whether the condition $P_2 = P_1$ can ever be satisfied in the experimental setup.

Considering the pressure gradient along a fluid element of length dx and integrating along the balloon length we have:

$$-\int_1^2 \frac{\partial P}{\partial x} dx = \rho \int_1^2 \left(\frac{\partial u}{\partial t} + g \sin \vartheta \right) dx$$

resulting in:

$$-\Delta P = \rho \frac{\partial u}{\partial t} L + \rho g \sin \vartheta L = P_1 - P_2$$

where L = length from 1 to 2.

Assuming L = 0.4 m (considering that a typical 40 cc balloon is 0.28 m long), ρ = 1000 kg/m^3 and θ = 30°:

$$-\Delta P = P_1 - P_2 = \rho \cdot \frac{\partial u}{\partial t} \cdot 0.4m + \rho \cdot 0.4m \cdot 5 \frac{m}{s^2}$$

Hence, in order for at least $P_1 = P_2$:

$$\frac{\partial u}{\partial t} = -5 \frac{m}{s^2}$$

and for (P_2-P_1) < 0 it would be needed $\frac{\partial u}{\partial t} < -5 \frac{m}{s^2}$

However, considering mean $\dot{V}_2 = k u_2$ during the inflation phase:

$\dot{V}_2 = \frac{20ml}{0.25s} \approx 0.00008 \frac{m^3}{s}$ for a 20 cc balloon with inflation time of 0.25 s,

and

$k = \pi r^2 = 0.00125 m^2$, given the radius of the glass tube r = 0.02 m,

$$\therefore u_2 = \frac{\dot{V}_2}{k} \approx 0.064 \frac{m}{s}$$

and considering the deceleration phase of inflation from t_R to end of inflation (for du/dt to be ≤ -5 m/s^2), hence over a time span of approximately 0.125 s:

$$\frac{\partial u}{\partial t} = -\frac{0.064 \frac{m}{s}}{0.125s} = -0.512 \frac{m}{s^2}.$$

So $\frac{\partial u}{\partial t} >> -5 \frac{m}{s^2}$, implying that the cross-over cannot occur. This reinforces the observation that inflation of the balloon at the angled case proceeds from tip to base. From a merely qualitative point of view, it appears

unrealistic to obtain such a high deceleration in such a short time span in the simplified setup assumed or in the actual setup used for filming.

In order to explain the observations on duration of inflation deduced from the visualisation results, the behaviour of the IAB should be assessed in terms of transmural pressure. Starting from the horizontal case, a substantial difference in duration of inflation is measured depending on the intra-luminal pressure surrounding the balloon.

For the case of low P_i, referring to the TPC described in Chapter 4, the balloon is operating in the "high P_t" region of the TPC, meaning that the balloon membrane is stretching and corresponding to a volume displacement larger than balloon nominal volume. According to the law of Laplace

$$P_t = P_{in} - P_{out} = \frac{Sh}{r} \qquad \textbf{Eq.10}$$

where P_{in} = internal pressure, P_{out} = external pressure, S = hoop stress on the membrane, h = membrane thickness and r = radius. The force acting circumferentially on the membrane of a flexible tube (or in our case the balloon) can be defined:

$$F_{membrane} = ShL \qquad \textbf{Eq.11}$$

where L = the length of the tube. Hence:

$$LP_t = \frac{ShL}{r} \qquad \textbf{Eq.12}$$

and

$$F_{membrane} = LrP_t. \qquad \textbf{Eq.13}$$

Given that in the above formulation L is the same for a horizontal balloon surrounded by low or high P_i, we deduce that for the case of the balloon operated at low P_i (membrane stretching) both P_t and r will be larger, resulting

in an overall larger $F_{membrane}$. This is equivalent to say that the rate of change of momentum induced by the balloon membrane (F = d/dt M) is larger and that therefore inflation is faster.

Considering then the case of the balloon being tilted, it should be noted that the balloon will be subjected to non-uniform P_i acting on the membrane, hence non-uniform P_t. Compared to the horizontal case and assuming (as is the case for semi-recumbent position analogy) that the balloon is hinged at the base or at any rate at the catheter, the tip of the balloon is subjected to higher P_t.

If the balloon was tilted from an initial condition of low P_i, the further reduction in P_i resulting from increasing angle would correspond to moving more in the "high P_t" region of the TPC. Because the balloon was already operating in the stretching region, this change does not result in a further increase in balloon volume. It has been shown, earlier in this chapter, that when the balloon is angled inflation proceeds gradually from the tip towards the base. Assuming that the balloon chamber consists of a number of equally-sized segments, theoretically, this process (inflation wave propagating from tip to base) can be visualised as the sequential inflation of one segment after the other starting from the tip. This process results in:

(1) the segments are inflated faster in the tip region and slower in the base region, so the velocity of the inflation wave is decreasing from tip to base; this is due to the fact that P_t is larger at the tip and hence the $F_{membrane}$ is larger (r and L being the same for all segments of the stretched balloon)

(2) in the horizontal position, P_t acts uniformly throughout the membrane as all balloon segments are expanded simultaneously by the shuttle gas.

However, at an angle P_t acts membrane-segment after membrane-segment as shuttle gas gradually fills the chamber from tip to base. Therefore $F_{membrane}$ can be built up uniformly for all segments in the horizontal case and progressively, segment by segment, at an angle. This suggests that the $F_{membrane}$ at an angle is lower than that generated horizontally and resulting in smaller rate of change of momentum (F = d/dt M), i.e. longer inflation.

If the balloon instead was tilted starting from high P_i, because of the reduction in P_i associated with increasing angle it is likely that part of the balloon would operate in the high P_t region of the TPC, instead of the low P_t. These segments of the balloon, located at the tip, where inflation is initiated, would now be able to stretch. The increase in r resulting from part of the membrane stretching and the increase in P_t resulting from the reduction in P_i in the tip region suggest that the tilted balloon would be able to generated a larger $F_{membrane}$ and inflate faster than the corresponding horizontal case. A further increase in angle would enhance the phenomenon, because more segments of the membrane would be stretching, confirming the decreasing trend of duration of inflation observed for the balloon operated at high P_i.

In synthesis, four scenarios can be highlighted, as shown in Figure 5.12.

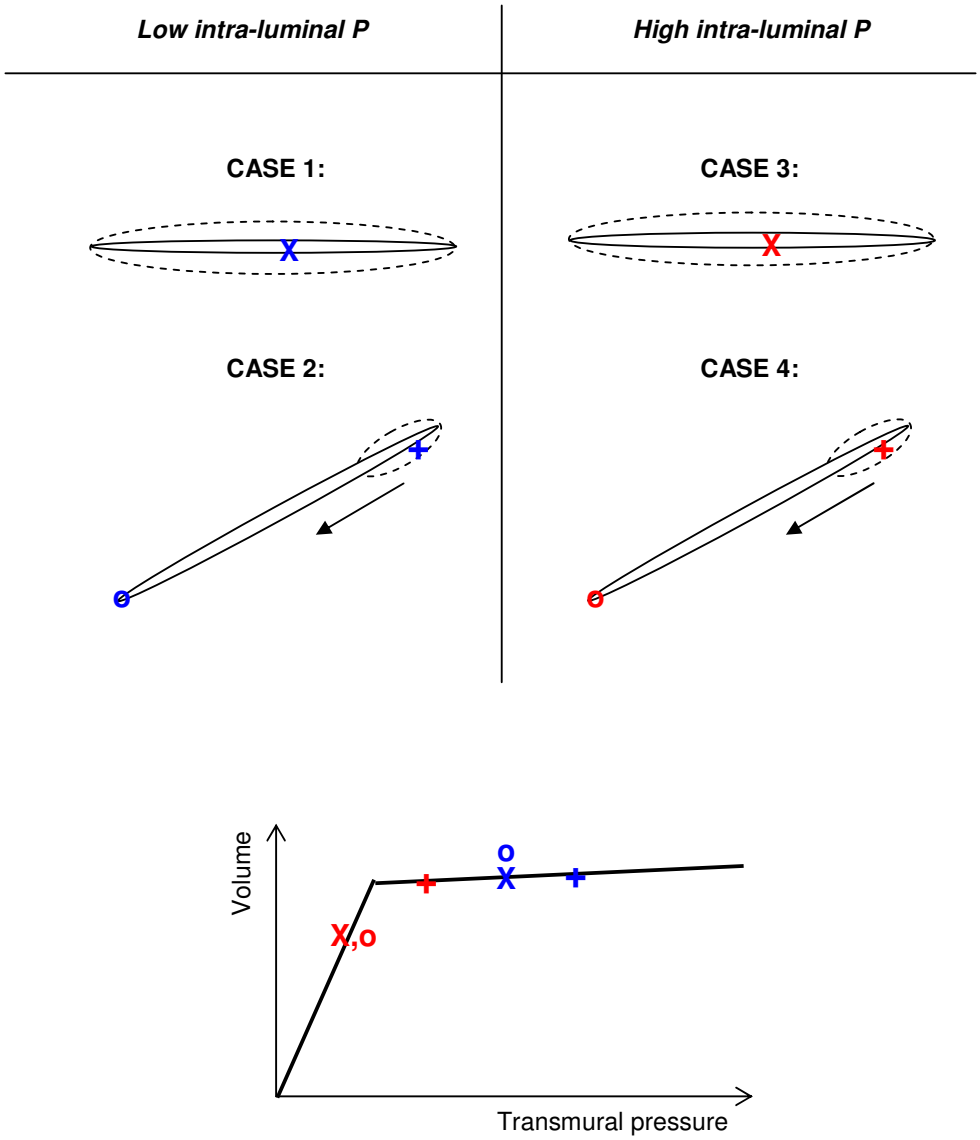

Figure 5.12: Balloons at different levels of intra-luminal pressure, horizontal and tilted, and the corresponding operating point on the transmural pressure – volume curve. For the tilted case, because inflation proceeds gradually tip-to-base, the tip and the base of the balloon membrane experience different transmural pressure.

5.3. High-speed camera movies: continuous pumping

The previous experiment shed light on both the effect of varying intra-luminal pressure and increasing angle on the pattern and the duration of balloon inflation/deflation. The choice of isolating one beat, operating the IABP at assisting frequency of 1:3, allowed full analysis of the inflation and the deflation

phases. However, producing one balloon pulse is an unrealistic scenario – albeit useful in the investigation of the mechanical behaviour of the balloon alone – since the IABP is pumping continuously in the clinical setting. The effect of tilting was therefore studied also with the IABP set on continuous assistance at 1:1 for all balloon shapes. Having identified already the effect of intra-luminal pressure, visualisation was carried out at one level of head pressure (intermediate head pressure, 80 mmHg).

5.3.1. Materials and methods

The experimental setup was the same as that described in section 4.2.1. The same balloons (cylindrical 40 cc, TDD, TID) were tested. The IABP was set on maximal volume augmentation, heart rate of 60 and 100 bpm and assisting frequency of 1:1. Images were acquired again at 500 frames/s.

In terms of image processing, one balloon cycle was selected from the recording sequence during analysis. The duration of inflation was calculated with frame by frame analysis. Because the IABP was operated at 1:1, the duration of deflation was not calculated in this case. Since the following inflation is automatically triggered by the IABP and not when deflation is completed, the balloon might not be able to deflate freely as in the case of an isolated pulse.

5.3.2. Results

An increase in angle of 75° resulted in extended duration of inflation, as shown in Figure 5.13. The cylindrical 40 cc balloon and the TDD exhibited significantly ($p < 0.005$) longer inflation, by 35% (0.196 at 0° vs 0.266 s at 75°) and 33% (0.185 at 0° vs 0.246 s at 75°) respectively. For the TID balloon, a

much more considerable increase of +281% was recorded (0.107 at 0° vs 0.408 s at 75°, $p < 0.005$).

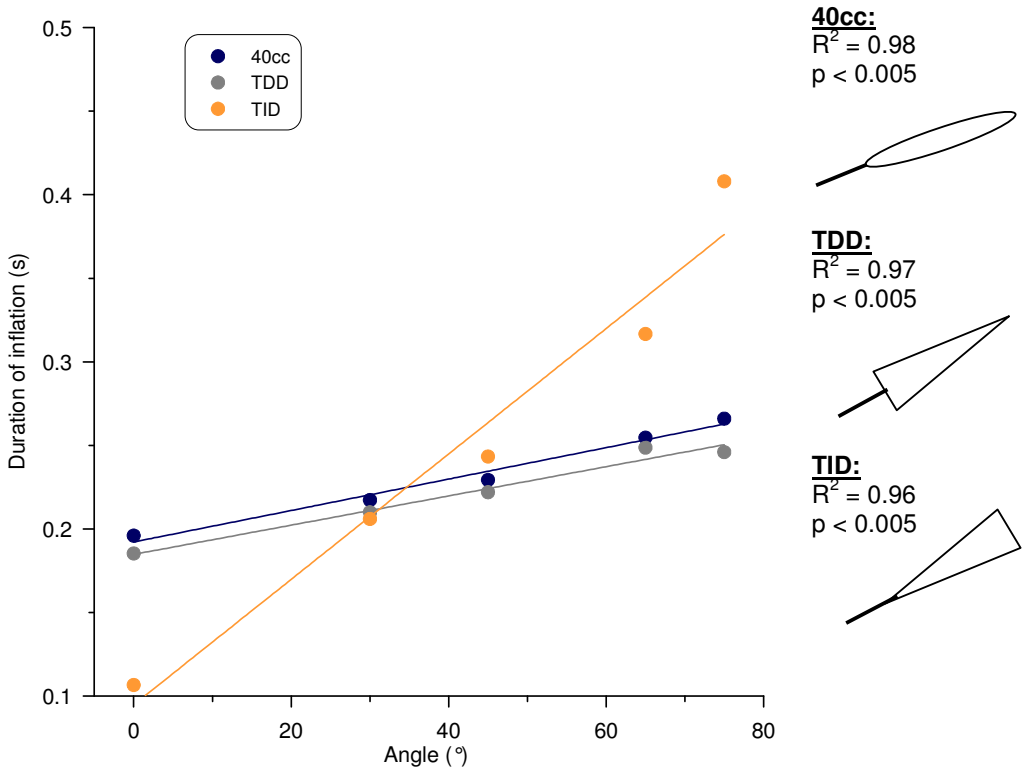

Figure 5.13: The effect of increasing angle on the duration of inflation of a cylindrical 40 cc balloon (blue full circles), a TDD (grey full circles) and a TID (orange full circles) balloon, with the IABP operated at 1:1 continuous assistance. For all cases, the duration of inflation was significantly increased with increasing angle.

5.3.3. Discussion

Comparing the results of the visualisation study performed at assisting frequency 1:1 with those at assisting frequency 1:3 for the same head pressure (80 mmHg) showed that the balloon is affected by assisting frequency in terms of duration of inflation. At 1:1, all tested shapes (cylindrical, TDD, TID) exhibited a statistically significant ($p < 0.005$) increase in inflation time with increasing angle. On the contrary, at 1:3 the duration of inflation was less affected over the

range of angles for all shapes. In order to investigate this difference, tracings of $P_{shuttle}$ have been compared (Figure 5.14). From this comparison it is clear that, both at the horizontal position (Figure 5.14a) and at an angle of 45° (Figure 5.14b) the balloon is not operated exactly in the same way. While the rapid initial stage of inflation and deflation appears to be unaffected, late inflation and late deflation exhibit a difference due to the change in assisting frequency. As reported in the reproducibility test in Chapter 2 (section 2.3.), $P_{shuttle}$ is a highly reproducible signal, therefore the differences reported in Figure 4.10 are considered to be of significance. Information on timing is obtained from the analysis of the movies by observing the changes of the balloon chamber over the time cycle and the end of inflation is assumed to be the frame when the balloon chamber is fully rounded. This is expected to happen at a specific transmural pressure across the balloon membrane. The pressure surrounding the balloon was the same for the tests at different assisting frequencies. However, analysis of the $P_{shuttle}$ signal shows that the same value of $P_{shuttle}$ in late inflation is reached at a different time, for example: in the horizontal case (Figure 4.10a) a value of $P_{shuttle}$ of 143 mmHg is reached 50 ms later at 1:3 assisting frequency with respect to 1:1 (20.188 s vs 20.138 s). When operated at 1:1, the continuous inflation/deflation of the balloon reduces the inertial behaviour of the system as compared to the case of an isolated pulsation from standstill (1:3). For this reason, inflation can occur more rapidly at 1:1, because the surrounding fluid effectively is already in motion, hence presenting less opposition to the opening of the balloon. This difference between assisting frequencies is further considered in the context of measurements in a mock circulatory system (page 187).

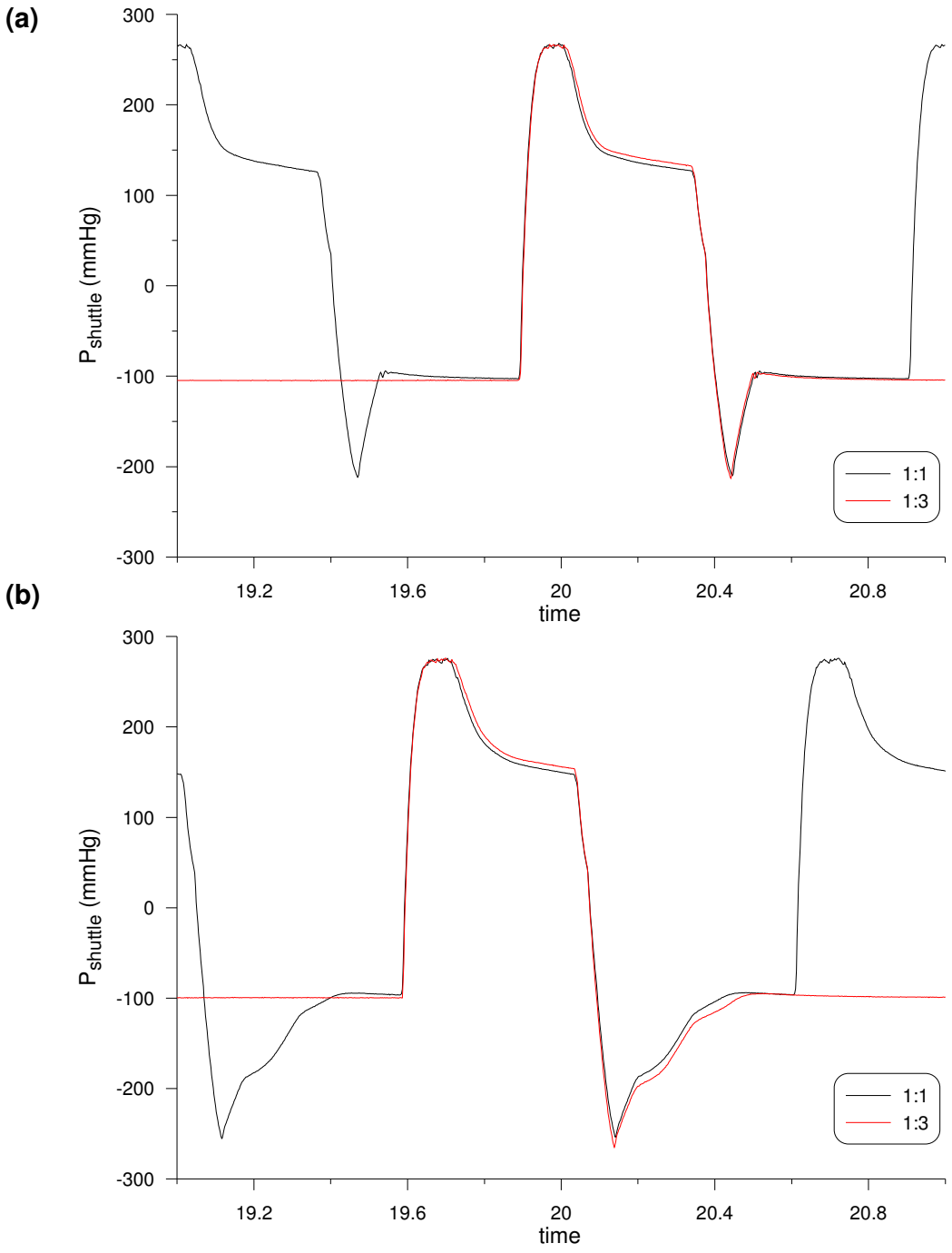

Figure 5.14: The different behaviour of a 40 cc balloon operated continuously at assisting frequency 1:1 and by isolating one pulse at assisting frequency 1:3, as observed from shuttle gas pressure, $P_{shuttle}$, tracings, both at the horizontal position (a) and at a 45º angle (b).

Results of visualisation with the IABP set to 1:1 assistance also showed a marked difference between balloons of different shape in terms of duration of inflation. In fact, the TID was dramatically affected by the change in posture, up to an increase of 281% at 75°. These results suggest clearly that the TID design, albeit in the horizontal setting inflating faster than the traditional cylindrical 40 cc balloon by 45% (0.107 vs 0.196 s), is severely affected by a change in angle. This increase in the duration of inflation can viewed in terms of changes in momentum. Given the relationship between radius and force (Eq.13) when the balloon is tilted and inflation proceeds from tip to base along subsequent membrane segments, the radius of the TID is drastically reduced compared to the tip region and this results in smaller d/dt(M) (longer inflation).

From these observations it is possible to conclude that, when operated continuously as in the clinical setting, the balloon will take longer to inflate at an angle (semi-recumbent position). However, the visualisation study focused on the mechanical behaviour of the balloon itself and did not model correctly the compliance of the aortic wall. In fact, because of the opacity of the walls, latex or silicone tubes were not regarded as suitable test bed for the visualisation study. Therefore, although the qualitative results about the effect of varying assisting frequency and/or intra-luminal pressure and/or angle on the duration of inflation and deflation are meaningful, their clinical relevance should be stated cautiously.

5.4. The effect of compliance

Following from the previous section, the visualisation experiments were carried in a glass tube because the opacity of the walls of a latex or silicone tube would render visualisation and analysis very difficult. However, as

indicated by the literature [14, 25, 73], compliance is a major factor affecting IABP counterpulsation. So, in order to understand the role played by compliance in these measurements, tests were performed in a glass tube and in a silicone tube measuring both balloon shuttle gas and internal pressure, accessing the balloon chamber with a pressure wire. This aimed to identify the difference induced by a more compliant setup on the balloon and to provide insight in the pressure changes inside the balloon chamber throughout the balloon cycle, which have not been reported in the literature before.

5.4.1. Materials and methods

A 40 cc balloon (Datascope) was tested inside a glass tube and a silicone tube[††] of equal dimensions (40 cm long, 4 cm ID). Both tubes were filled with water and connected, by means of lateral tygon tubes of equal length, to a overhead reservoir providing head pressure. An isolated pulse was generated at 1:3 assisting frequency, maximal volume augmentation and 60 bpm heart rate. Balloon pressure was measured at two locations: at the balloon catheter and inside the balloon chamber (Figure 5.15). Catheter pressure $P_{shuttle}$ was measured with a 5F transducer-tipped catheter (Gaeltec), positioned just before the balloon catheter. By means of a three-way connection, a pressure wire (Radi Medical Systems AB, Uppsala, Sweden) was inserted in the balloon catheter and pushed along the catheter until positioned inside the balloon chamber. A third catheter (Gaeltec) monitored pressure in the liquid surrounding the balloon. All sensors were calibrated after the measurements with the

[††] A silicone tube was chosen in order to provide a substantial variation in compliance with respect to the glass tube, not necessarily replicating a physiological environment. Unpublished data from a tensile strength experiment carried out within the Biofluid Mechanics group of Brunel University showed that Young's modulus (E) was E = 2.0 MPa for the silicone tube and E = 0.72 MPa for an aortic specimen.

methods of the column of water. Data was collected at 500 Hz in Labview and later analysed in MatLab.

The Radi equipment suffered from poor digital discrimination, as will be visible in the Results, with a coarser tracing compared to the Gaeltec equipment. Also, the same Gaeltec catheter and Radi wire used during the measurements were compared in a simple setup where suction was produced in a small, sealed Perspex tube by means of a syringe, with each pressure sensor measuring subsequently the pressure inside the tube. As shown in Figure 5.16, the Radi wire could not measure below – 57 mmHg, as opposed to the Gaeltec catheter, which could record throughout the suction phase without any threshold. Despite these limitations, it is important to have gained insight into the internal behaviour of the balloon. The possibility of commenting – at least qualitatively – on $P_{internal}$ was outweighing the technical constraints.

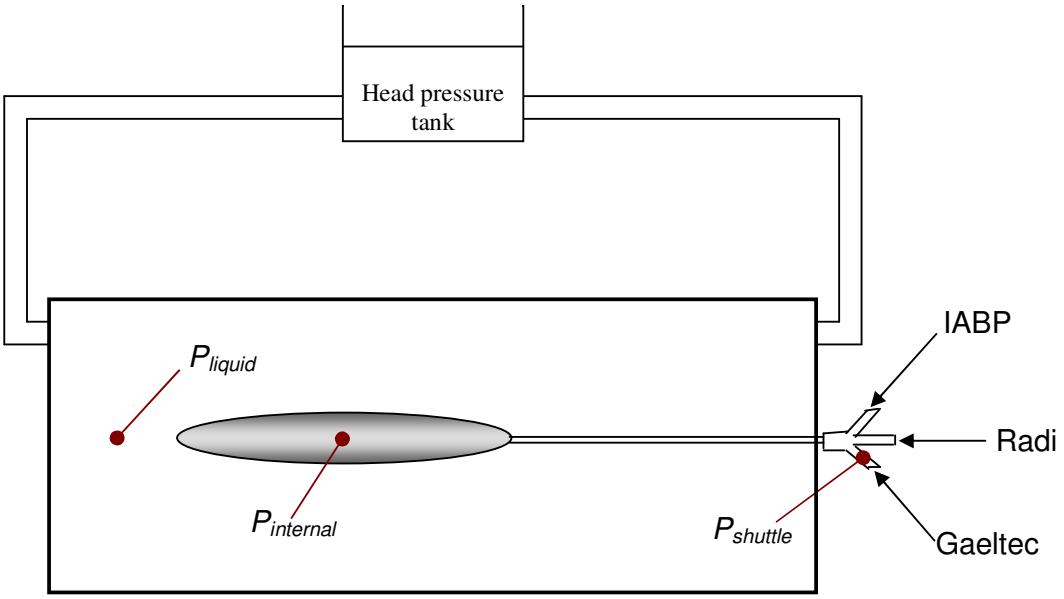

Figure 5.15: The black arrows indicate the insertion of the Radi and Gaeltec pressure catheters via the three-way connection, which is also attached to the IABP. The red closed circles indicate the measuring sites of catheter pressure ($P_{shuttle}$) and liquid pressure (P_{liquid}) acquired with the Gaeltec catheters, and balloon internal pressure ($P_{internal}$) acquired with the Radi pressure wire.

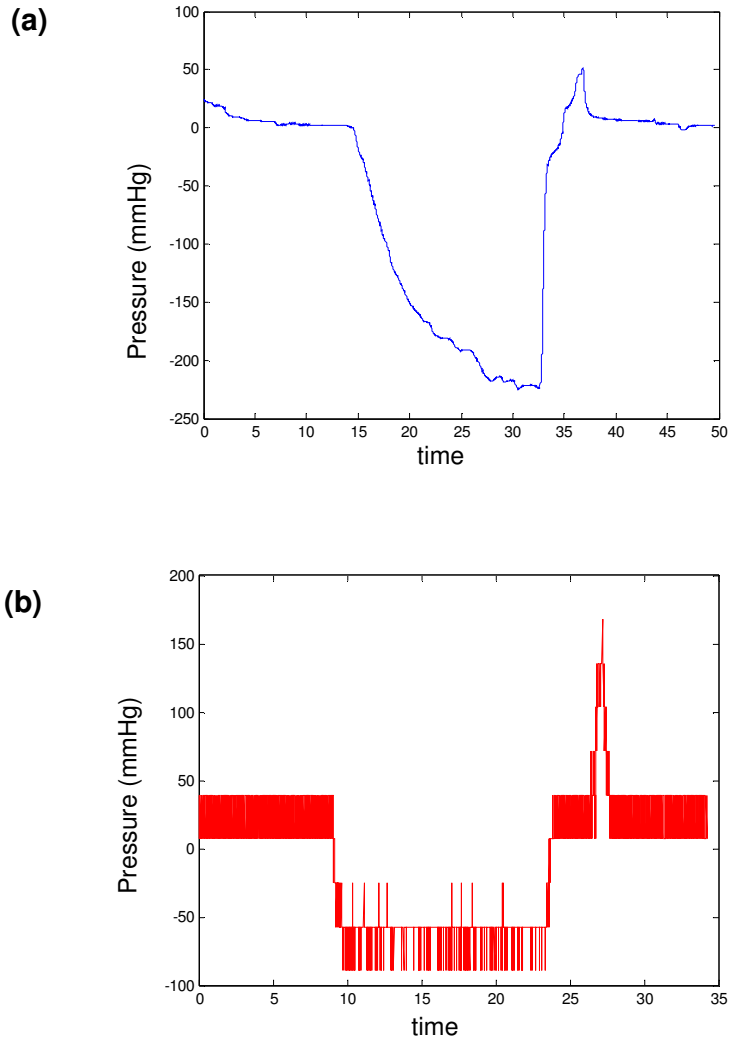

Figure 5.16: Measurements of negative pressre, induced by suction, comparing the Gaeltec catheter (a) and the Radi wire (b), showing the inability of the Radi wire to read below – 57 mmHg, as opposed to the Gaeltec catheter. The two measurements were not simultaneous.

5.4.2. Results

Comparison of $P_{internal}$ and $P_{shuttle}$ highlighted the difference between operating the balloon inside a glass tube and inside a silicone tube.

Comparing glass and silicone using $P_{shuttle}$ (Figure 5.17) and $P_{internal}$ (Figure 5.17), the major features are:

- $P_{shuttle}$: during late inflation, and up to the onset of deflation, when operating the balloon in glass $P_{shuttle}$ exhibits an oscillatory behaviour, whereas in silicone it does not; the same recordings in glass and silicone also do not coincide in late deflation.
- $P_{internal}$: despite the poor quality of the Radi signal it is possible to observe that, when operating the balloon in glass, $P_{internal}$ also exhibits an oscillatory behaviour during late inflation up to the onset of deflation; even more interestingly, it is possible to identify a large increase in $P_{internal}$ (up to 350 mmHg) at the end of deflation, only when operating the balloon in glass, whereas this spike is not visible when operating the balloon in silicone.

Plotting $P_{shuttle}$ and $P_{internal}$ together depending on the compliance of the tube (Figure 5.18), it is interesting to observe the substantial augmentation in $P_{internal}$ recorded inside the balloon. This is not only absent from the $P_{internal}$ tracing for the case of the silicone tube, but also not visible on the $P_{shuttle}$ signal of the same glass tube measurement.

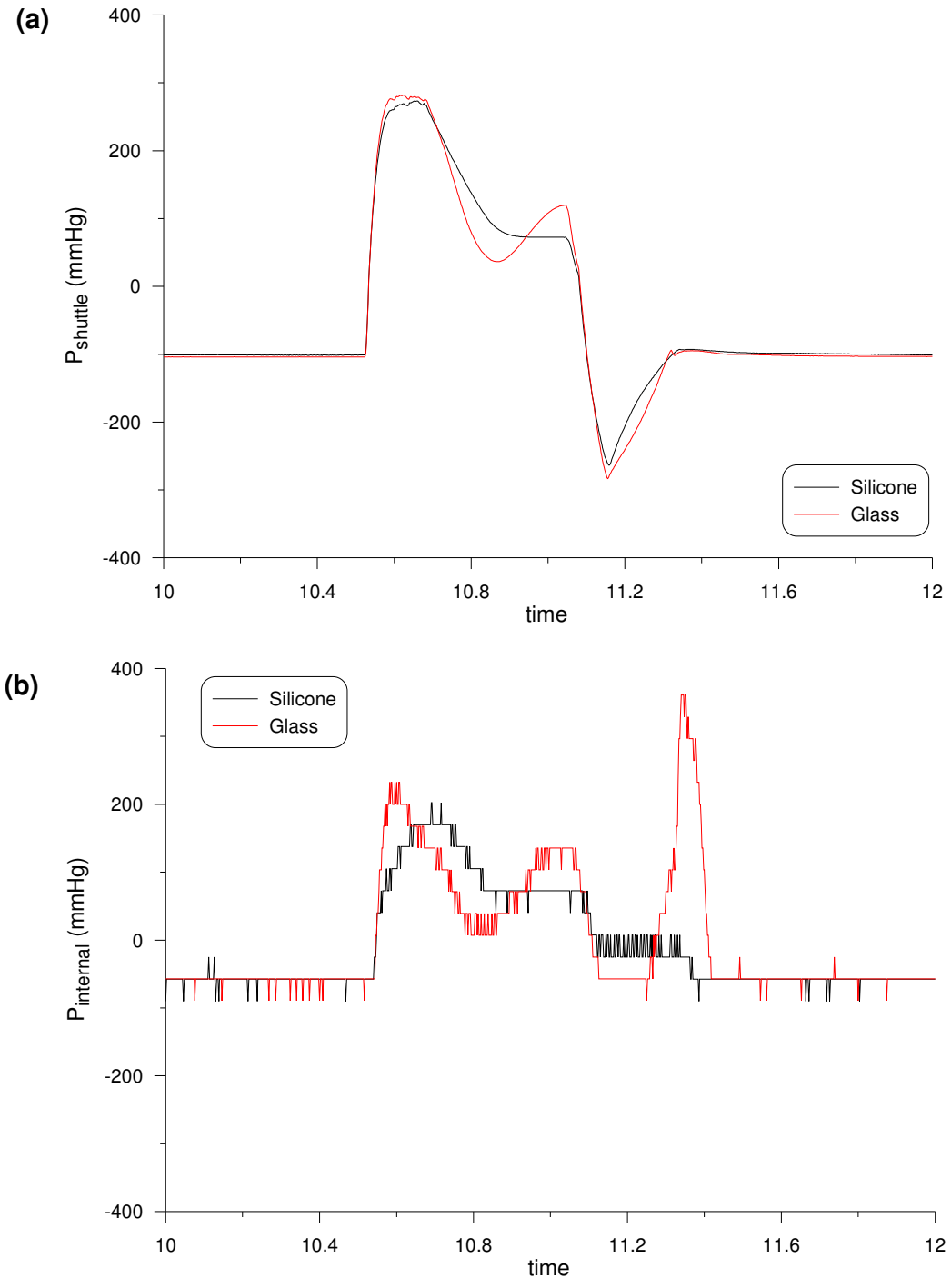

Figure 5.17: Measurements of shuttle gas pressure, $P_{shuttle}$ (a) and balloon internal pressure, $P_{internal}$ (b) with the balloon operated both in a glass and in a silicone tube.

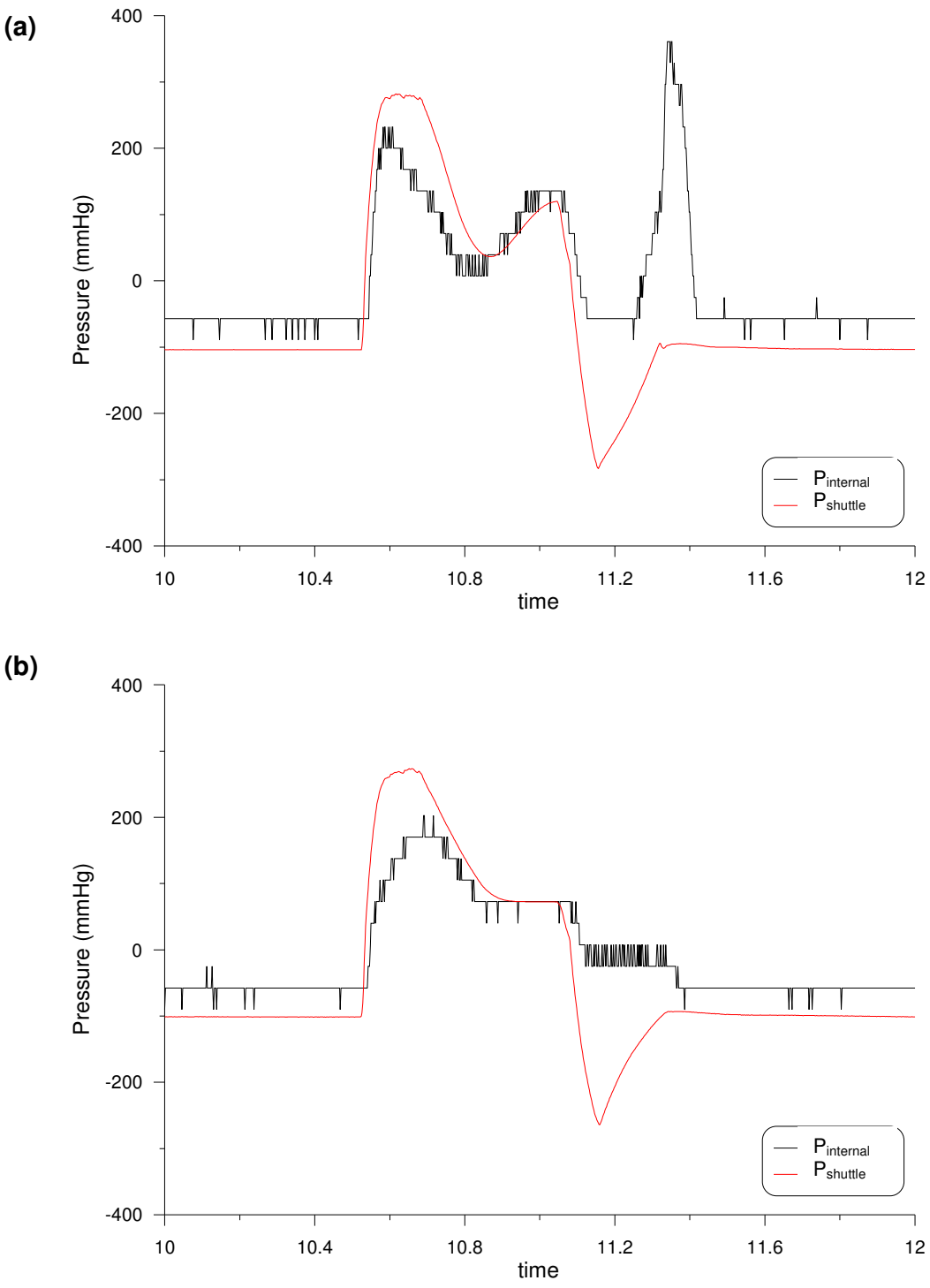

Figure 5.18: Comparison of shuttle gas pressure measured with the Gaeltec catheter and balloon internal pressure measured with the Radi wire. The balloon is operated in a glass tube (a) and in a silicone tube (b).

5.4.3. The "stopping shock" phenomenon

The results presented above highlighted the difference induced by the compliance of the test bed on the mechanics of the balloon. The main differences resulting from a drastic change in compliance were the fluctuations in both $P_{shuttle}$ and $P_{internal}$ recorded in glass during late inflation and the large increase in $P_{internal}$ at the end of deflation again for the case of the glass tube.

Measurements of balloon internal pressure are not reported in the literature about IABP and confirmed (and reinforced) the information obtained via $P_{shuttle}$. It also highlighted the presence of the increase in pressure at the end of deflation which otherwise would have not been observed.

When operating the balloon in a glass tube, a major increase in $P_{internal}$ was recorded with the Radi wire at the end of deflation (Figure 5.17b and Figure 5.18a). This was not recorded either when operating the balloon in a silicone tube or by measuring $P_{shuttle}$ at the balloon catheter with the balloon inside the glass tube. Also, measuring the pressure of the liquid surrounding the balloon, a similar increase was measured in the glass tube, as shown in Figure 5.19. Furthermore, by manipulating the onset of balloon deflation with the appropriate slide commands on the IABP, delaying and preceding deflation by 80 ms, it was clear that this increase was timed with the end of deflation, taking place always about 200 ms after the onset of deflation. This is also shown in Figure 5.19.

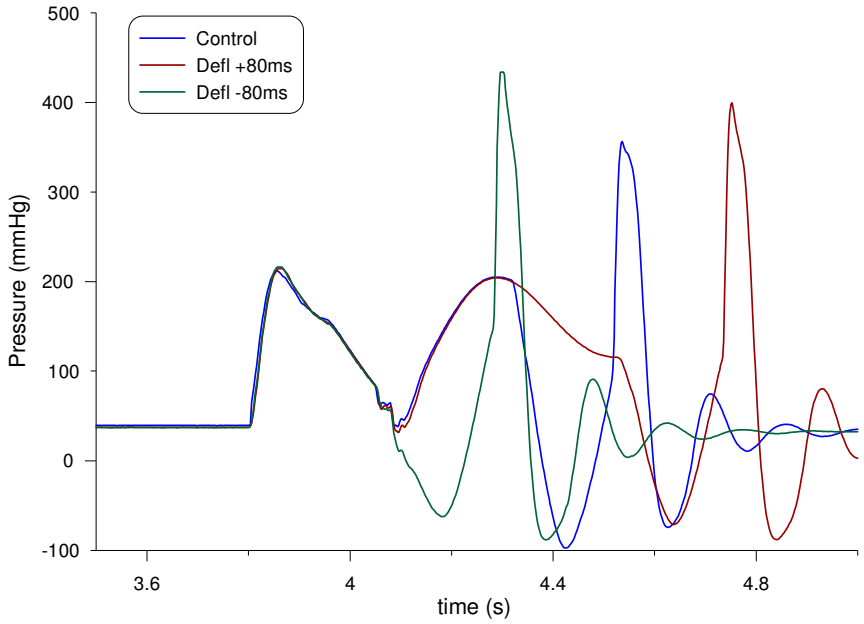

Figure 5.19: Pressure measurements of the liquid surrounding the balloon in the glass tube showing the "stopping shock" phenomenon coinciding with the end of deflation. Deflation is set at control (blue) and at +80 ms (green) and -80 ms (red) from the IABP commands. For all cases the corresponding stopping shock is clearly recognizable.

This phenomenon can be named as "stopping shock", following from a definition given by McMahon in 1969 based on measurements outside the balloon [129]. His observation was that "[…] the end of balloon deflation was marked by a stopping shock, an instantaneously high pressure measured in the liquid in the region around the balloon. It was established that this stopping shock occurred just at the time when the balloon reached its minimum volume i.e. when the radial liquid motions associated with the collapse of the balloon suddenly terminated as the balloon touched the catheter". Also: "If the arteries were inextensible and the blood completely incompressible, such an abrupt change in the momentum of the blood would cause infinite pressures to be

generated at the balloon node" in the pressure-node model of the balloon. "The rate of change of momentum of the column of blood is ρuc per unit area of cross section, where ρ is density of blood, u is the velocity the blood had just before it stopped, and c is the local pulse-wave velocity".

This reasoning was then applied to the current case, where observations are based on balloon internal pressure.

ρuc has units of pressure, kg/m·s^2 .

Modelling the collapse of a 40 cc balloon, it is appropriate to assume a deflation time of 0.3 s, resulting in

$$40/0.3 = 0.0001333 \text{ m}^3/\text{s}$$

indicating that the balloon is collapsing at a rate of approximately 7.9 l/min.

Measurements were carried out in water, thus ρ = 1000 kg/m^3.

In order to calculate u, we can relate it to the change in volume, V, defined as

$$\dot{V} = ku$$

where k has units of area, with the radius of the tube being 0.02 m, both for the silicone tube and the glass tube. So:

$$u = \dot{V}/k = 0.0001333/0.00125 = 0.10664 \text{ m/s.}$$

For the case of the silicone tube let us assume c = 8 m/s. In this case the amplitude of the stopping shock would be:

$$\rho uc = 1000 \cdot 0.10664 \cdot 8 = 853.12 \frac{kg}{m \cdot s^2} = 6.4 mmHg$$

For the case of the glass tube let us assume c = 300 m/s. In this other case the amplitude of the stopping shock would be:

$$\rho uc = 1000 \cdot 0.10664 \cdot 300 = 31992 \frac{kg}{m \cdot s^2} = 240 mmHg \text{ .}$$

These results show that the theoretical amplitude of the stopping shock is very large when calculated in the glass tube, confirming the differences observed in the experiment.

Also, the theoretical calculation of the stopping shock shows that the stopping shock phenomenon is also present when operating the balloon in the silicone tube, although it has much smaller amplitude, so it might not be recognizable in the noisy tracing of $P_{internal}$ measured with the Radi wire.

It is also worth noting that the stopping shock was noted only on the $P_{internal}$ trace and not on the $P_{shuttle}$ trace. This can be explained following from the above description of the phenomenon. In fact, the stopping shock occurs in the liquid surrounding the balloon, not in the shuttle gas inside the balloon. It is timed with the end of the deflation phase. At this instant, it is read by the Radi wire inside the balloon chamber because it is read through the balloon membrane. However, the balloon chamber is fully empty at end deflation and therefore the stopping shock cannot be read by the Gaeltec catheter measuring $P_{shuttle}$, which is positioned at the beginning of the balloon catheter.

Finally, the stopping shock phenomenon has not been reported for the case of *in vivo* measurements. This can be ascribed to the low values of wave speed measured in the compliant aorta.

5.5. Conclusion

The visualisation study reported in this chapter showed that at an angle the balloon is inflated from tip to base instead of uniformly. It also showed that increasing intra-luminal pressure results in reduced duration of inflation and longer duration of deflation while increasing angle results in longer duration of

both inflation and deflation. The intertwined effect of these two parameters has been distinguished.

Three balloon shapes were filmed and it was shown that, when the IABP is operated continuously, the TID balloon is more affected by an increment in angle than the TDD balloon or a 40 cc cylindrical balloon.

Since visualisation had to be performed in a rigid glass tube, knowledge of balloon internal pressure was acquired to show the effect of tube compliance of balloon mechanics. A major difference between the case of the balloon operating in a silicone and that of the balloon operating in a glass tube was shown at the end of deflation and identified as the “stopping shock” phenomenon.

CHAPTER 6

DESIGNING A MOCK CIRCULATORY SYSTEM FOR IABP TESTING[‡‡]

6.1. Introduction

This chapter will describe the design of a mock circulatory system specifically designed and assembled for the purpose of IABP testing. A mock circulatory system, or mock loop, is an artificial analogue of the human circulation, more or less detailed, in which physiological pressure and flow conditions are recreated *in vitro* for the purpose of studying cardiovascular phenomena or testing cardiac devices. A mock loop usually allows data collection in a controlled (hence, to a varying degree, simplified) environment. Richard Skalak defined a complete mock circulation system as "any system or preparation which contains some part of each category: arterial, capillary and venous networks connected in their usual and natural sequence" adding that the choice of model on which to base the system "depend[s] on the purposes one has in mind" [130].

In elucidating the main characteristics of different models, Skalak indicated the lumped parameter model, based on Otto Frank's Windkessel theory [131], as the most suitable for the study of cardiac assist devices: "Another recent use of lumped parameter models is in the analysis of cardiac pumping assist devices, particularly for intra-arterial counterpulsation methods. In this application the details of wave propagation are not so important as the gross volumetric and elastic parameters and their variation in time" [130].

[‡‡] *Partly in: C Kolyva, G Biglino, JR Pepper and AW Khir, A mock circulatory system with physiological distribution of terminal resistance and compliance: application for testing the intra-aortic balloon pump, Artif Organs (under revision)*

The Windkessel model, as originally proposed by Frank [131], essentially describes the arterial system as a flowing system with a cushioning effect. By using the Windkessel model it is possible to represent the arterial system as a compartment (Windkessel = air chamber, in German) including the arteries, with a pressurised volume, and a capacitance and a resistance representing the microvasculature and providing nearly-constant flow to the tissues.

An early study (1968) by Jones et al. applied the Windkessel model to arterio-arterial pumps, which are counterpulsating devices such as a simple pulsating bulb or the IABP [132]. McMahon et al. (1971) constructed a hydraulic model specific for the study of the IABP, in which the compliance of the arterial system was modelled as three lumped capacitance elements and the peripheral resistance was implemented with porous tubes [133]. Wolf and Clinch (1972) proposed a mock circulatory system consisting of a left heart analog, compliant arteries, peripheral resistance and venous return and the authors explicitly stated that "no attempt was made to model the right heart and pulmonary circuit since these seemed unnecessary for IAB testing" [134].

Another application specific to IABP testing is described by Bowles et al. (1990). Mock loops are valuable tools for testing and comparing cardiac assist devices *in vitro* and in this case the mock circulation system was used to assess the performance of extra-aortic counterpulsation[§§] and IABP counterpulsation [135]. The authors used a Windkessel model with lumped compliance and resistance. Both compliance and resistance were divided into proximal and distal and implemented with Windkessel chambers and adjustable laminar resistors respectively.

[§§] Extra-aortic counterpulsation implies the use of trained skeletal muscle wrapped around the proximal descending aorta [135].

A more recent example (2004) is provided by Pantalos et al. This model included left atrium, left ventricle, systemic and coronary vasculature. As in the case of the previous model, resistance and compliance were divided between proximal and peripheral resistance and systemic and venous compliance, respectively [136]. An application of this mock loop was proposed by Koenig et al. in order to test a new counterpulsation device [137].

Another relevant example of a mock loop is the setup designed by Vandenberghe et al. [138] for comparison of IABP and a PUCA II device ("PUlsatile CAtheter" device, combining the characteristics of traditional counterpulsation with an actual blood pump). In this case a pulse duplicator, comprising two silicone sacs (left ventricle and left atrium) and bileaflet and bovine pericardial valves (mitral and aortic valves), was used in combination with a silicone aorta. The aorta had eight branches, each terminating in a resistor made of compressible foam, used to regulate flow distribution.

Finally, a "hybrid" type of mock loop system has been conceived. According to Ferrari et al.: "Flexibility and accuracy can be improved by merging numerical models with physical models, thus obtaining a hybrid model where numerical and physical sections are connected by an electrohydraulic interface" [139]. This concept has also been applied for IABP testing [140, 141].

In terms of the IABP, as highlighted in Chapter 1, compliance is a major variable affecting IABP performance [25, 73]. Sensitivity to heart rate [77, 78] and to timing of inflation and deflation [29] are equally important aspects. Following from the existing knowledge on artificial circulation, the aim of this study is to design a mock circulatory system (MCS) which will be suitable for replicating the cardiovascular system for IABP testing.

In order to achieve the scope, the major design criteria of the process are: physiological distribution of peripheral resistance and compliance, anatomical accuracy, the possibility of varying the inclination of the MCS to replicate the semi-recumbent position and good control over balloon timing.

6.2. The mock circulation system (MCS)

6.2.1. Artificial aorta

The MCS was constructed around an artificial aorta (Ranier, Cambridge, UK), made of a polyurethane compound and including 14 main branches: right and left coronaries, right and left carotid arteries, right and left subclavian arteries, splenic, mesenteric, right and left renal arteries, right and left iliac branching into right and left femoral and deep femoral. A representation of the aorta is provided in Figure 6.1. The dimensions, tapering and elastic properties of the aorta ensured a physiological environment for *in vitro* testing; however, the aortic arch was straightened.

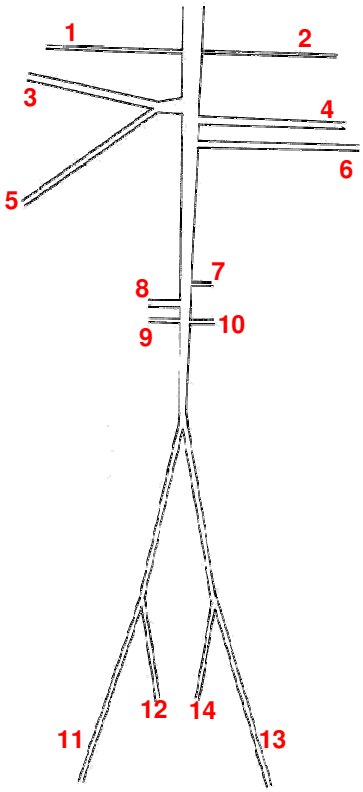

Figure 6.1: Schematic representation of the polyurethane aorta. Arterial segments: (1) right coronary, (2) left coronary, (3) right carotid, (4) left carotid, (5) right subclavian, (6) left subclavian, (7) splenic, (8) mesenteric, (9) right renal, (10) left renal, (11) right femoral, (12) right deep femoral, (13) left femoral and (14) left deep femoral.

6.2.2. Resistance and compliance

Since part of the IABP testing in the MCS will involve the flow-volume displaced during IAB inflation, it is important to ensure a physiological flow distribution by setting the appropriate terminal resistances at the end of each branch. Also, being that the IAB is greatly affected by changes in compliance, suitable implementation and distribution of compliance was regarded as a second crucial parameter to control. Hence, the end of each branch of the aorta was fitted with an arrangement of a syringe and a capillary tube, representing respectively distal compliance and peripheral resistance. This is explained in detail in the following section.

6.2.2.1. Theoretical models

In 1992 Stergiopulos et al. proposed a computer model comprising 55 arterial segments, excluding the coronary circulation [142]. This is shown in Figure 6.2. Distribution of resistance and compliance in the MCS is mainly based on this model.

The main physiological parameters of the Stergiopulos model are derived reducing the number of branches from a previous (1969) model by Westerhof et al., an electrical analog of the circulation based on pulsatile flow theory in which the viscous, inertial and compliant properties of arterial blood flow are represented by electrical resistance, inertance and capacitance respectively [143]. The Westerhof model provides physiological proximal resistance and compliance data per arterial segment and arterial dimensions from a subject with height of 175 cm and mass of 75 kg [143]. This model did not include the coronary circulation.

The values of terminal resistance used in the Stergiopulos model were provided by the 1972 mathematical model by Schaaf and Abbrecht [144], in which these values were "calculated from the specified total peripheral resistance and the distribution of flow estimated from physiological data".

In terms of terminal compliance, Stergiopulos et al. assumed a value of total compliance of 1 ml/mmHg, subtracted from this value the summation of each vessel's volume compliance (0.835 ml/mmHg) and the remaining 0.165 ml/mmHg was distributed in the terminal branches in proportion to the mean flow [142].

Since our model also includes two coronary vessels, a value of coronary microvascular resistance was obtained from a recent human study by Verhoeff et al. [145], as described in the following section.

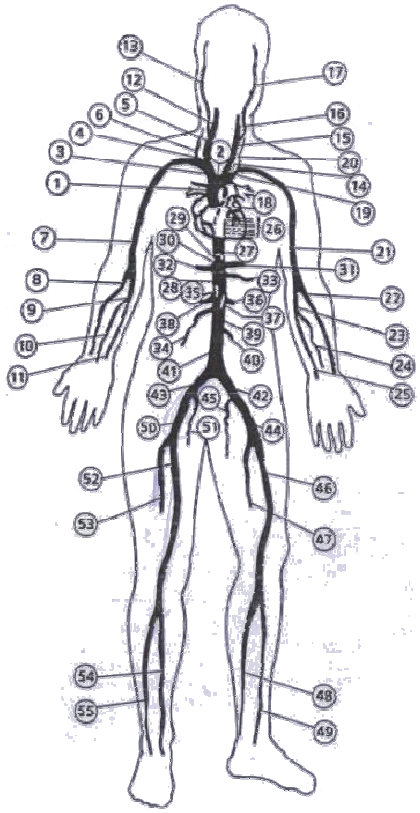

Figure 6.2: The model of human circulation proposed by Stergiopulos in 1992, comprising of 55 main vessels [142]. The Stergiopulos computational model fuses the resistance and compliance values from the Westerhof model [143] and the data on terminal resistance and compliance from the Schaaf and Abbrecht model [144].

6.2.2.2. Total resistance

The total resistance, R, implemented in the aortic model was divided between proximal, R_{prox}, and terminal, R_t, resistance. The geometry of the aorta accounted for R_{prox}, while R_t was applied at each branch by means of capillary tubes. Since fully-developed laminar flow could not be guaranteed inside any of the capillary endings, the Poiseuille formula was not applied for quantifying their resistance, R_c, based on their dimensions. Instead, pressure drop-flow curves were obtained for a range of capillary diameters (with ID of 1, 1.5, 2 and 3 mm) and lengths (from 3 to 60 cm). Pressure drop, ΔP, across and flow, Q, through each capillary tube were measured, and a value of $R_c = \Delta P/Q$ was estimated as

the slope of the curve at the range of flows expected in each branch, as indicated in Figure 6.3. The curve in Figure 6.3 represents the case of 15 cm long capillary with diameter of 1.5 mm. The curve exhibits a biphasic behaviour with a change in slope occurring at Re = 1900 (at Q = 0.17 l/min), likely to be due to the transition from laminar to turbulent flow.

A relationship between capillary length and R_c could thus be obtained for each capillary diameter. This provided a way to convert capillary dimensions to R_c. This relationship is shown in Figure 6.4.

The required values of total resistance, R, for all branches of the aortic model, except for the coronary branches, were obtained by reducing the 55 branches of the Stergiopulos model into 12 branches by adding resistances in series or in parallel according to electric circuit theory (Table 6.1). Since for each aortic branch R_{prox} in the aortic model was estimated to be approximately three orders of magnitude smaller than the R needed to be implemented according to the Stergiopulos model, the approximations $R = R_t$ was considered valid in the physical model. The resulting theoretical values of R_t for the 12 branches are reported in Table 6.2. The table also includes the value of microvascular resistance downstream healthy coronary arteries obtained from an experimental study in humans [145]. This value was used as theoretical R for the coronary branches.

From the previously calculated conversion lines between capillary dimensions and R_c it was possible to derive the correct combination of capillary length and diameter so that for each branch of the aorta $R_t = R_c$. This process ensured a physiological distribution of peripheral resistance across the aortic model. When there was a choice, capillary diameter was chosen so that, in order to achieve the desired R_c, capillary length was 15-20 cm.

Vessel (Stergiopulos)	Vessel (current model)	Arrangement
1) Ascending aorta 2) Aortic arch I 3) Brachiocephalic 4) R subclavian I 5) R carotid 6) R vertebral	R subclavian	10 and 11 in parallel, in series with 9, in parallel with 8, in series with 7, in parallel with 6, in series with 4
7) R subclavian II 8) R radius 9) R ulnar I 10) R interosseous 11) R ulnar II 12) R internal carotid	L subclavian	24 and 25 in parallel, in series with 23, in parallel with 22, in series with 21, in parallel with 20, in series with 19
13) R external carotid 14) Aortic arch II 15) L carotid 16) L internal carotid	R carotid	12 and 13 in parallel, in series with 5
17) L external carotid 18) Thoracic aorta I 19) L subclavian I 20) Left vertebral	L carotid	16 and 17 in parallel, in series with 15
21) L subclavian II 22) L radius 23) L ulnar I 24) L interosseous	Splenic	31, 32 and 33 in parallel, in series with 29 and 30
25) L ulnar II 26) Intercostals 27) Thoracic aorta II 28) Abdominal aorta I	Mesenteric	34
29) Celiac I 30) Celiac II 31) Hepatic 32) Gastric	R renal	38
33) Splenic 34) Superior mesenteric 35) Abdominal aorta II 36) L renal	L renal	36
37) Abdominal aorta III 38) R renal 39) Abdominal aorta IV 40) Inferior mesenteric 41) Abdominal aorta V	R femoral	54 and 55 in parallel, in series with 52, in parallel with 53
42) R common iliac 43) L common iliac 44) L external iliac 45) L internal iliac 46) L femoral	L femoral	48 and 49 in parallel, in series with 46, in parallel with 47
47) L deep femoral 48) L posterior tibial 49) L anterior tibial 50) R external iliac 51) R internal iliac	R deep femoral	Occluded for insertion of pressure catheter
52) R femoral 53) R deep femoral 54) R posterior tibial 55) R anterior tibial	L deep femoral	Occluded for insertion of balloon catheter

Table 6.1: The 55 vessels of the Stergiopulos model have been reduced to the 12 branches of the current model (does not include the coronary branches).

Vessel	Resistance			Compliance	
	Theoretical R (mmHg/l/min)	Capillary L (cm)	Capillary D (mm)	Theoretical C (ml/mmHg*10^{-3})	Syringe volume (ml)
Right coronary	2187.5	69.2	1.5	-	-
Left coronary	2187.5	69.2	1.5	-	-
Right carotid	230.7	14.7	2	1.4	10
Left carotid	230.7	14.7	2	1.4	10
Right subclavian	878.5	22.8	1.5	2.5	20
Left subclavian	878.6	22.8	1.5	2.5	20
Splenic	141.7	3.2	2	0.7	10
Mesenteric	116.4	0	-	9.1	60
Right renal	142.0	3.1	2	2.0	10
Left renal	142.0	3.1	2	2.0	10
Right femoral	223.4	12.4	2	3.6	40
Left femoral	223.4	12.4	2	3.6	40

Table 6.2: Values of resistance (R) and compliance (C) obtained reducing the 55 vessels of the Stergiopulos model into the 12 vessels of the current physical model according to circuit theory. L = length and D = internal diameter.

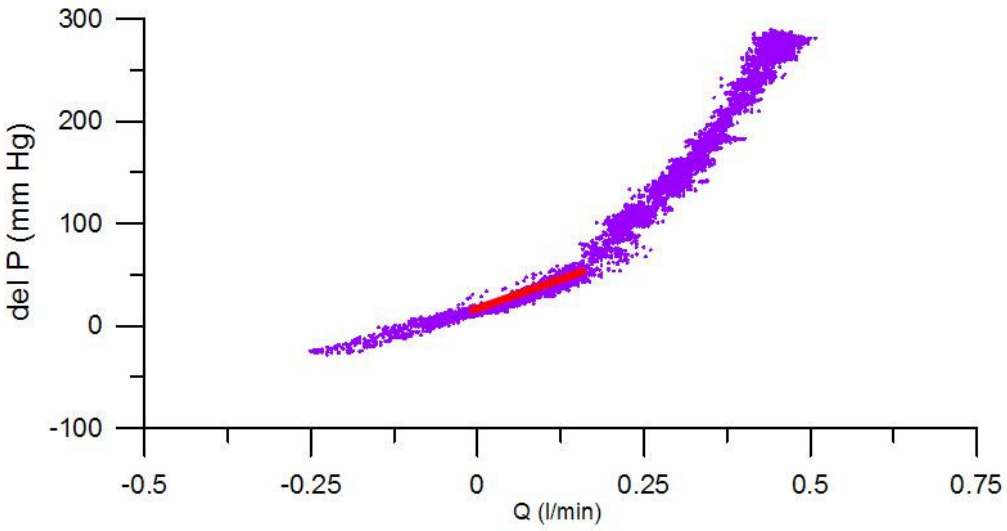

Figure 6.3: An example of pressure drop-flow curve, calculated for a capillary tube of 1.5 mm ID and 15 cm long. A transition is occurring at Q = 0.17 l/min. The slope of the curve over the flow range of interest (red line) yields the value of R. Given that cardiac output was fixed at 2.7 l/min, Q was rarely expected > 0.170 l/min, and for those vessels for which this was the case (eg. renals) a larger diameter of capillary was chosen.

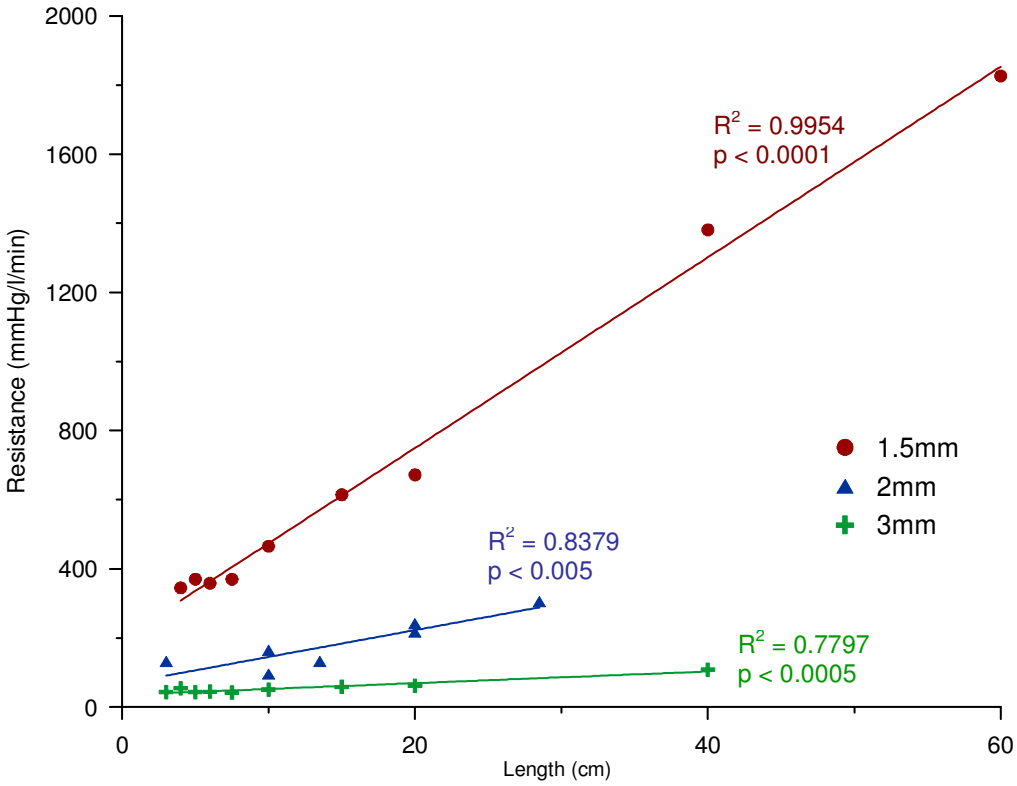

Figure 6.4: Relationship between capillary tube length and resistance for capillaries of different sizes (1.5, 2 and 3 mm ID). Each point was obtained from the slope of a pressure drop-flow curve. These conversion lines enable us to determine the length of capillary tube needed in order to implement a desired value of theoretical resistance.

6.2.2.3. Proximal compliance

Total compliance, C, of the aortic model was also divided into proximal, C_{prox}, and distal, C_d, compliance. The elastic properties of the aorta determined C_{prox}, while C_d was implemented by means of syringes.

C_{prox}, represented by the compliance of the polyurethane aorta itself, was measured according to a method previously reported by Segers et al. [146]. All aortic ends were closed and the aorta was filled with water to create a closed volume. Volume, V, was increased by 60 ml in steps of dV = 5 ml by injecting water with a syringe, and then decreased gradually by removing water in equal

steps. Pressure, P, was continuously measured inside the aorta with a transducer-tipped catheter throughout the loading and unloading phases. This process results in a PV loop, as shown in Figure 6.5. Compliance at a certain pressure level is the slope of the PV loop at this pressure, according to the definition of compliance (C = –dV/dP). The hysteresis between the loading and unloading part of the loop is related to the viscoelastic properties of the material of the aortic walls.

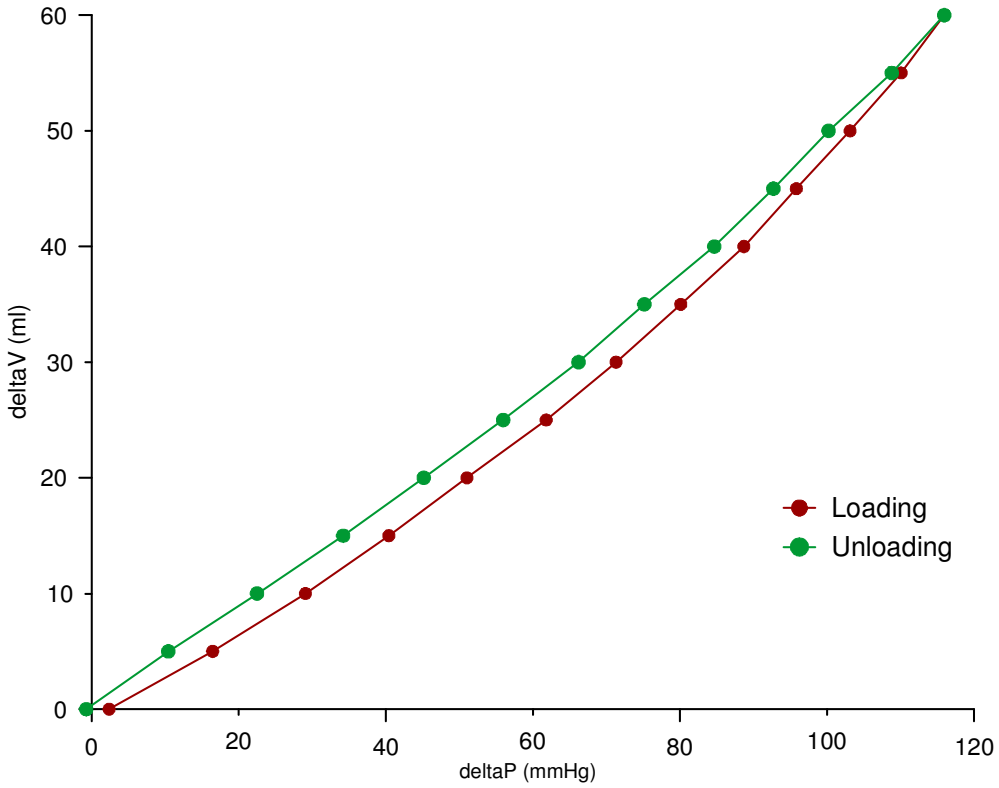

Figure 6.5: Calculation of proximal compliance, C_{prox}. A PV loop relating the change in volume, V, and pressure, P, inside the aorta was obtained during loading and unloading. The average of the slopes of linear fits over the loading and unloading curves for P > 70 mmHg yielded the value of C_{prox}. The hysterisis relates to the viscoelastic properties of the material of the aortic wall.

6.2.2.4. Distal compliance

As originally proposed by Westerhof, an "air bubble" is a compliant element, effectively acting as a Windkessel [147]. Air chambers representing C_d were implemented in the MCS by means of syringes containing air.

Following the same procedure described for the resistances, the required physiological distribution of total compliance C in the aortic model was derived from the compliance values provided in the Stergiopulos model and these values of theoretical C are reported in Table 6.1. The distal compliance accommodated by a certain air volume v enclosed in a syringe under pressure p can be derived from the gas law, $pv^n = \text{const}$ assuming an isothermal process (n = 1). It was ensured that the distribution of C_d in the aortic model was proportional to the theoretical distribution of C. Syringes with air volume between 10 and 60 ml were used. So, the compliance implemented by a syringe, following from [135], was for example:

- Syringe air volume = v =10 ml
- P atmospheric = 760 mmHg
- Working P = 95 mmHg
- Assuming n = 1 in $pv^n = \text{const}$,

$$C_d = \frac{dv}{dp} = \frac{-v^n}{(pnv)^{n-1}} = -\frac{1}{n} \cdot \frac{v}{p} = \frac{10ml}{760 + 95mmHg} = 0.0117 \frac{ml}{mmHg}.$$

Syringes were distributed in order to achieve a total compliance of approximately 1 ml/mmHg, in accordance with the Stergiopulos model [142].

6.2.2.5. Resistance and compliance arrangement

The connection of terminal resistance and distal compliance at the end of each branch was in parallel, forming a 2-element Windkessel arrangement. In order to connect the syringes at the end of a branch before the capillary tube a 4-way luer valve was used. Isolating the 4-way valve and testing its hemodynamic behaviour it was possible to discern that it behaves as a stenosis, as can be seen by the shape of the pressure-drop curve presented in Figure 6.6: typical of stenotic behaviour, resistance was flow rate dependent.

In order to compensate for this, the resistance of the 4-way valve was estimated in the range of flows expected in the arterial segments. This resistance was subtracted from the resistance that needed to be implemented at the end of each branch with a capillary in order to maintain the total resistance constant.

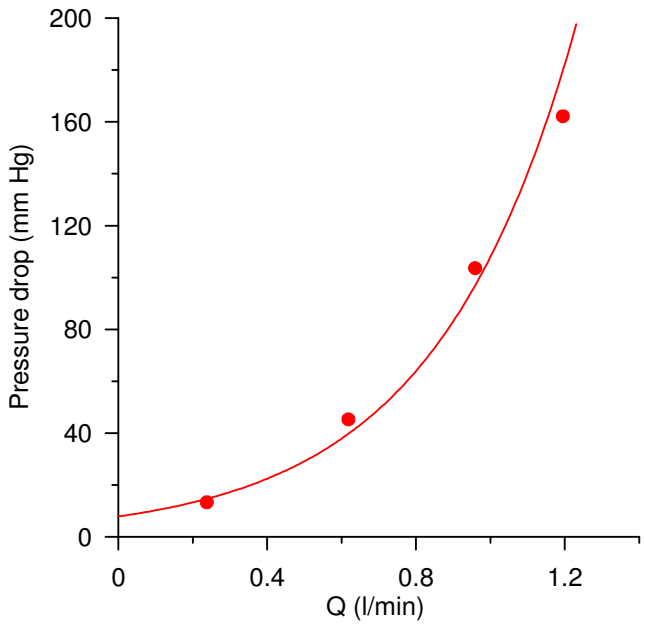

Figure 6.6: Pressure-drop curve for a 4-way valve used in order to connect syringes in the system and implement distal compliance. The plot shows that a 4-way valve induces a stenosis in the system.

6.2.3. Other components

Pulsatile flow in the aortic model was provided by an Abiomed BVS 5000 ventricular assist device (Abiomed Inc, MA, USA). The BVS 5000 is a dual-chamber device and simulates the left ventricle (LV) and left atrium (LA) in the MCS. The device also includes equivalents for the aortic and mitral valves. It is pneumatically driven by an external stepper motor driver (Placepower, Norfolk, UK) connected to the LV. The driver is controlled with specific software (Easitools, v 1.5, Parker Hannifin Corp, Dorset, UK) and can generate a variety of flow profiles with accurate control over stroke volume, period and systolic/diastolic duration. Because of its design, the driver is also independent of afterload and is suitable for synchronisation with the IABP. This last point will be expanded in section 6.4.

The LV of the BVS 5000, consisting of a silicone sac, was connected to the aortic root of the arterial model, while the LA was connected to an overhead reservoir, providing constant atrial pressure of 10 mm Hg. Each aortic branch ending was fitted with a capillary tube of specific dimensions and a syringe of suitable air volume for the purpose of providing the desired physiological values and distribution of resistance and compliance across the aortic model. The outlets of the branches were then connected to a common silicone drainage tube (ID of 8 mm) simulating the venous system. The venous return was in turn coupled to the overhead reservoir. The main components of the MCS, connection of the BVS 5000 to the aortic root and connection of the capillaries to the venous return are shown in Figure 6.7.

The LV was driven with water by the stepper motor driver. Cardiac output was set at 2.7 l/min. This is also a restriction imposed by the maximum capacity

of the BVS 5000 [148]. Images of the Abiomed BVS 5000 and of the driver showing their main components are provided in Figure 6.8a and Figure 6.8b respectively.

The volume profile of the driver with sweep volume set at 45 ml in order to achieve cardiac output of 2.7 l/min was extracted from the software that controls the driver and is shown in Figure 6.9a. The flow profile of the driver as calculated from differentiation of the volume profile is shown in Figure 6.9b.

Heart rate was set at 60 bpm and diastolic time fraction was 68%.

The MCS was assembled on a hinged platform in order to simulate different patient postures by different platform inclinations (0, 10, 20, 30 and 45°).

Water at room temperature (20 °C) was used as test fluid.

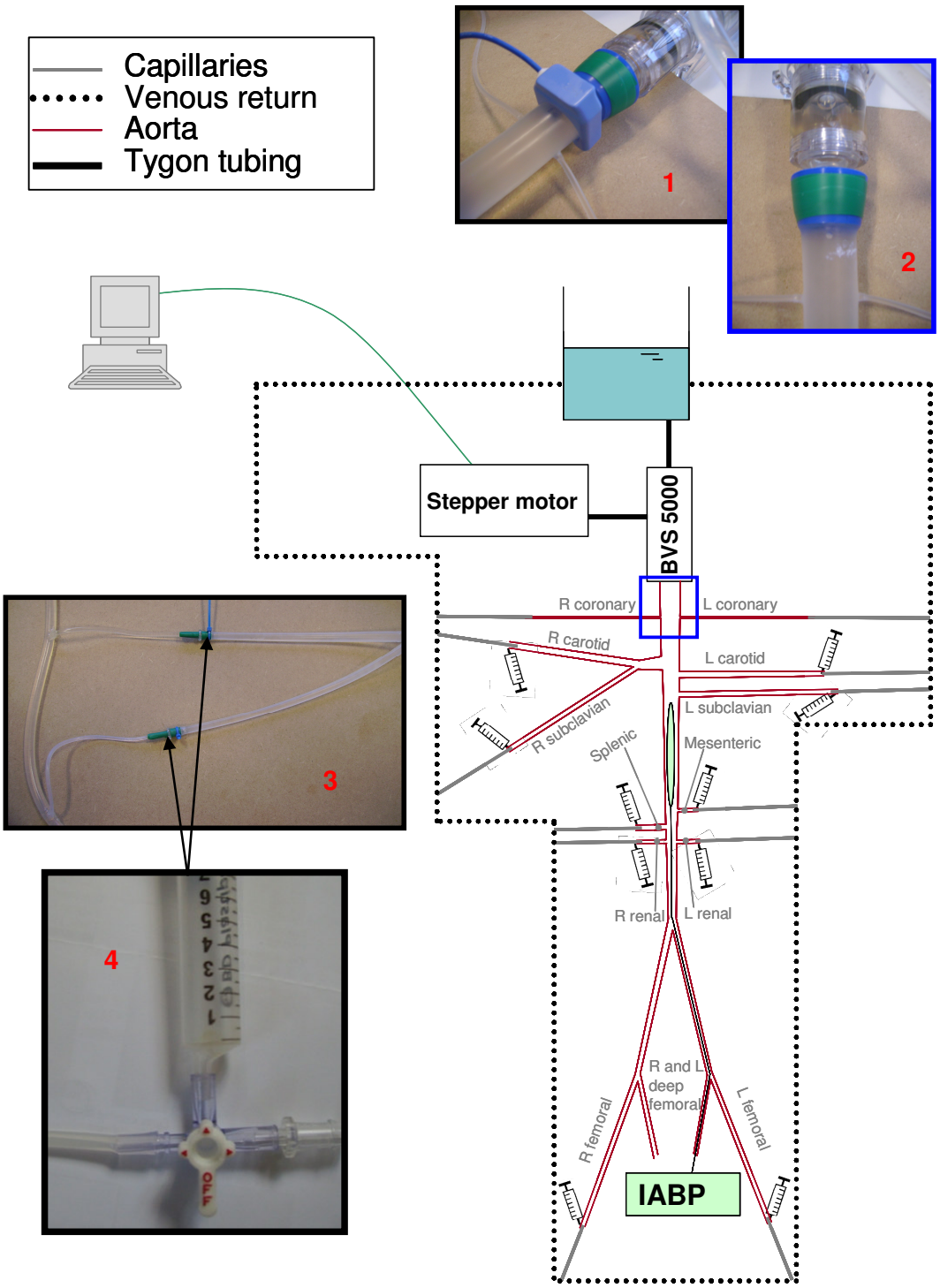

Figure 6.7: Diagram of the artificial aorta. The connection between the Abiomed BVS ventricle and the aortic root is shown, with (1) and without (2) the 28 mm flowprobe measuring Q_{root}. The connection between the branches and the venous return is also shown (3), together with an image of the arrangement of 2-element Windkessel at each branch (4).

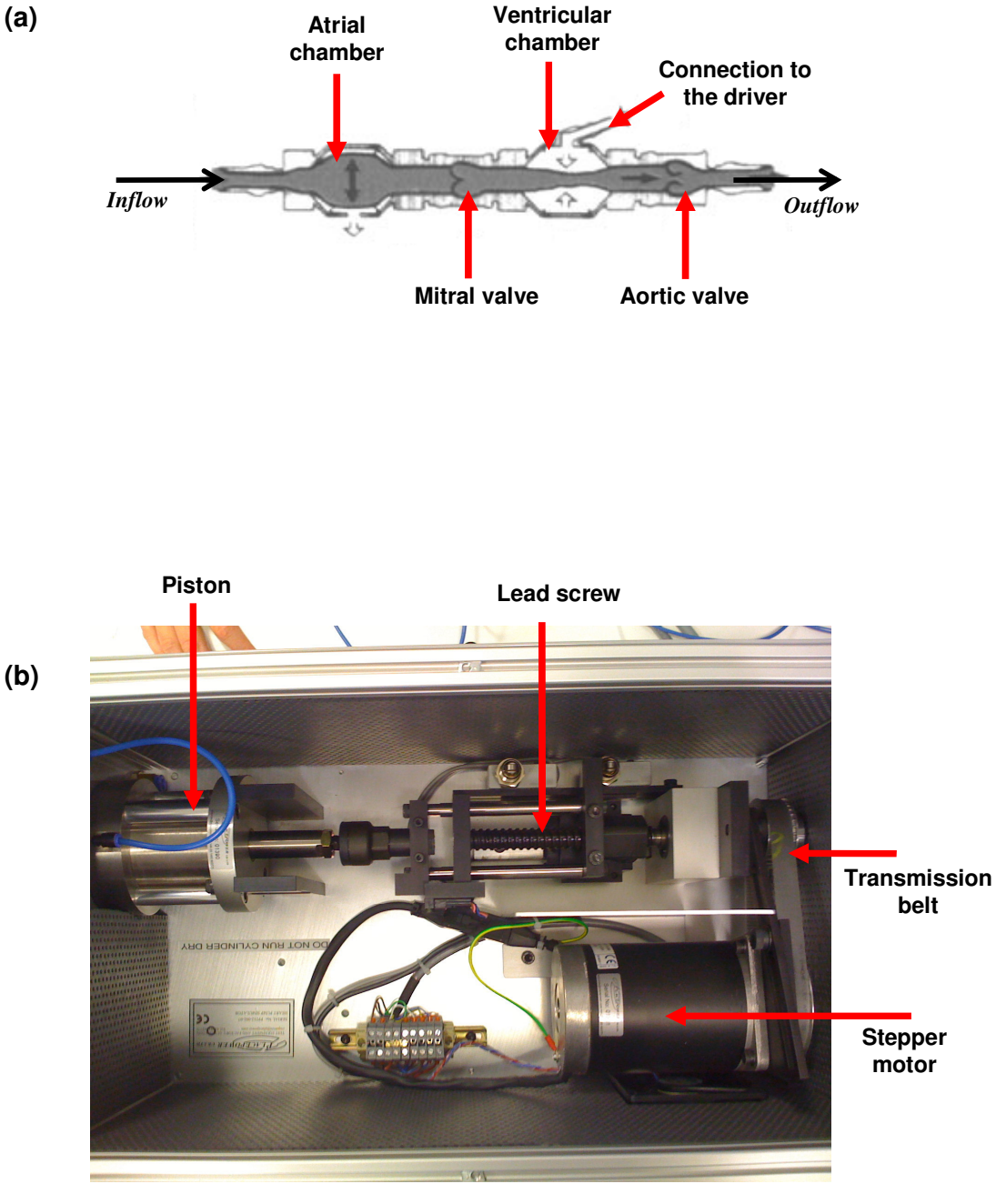

Figure 6.8: Components controlling the flow in the MCS: (a) top view of the Abiomed BVS 5000, redrawn from [149] and (b) top view of the driver of the MCS (lid removed).

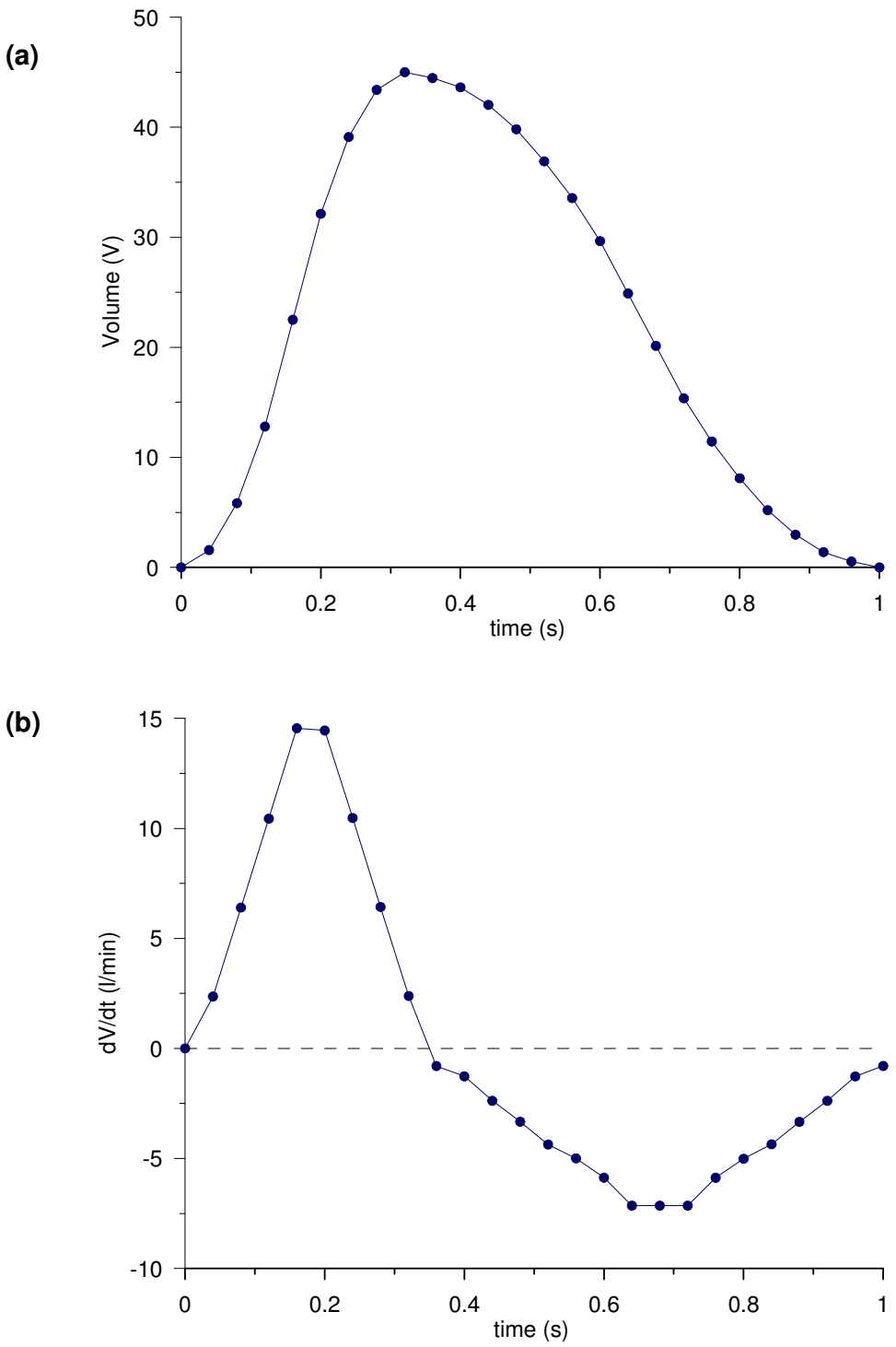

Figure 6.9: The profile of the volume displaced by the piston of the stepper motor driver (a) and the flow profile generated by the stepper motor driver (b). The sweep volume of the driver was set at 45 ml, in order to achieve cardiac output of 2.7 l/min (at 60 bpm). The flow profile is calculated from differentiation of the volume profile.

6.2.4. Measurements

Pressure was measured with 7F and 5F transducer-tipped pressure catheters (Gaeltec Ltd, Isle of Skye, UK and Millar Instruments, TX, USA). The pressure catheters were calibrated with the method of the "column of water".

Flow was measured with ultrasonic flow probes (Transonic Systems Inc, NY, USA) of different sizes (3, 8, 10, 20 and 28 mm). All probes were calibrated before the measurements at a range of flows (0-1.5 l/min) with the method of timed-collection.

In order to ensure good agreement between the theoretical and experimental values of R for each aortic branch and to confirm physiological flow distribution, measurements of pressure drop across and flow through each aortic branch were performed. Pressure was measured simultaneously before and after each branch, in the aorta and the venous tube. Flowprobes of 3, 8 or 10 mm were used, according to the dimensions of each branch. Measurements were obtained under constant flow rate of 3 l/min.

Measurements were also taken to verify that mean and phasic pressure hemodynamic signals in the MCS were physiological. Aortic pressure was measured in the aortic arch. Left ventricular pressure was measured by inserting a catheter into the LV chamber of the BVS 5000 through the aortic valve. Pressure at the IAB catheter was also recorded in order to acquire insight into the behaviour of the IAB during its cycle. Aortic flow was measured at two locations: (a) at the aortic root, with a 28 mm Transonic flow probe, as shown in Figure 6.7, and (b) retrograde the IAB tip, 1-2 cm below the subclavian branches, with a 20 mm Transonic flow probe.

6.3. Results

Resistance distribution was measured across the aortic model and matched well the desired R distribution according to the theoretical model. This is shown in Figure 6.10. Total measured peripheral resistance of the aortic model was 20.3 ± 3.3 mmHg/l/min, close to the theoretical value of 19.8 mmHg/l/min. Correct resistance distribution is a crucial factor in the design of the MCS since it reflects on any observation on flow distribution.

Physiological flow distribution at the major vascular beds was achieved in this physical model and was in good agreement with values reported in the literature, as summarized in Table 6.3.

A value of C_{prox} of 0.64 ml/mmHg was derived as the average of the slopes of linear fits over the loading and unloading curves for pressure higher than 70 mmHg [146].

C_d was calculated for each branch at average working pressure of 95 mmHg resulting in $\sum C_d$ = 0.3 ml/mmHg.

Total compliance was obtained as $C = C_{prox} + \sum C_d$. The value of total compliance, C = 0.94 ml/mmHg, is in a physiological range, with C_d distributed physiologically in each branch, and in good agreement with the Stergiopulos model.

Waveforms of aortic pressure and flow recorded without the IABP counterpulsating are shown in Figure 6.11 alongside with LV pressure. A physiological hemodynamic profile was achieved in the MCS. Mean aortic pressure was 95 mmHg. Integration of the aortic flow signal measured at the aortic root confirmed that cardiac output was 2.7 l/min.

Vascular bed	% flow (measured)	% flow [146]	% flow [150]
Coronaries	3.0	-	4
Head	15.4	14.2	13
Arms	5.3	5.2	-
Abdomen	46.5	52.9	48
Legs	31.2	17.6	26

Table 6.3: Measured flow distribution at the major vascular beds was in good agreement with data reported in the literature by Segers et al. [146] and Nichols and O' Rourke [150].

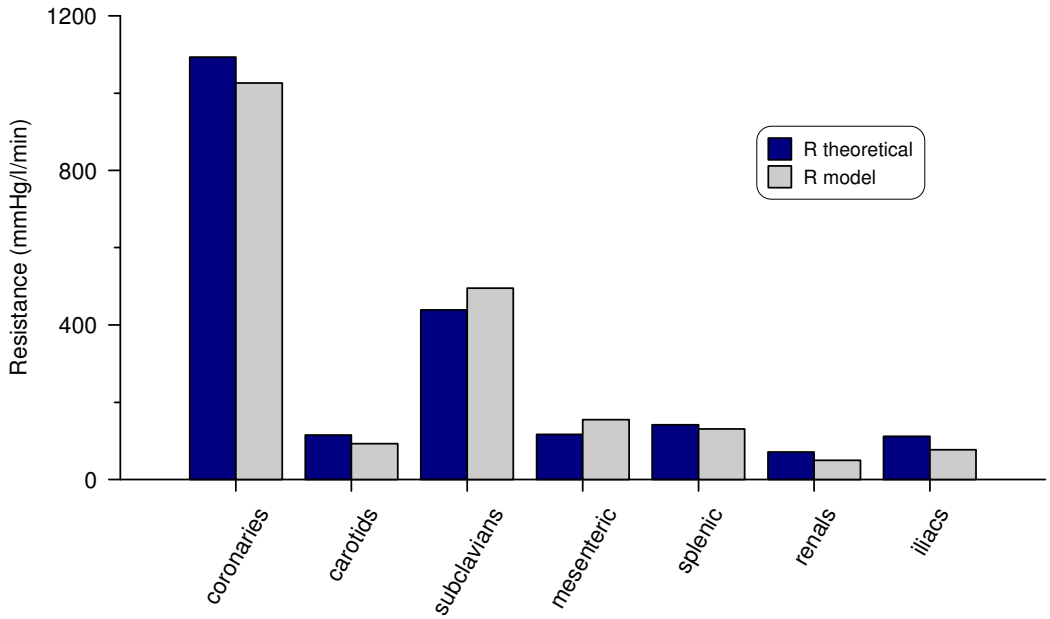

Figure 6.10: Comparison of expected ("R theoretical") and measured ("R model") resistance for different branches of the aortic model showed that resistance distribution implemented with capillary tubes in the MCS was in good agreement with the theoretical values.

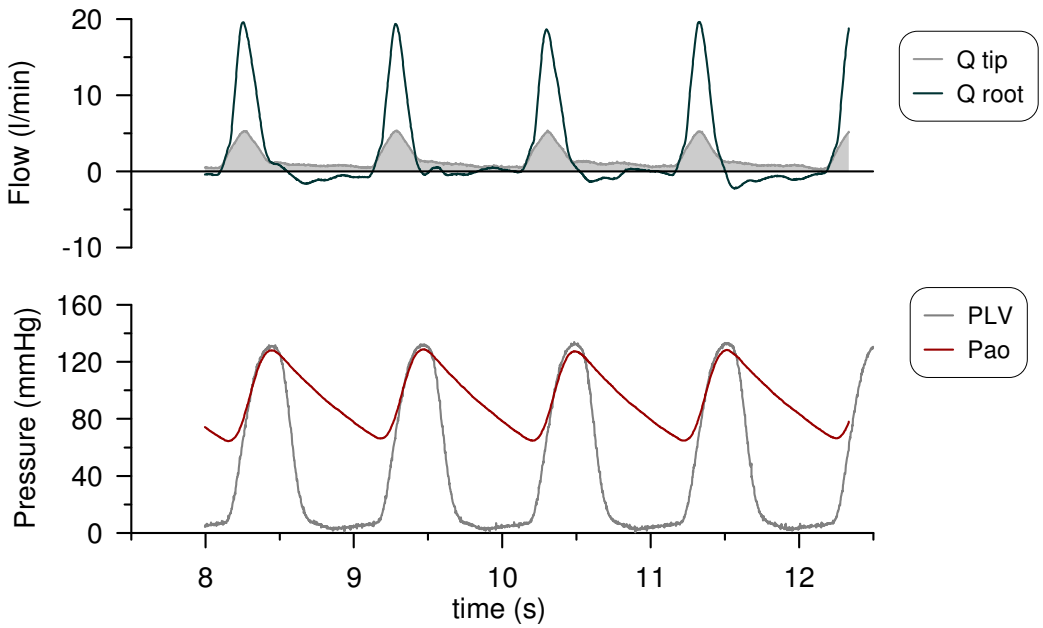

Figure 6.11: Measurements of pressure and flow in the MCS without the IABP, showing physiological hemodynamic profiles. Aortic flow at the aortic root (Q_{root}, solid black line, measured with the 28 mm probe) and 2 cm retrograde from the balloon tip (Q_{tip}, shaded, measured with the 20 mm probe) are shown at the top. Aortic pressure measured in the aortic arch is shown together with LV pressure in the bottom panel.

6.4. Simulating the principle of counterpulsation

In order to simulate the principle of counterpulsation *in vitro*, the stepper motor driver and the IABP (System 98, Datascope) had to be synchronized. A short square pulse signal (0.054 s) generated by the driver at the start of every forward movement of the piston was used as an ECG-surrogate signal for triggering IABP inflation and deflation. The synchronization signal is generated by a spare output from the stepper drive. The driver is connected with a BNC cable to the appropriate ECG input port on the IABP, the same port where previously a patient simulator was attached for the same purpose.

According to the IABP instructions, the front end panel can accept an external ECG signal of 1 V while the square pulse signal was 24 V in

magnitude. For this reason, a potential divider was added to the driver, in order to reduce the voltage of the synchronisation signal to a level more suitable for the IABP. This arrangement is shown in Figure 6.12.

Once the scaled ECG-equivalent signal was read by the IABP, further fine-tuning of the timing of inflation and deflation was possible – if necessary – via the controls of the IABP panel.

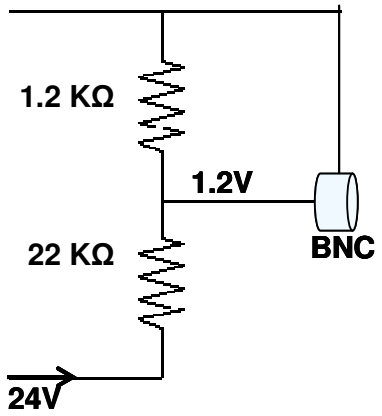

Figure 6.12: A potential divider ensured that the square pulse signal extracted from the stepper motor driver (24 V) was scaled down in order to be read as an ECG-trigger by the IABP. The BNC port is located on the back of the driver and can then be connect to the IABP.

Once the driver and the IABP were synchronised, counterpulsation was simulated in the MCS. Results with a 40 cc balloon (Datascope) inserted via the right deep-femoral artery showed that the major features of counterpulsation were obtained, namely:

1) early diastolic pressure augmentation during balloon inflation

2) inflection point on the aortic pressure signal at the onset of deflation

3) end-diastolic pressure reduction at the end of deflation, preceding the following systole

4) the contribution of balloon inflation and deflation to aortic flow was clearly visible by a negative and positive peak in the Q_{tip} signal during early and late diastole respectively.

These features are shown in Figure 6.13. In this case mean aortic pressure was 99 mmHg.

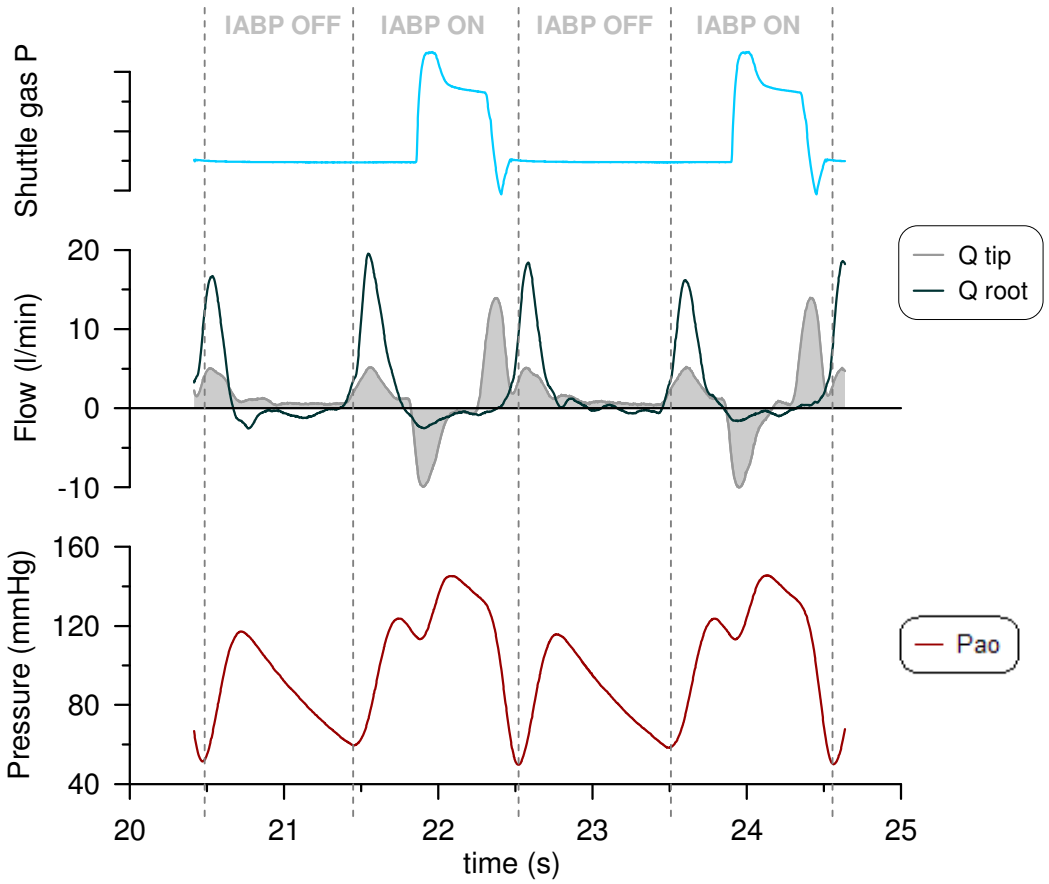

Figure 6.13: Simulation in the MCS showing physiological hemodynamic profiles. Shuttle gas pressure is reported as a reference of the balloon cycle (top) with the IABP operated at 1:2 assisting frequency. Aortic flow at the aortic root (Q_{root}, solid black line, measured with the 28 mm probe) and 2 cm retrograde from the balloon tip (Q_{tip}, shaded, measured with the 20 mm probe) are show at the centre. The contribution of balloon inflation and deflation is clearly visible especially at the balloon tip. Aortic pressure (bottom) shows the main features of counterpulsation, namely: early diastolic augmentation, inflection point at the onset of deflation and end-diastolic pressure reduction.

6.5. Methodological considerations

The design of a MCS which is suitable for IABP testing has been described. The MCS has physiologically correct distribution of resistance and compliance and the artificial aorta ensured physiological anatomy. Pressure and flow recordings in the MCS exhibited physiological features both with and without the IABP counterpulsating, as desired. Some of the advantages, limitations and distinctive features of the MCS are here described.

The MCS was designed to operate at a cardiac output of 2.7 l/min. This was a restriction imposed by the choice of LVAD, which is not designed to provide flow augmentation higher than 3 l/min [148]. This represents a limitation in terms of the range of cardiac outputs that can be simulated in the MCS. However, a choice of 2.7 l/min, although seemingly low, is considered physiologically realistic for patients in need of IABP assistance. A similar value of cardiac output (2.6 l/min) was in fact chosen for a previous counterpulsation study [25].

In agreement with the observation by Wolf and Clinch [134] this MCS does not include the right ventricle and atrium nor the pulmonary circulation because the effects of IABP assistance are not relevant to these components.

The way in which terminal resistance was implemented at the end of each branch prevented the possibility of readily adjusting the resistances in order to simulate conditions of vasoconstriction or vasodilation. However, these fixed resistances and their distribution were based on published data. Resistance was not adjusted by regulation of R_t in order to tune the system until flow distribution was satisfactory or until the shape and amplitude of the hemodynamic signals were physiological. Instead, this method provides

certainty that during IAB pumping the flow generated by the IAB will be distributed in a physiological way through each aortic branch.

The mechanism of coronary systolic flow impediment was not reproduced in the MCS, consequently leading to predominantly systolic coronary flow in the system. A physiologic value of mean coronary microvascular resistance, based on patient data [145], was however implemented in both coronary vessels, leading to admittedly not accurate shape of coronary blood flow, but to realistic mean coronary flow. Given that the MCS was designed to study the IABP, and that coronary flow augmentation is an important parameter in this context, it was attempted to measure coronary flow in fully opened coronary vessels in the MCS, to confirm that quantification of coronary augmentation in the absence of the mechanism of coronary systolic flow impediment would be misleading. A sample of coronary flow at the horizontal position is presented in Figure 6.14a. From observation of this trace and from the comparison with an *in vivo* trace of coronary flow during counterpulsation (Figure 6.14b), it is clear that the coronaries in the current model are perfusing during systole and do not present the flow pattern typical of coronary flow. Despite the balloon contribution being easily recognisable on the traces, information extracted from such signals would be inaccurate. As indicated in the Future work section of Chapter 8, implementing the mechanism of coronary systolic flow impediment would be a substantial improvement to the current design.

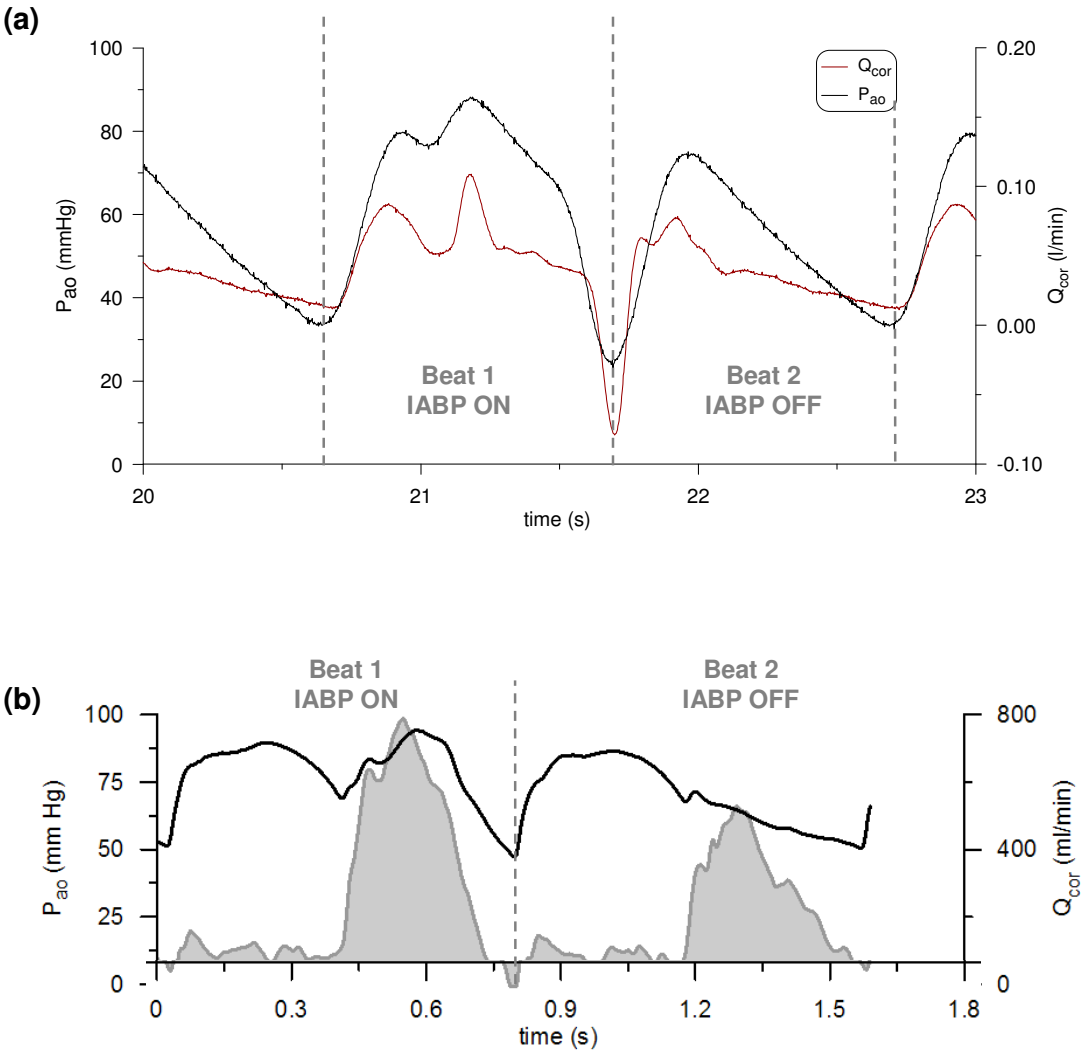

Figure 6.14: Sample of coronary flow measured in the MCS in fully open right coronary at the horizontal position (a). An assisted and a non-assisted beat are presented. It is clear, especially from the non-assisted beat, that qualitatively the trace exhibits aortic flow characteristics rather than coronary flow characteristics. This is due to the absence of the coronary systolic flow impediment mechanism in the MCS. Comparison with an in vivo coronary flow trace from unpublished data obtained by Louisville University and analysed by the Biofluid mechanics group at Brunel University (b) highlights the not physiological shape of coronary flow in the MCS.

The dicrotic notch was not adequately reproduced in the aortic pressure signal at valve closure (Figure 6.11). Despite the absence of the dicrotic notch, the ability to regulate the length of systole and diastole from the software controlling the driver provides accurate knowledge of the onset of diastole without the necessity for a visual marker, such as the notch. Therefore, the onset balloon inflation can still be set at the beginning of diastole, as appropriate. Further tuning is also possible from the console of the IABP.

Several studies about MCSs in the literature suggest that a solution of water and glycerine is a suitable blood analogue. The recommended percentage of glycerine in the solution varies between 30% [146] and 40% [138]. The present study however was not focusing on viscous effects and therefore water alone was used as test fluid. Alongside other example of MCSs employing water alone as flowing medium [151-153], Papaioannou et al. chose water as flowing medium for an MCS designed to test the effect of compliance specifically on IABP effectiveness [25]. In addition, McMahon et al. [133] also used water as circulating fluid in a hydraulic model of the circulation for IABP testing and pointed out that viscous effects "are not likely to modify substantially the phenomena of balloon opening and closing". In terms of the design of the MCS, which is the focus of this Chapter, different flowing medium would result in a need to change the capillaries implementing R. In fact the viscosity (μ) of an aqueous glycerine solution (40% glycerine) is μ = 3.72 mPa·s at 20°C [154], whereas for water alone μ = 1.002 mPa·s at 20°C. Given R = ΔP/Q, and that ΔP is proportional to μ according to $\Delta P = \frac{8\mu LQ}{\pi r^4}$ (Hagen-Poiseuille equation) then the capillary lengths would have to be shorter in order to achieve them same R. On the other hand, flow distribution would not be affected by this change, with

the more irrigated vessels still receiving a larger proportion of Q and overall physiological flow distribution. Considering that a main parameter of interest is the amount displaced retrograde by the balloon and the variations of this quantity with angle, this parameter is not likely to be affected by variations in μ. In fact, flow observations in the MCS are mostly focused on the region corresponding to the ascending and descending aorta and "the effect of using lower viscosity fluid on the flow profile [is] negligible due to the typical high Womersley number (> 10) in the large vessels" [155], where the Womersley number is the dimensionless quantity expressing the relation between pulsatile flow frequency and viscous effects.

In this MCS, compliance was distributed according to the theoretical model and not set in order to "tune" the signals generated by the driver. Branches with a similar value of R can exhibit substantial differences in their value of C, as in the case of the splenic and the mesenteric arteries, with the mesenteric being about 13 times more compliant (Table 6.1). For this reason, equal attention was put on the distribution of C as for the distribution of R. Furthermore, measured C (0.94 ml/mmHg) was in good agreement with the value proposed in the Stergiopulos model (1 ml/mmHg).

The MCS was compact enough to be positioned on a hinged platform. This characteristic represents an advantage of the MCS and is of clinical relevance, since it allows varying the inclination of the MCS simulating the commonly adopted semi-recumbent position in the ICU. This characteristic of the MCS will be fully exploited in the work presented in Chapter 7 of this thesis, investigating the effect of angle on the balloon when the IABP is counterpulsating with the LV.

Another advantage of the current MCS is the very flexible driver that was used to generate flow. It allowed direct control of stroke volume and heart rate as well as selection of different diastolic duration. This driver is independent of the afterload and generates reproducible flow profiles.

Finally, the MCS is regarded as sufficiently simple and flexible to allow other VADs to be studied with some modifications. It is envisaged that acute hemodynamics of destination therapy devices could be tested by removing the driver and LVAD (Abiomed) altogether and replacing them with the new device to be investigated. Some modifications to the MCS would be required in this case.

6.6. Conclusion

A MCS was designed and tested with an IABP application. The system had physiological distribution of terminal resistance and compliance. The simulation of IABP counterpulsation was successful, exhibiting major features such as early diastolic pressure augmentation and end-diastolic pressure reduction together with inflation and deflation volume displacement. Further IABP testing in the MCS will be carried out, exploiting the advantage of the MCS being positioned on a hinged platform simulating the semi-recumbent position, as described in Chapter 7.

CHAPTER 7

THE EFFECT OF ANGLE ON IABP MECHANICS:

MEASUREMENTS IN THE MOCK CIRCULATORY SYSTEM

7.1. Introduction

Mock circulatory systems (MCSs) have been successfully employed over the years as test beds for ventricular assist devices (VADs) and for other cardiovascular applications. Limiting the examples to recent literature, in 2004 a pulsatile mock circulation loop was used to test a centrifugal pump as a biventricular VAD [156]. In 2005 *in vitro* experiments were conducted in a mock loop to study the MicroMed DeBakey VAD [157] and a mock loop comprising of both systemic and pulmonary circulations was used to test a prototype LVAD [158]. Evaluation of a naturally shaped silicone ventricle was carried out in a mock circulatory loop in 2009 [159] and a mock loop was also used as a tool in the development of an algorithm, as in the case of a MCS with sheep blood in which an artificial heart was tested to identify a possible method for failure detection [160]. Heart valves have also been tested in mock circulation, including mechanical valves, such as the Omnicarbon tilting disc valve [161], and prosthetic valves, such as the On-x mitral valve [162]. MCSs can also be used as a term of comparison for the evaluation of computational [163] and numerical models [164]. In addition, a MCS can be used as a teaching tool [165]. This highlights the versatility of MCSs as a tool in cardiovascular research.

As discussed in the previous chapter, specific MCSs with various degrees of complexity have also been developed for the application of IABP

testing [135, 137, 138]. As part of the present work, a new mock loop with physiological distribution of terminal resistance and compliance has been proposed for this application in Chapter 6, where the designs steps have been described and the pilot measurements showed that this MCS was able to reproduce physiological signals both in the absence of and during IABP counterpulsation.

Following from previous observation about the effect of posture on IABP operation, from the literature [90] and from this work, it is now aimed to investigate the effect of angle on IABP operation when the balloon is counterpulsating with the left-ventricle (LV) in an anatomically correct and physiologically resembling setup. The clinical relevance of testing the IABP at varying inclinations is linked with the semi-recumbent position [88, 89]. Merging knowledge from previous chapters, it has been suggested that angle affects IABP performance, in terms of duration of inflation and deflation (Chapter 4), end-diastolic pressure reduction (Chapter 5) and flow-volume displacement in the direction of the coronary circulation (Chapters 3 and 5). These parameters will be further tested at a range of angles while simulating *in vitro* the principle of counterpulsation. Also, having established knowledge about the wave intensity pattern associated with the IABP alone at the horizontal position(Chapter 5), it is aimed to observe the changes in the energy carried by the inflation and deflation waves at an angle with the IABP counterpulsating.

7.2. Materials and methods

The MCS used for this investigation is described in Chapter 6. Given that the artificial aorta was designed from the dimensions of a 175 cm tall patient

from the Westerhof model [143], a 40 cc balloon (Datascope) was the correct choice to fit the anatomy, according to Table 1.1.

The balloon was introduced via the left deep-femoral artery and pushed until it reached the thoracic aorta. More specifically, the tip of the balloon was positioned 2-3 cm below the departure of the left subclavian branch. However, once in place, the base of the balloon extended below the renal bifurcation. The balloon was driven with the IABP (System 98, Datascope) which was counterpulsating with the LV, represented by the BVS 5000 Abiomed VAD. The LV, as previously described, was driven by a stepper motor driver, which throughout these experiments was set to produce a cardiac output of 2.7 l/min. Heart rate was 60 bpm and diastolic time fraction was 68%. The IABP and the driver were synchronized and fine-tuning of onset of inflation of the balloon was further achieved using the slide controls on the IABP console. In order to observe changes induced by different assisting frequency, the latter was set at 1:1, 1:2 and 1:3.

Exploiting in full the portability of the MCS and its ability to operate at different inclinations, the semi-recumbent position was simulated and measurements were performed in the horizontal position and at angles of 10, 20, 30 and 45°.

Aortic pressure (P_{ao}) was measured in the aortic arch using a 7F transducer-tipped catheter (Gaeltec), which was inserted via the right deep-femoral artery. Balloon shuttle gas pressure was measured as a reference of the balloon cycle with a 5F transducer-tipped catheter (Millar). Flow was measured at the aortic root with a 28 mm ultrasonic flowprobe (Transonic) and just below the left subclavian artery with a 20 mm ultrasonic flowprobe (Transonic). The latter (Q_{tip}) was recorded in order to identify the full

contribution of balloon inflation and deflation on the flow pattern, before part of the flow-volume displaced by the inflating/deflating balloon was dispersed in the arch vessels. Although the major effects of balloon counterpulsation do not reflect on carotid flow and subclavian flow, both these measurements were performed in order to monitor mean flow in the arch vessels. Hence, carotid flow was measured in the right carotid with a 10 mm ultrasonic flowprobe (Transonic) and subclavian flow was measured in the right subclavian with a 8 mm ultrasonic flowprobe (Transonic). Because the MCS cannot replicate the mechanism of coronary systolic flow impediment, there was no interest in monitoring coronary flow. A schematic representation of the locations where the measurements were performed can be found in Figure 7.1. The pressure sensors were calibrated with the method of the column of water. The flow-measuring equipment was calibrated *in situ* before the measurements with the method of timed collection.

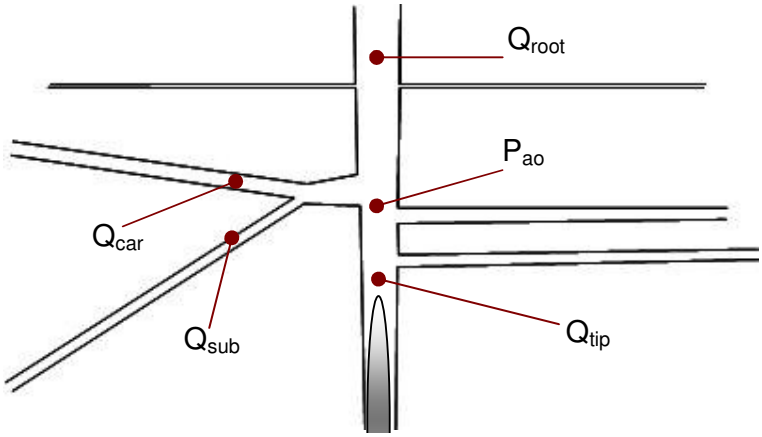

Figure 7.1: Schematic representation of the aortic arch, showing the position of the tip of the balloon 2 cm below the left subclavian. Measurement sites are indicated with red circles: P_{ao}, aortic pressure; Q_{tip}, aortic flow at the tip of the balloon before it is dispersed in the arch vessels;, Q_{root}, flow at the aortic root; Q_{car}, carotid flow; Q_{sub}, subclavian flow.

Data were acquired in Labview at 500 Hz and then processed in Matlab. For any combination of angle and assisting frequency, five control beats and five assisted beats were analysed and averaged. In the case of assisting frequency of 1:3, one non-assisted beats following each assisted one was also analysed. The effectiveness of balloon counterpulsation was quantified in terms of

- diastolic aortic pressure augmentation (DPA, Figure 7.2), as a measure of the benefit of balloon inflation in terms of pressure
- end-diastolic pressure reduction (EDPR, Figure 7.2), as a measure of the benefit of the unloading action of balloon deflation
- retrograde volume displacement (V_{up}), as an indication of the benefit of balloon inflation in terms of flow; this volume was calculated by integrating the negative peak in Q_{tip} during balloon inflation as shown in Figure 7.3.

The way in which the inflation volume was calculated from Q_{tip} was based on previous observations (Chapter 3 and Appendix A): since recirculation and reversed flow are observed in late balloon inflation before the onset of deflation, it is preferred to quantify the inflation volume on the basis of the volume displacement towards the arch rather than the net volume displaced over the whole inflation phase.

Wave intensity analysis was performed in order to study the wave pattern during balloon counterpulsation and quantify any changes deriving from the variation in angle. As shown in Chapter 4, when a horizontal balloon operates without systolic flow it generates a backward compression wave during inflation and a backward expansion wave during deflation. Flow velocity U was derived from Q_{tip} by dividing with the nominal cross-sectional area of the 20 mm flowprobe and wave intensity analysis was applied to phasic P_{ao} and U

corresponding to adjacent measuring sites retrograde the balloon tip. Wave speed was calculated with the PU loop method [109] and separated forward and backward wave intensities were computed. From the integration of the dI_+ pattern over time it was possible to calculate the energy carried by the backward compression and expansion waves, during inflation and deflation respectively.

Since the 40 cc balloon extended below the renal bifurcation, the effect of choosing the wrong balloon with respect to patient size was shown in this study by inserting also a 25 cc instead of the 40 cc balloon and repeating all the same measurements of pressure and flow over the same range of angles. IABP settings and settings of cardiac output and heart rate were kept constant. The difference induced in the system by using the smaller 25 cc balloon consists mainly in the balloon chamber not extending below the renal bifurcation, according to IABP guidelines. This is shown in Figure 7.4.

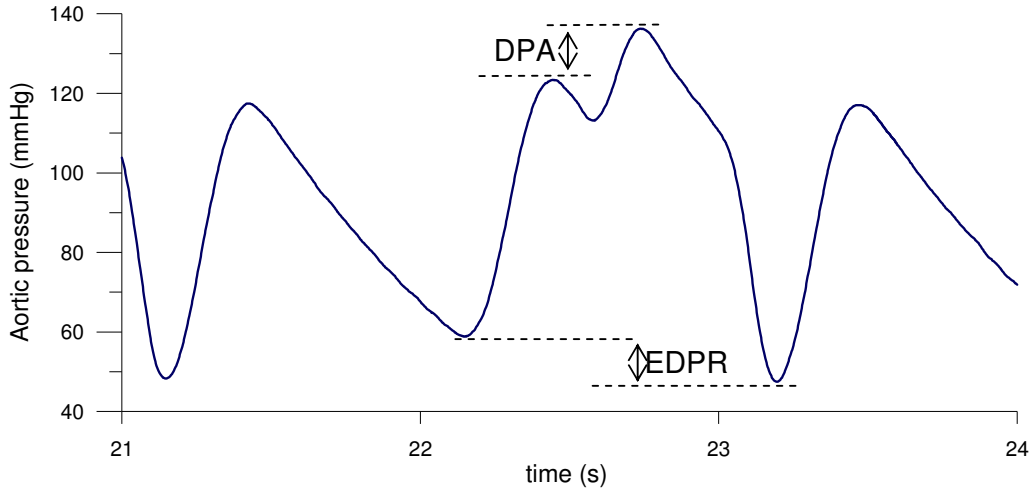

Figure 7.2: An example of the aortic pressure signal measured during IABP counterpulsation with the 25 cc balloon in the MCS. Diastolic pressure augmentation (DPA) and end-diastolic pressure reduction (EDPR) are shown on the assisted beat.

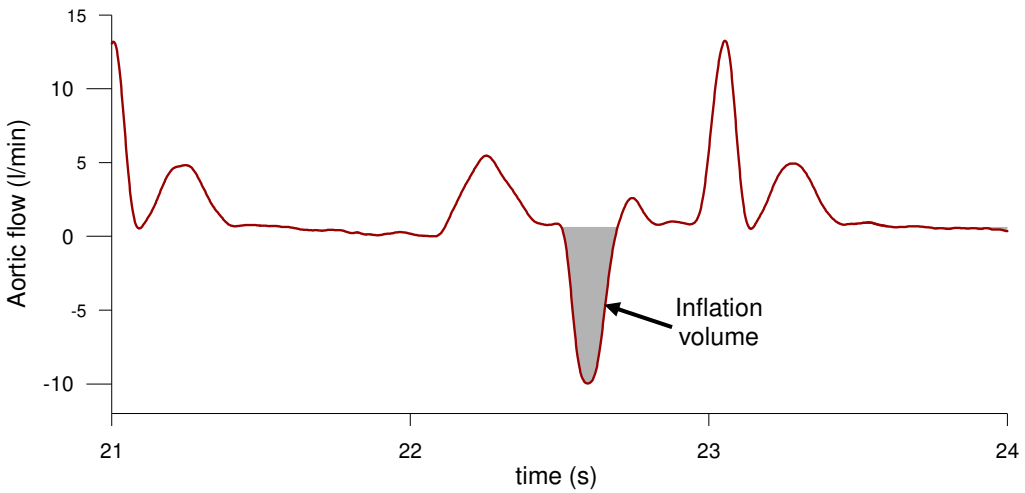

Figure 7.3: An example of the aortic flow signal measured during IABP counterpulsation with the 25 cc balloon in the MCS. The trace represents Q_{tip}, i.e. flow measured before the aortic arch with the 20 mm ultrasonic flowprobe. The volume displaced during balloon inflation is shown by the shaded area.

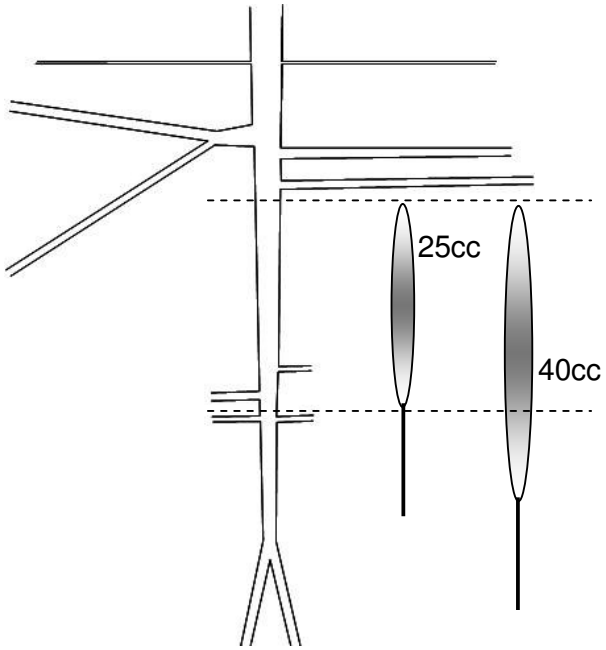

Figure 7.4: Both a 25 cc and 40 cc balloon were tested in the aorta, demonstrating the effect of choice of balloon size. As shown, the 40 cc in this case extended below the renal bifurcation.

7.3. Results

7.3.1. The 25 cc balloon

Pressure measurements highlighted the effect of angle and assisting frequency on DPA (Figure 7.5a) and EDPR (Figure 7.5b). DPA was significantly reduced with increasing angle at 1:1 ($p < 0.05$) and 1:3 ($p < 0.005$). EDPR was reduced significantly at all frequencies ($p < 0.05$ or smaller). In both cases, 1:1 ratio produced a larger benefit, in terms of a more substantial DPA or EDPR.

Flow measurements showed that V_{up} did not vary either with angle or with assisting frequency (Figure 7.6). It was also observed that a larger proportion of balloon volume is displaced in the retrograde direction rather than towards the renal arteries. In the horizontal case, V_{up} was 79% of balloon volume (19.8 ml), from V_{up} displaced on average at the three different assisting frequencies.

The WIA pattern associated with counterpulsation is shown in Figure 7.7.

From wave intensity results, the BCW (Figure 7.8a) was significantly reduced with increasing angle at 1:1 ($p < 0.005$) and 1:3 ($p < 0.05$). The BEW (Figure 7.8b) was also significantly reduced with increasing angle at 1:1 and 1:3 ($p < 0.05$), this mirroring the case of DPA and EDPR. These results also confirmed that 1:1 assistance generated a larger benefit, since at this frequency both BCW and BEW carried higher energy.

In addition, the incremental change in angle did not show a marked effect of mean carotid flow. Comparing the horizontal (Figure 7.9a) and 45° angle (Figure 7.9b) case, mean Q_{car} of the assisted beats remained constant at all assisting frequencies. Instead, it was not possible to identify a clear pattern of variations in subclavian flow. Mean Q_{sub} at the horizontal case and at 45° angle is shown in Figure 7.10a and 7.10b respectively.

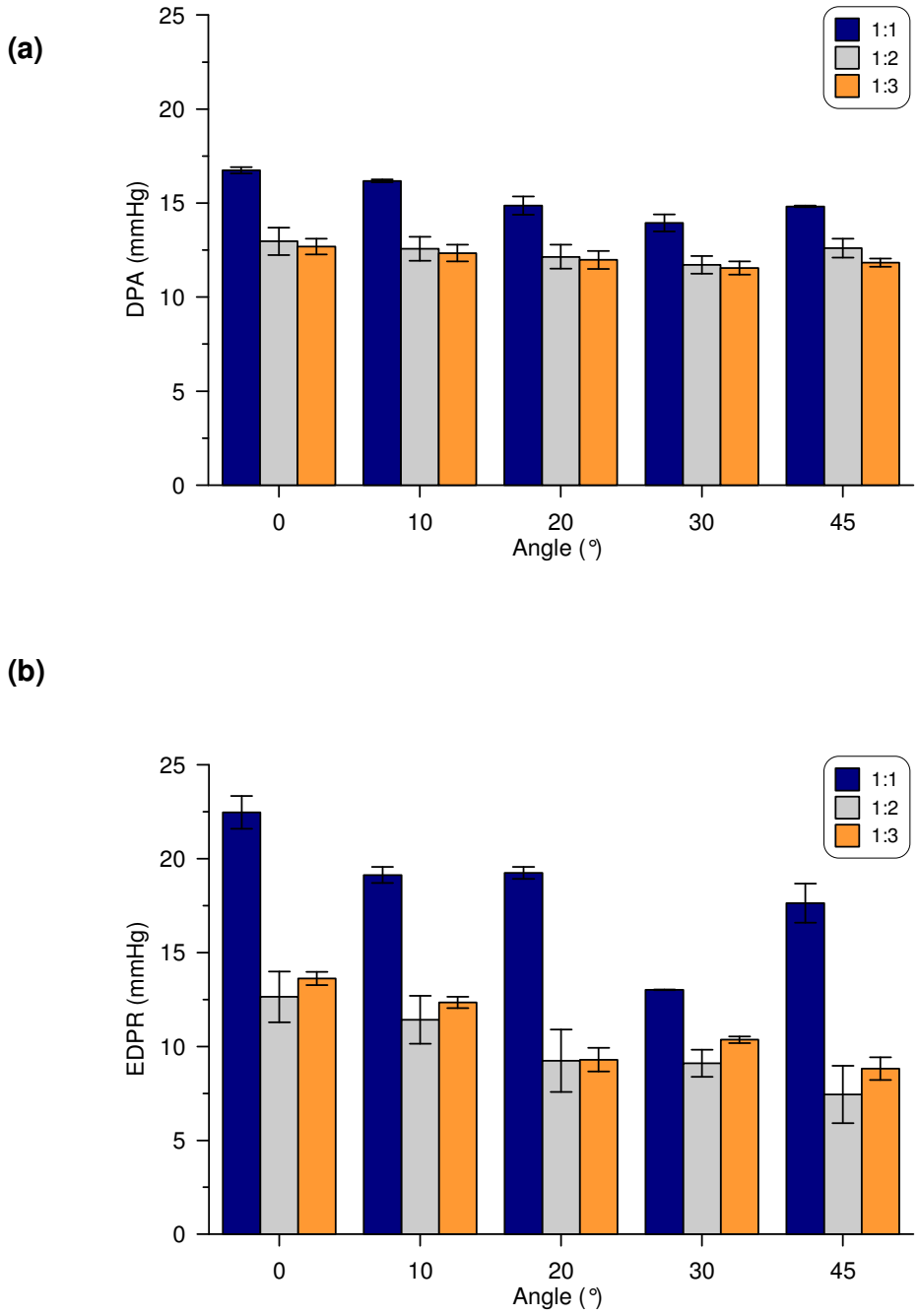

Figure 7.5: Changes in diastolic pressure augmentation, DPA (a) and end-diastolic pressure reduction, EDPR (b) with increasing angle for the 25 cc balloon. Each bar represents the average of 5 measurements and error bars represent SD.

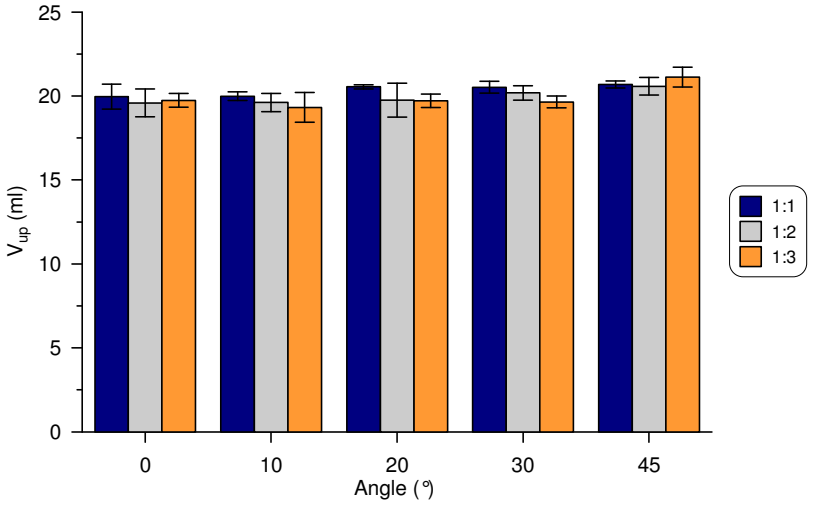

Figure 7.6: Changes in flow-volume displacement opposite to the balloon tip in the direction of the coronary circulation with increasing angle for the 25 cc balloon. Each bar represents the average of 5 measurements and error bars represent SD.

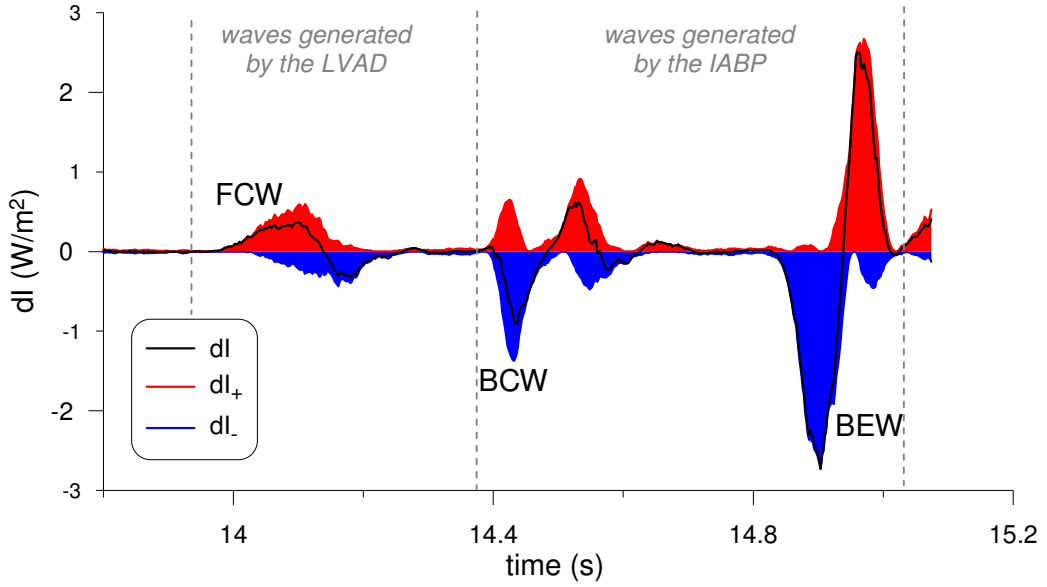

Figure 7.7: The wave intensity pattern associated with balloon counterpulsation in vitro. A full assisted heart beat is depicted. Left-ventricular ejection is associated with a forward compression wave (FCW). During balloon assistance, a backward compression wave (BCW) associate with balloon inflation and a backward expansion wave (BEW) associated with balloon deflation can be identified.

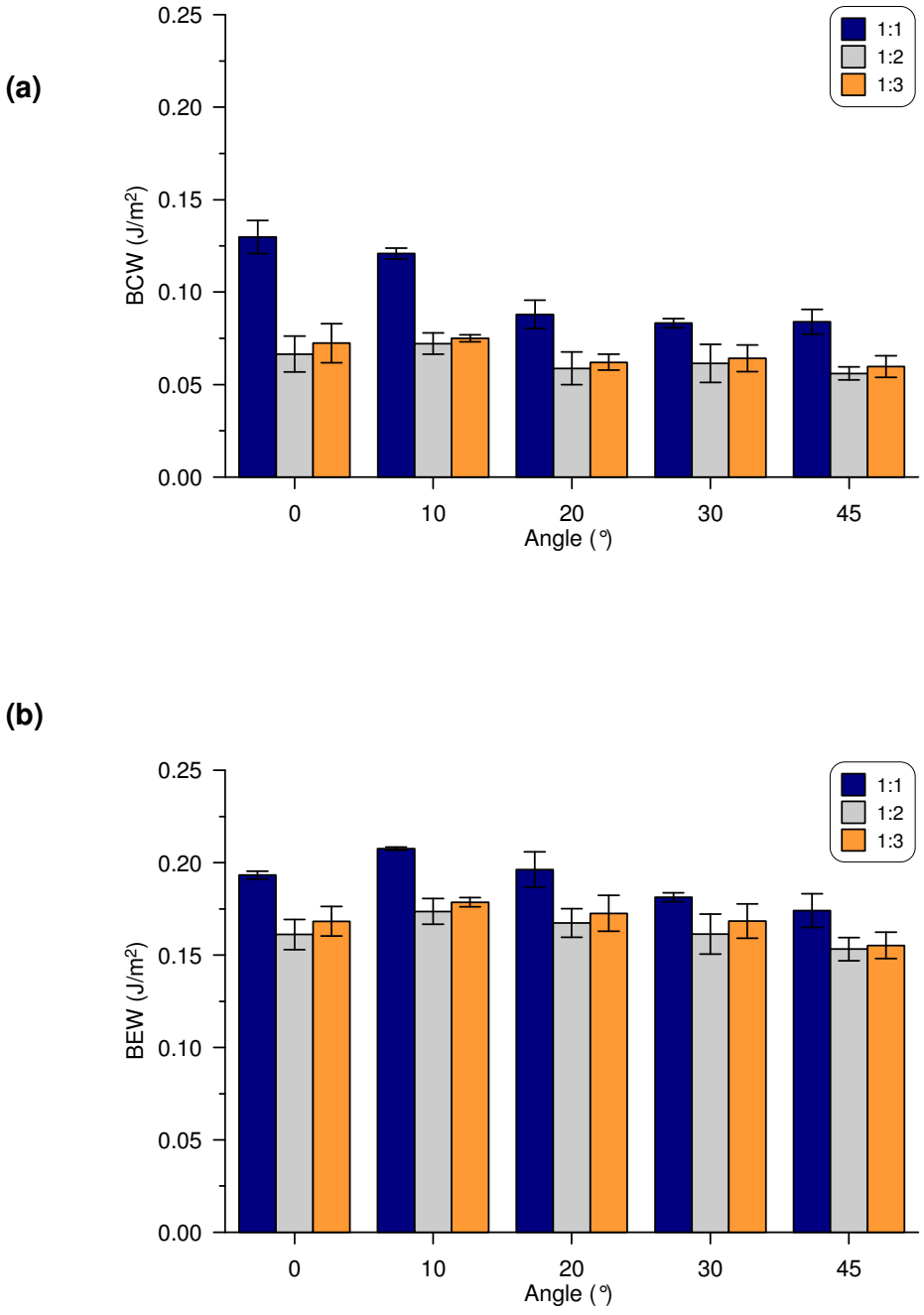

Figure 7.8: Changes in the energy carried by the BCW associated with balloon inflation (a) and the BEW associated with balloon deflation (b) with increasing angle for the 25 cc balloon. Each bar represents the average of 5 measurements and error bars represent SD.

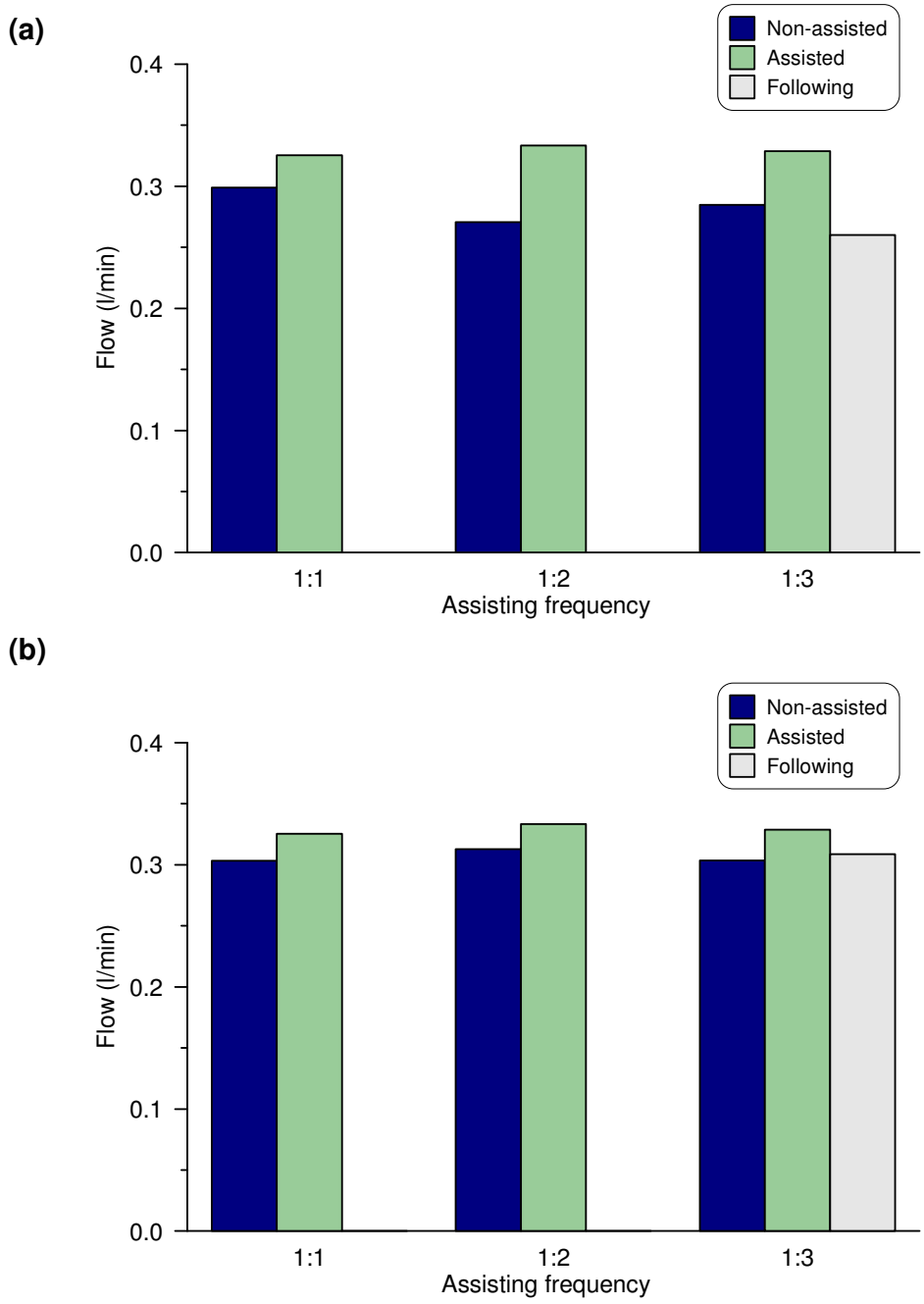

Figure 7.9: Changes in mean flow in the right carotid artery during balloon assistance (25 cc balloon). Mean flow for each assisting frequency is reported for the assisted beats, their preceding non-assisted beats and, in the case of 1:3 assisting frequency, also for the non-assisted beats following the assisted ones. The horizontal (a) and 45° angled case (b) are depicted.

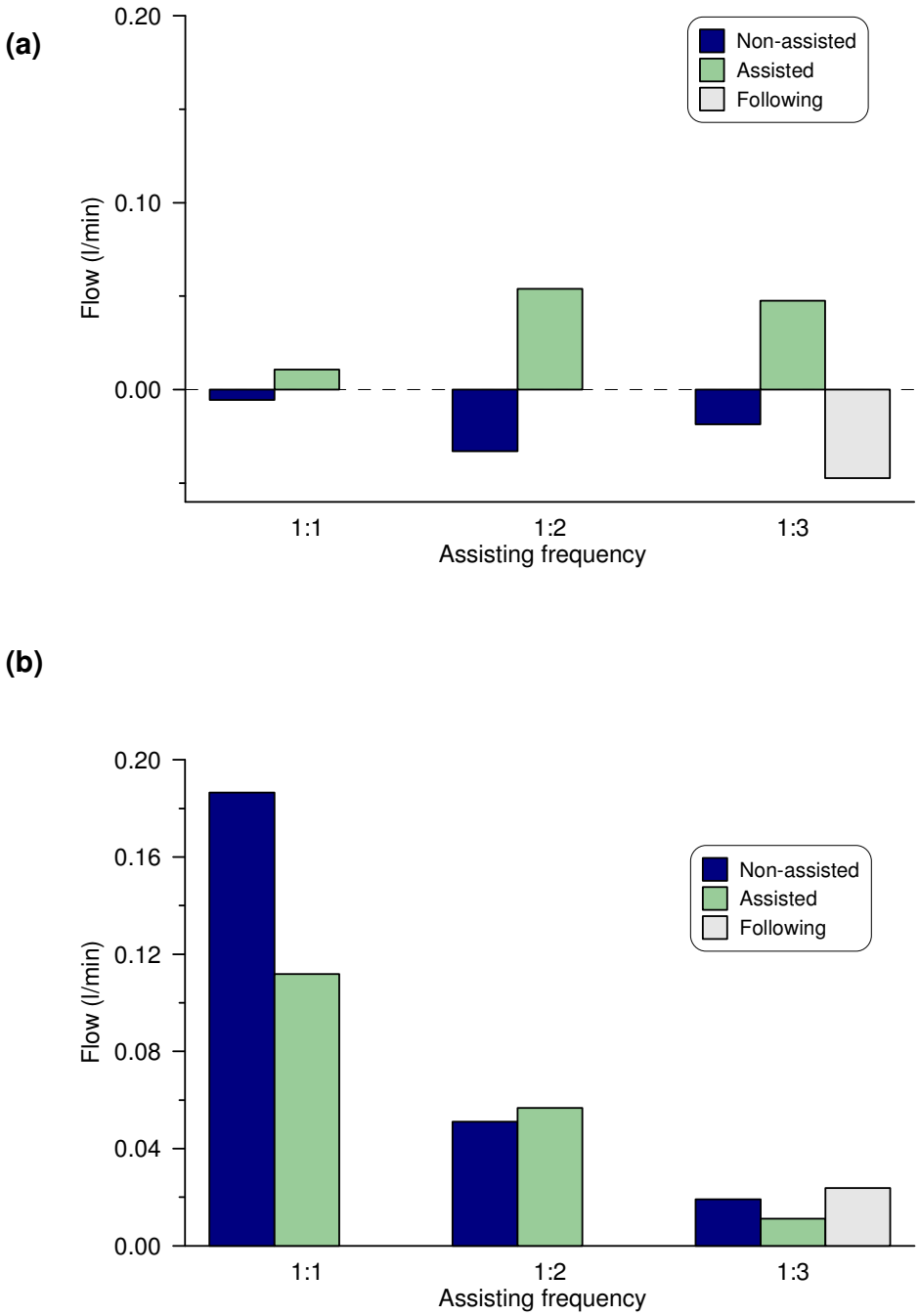

Figure 7.10: Changes in mean flow in the right subclavian artery during balloon assistance (25 cc balloon). Mean flow is reported for each assisting frequency for the assisted beats, their preceding non-assisted beats and, in the case of 1:3 assisting frequency, also for the non-assisted beats following the assisted ones. The horizontal (a) and 45° angled case (b) are depicted.

7.3.2. The 40 cc balloon

Measurements performed with the 40 cc balloon in the MCS showed similar results as those described for the 25 cc balloon, but in some cases – as shown below – the effect of angle was more pronounced.

DPA (Figure *7.*11a) was significantly reduced with increasing angle at all assisting frequencies ($p < 0.005$ or smaller). Equally EDPR (Figure 7.11b) was significantly reduced across the range of operating angles ($p < 0.005$) and in this case it is interesting to note that at 45° EDPR has negative values. This observation indicates that the deflation benefit is lost at the highest angle (end-diastolic pressure cannot be lowered).

In opposition to the 25 cc flow-volume results, in this case V_{up} was reduced at 45° by 15% compared to the horizontal position (Figure 7.12). This reduction was significant for all frequencies ($p < 0.05$ for 1:1, $p < 0.005$ for 1:2, $p < 0.001$ for 1:3).

Wave energy also showed a reduction due to angle. Both BCW (Figure 7.13a) and BEW (Figure 7.13b) were significantly reduced from 0 to 45° (always $p < 0.0001$).

As for the case of the 25 cc balloon, mean values of Q_{car} and Q_{sub} are provided (Figure 7.14 and 7.15 respectively).

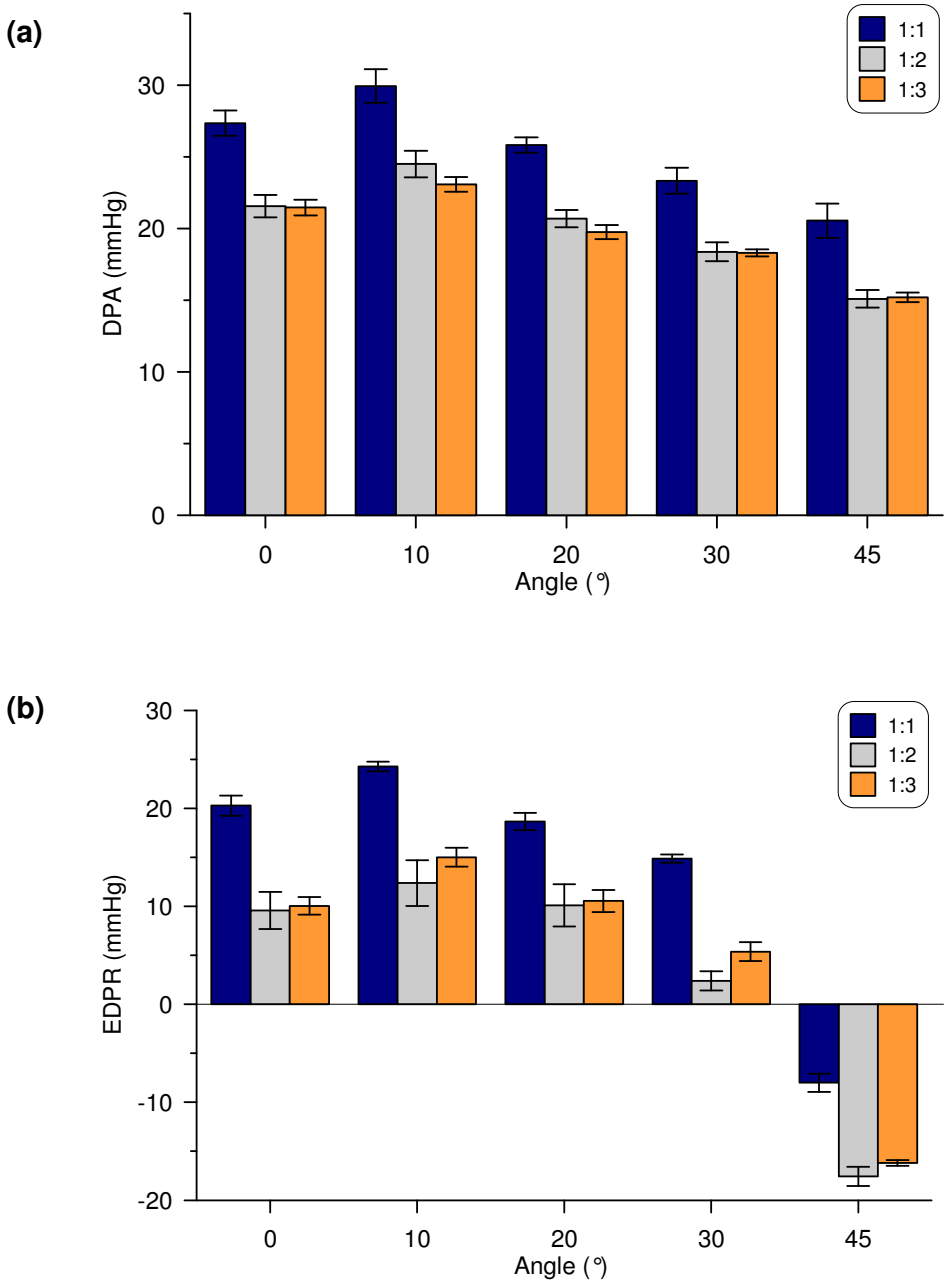

Figure 7.11: Changes in diastolic pressure augmentation, DPA (a) and end-diastolic pressure reduction, EDPR (b) with increasing angle for the 40 cc balloon. Each bar represents the average of 5 measurements and error bars represent SD. In (b) negative pressure values at 45° angle indicate the inability of balloon deflation to reduce end-diastolic pressure.

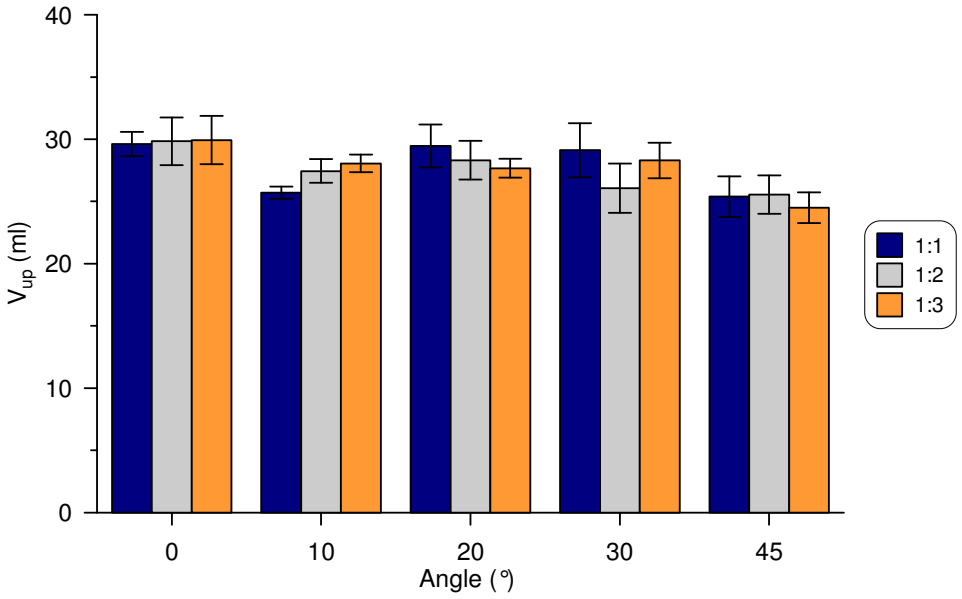

Figure 7.12: Changes in flow-volume displacement opposite to the balloon tip in the direction of the coronary circulation with increasing angle for the 40 cc balloon. Each bar represents the average of 5 measurements and error bars represent SD.

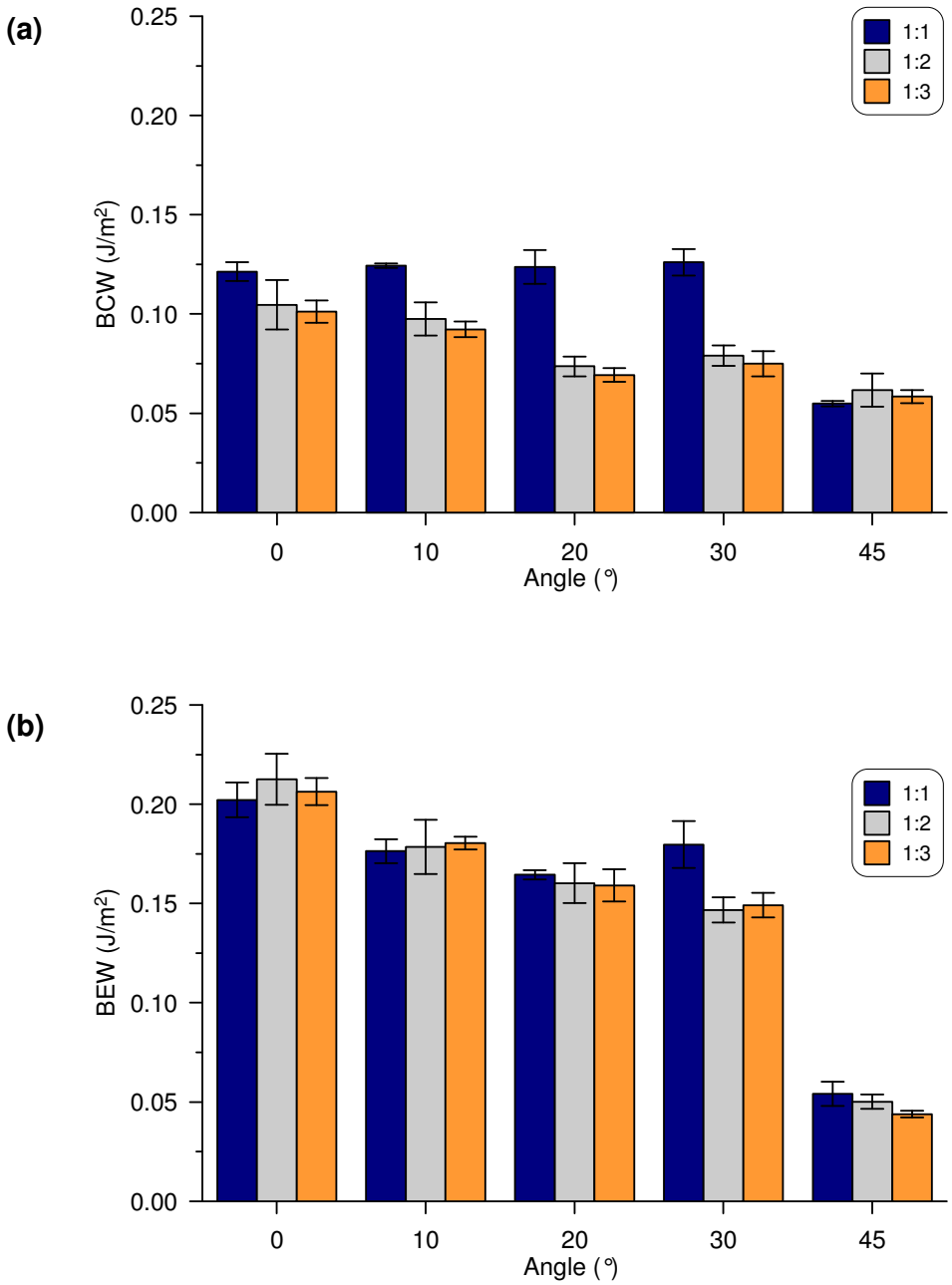

Figure 7.13: Changes in the energy carried by the BCW associated with balloon inflation (a) and the BEW associated with balloon deflation (b) with increasing angle for the 40 cc balloon. Each bar represents the average of 5 measurements and error bars represent SD.

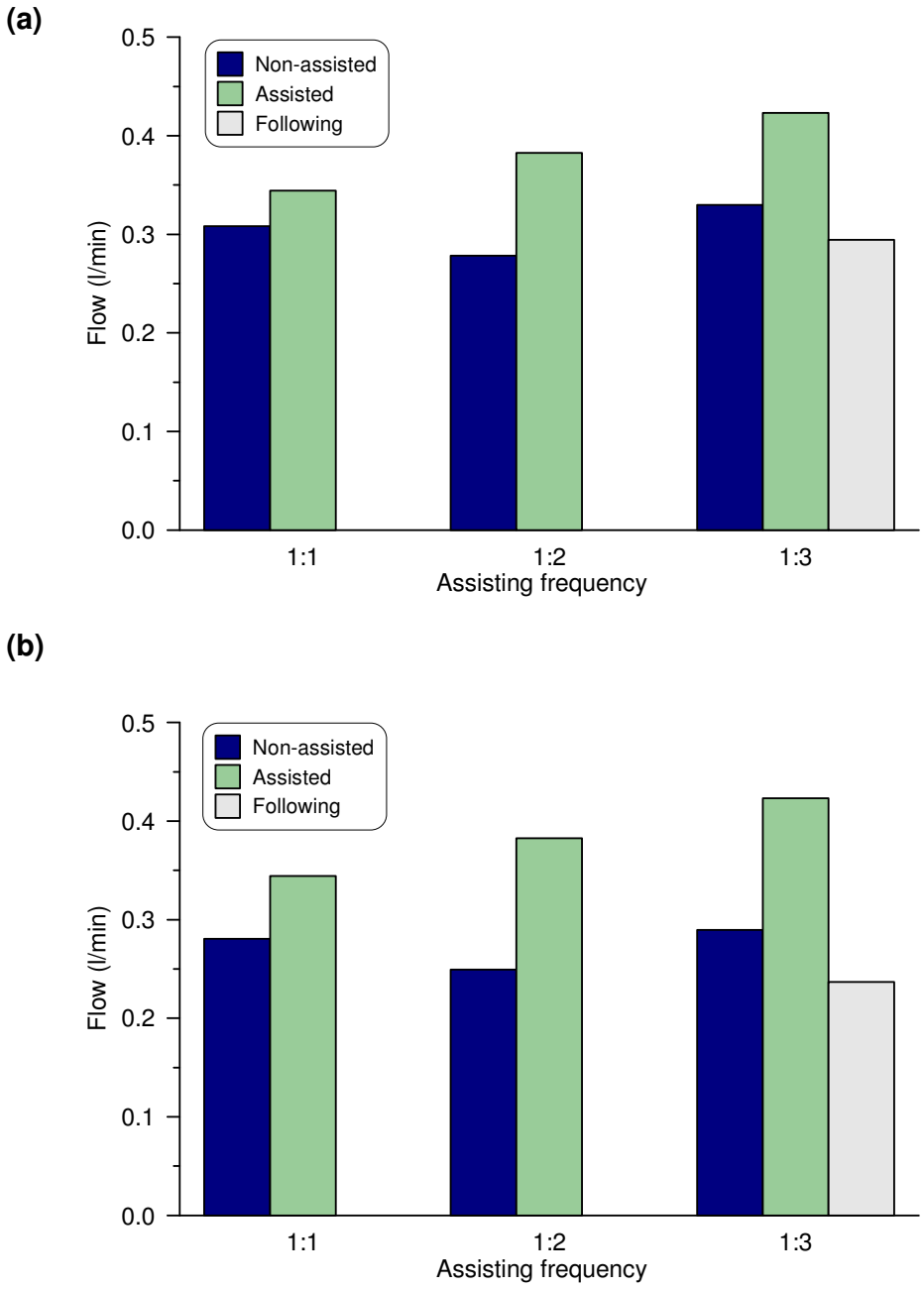

Figure 7.14: Changes in mean flow in the right carotid artery during balloon assistance (40 cc balloon). Mean flow for each assisting frequency is reported for the assisted beats, their preceding non-assisted beats and, in the case of 1:3 assisting frequency, also for the non-assisted beats following the assisted ones. The horizontal (a) and 45° angled case (b) are depicted.

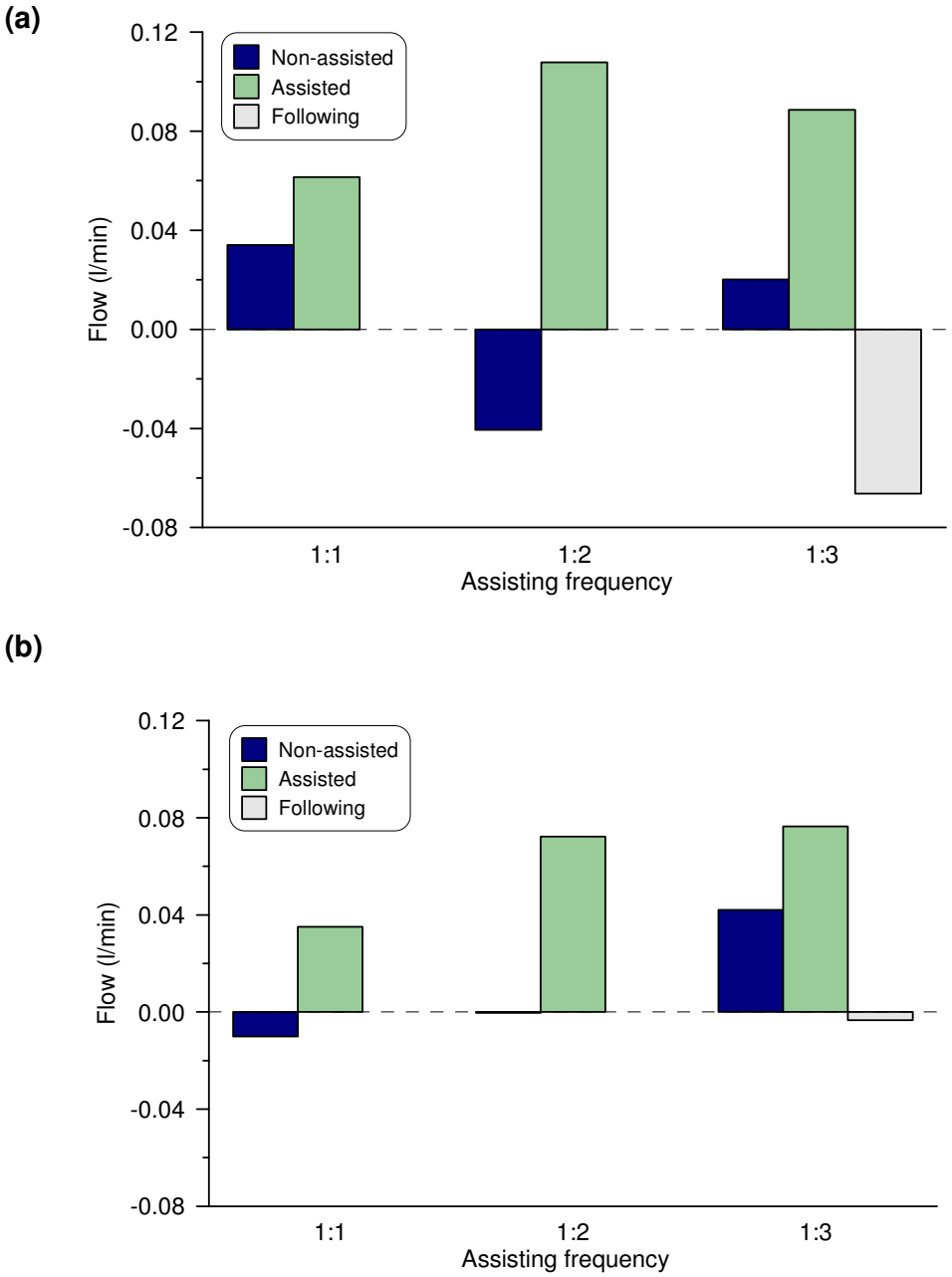

Figure 7.15: Changes in mean flow in the right subclavian artery during balloon assistance (40 cc balloon). Mean flow for each assisting frequency is reported for the assisted beats, their preceding non-assisted beats and, in the case of 1:3 assisting frequency, also for the non-assisted beats following the assisted ones. The horizontal (a) and 45° angled case (b) are depicted.

7.4. Discussion

This study focused on the effect of angle on balloon mechanics during counterpulsation. It was carried out in the MCS described in Chapter 6, which provided physiological distribution of terminal resistance and compliance. A 25 cc balloon and a 40 cc balloon were tested. Results showed that both diastolic aortic pressure augmentation and end-diastolic aortic pressure reduction are reduced with increasing angle. On the other hand, V_{up} remained unchanged over the range of angles for the 25 cc balloon, while it was reduced by about 15% at 45° in the case of the 40 cc balloon, showing that the balloon of incorrect size underperformed. Furthermore, wave intensity analysis was performed, offering an alternative way to assess the effect of angle on balloon inflation and deflation. As well as the effect angle, this study highlighted the impact of assisting frequency on balloon operation and especially on the pressure parameters.

In terms of pressure, DPA and EDPR have been analysed, chosen as indicators of the action of balloon inflation and deflation respectively. EDPR was more affected by an increment in angle. For the case of the 25 cc balloon, an average (taking into account the three different assisting frequencies) reduction of 32 ± 9.7 % was observed from 0 to 45°. This suggests that the benefit associated with balloon deflation, namely the unloading action resulting in reduced LV afterload, is jeopardized by the angled position. Taking into account EDPR and DPA it was also observed that in both cases operating the balloon at assisting frequency of 1:1 resulted in increased EDPR and DPA. Specifically, in the horizontal position, EDPR was 78% higher than 1:2 and 65% higher than 1:3 and DPA was 29% higher than 1:2 and 32% higher than 1:3, likewise in the

angle position EDPR was 138% higher than 1:2 and 100% higher than 1:3 and DPA was 18% higher than 1:2 and 26% higher than 1:3. These results suggest that a possible increased benefit may be achieved both in terms of inflation (DPA) and deflation (EDPR) when operating the IABP at 1:1, assisting every heart beat.

A similar picture emerges when considering the pressure results obtained with the 40 cc balloon counterpulsating in the MCS. As for the 25 cc, increasing angle resulted in a reduction of DPA and EDPR, with assisting frequency 1:1 again yielding better results than the other frequencies. The major difference to be highlighted is in terms of EDPR. At an angle of 45°, the deflating 40 cc balloon was not able to reduce end-diastolic pressure, as shown by the negative values of EDPR recorded at this position for all assisting frequencies. It should be noted that the 40 cc balloon was oversized for the dimensions of the artificial aorta. Results of EDPR indicate that a balloon of incorrect size may result in reduced (even lost) benefit of balloon deflation when operating at an angle, with 45° being a possible backrest angle for patients nursed in the semi-recumbent position.

Examining flow results, V_{up}, an indicator of coronary flow augmentation, was used to quantify the hemodynamic benefit associated with balloon inflation. The Q_{tip} signal clearly showed the volume displaced by balloon inflation before it gets partly dispersed in the arch vessels (Figure *7*.3). Overall, neither angle nor assisting frequency affected the amount of retrograde flow-volume displaced by the inflating balloon. Considering the 25 cc balloon, V_{up} was on average 19.8 ml at the horizontal position and 20.8 ml at the maximum angle (45°). This result suggests that the action of balloon inflation in terms of volume displacement is not affected by variations in posture, for all assistance ratios. Previous

observations in an artificial aorta but in the absence of counterpulsation (Chapter 4) have shown that the effect of increasing angle on V_{up} is related to the level of intra-luminal pressure, with flow-volume decreasing with increasing angle for low intra-luminal pressure (45 mmHg) and on the contrary flow-volume overall lower but unchanged by angle for high intra-luminal pressure (115 mmHg). Intra-aortic pressure in the MCS was about 97 mmHg. The behaviour of V_{up} – constant with increasing angle – is thus related to the level of intra-aortic pressure.

However, a different scenario was observed for the case of the 40 cc balloon. In this case, V_{up} was affected by increasing angle, with a reduction of 15% from 0 to 45°. This reduction was significant for all three assisting frequencies. It should be noted, though, that the net amount of V_{up} is larger when the 40 cc was pumping, despite this amount being affected by an increase in angle. Effectively, it is the larger balloon that displaces the more retrograde volume, resulting in larger inflation benefit.

Despite this difference, in both cases (25 and 40 cc balloons) the majority of balloon volume is displaced in the direction of the arch; just looking at the horizontal position, 79% and 75% of balloon nominal volume was displaced retrograde, for the 25 cc and 40 cc balloon respectively; this result confirms previous observations in latex tubes (Chapter 3) and in the artificial aorta (Chapter 4).

In addition to pressure and flow results, wave intensity analysis was performed in this study. The wave intensity pattern during balloon counterpulsation *in vitro* (Figure *7.*7) shows the FCW generated by LV ejection and its reflection from the periphery, the BCW associated with balloon inflation and the BEW associated with the suction generated by balloon deflation. It is

noted that the expansion wave due to LV relaxation usually seen in a conventional WIA aortic pattern here is not visible, because the mechanism operating the LVAD does not mimic LV relaxation. The BCW and BEW were previously identified *in vitro* (Chapter 4) in the absence of counterpulsation. Results of WIA suggest that this analysis can provide an alternative way to assess the effect of angle on the hemodynamic parameters under investigation.

Similar changes between hemodynamic parameters and wave energy were observed with changes in assistance frequency and angle. Pressure results showed that assisting frequency of 1:1 produced higher DPA and higher EDPR. The same can be observed about the energy carried by the BCW and BEW; particularly for the BCW, 1:1 assistance resulted in higher amount of energy. Further, an increase in angle induced a reduction both in DPA and BCW energy and similarly both in EDPR and BEW energy. These observations warranted further investigation of the relationship between pressure parameters of balloon benefit and wave energy.

Both for the 40 cc and the 25 cc balloon, significant correlations between DPA and BCW energy (Figure 7.16a) and between EDPR and BEW energy (Figure 7.16b) were found. There correlations highlight the fact that results from wave intensity analysis can be used as an alternative to assess the effect of angle on balloon mechanics. The wave intensity pattern can be an important tool in the understanding of its mechanical behaviour, containing a considerable amount of information related to the behaviour of the balloon. It is foreseen that wave intensity analysis could be a viable alternative for the quantification of the balloon benefits, both for inflation and deflation.

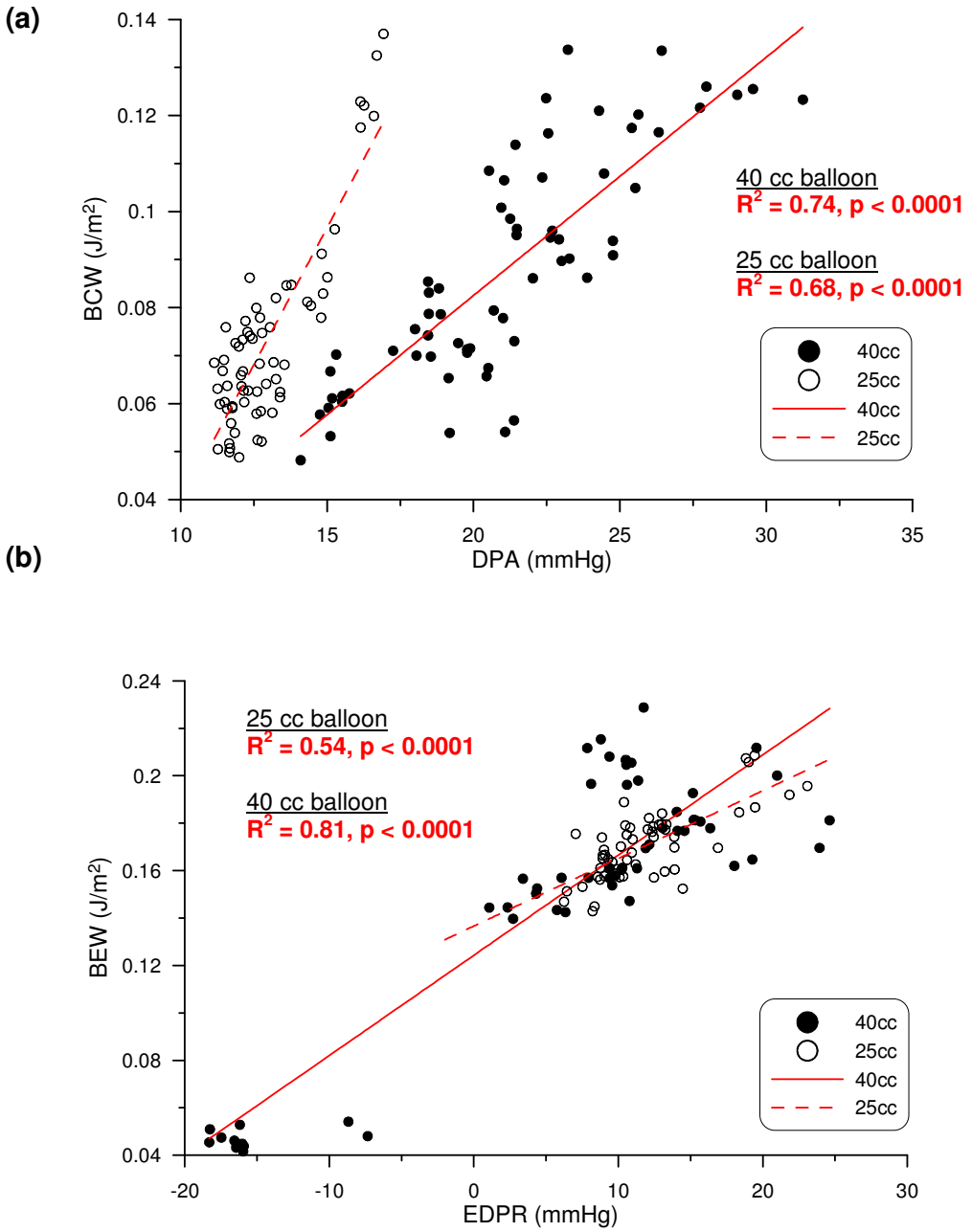

Figure 7.16: Correlation between diastolic artic pressure augmentation (DPA) and the energy carried by the backward compression wave (BCW) associated with balloon inflation for the 25 cc balloon (a) and the 40 cc balloon (b).

The usefulness of wave intensity analysis in assessing balloon performance raises a more general question: How should the benefits of balloon counterpulsation be assessed? First of all, in the context of this work, it is necessary to note that, although the MCS used for these measurements is more complex and more physiological than the setups described in Chapter 3 or Chapter 4, an *in vitro* investigation is always an approximation. So comparisons with the literature relative to IABP *in vivo* should be stated with caution. However, by referring to previous studies relative to the IABP, it is clear that there is not a commonly recognised method to quantify balloon performance. Performance indexes have been proposed, for example by Jaron et al. [63, 166] and by Kao and Ohley [77]. Besides, it is arguable whether the benefit of IABP counterpulsation should be assessed in terms of pressure or flow. Previous studies have supported the theory that the real benefit of IABP is its unloading action during deflation especially in the presence of coronary artery stenosis [59, 93, 167], disregarding the contribution to the coronary perfusion during inflation.

In the light of these observations, assessing the effect of increasing angle in terms of pressure, it is clear that the reduction of both DPA and EDPR indicates the negative effect of posture on balloon performance. Considering also the effect of increasing angle on volume displacement, especially considering the case of the 25 cc balloon which is the correct choice of balloon given the dimensions of the artificial aorta, it could be argued that increasing angle does not influence the inflation benefit of the balloon by observing the constant behaviour of V_{up}. These observations are based on this set of experiments but direct comparison with the *in vivo* case should be stated with caution.

Considering coronary perfusion augmentation, the MCS did not model the mechanism of coronary systolic flow impediment. Deductions about flow were mainly based on knowledge of Q_{tip}, which was regarded as a useful source of information since the total contribution of the inflating balloon is not yet dispersed into the arch vessels. On top of this, measurements of carotid and subclavian flow were performed. Correct flow distribution in the aortic arch was ensured in this case by the correct distribution of terminal resistance, previously demonstrated in Chapter 6. From the measurements of carotid and subclavian flow it was possible to identify the contribution of the inflating balloon, as shown in the examples provided in Figure *7.*17. Following from this observation, it is deduced that V_{up} – accounting for 79% and 75% of the balloon nominal volume for the 25 cc and the 40 cc balloon respectively – is partly distributed in the carotid and the subclavian vessels before reaching the coronary circulation.

An additional remark to be made about mean subclavian flow is that, as observed in Figure 7.10 and 7.15, the negative mean value of Q_{sub} suggests the possible presence of a steal phenomenon induced by balloon deflation. The steal phenomenon is usually observed in the coronary circulation, and a coronary-subclavian steal has been reported in the presence of coronary artery bypass graft (CABG) [168].

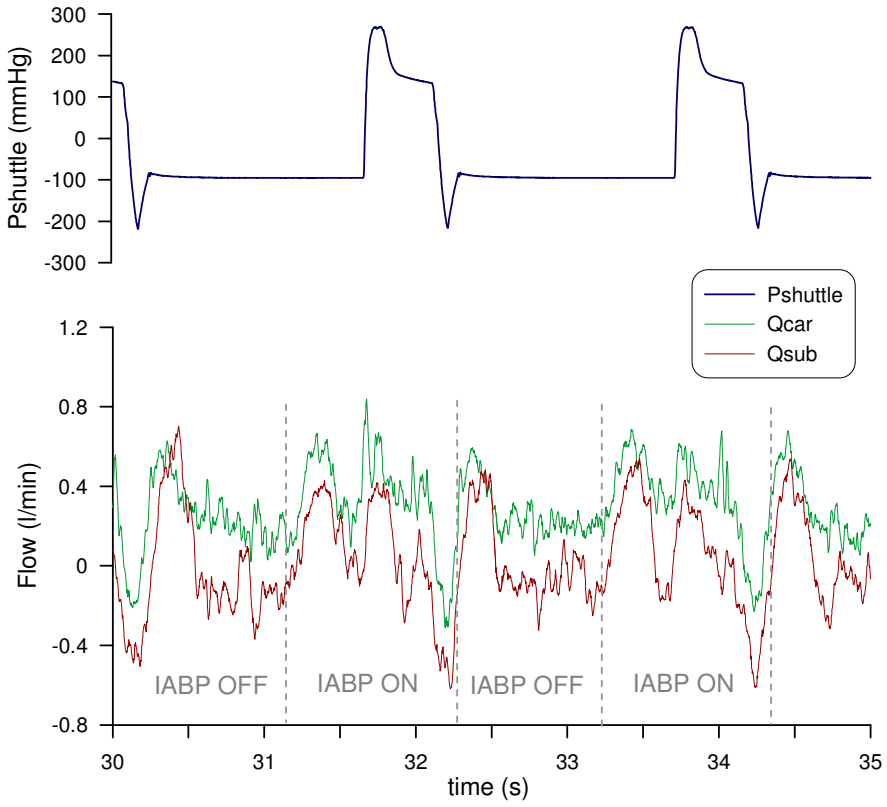

Figure 7.17: An example of flow measured in the right carotid (Q_{car}) and in the right subclavian (Q_{sub}) exhibiting the contribution of balloon inflation and deflation on the flow pattern. Shuttle gas pressure ($P_{shuttle}$) is also shown as a reference of the balloon cycle.

Finally, albeit not the original focus of the study, assisting frequency clearly emerged throughout the results as a parameter affecting the IABP, especially the pressure parameters, with 1:1 frequency emerging as the option that would deliver the greater benefit. This result is in agreement with an earlier observation, namely that, in the context of patient weaning, reduction of assisting frequency from 1:1 to 1:2 reduces augmentation of coronary perfusion and diastolic aortic pressure by 50% [169]. This observation was also extended

to the deflation phase. The greater benefit of continuous assistance is linked with the fact that the periodic action of the IABP during 1:1 lowers the baseline pressure at which the system operates, as indicated in Figure 7.18, while Q remains unaffected. Such a reduction indicates that, overall, peripheral resistance is also lower. Hence, pumping against a lower resistance, the balloon is operating more effectively. Moreover, the periodicity of 1:1 assistance in comparison with 1:2 and 1:3 results in lower inertial effects [170], supporting the fact that 1:1 assistance can generate larger DPA and EDPR (and also BCW and BEW), because the balloon motion in the fluid is less opposed to.

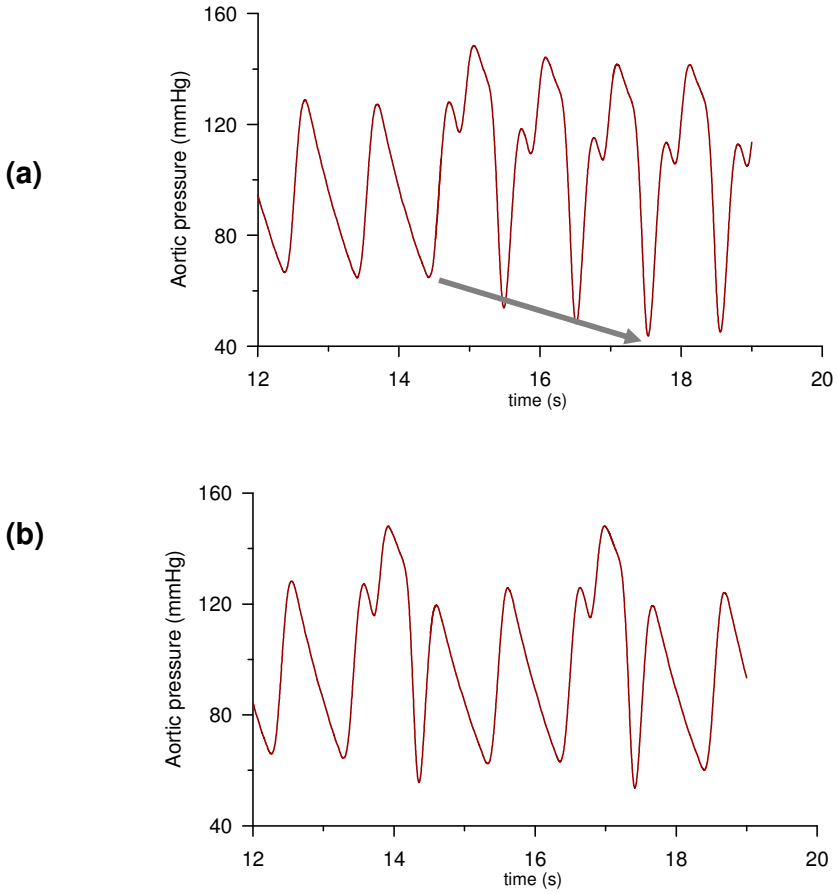

Figure 7.18: Sample of aortic pressure in MCS (horizontal position, 40 cc) with assistance set at 1:1 (a) and 1:3 (b), showing the reduction in baseline pressure at 1:1 which results in overall more effective pumping, since the balloon is essentially working against a lower resistance.

Methodological considerations:

The experiments in the MCS were repeated for two balloons of different size (25 cc and 40 cc). However, balloons of different shape could not be tested. The tapered balloons, TDD and TID, previously described (Chapter 3 and Chapter 5) resulted to be excessively long for the dimensions of the artificial aorta. Not only the base of the balloons extended below the renal bifurcation and the tip of the balloon was positioned into the aortic arch, way past the left subclavian artery, hence disregarding traditional guidelines of balloon placement; but also, because of their length, it would not have been possible to perform measurements at the same measurement sites used for the 25 cc and 40 cc balloons, rendering any comparison very difficult.

As said, the mechanism of coronary systolic flow impediment was not modelled in the MCS used for the experiments. Consequently, given that the flow profile of coronary flow would not have been physiological, coronary flow was not measured during this study.

Also, the forward expansion wave associated with LV relaxation was not detected in the wave intensity profile. This might be related to the Abiomed LVAD not mimicking this phenomenon.

7.5. Conclusion

This *in vitro* study in a MCS with physiological distribution of terminal resistance and compliance highlighted that the effect of increasing angle on balloon performance can be considered as adverse if assessed in terms of pressure. Changes have been recorded both in terms of diastolic pressure augmentation and end-diastolic aortic pressure reduction, relating with balloon

inflation and deflation respectively. On the other hand, the amount of flow displaced during inflation into the aortic arch toward the coronary circulation was less affected by increasing angle, especially in the case of the 25 cc balloon.

These changes have also been identified by means of wave intensity analysis. A significant correlation was found between the compression wave associated with balloon inflation and diastolic pressure augmentation and between the expansion wave associated with balloon deflation and end-diastolic pressure reduction. Wave intensity is thus regarded as a resourceful analytical tool to understand the wave pattern associated with counterpulsation.

It was further observed that the IABP assisting frequency had a marked effect on the measured parameters. Frequency set at 1:1 appeared to be more beneficial than 1:2 or 1:3, especially according to the pressure parameters and reinforced by wave intensity. This result is in agreement with the literature [169].

CHAPTER 8

CONCLUSIONS AND FUTURE OUTLOOK

The IABP has been clinically employed for decades; however, some aspects of the operation of the intra-aortic balloon had not been investigated before. This thesis focused on the mechanics of the intra-aortic balloon. Pressure and flow measurements have been carried out *in vitro* in gradually more physiological setups, from a single latex tube (Chapter 3) to a mock circulatory system with physiological distribution of terminal resistance and compliance (Chapter 7). Also, observations based on hemodynamic measurements have been supported with a visualisation study (Chapter 5).

Considering the semi-recumbent position adopted in the clinical setting, the effect of angle on balloon mechanics was investigated. This parameter was also distinguished from the effect of intra-luminal pressure, since a change in angle is necessarily accompanied by a variation in the intra-luminal pressure surrounding the balloon. In summary, it was observed that:

- End-diastolic pressure reduction, taken as an indicator of the benefit of balloon deflation, is reduced with increasing angle, as shown in an artificial aorta (Chapter 4) and in the mock circulatory system (Chapter 7). For the case of an horizontal balloon, it was shown that increasing intra-luminal pressure increased end-diastolic pressure reduction (Chapter 4).
- In terms of the amount of retrograde volume displacement, a larger proportion of the balloon nominal volume is displaced in the retrograde direction. This was observed both in a single latex tube (Chapter 3) as well as in the mock circulatory system (Chapter 7). The percentage of retrograde

flow-volume displacement varies up to 79% of the balloon nominal volume. This quantity was shown to depend on intra-luminal pressure. A reduction in flow-volume with increasing angle (0-45°) was measured at low intra-luminal pressure and an overall lower amount but constant over the range of angles at high intra-luminal pressure (Chapter 4).

- The duration of inflation is prolonged with higher intra-luminal pressure and varies with increasing angle depending on the level of transmural pressure across the membrane of the balloon, while the duration of deflation is shortened with higher intra-luminal pressure and increased with increasing angle (Chapter 5).
- The amount of energy carried by the compression wave associated with balloon inflation was reduced at higher intra-luminal pressure (Chapter 4) and also reduced with increasing angle (Chapter 7). The amount of energy carried by the expansion wave associated with balloon deflation was increased at higher intra-luminal pressure (Chapter 4) and reduced with increasing angle (Chapter 7).
- Assistance frequency was not one of the major parameters under investigation, but results of diastolic aortic pressure augmentation and end-diastolic pressure reduction from the mock circulation experiment (Chapter 7) suggested that 1:1 frequency would result in marked increased benefit from IABP counterpulsation, in agreement with a previous observation [169].

In general, the effect of angle on balloon mechanics, with reference to the semi-recumbent position, was studied throughout this thesis (Chapters 3, 4, 5 and 7) and a summary is provided in Figure 8.1, showing that counterpulsation is more effective at the horizontal position.

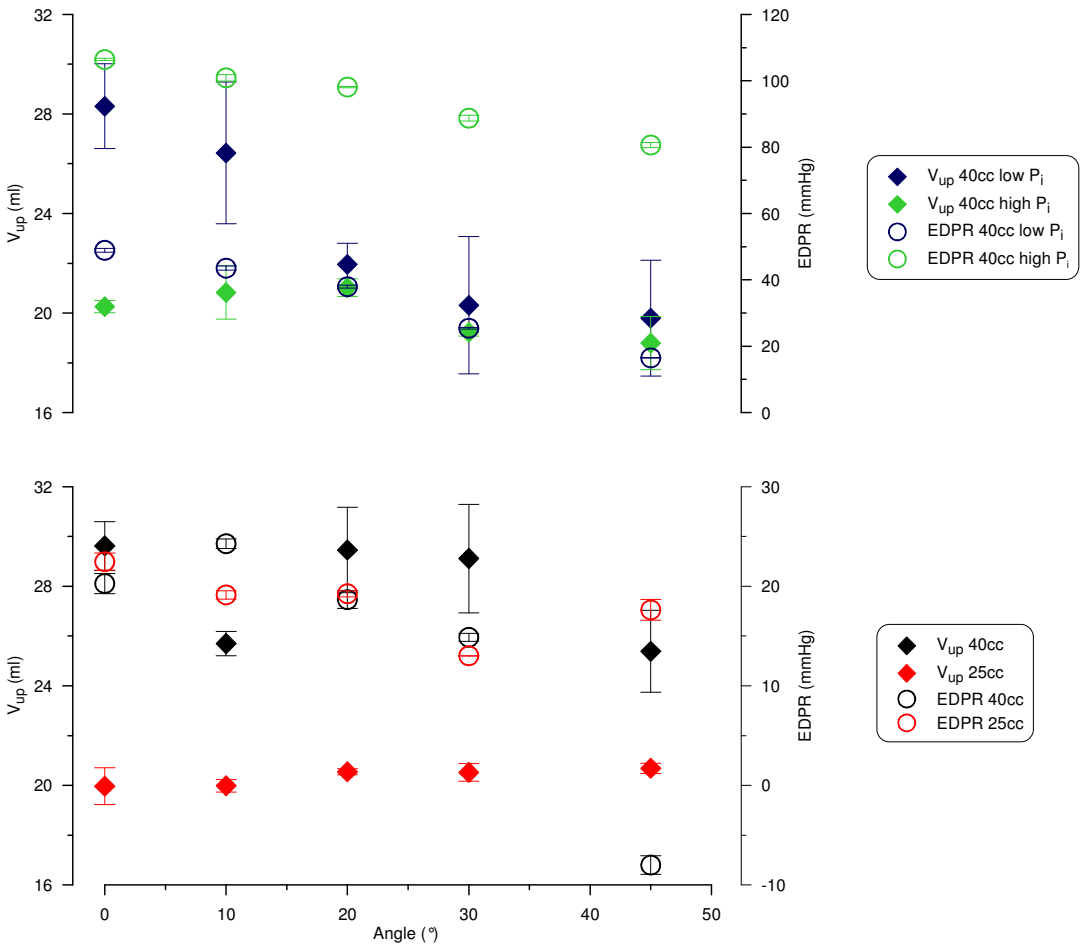

Figure 8.1: Summary plot, merging results from different setups (Chapter 4 and Chapter 7), summarizing changes in V_{up} (inflation benefit) and EDPR (deflation benefit). It shows that the largest counterpulsation benefit is achieved in the horizontal position with a balloon of large volume.

Initially it was shown that, in a single latex tube (Chapter 3), a small increment in angle (19°) resulted in a reduction of the amount of flow-volume displaced in the retrograde direction. It was further shown (Chapter 4) that this effect depends on the level of transmural pressure across the balloon membrane. Measurements in a more physiological setup (Chapter 7) have shown that angle does not affect the volume displaced during inflation. On the other hand a reduction of the benefit of balloon deflation was associated with

the increase in angle. One of the two major benefits of IABP therapy, namely the reduction of afterload reflecting as decreased workload for the recovering myocardium, achieved with balloon deflation, is affected by a change in posture. By quantifying the benefit of deflation by means of end-diastolic pressure reduction, it was shown both in an inclined artificial aorta (Chapter 4) and in a complete mock circulatory system (Chapter 7) that increasing angle results in lesser end-diastolic pressure reduction.

Combining these observations it was apparent that in order to assess the effect of angle on balloon mechanics it was necessary to decide whether to weight the benefit of IABP in terms of balloon inflation (coronary perfusion augmentation) or balloon deflation (myocardial unloading). In agreement with previous observations [59, 93, 167], the unloading action of balloon deflation can be regarded as the main benefit of the IABP. Hence, *in vitro* results suggest that angle has overall a negative effect of IABP therapy. Also, increasing intra-luminal pressure resulted in larger end-diastolic pressure reduction and hence increased the unloading action of balloon deflation. In this sense, it is concluded that it is preferable to operate the balloon at high intra-luminal pressure. This is in agreement with the literature [120, 121].

The visualisation study showed changes in the timing of the balloon cycle with posture. The dependence of the duration of inflation and deflation on angle is an indication that, in clinical terms, adjustments of the onset of inflation and deflation with the apposite commands on the IABP panel may (completely or to some extent) compensate for the adverse effect of increasing angle.

Changes in the amount of flow-volume have been further explained by examining volume displacement in relation to the level of intra-luminal pressure surrounding the balloon (Chapter 4) and changes in balloon cross-sectional

area at different transmural pressures. Furthermore, flow recirculation during late balloon inflation has been detected (Chapter 3 and Appendix A).

Wave intensity analysis was applied to the case of IABP counterpulsation. This analysis has not been employed yet in the study of cardiac assist devices. Not only it was useful for the purpose of identifying the waves generated by the inflation and deflation of the balloon (Chapter 4) but more importantly it showed that the assessment of balloon performance could alternatively be performed by quantifying the energy carried by the waves generated by balloon inflation and deflation (Chapter 7). In fact a significant correlation was found between the energy carried by the compression wave generated during balloon inflation and diastolic pressure augmentation and between the energy carried by the expansion wave generated during balloon deflation and end-diastolic pressure reduction.

Measurements of balloon internal pressure, previously not available, were performed (Chapter 5). These highlighted the difference between operating the balloon in a compliant tube or in a rigid tube. Major qualitative differences were exhibited, confirming previous observations about the significant effect of compliance on IABP. Such difference was also quantified as the “stopping shock” phenomenon, which coincides with the end of balloon deflation.

Finally, this work involved testing prototypes of balloons with a novel shape, with increasing/decreasing tapered diameter from the catheter to the tip. These balloons showed differences in terms of pressure distribution (Chapter 3) and duration of inflation and deflation (Chapter 5) with respect to traditional cylindrical balloons. However, the novel balloons presented a problem in terms of their dimensions and were too long to be tested in the mock circulatory system (Chapter 7) so a full set of data for the prototype is still lacking.

These results overall bear clinical relevance. It is in fact suggested that, in the case of a patient nursed in the semi-recumbent position, the benefit of IABP therapy will be compromised (Figure 8.1). Also, pressure results and results on intra-luminal pressure indicate that hypotensive patients may not receive the full benefit of balloon deflation as quantified by the related reduction of myocardial workload. However, such remarks should be stated with caution, because these results were obtained *in vitro* and in the case of *in vitro* experiments it is not possible to reproduce biological phenomena and autoregulation [93, 171]. Moreover, some components of the test beds were not modelled physiologically (such as the mechanism of coronary systolic flow impediment in the case of the mock circulatory system described in Chapter 6). Conversely, the benefit of performing experiments *in vitro* is that it is possible to reduce the number of variables under investigation, dissecting the problem and studying each variable separately.

In conclusion, this work clarified some aspects of IABP that were not previously reported. With respect to the aims enunciated in Chapter 1, it was shown that:

(1) operating the balloon at an angle reduces the efficacy of counterpulsation

(2) variations in intra-luminal pressure, translating in variations in transmural pressure across the balloon membrane, affect the mechanisms of balloon inflation/deflation

(3) a mock circulatory system suitable for IABP testing was constructed and its strengths (physiological distribution of terminal resistance and compliance, portability, driver independent of afterload) and limitations (lack of coronary systolic flow impediment mechanism) were described

(4) wave intensity analysis proved to be a suitable descriptor of balloon operation

Finally, it is foreseen that – although IABP therapy has been employed for decades and currently the IABP is the most widely used temporary VAD – the benefit of this device might be further enhanced, possibly exploring new balloon shapes, as attempted by including in this work preliminary results on novel balloons with tapered diameter.

In the light of these conclusions and of the results presented in this thesis, some points are here proposed for future development:

- the balloons of novel shape deserve further study, since – as said – they could not be tested in the mock circulatory system, which would have provided a physiological environment in which to expand the encouraging results presented in Chapter 3. The current available tapered design necessarily requires a balloon longer that those commercially available and the extra length results in incorrect balloon placement according to the commonly adopted guidelines. If however further study in more physiological test beds confirms the benefits of the rationale behind the novel design, it is put forward that such rationale may be incorporated into a cylindrical balloon by manufacturing a balloon membrane of non-uniform thickness. This would not compromise the design in terms of length.

- PIV measurements have proved to be a resourceful tool in the study of the flow pattern generated during balloon inflation (as indicated in Chapter 3 and reported in Appendix A). However, in this context an *ad hoc* study was

referred to. It is envisaged that by further exploiting the PIV technique to study the flow generated during balloon inflation and deflation interesting results may be achieved.

- With the aid of appropriate software, simultaneous measurements of balloon pressure and high-speed camera recording may be performed. This would be beneficial, by allowing mapping of the events occurring during the balloon cycle on the balloon pressure signal, providing detailed resourceful information.

- The mock circulatory system presented in Chapter 7 can be further improved, chiefly by devising a method to reproduce the mechanism of coronary systolic flow impediment. Such an improvement would allow measurements of flow in the coronary vessels. Furthermore, although these were not the priority of the study, measurements of carotid and subclavian flow have been carried out in the mock loop and they indicated the contribution of balloon inflation and deflation to the flow pattern of arch vessels. It was thus envisaged that part of the aforementioned amount of balloon volume displaced retrograde from the tip toward the coronary circulation may be dispersed in the arch vessels. This point can be further studied by means of more detailed measurements of flow distribution in the aortic arch.

APPENDIX A

PIV VISUALISATION CONFIRMING FLOW RECIRCULATION

DURING INTRA-AORTIC BALLOON INFLATION

Particle Image Velocimetry (PIV) is an optical measurement technique used to obtain velocity information of whole flow fields in fractions of a second [172].

Observations during a PIV visualisation experiment, performed with equipment from Dantec Dynamics (Dantec Dynamics, Tonsbakken, Denmark), confirmed the presence of flow recirculation during late balloon inflation, before the onset of deflation.

A 40 cc balloon was submerged in a water bath, adequately seeded for PIV visualisation. The balloon was inflated and deflated only once, at 1:3 assisting frequency and 60 bpm heart rate. A 200 ms recording was obtained at 500 frames/s, after the onset of inflation but before the onset of deflation. The acquired images clearly showed the velocity vectors turning from the direction opposite to the balloon tip (sample 1 and 30) back towards the balloon (sample 60 and 99). These results confirmed visually the observations in Chapter 3, where flow recirculation was observed on the flow waveforms obtained in a latex tube.

Four images are here shown in sequence to demonstrate this phenomenon (samples 1, 30, 60 and 99 from the recording, the time of the sample reported in brackets). The pink arrows represent the velocity vectors and indicate the direction of flow. The tip of the balloon is easily recognisable on each image as an elongated white oval.

Sample 1 (t = 2 ms):

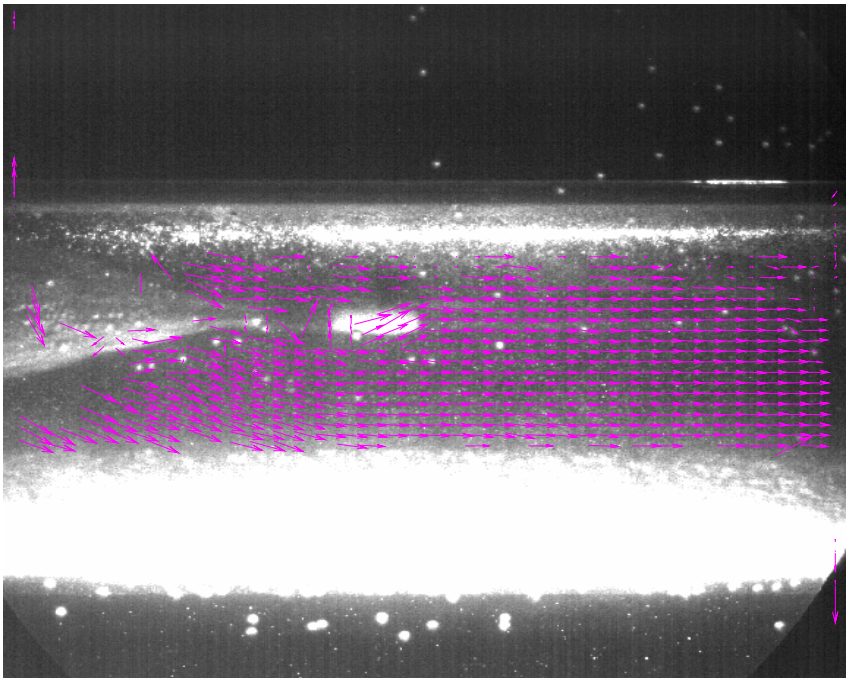

Sample 30 (t = 60 ms):

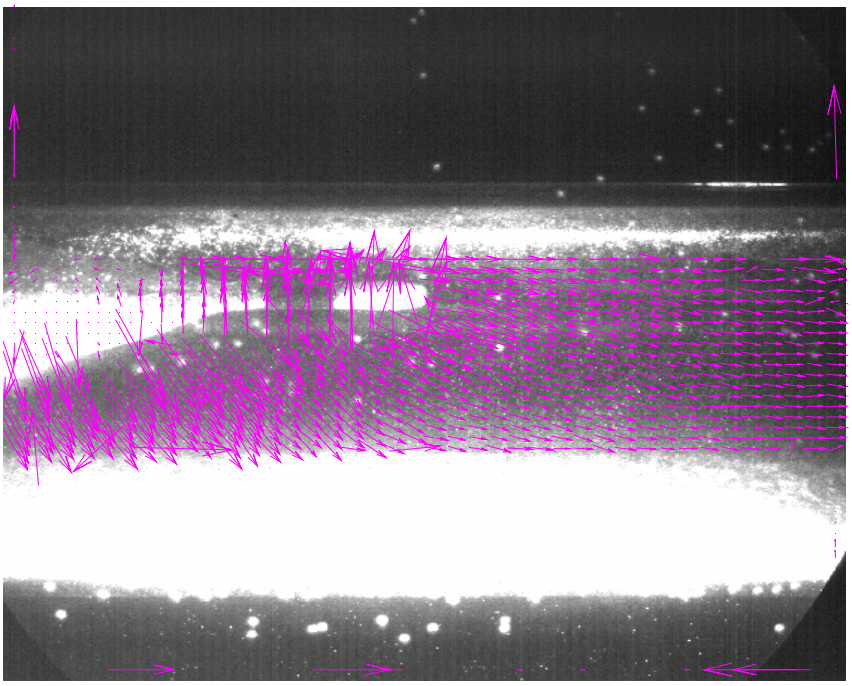

Sample 60 (t = 120 ms):

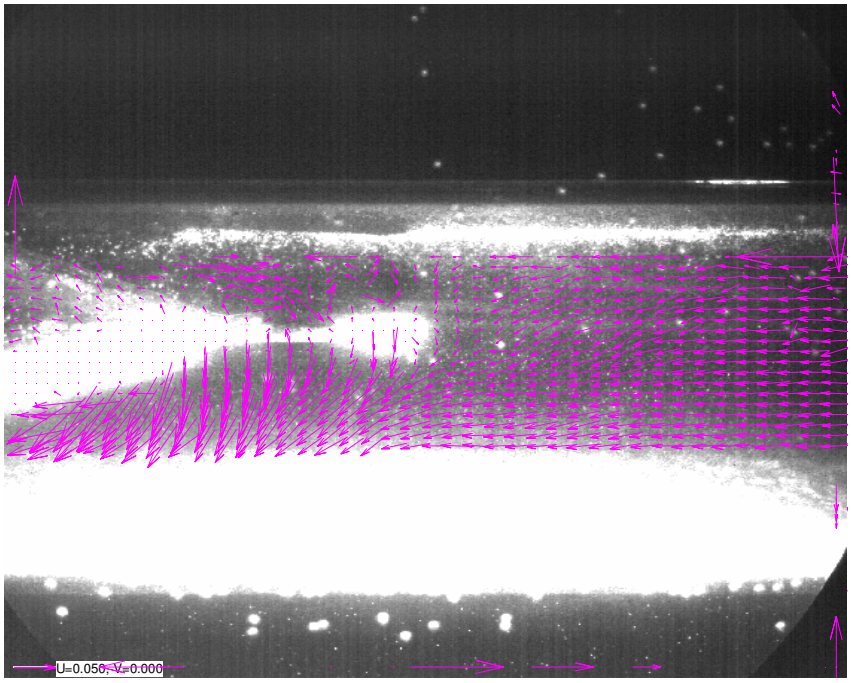

Sample 99 (t = 198 ms):

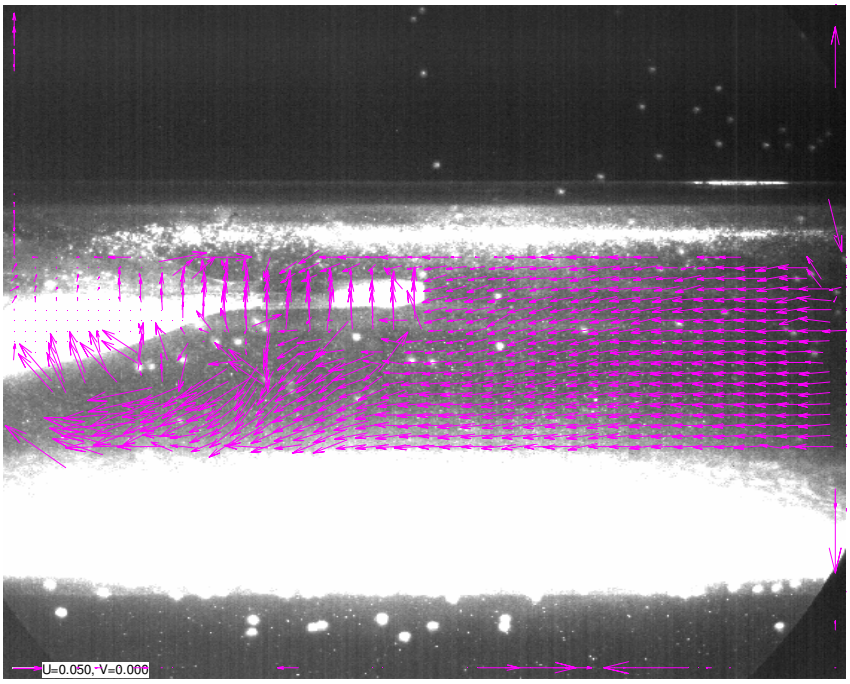

APPENDIX B

TRANSMURAL PRESSURE CURVE FOR DIFFERENT BALLOONS

In order to check the reproducibility of the concept of the transmural pressure curve (TPC) obtained in Chapter 5 for a 40 cc balloon, such curve was obtained for balloons of different volumes (25, 34 and 50 cc, in addition to the 40 cc) and of different shape (TID and TDD balloons).

The curves were obtained in the same way as previously described, with each balloon submerged in a water bath and rapidly inflated once at increasingly high pressure, measuring the volume displaced by the balloon with a measuring cylinder.

As shown in Figure B.1, all balloons exhibited a similar behaviour and for all it was possible to identify a linear part and a plateau region of the TPC, as expected from Chapter 5.

Interestingly, it should be pointed out that, while the commercially-available cylindrical balloons of different sizes were all able to displace more than their nominal volume at high P, the tapered balloons could displace only up to the total original volume. This difference was explained in terms of wall thickness. The TDD and TID balloons are prototypes and are not commercially-available and the thickness of the membrane was higher than that of the cylindrical balloons. Wall thickness was measured with a calliper and it was estimated 0.128 mm for all cylindrical balloons and 0.275 mm for the tapered balloons. As a result, it was alleged that it was more difficult for the TID and TDD balloons to stretch.

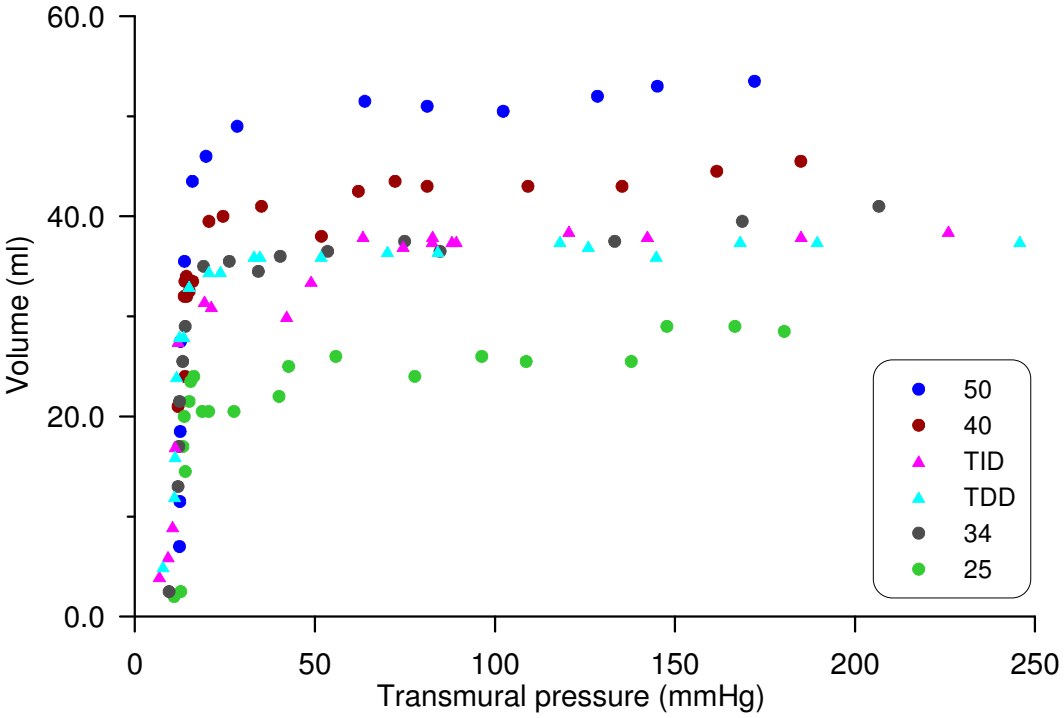

Figure B.1: The TPC was calculated for balloons of different size (25, 34, 40 and 50 cc) and shape (cylindrical, TDD and TID). In all cases, the curve of each balloon exhibited the same behaviour, with a linear part at low P range and a near-plateau region at high P range. However, the TID and TDD balloons were not able to displace more than their total nominal volume at high P, and this was believed to be due to the thicker balloon membrane of the tapered balloons.

APPENDIX C

LIST OF PUBLICATIONS

Papers

Biglino G, Whitehorne M, Pepper JR and Khir AW, Pressure and flow-volume distribution associated with intra-aortic balloon inflation: an in vitro study, Artificial Organs 2008; 32(1):19-27

Bowles CT, New S, Van Loon R, Dreger SA, Biglino G, Chan C, Parker KH, Chester AH, Yacoub MH and Taylor PM, Hydrodynamic evaluation of a bioreactor for tissue engineering heart valves, Cardiovascular Engineering and Technology, Cardiovascular Engineering and Technology 2010; 1(1):10-17

Biglino G, Kolyva C, Whitehorne M, Pepper JR and Khir AW, Variations in aortic pressure affect the mechanics of the intra-aortic balloon, Artificial Organs (in press)

Kolyva C, Biglino G, Whitehorne M, Pepper JR and Khir AW, A mock circulatory system with physiological distribution of terminal resistance and compliance: application for testing the intra-aortic balloon pump, Artificial Organs (under revision)

Biglino G, Kolyva C, Pepper JR and Khir AW, Waves generated during counterpulsation in a mock circulatory system: variations with angle and assisting frequency, Journal of Biomechanics (in preparation)

Conferences

Biglino G, Kolyva C and Khir AW, Effect of angle on IAB mechanics in a mock circulation (talk), European Society for Artificial Organs (ESAO) 9/2009, Compiègne, France

Kolyva , Biglino G and Khir AW, "Distribution of volume displaced during intra-aortic balloon pump inflation in vitro" (poster), European Society for Artificial Organs (ESAO) 9/2009, Compiègne, France

Biglino G, Kolyva C and Khir AW, Mechanics of IABP inflation: in vitro and visualisation studies (talk), Royal Society of Engineering 9/2008, London, UK

Biglino G, Kolyva C, Whitehorne M, Pepper JR and Khir AW, Mechanics of IAB inflation: the combined effect of pressure and posture (poster), American Society for Artificial Internal Organs (ASAIO) 6/2008, San Francisco, USA

Biglino G, Kolyva C, Whitehorne M, Pepper JR and Khir AW, The effect of shape and angle on intra-aortic balloon pump performance (poster), ESAO 9/2007, Krems, Austria

Khir AW, Biglino G, Whitehorne M and Pepper JR, A new face to an old technology: effect of shape on IAB performance (talk), ASAIO 6/2007, Chicago, USA

Biglino G, An in vitro study of the dynamics of the intra-aortic balloon (poster), 9th Great British Research and R&D Show, 3/2007, London, UK

Biglino G, Whitehorne M, Pepper JR and Khir AW, Pressure and wave intensity distribution along the intra-aortic balloon: an in vitro study (poster), ASAIO 6/2006, Chicago, USA

LIST OF CITATIONS

1. HARVEY W., The circulation of blood. London: Everyman *1993*.
2. WORLDHEALTHORGANISATION, Who.Int/cardiovascular_diseases/en/.*last accessed on 24/6/2009*.
3. AMERICANHEARTASSOCIATION, Heart disease and stroke statistics - 2009 update (at-a-glance version), americanheart.Org/presenter.Jhtml?Identifier=3037327.*last accessed on 27/6/2009*.
4. KURUSZ M., Cardiopulmonary bypass: Past, present, and future. Asaio J, **50**(6): p. xxxiii-xxxvi,*2004*.
5. WELKOWITZ W., Engineering hemodynamics: Application to cardiac assist devices. New York: New York University Press. *1987*.
6. HIRSCH D.J. and COOPER J.R.J., Cardiac failure and left ventricular assist devices. Anesthesiol Clin North America **21**(3): p. 625-38,*2003*.
7. DYKE D.B., PAGANI F.D., and AARONSON K.D., Circulatory assist devices 2000: An update. Congest Heart Fail, **6**(5): p. 259-271,*2000*.
8. WHEELDON D.R., Mechanical circulatory support: State of the art and future perspectives. Perfusion, **18**(4): p. 233-43,*2003*.
9. REUL H. and AKDIS M., Temporary or permanent support and replacement of cardiac function. Expert Rev Med Devices, **1**(2): p. 215-27,*2004*.
10. GOLDSTEIN D.J. and OZ M.C., Cardiac assist devices. 1st ed. London: Wiley-Blackwell. *2000*.
11. PARAMESHWAR J. and WALLWORK J., Left ventricular assist devices: Current status and future applications. Int J Cardiol, **62 Suppl 1**: p. S23-7,*1997*.
12. WELKOWITZ W. and LI J.K.J., Control aspects of intraaortic balloon pumping: An overview. Proceedings of the IEEE, **76**(9): p. 1210-1217,*1988*.
13. KANTROWITZ A., Restoring cardiac function: An emerging spectrum of therapeutic options. J Biomater Appl, **1**(1): p. 13-38,*1986*.
14. PAPAIOANNOU T.G., MATHIOULAKIS D.S., STAMATELOPOULOS K.S., GIALAFOS E.J., LEKAKIS J.P., NANAS J., STAMATELOPOULOS S.F., and TSANGARIS S.G., New aspects on the role of blood pressure and arterial stiffness in mechanical assistance by intra-aortic balloon pump: In-vitro data and their application in clinical practice. Artif Organs, **28**(8): p. 717-27,*2004*.
15. PAPAIOANNOU T.G. and STEFANADIS C., Basic principles of the intraaortic balloon pump and mechanisms affecting its performance. Asaio J, **51**(3): p. 296-300,*2005*.

16. MIN B., WELKOWITZ W., FICH S., JARON D., and KANTROWITZ A., Dynamic optimization of in-series cardiac assistance by means of intra-aortic balloon pumping. Bull Math Biol, **37**(1): p. 19-35,*1975*.

17. JEEVANANDAM V., JAYAKAR D., ANDERSON A.S., MARTIN S., PICCIONE W., JR., HEROUX A.L., WYNNE J., STEPHENSON L.W., HSU J., FREED P.S., and KANTROWITZ A., Circulatory assistance with a permanent implantable iabp: Initial human experience. Circulation, **106**(12 Suppl 1): p. I183-8,*2002*.

18. KANTROWITZ A., Experimental augmentation of coronary flow by retardation of the arterial pressure pulse. Surgery, **34**(4): p. 678-87,*1953*.

19. KANTROWITZ A., Origins of intraaortic balloon pumping. Ann Thorac Surg, **50**(4): p. 672-4,*1990*.

20. MOULOPOULOS S.D., TOPAZ S., and KOLFF W.J., Diastolic balloon pumping (with carbon dioxide) in the aorta--a mechanical assistance to the failing circulation. Am Heart J, **63**: p. 669-75,*1962*.

21. KANTROWITZ A., TJONNELAND S., FREED P.S., PHILLIPS S.J., BUTNER A.N., and SHERMAN J.L., JR., Initial clinical experience with intraaortic balloon pumping in cardiogenic shock. Jama, **203**(2): p. 113-8,*1968*.

22. KANTROWITZ A., TJONNELAND S., FREED P.S., PHILLIPS S.J., BUTNER A.N., and SHERMAN J.L., JR., Intraaortic balloon pumping. Jama, **203**(11): p. 988,*1968*.

23. KANTROWITZ A., TJONNELAND S., KRAKAUER J.S., PHILLIPS S.J., FREED P.S., and BUTNER A.N., Mechanical intraaortic cardiac assistance in cardiogenic shock. Hemodynamic effects. Arch Surg, **97**(6): p. 1000-4,*1968*.

24. LEVICK R.J., An introduction to cardiovascular physiology. 4th ed. London: Arnold. *2003*.

25. PAPAIOANNOU T.G., MATHIOULAKIS D.S., NANAS J.N., TSANGARIS S.G., STAMATELOPOULOS S.F., and MOULOPOULOS S.D., Arterial compliance is a main variable determining the effectiveness of intra-aortic balloon counterpulsation: Quantitative data from an in vitro study. Med Eng Phys, **24**(4): p. 279-84,*2002*.

26. DUCAS J. and GRECH E.D., Abc of interventional cardiology. Percutaneous coronary intervention: Cardiogenic shock. Bmj, **326**(7404): p. 1450-2,*2003*.

27. DATASCOPE.COM/CA/SENSATION_CS300_SYS.HTML,*last accessed on 27/6/2009*.

28. DATASCOPE.COM/CA/CS100.HTML,*last accessed on 27/6/2009*.

29. ARROWINTERNATIONAL®, Counterpulsation applied: An introduction to intra-aortic balloon pumping. part number ABT-TG,Revision 12/04 ed. Reading, PA, U.S.A. . *2004*.

30. QUAAL S.J., Comprehensive intraaortic balloon counterpulsation. St Louis: Mosby. *1993*.

31. COHEN M., URBAN P., CHRISTENSON J.T., JOSEPH D.L., FREEDMAN R.J., JR., MILLER M.F., OHMAN E.M., REDDY R.C., STONE G.W., and FERGUSON

J.J., 3RD, Intra-aortic balloon counterpulsation in us and non-us centres: Results of the benchmark registry. Eur Heart J, **24**(19): p. 1763-70,*2003*.

32. FERGUSON J.J., 3RD, COHEN M., FREEDMAN R.J., JR., STONE G.W., MILLER M.F., JOSEPH D.L., and OHMAN E.M., The current practice of intra-aortic balloon counterpulsation: Results from the benchmark registry. J Am Coll Cardiol, **38**(5): p. 1456-62,*2001*.

33. SEYFARTH M., SIBBING D., BAUER I., FROHLICH G., BOTT-FLUGEL L., BYRNE R., DIRSCHINGER J., KASTRATI A., and SCHOMIG A., A randomized clinical trial to evaluate the safety and efficacy of a percutaneous left ventricular assist device versus intra-aortic balloon pumping for treatment of cardiogenic shock caused by myocardial infarction. J Am Coll Cardiol, **52**(19): p. 1584-8,*2008*.

34. KERN M.J., AGUIRRE F., BACH R., DONOHUE T., SIEGEL R., and SEGAL J., Augmentation of coronary blood flow by intra-aortic balloon pumping in patients after coronary angioplasty. Circulation, **87**(2): p. 500-11,*1993*.

35. BASKETT R.J., GHALI W.A., MAITLAND A., and HIRSCH G.M., The intraaortic balloon pump in cardiac surgery. Ann Thorac Surg, **74**(4): p. 1276-87,*2002*.

36. CHRISTENSON J.T., BADEL P., SIMONET F., and SCHMUZIGER M., Preoperative intraaortic balloon pump enhances cardiac performance and improves the outcome of redo cabg. Ann Thorac Surg, **64**(5): p. 1237-44,*1997*.

37. LAZAR H.L., BAO Y., RIVERS S., TREANOR P.R., and SHEMIN R.J., Decreased incidence of arterial thrombosis using heparin-bonded intraaortic balloons. Ann Thorac Surg, **67**(2): p. 446-9,*1999*.

38. NORKIENE I., RINGAITIENE D., RUCINSKAS K., SAMALAVICIUS R., BAUBLYS A., MINIAUSKAS S., and SIRVYDIS V., Intra-aortic balloon counterpulsation in decompensated cardiomyopathy patients: Bridge to transplantation or assist device. Interact Cardiovasc Thorac Surg, **6**(1): p. 66-70,*2007*.

39. GJESDAL O., GUDE E., ARORA S., LEIVESTAD T., ANDREASSEN A.K., GULLESTAD L., AABERGE L., BRUNVAND H., EDVARDSEN T., GEIRAN O.R., and SIMONSEN S., Intra-aortic balloon counterpulsation as a bridge to heart transplantation does not impair long-term survival. Eur J Heart Fail, **11**(7): p. 709-14,*2009*.

40. KORMOS R.L., The role of the intraaortic balloon as a bridge to cardiac transplantation. Cardiac Assists, **3**(1),*1987*.

41. OVERWALDER P.J., Intra aortic balloon pump (iabp) counterpulsation. The internet journal of thoracic and cardiovascular surgery **2**(2),*1999*.

42. PETERSON J.C. and COOK D.J., Intra-aortic balloon counterpulsation pump therapy: A critical appraisal of the evidence for patients with acute myocardial infarction. Crit Care, **2**(1): p. 3-8,*1998*.

43. BREGMAN D. and CASARELLA W.J., Percutaneous intraaortic balloon pumping: Initial clinical experience. Ann Thorac Surg, **29**(2): p. 153-5,*1980*.

44. HAUSER A.M., GORDON S., GANGADHARAN V., RAMOS R.G., WESTVEER D.C., GARG A.K., and TIMMIS G.C., Percutaneous intraaortic balloon

counterpulsation. Clinical effectiveness and hazards. Chest, **82**(4): p. 422-5,*1982*.

45. SELDINGER S.I., Catheter replacement of the needle in percutaneous arteriography; a new technique. Acta radiol, **39**(5): p. 368-76,*1953*.

46. MENON P., TOTARO P., YOUHANA A., and ARGANO V., Reduced vascular complication after iabp insertion using smaller sized catheter and sheathless technique. Eur J Cardiothorac Surg, **22**(3): p. 491-2; author reply 492-3,*2002*.

47. MAYER J.H., Subclavian artery approach for insertion of intra-aortic balloon. J Thorac Cardiovasc Surg, **76**(1): p. 61-3,*1978*.

48. SHAW J., TAYLOR D.R., and PITT B., Effects of intraaortic balloon counterpulsation on regional coronary blood flow in experimental myocardial infarction. Am J Cardiol, **34**(5): p. 552-6,*1974*.

49. KANTROWITZ A., WASFIE T., FREED P.S., RUBENFIRE M., WAJSZCZUK W., and SCHORK M.A., Intraaortic balloon pumping 1967 through 1982: Analysis of complications in 733 patients. Am J Cardiol, **57**(11): p. 976-83,*1986*.

50. MACCIOLI G.A., LUCAS W.J., and NORFLEET E.A., The intra-aortic balloon pump: A review. J Cardiothorac Anesth, **2**(3): p. 365-73,*1988*.

51. DATASCOPE®, 9.5 fr. True sheathlesstm intra-aortic balloon catheter for sheathless insertion, instructions for use *Document no. 0065-00-0160 R132-97*.

52. ONORATI F., BILOTTA M., PEZZO F., IMPIOMBATO B., CAROLEO S., SANTANGELO E., and RENZULLI A., Transbrachial insertion of a 7.5-fr intra-aortic balloon pump in a severely atherosclerotic patient. Crit Care Med, **34**(8): p. 2231-3,*2006*.

53. ALDERMAN J.D., GABLIANI G.I., MCCABE C.H., BREWER C.C., LORELL B.H., PASTERNAK R.C., SKILLMAN J.J., STEER M.L., and BAIM D.S., Incidence and management of limb ischemia with percutaneous wire-guided intraaortic balloon catheters. J Am Coll Cardiol, **9**(3): p. 524-30,*1987*.

54. BAVIN T.K. and SELF M.A., Weaning from intra-aortic balloon pump support. Am J Nurs, **91**(10): p. 54-9,*1991*.

55. BARNEA O., MOORE T.W., DUBIN S.E., and JARON D., Cardiac energy considerations during intraaortic balloon pumping. IEEE Trans Biomed Eng, **37**(2): p. 170-81,*1990*.

56. SUGA H., HAYASHI T., SUEHIRO S., HISANO R., SHIRAHATA M., and NINOMIYA I., Equal oxygen consumption rates of isovolumic and ejecting contractions with equal systolic pressure-volume areas in canine left ventricle. Circ Res, **49**(5): p. 1082-91,*1981*.

57. SUGA H., YASUMURA Y., NOZAWA T., FUTAKI S., IGARASHI Y., and GOTO Y., Prospective prediction of o2 consumption from pressure-volume area in dog hearts. Am J Physiol, **252**(6 Pt 2): p. H1258-64,*1987*.

58. VINTEN-JOHANSEN J., DUNCAN H.W., FINKENBERG J.G., HUME M.C., ROBERTSON J.M., BARNARD R.J., and BUCKBERG G.D., Prediction of myocardial o2 requirements by indirect indices. Am J Physiol, **243**(6): p. H862-8,*1982*.

59. WILLIAMS D.O., KORR K.S., GEWIRTZ H., and MOST A.S., The effect of intraaortic balloon counterpulsation on regional myocardial blood flow and oxygen consumption in the presence of coronary artery stenosis in patients with unstable angina. Circulation, **66**(3): p. 593-7,*1982*.

60. OHLEY W.J., Counterpulsation: Theory and practice. IEEE Eng Med Biol Mag, **5**(1): p. 14-8,*1986*.

61. KANTROWITZ A., FREED P.S., CARDONA R.R., GAGE K., MARINESCU G.N., WESTVELD A.H., LITCH B., SUZUKI A., HAYAKAWA H., TAKANO T., and ET AL., Initial clinical trial of a closed loop, fully automatic intra-aortic balloon pump. Asaio J, **38**(3): p. M617-21,*1992*.

62. OAKS T.E. and KINCAID E.H.K., Indications for intra-aortic balloon pump placement, in Cardiac surgery secrets, P.R. Soltoski, H.R. Karamanoukian, and T.A. Salerno: Hanley&Belfus. *2003*.

63. JARON D., MOORE T.W., and HE P., Control of intraaortic balloon pumping: Theory and guidelines for clinical applications. Ann Biomed Eng, **13**(2): p. 155-75,*1985*.

64. UNDERWOOD M.J., FIRMIN R.K., and GRAHAM T.R., Current concepts in the use of intra-aortic balloon counterpulsation. Br J Hosp Med, **50**(7): p. 391-7,*1993*.

65. ELTCHANINOFF H., DIMAS A.P., and WHITLOW P.L., Complications associated with percutaneous placement and use of intraaortic balloon counterpulsation. Am J Cardiol, **71**(4): p. 328-32,*1993*.

66. FUNK M., GLEASON J., and FOELL D., Lower limb ischemia related to use of the intraaortic balloon pump. Heart Lung, **18**(6): p. 542-52,*1989*.

67. STAVARSKI D.H., Complications of intra-aortic balloon pumping. Preventable or not preventable? Crit Care Nurs Clin North Am, **8**(4): p. 409-21,*1996*.

68. MACKENZIE D.J., WAGNER W.H., KULBER D.A., TREIMAN R.L., COSSMAN D.V., FORAN R.F., COHEN J.L., and LEVIN P.M., Vascular complications of the intra-aortic balloon pump. Am J Surg, **164**(5): p. 517-21,*1992*.

69. ELAHI M.M., CHETTY G.K., KIRKE R., AZEEM T., HARTSHORNE R., and SPYT T.J., Complications related to intra-aortic balloon pump in cardiac surgery: A decade later. Eur J Vasc Endovasc Surg, **29**(6): p. 591-4,*2005*.

70. WOLVEK S., The hostile environment of the aging human aorta and the smaller patient--their implications for the intra-aortic balloon. Perfusion, **9**(2): p. 87-94,*1994*.

71. GRANDE A.M., MARTINELLI L., GRAFFIGNA A., and VIGANO M., Retained intraaortic balloon. Case report and review of the literature. Tex Heart Inst J, **22**(4): p. 332-4,*1995*.

72. SHAFEI H. and AL-EBRAHIM K., Awareness of a serious complication of the intraaortic balloon pump: "Entrapping". Ann Thorac Surg, **57**(5): p. 1373,*1994*.

73. PAPAIOANNOU T.G., LEKAKIS J.P., DAGRE A.G., STAMATELOPOULOS K.S., TERROVITIS J., GIALAFOS E.J., KANAKAKIS J., NANAS J., STAMATELOPOULOS S.F., and MOULOPOULOS S., Arterial compliance is an independent factor

predicting acute hemodynamic performance of intra-aortic balloon counterpulsation. Int J Artif Organs, **24**(7): p. 478-83,*2001*.

74. MINICH L.L., TANI L.Y., HAWKINS J.A., BARTKOWIAK R.R., ROYALL M.L., and PANTALOS G.M., In vitro evaluation of the effect of aortic compliance on pediatric intra-aortic balloon pumping. Pediatr Crit Care Med, **2**(2): p. 139-44,*2001*.

75. PANTALOS G.M., MINICH L.L., TANI L.Y., MCGOUGH E.C., and HAWKINS J.A., Estimation of timing errors for the intraaortic balloon pump use in pediatric patients. Asaio J, **45**(3): p. 166-71,*1999*.

76. PAUL COLLISON S. and SINGH DAGAR K., The role of the intra-aortic balloon pump in supporting children with acute cardiac failure. Postgrad Med J, **83**(979): p. 308-11,*2007*.

77. KAO C. and OHLEY W.J., Influence of vascular parameters on the effectiveness of intra-aortic balloon pumping: A model study. Med Biol Eng Comput, **20**(5): p. 529-38,*1982*.

78. PAPAIOANNOU T.G., TERROVITIS J., KANAKAKIS J., STAMATELOPOULOS K.S., PROTOGEROU A.D., LEKAKIS J.P., NANAS J.N., and STAMATELOPOULOS S.F., Heart rate effect on hemodynamics during mechanical assistance by the intra-aortic balloon pump. Int J Artif Organs, **25**(12): p. 1160-5,*2002*.

79. COHEN M., FASSEAS P., SINGH V.P., MCBRIDE R., ORFORD J.L., and KUSSMAUL W.G., 3RD, Impact of intra-aortic balloon counterpulsation with different balloon volumes on cardiac performance in humans. Catheter Cardiovasc Interv, **57**(2): p. 199-204,*2002*.

80. STAMATELOPOULOS S.F., NANAS J.N., SARIDAKIS N.S., ZAKOPOULOS N.A., LYROPOULOS S., MAKRAKIS G., LIBERIDIS A., and MOULOPOULOS S.D., Treating severe cardiogenic shock by large counterpulsation volumes. Ann Thorac Surg, **62**(4): p. 1110-7,*1996*.

81. BAI J., LIN H., YANG Z., and ZHOU X., A study of optimal configuration and control of a multi-chamber balloon for intraaortic balloon pumping. Ann Biomed Eng, **22**(5): p. 524-31,*1994*.

82. BREGMAN D. and GOETZ R.H., Clinical experience with a new cardiac assist device. The dual-chambered intra-aortic balloon assist. J Thorac Cardiovasc Surg, **62**(4): p. 577-91,*1971*.

83. BREGMAN D., KRIPKE D.C., and GOETZ R.H., The effect of synchronous unidirectional intra-aortic balloon pumping on hemodynamics and coronary blood flow in cardiogenic shock. Trans Am Soc Artif Intern Organs, **16**: p. 439-46,*1970*.

84. BIAN X. and DOWNEY H.F., Enhanced intra-aortic balloon pump: Markedly improved systemic hemodynamics and cardiac function in canines with severe, acute left ventricular failure. Artif Organs, **26**(8): p. 727-33,*2002*.

85. MEYNS B.P., NISHIMURA Y., JASHARI R., RACZ R., LEUNENS V.H., and FLAMENG W.J., Ascending versus descending aortic balloon pumping: Organ and myocardial perfusion during ischemia. Ann Thorac Surg, **70**(4): p. 1264-9,*2000*.

86. KOLLEF M.H., Prevention of hospital-associated pneumonia and ventilator-associated pneumonia. Crit Care Med, **32**(6): p. 1396-405,*2004*.

87. LORENTE L., BLOT S., and RELLO J., Evidence on measures for the prevention of ventilator-associated pneumonia. Eur Respir J, **30**(6): p. 1193-207,*2007*.

88. LI T.S., JOYNT G.M., SO H.Y., GOMERSALL C.D., and YAP F.H., Semi-recumbent position in icu. Crit Care & Shock, **11**(2): p. 61-66,*2008*.

89. WILKINSON F., Organ donor managment - care bundle. NHS Lancashire and South Cumbria critical care network. *Review date 2008*.

90. KHIR A.W., PRICE S., HALE C., YOUNG D.A., PARKER K.H., and PEPPER J.R., Intra-aortic balloon pumping: Does posture matter? Artif Organs, **29**(1): p. 36-40,*2005*.

91. AKYUREKLI Y., TAICHMAN G.C., and KEON W.J., Effectiveness of intra-aortic balloon counterpulsation on systolic unloading. Can J Surg, **23**(2): p. 122-6,*1980*.

92. GEWIRTZ H., OHLEY W., WILLIAMS D.O., SUN Y., and MOST A.S., Effect of intraaortic balloon counterpulsation on regional myocardial blood flow and oxygen consumption in the presence of coronary artery stenosis: Observations in an awake animal model. Am J Cardiol, **50**(4): p. 829-37,*1982*.

93. KIMURA A., TOYOTA E., LU S., GOTO M., YADA T., CHIBA Y., EBATA J., TACHIBANA H., OGASAWARA Y., TSUJIOKA K., and KAJIYA F., Effects of intraaortic balloon pumping on septal arterial blood flow velocity waveform during severe left main coronary artery stenosis. J Am Coll Cardiol, **27**(4): p. 810-6,*1996*.

94. SCHREUDER J.J., CASTIGLIONI A., DONELLI A., MAISANO F., JANSEN J.R., HANANIA R., HANLON P., BOVELANDER J., and ALFIERI O., Automatic intraaortic balloon pump timing using an intrabeat dicrotic notch prediction algorithm. Ann Thorac Surg, **79**(3): p. 1017-22; discussion 1022,*2005*.

95. DATASCOPE.COM/CA/BALLOON_PUMPS.HTML,*last accessed on 21/6/2009*.

96. DATASCOPE.COM/CA/SYS98XT.HTML,*last accessed on 27/6/2009*.

97. PMSINSTRUMENTS.CO.UK/PDF/PCU2000.PDF,*last accessed on 21/6/2009*.

98. TRANSONIC.COM/CO_PROBE_VALIDATION.PDF,*last accessed on 21/6/2009*.

99. TRANSONIC.COM/TN_94_FREQUENCY_RESPONSE.PDF,*last accessed on 21/6/2009*.

100. TRANSONIC.COM/TN_5REVD.PDF,*last accessed on 21/6/2009*.

101. PARKER K.H. and JONES C.J.H., Forward and backward running waves in the arteries: Analysis using the method of characteristics. Journal of Biomedical Engineering, **112**: p. 322-326,*1990*.

102. AVOLIO A., WESTERHOF B.E., SIEBES M., and TYBERG J.V., Arterial hemodynamics and wave analysis in the frequency and time domains: An evaluation of the paradigms. Med Biol Eng Comput, **47**(2): p. 107-10,*2009*.

103. PARKER K.H., An introduction to wave intensity analysis. Med Biol Eng Comput, **47**(2): p. 175-88,*2009*.

104. PARKER K.H., A brief history of arterial wave mechanics. Med Biol Eng Comput, **47**(2): p. 111-8,*2009*.

105. MOENS A.I., *Over de voortplantingssnelheid van den pols*. 1877, Academisch Profschrift: Leiden. p. 1-72.

106. KORTEWEG D.J., *Over voortplantings-snelheid van golven in elastische ruizen*. 1877: Leiden. p. 525-542.

107. MILNOR W.R., Hemodynamics. 2nd ed. Baltimore: Williams & Wilkins. *1989*.

108. DAVIES J.E., WHINNETT Z.I., FRANCIS D.P., WILLSON K., FOALE R.A., MALIK I.S., HUGHES A.D., PARKER K.H., and MAYET J., Use of simultaneous pressure and velocity measurements to estimate arterial wave speed at a single site in humans. American Journal of Physiology Heart and Circulatory Physiology, **290**(2): p. H878-885,*2006*.

109. KHIR A.W., O'BRIEN A.B., GIBBS J.S.R., and PARKER K.H., Determination of wave speed and wave separation in the arteries. Journal of Biomechanics, **34**: p. 1145-1155,*2001*.

110. TIJSSELING A.S. and ANDERSON A., Johannes von kries and the history of waterhammer. J Hydr Eng, **133**: p. 1-8,*2007*.

111. FENG J. and KHIR A.W., The compression and expansion waves of the forward and backward flows: An in-vitro arterial model. Proc Inst Mech Eng H, **222**(4): p. 531-42,*2008*.

112. SWALEN M.J. and KHIR A.W., Resolving the time lag between pressure and flow for the determination of local wave speed in elastic tubes and arteries. J Biomech, **42**(10): p. 1574-7,*2009*.

113. SUGAWARA M., NIKI K., OHTE N., OKADA T., and HARADA A., Clinical usefulness of wave intensity analysis. Med Biol Eng Comput, **47**(2): p. 197-206,*2009*.

114. PARKER K.H., JONES C.J.H., DAWSON J.R., and GIBSON D.G., What stops the flow of blood from the heart? Heart and Vessels, **4**: p. 241-245,*1988*.

115. DAVIES J.E., WHINNETT Z.I., FRANCIS D.P., MANISTY C.H., AGUADO-SIERRA J., WILLSON K., FOALE R.A., MALIK I.S., HUGHES A.D., PARKER K.H., and MAYET J., Evidence of a dominant backward-propagating "Suction" Wave responsible for diastolic coronary filling in humans, attenuated in left ventricular hypertrophy. Circulation, **113**(14): p. 1768-1778,*2006*.

116. WANG Z., JALALI F., SUN Y.H., WANG J.J., PARKER K.H., and TYBERG J.V., Assessment of left ventricular diastolic suction in dogs using wave-intensity analysis. Am J Physiol Heart Circ Physiol, **288**(4): p. H1641-51,*2005*.

117. HOLLANDER E.H., WANG J., JR., DOBSON G.M., PARKER K.H., and TYBERG J.V., Negative wave reflections in pulmonary arteries. American Journal of Physiology Heart and Circulatory Physiology, **281**(2): p. H895-902,*2001*.

118. OHTE N., NARITA H., SUGAWARA M., NIKI K., OKADA T., HARADA A., HAYANO J., and KIMURA G., Clinical usefulness of carotid atrerial wave intensity in

assessing left ventricular systolic and early diastolic performance. Heart and Vessels, **18**: p. 107-111,*2003*.

119. ZAMBANINI A., CUNNINGHAM S.L., PARKER K.H., KHIR A.W., MCG. THOM S.A., and HUGHES A.D., Wave-energy patterns in carotid, brachial, and radial arteries: A noninvasive approach using wave-intensity analysis. American Journal of Physiology Heart and Circulatory Physiology, **289**(1): p. H270-276,*2005*.

120. CHARITOS C.E., NANAS J.N., KONTOYIANNIS D.A., NANAS S.N., STAMATOPOULOS G.Z., RAPTI A.C., STAMATELOPOULOS S.F., and MOULOPOULOS S.D., The efficacy of the high volume counterpulsation technique at very low levels of aortic pressure. J Cardiovasc Surg (Torino), **39**(5): p. 625-32,*1998*.

121. MOULOPOULOS S.D., The limits of counterpulsation. Int J Artif Organs, **16**(12): p. 803-5,*1993*.

122. PEDLEY T.J., The fluid mechanics of large blood vessels. Cambridge: Cambridge University Press. *1980*.

123. SHAPIRO A.H., Steady flow in collapsible tubes. ASME Journal of Biomechanical Engineering, **99**: p. 126-147,*1977*.

124. MBAKOGU F.C. and PAVLOVIC M.N., Bending and stretching actions in shallow domes. Part 1. Analytical derivations. Thin-walled structures, **26**: p. 61-82,*1996*.

125. VON MÜNSTER T., *Der einfluss der körperposition auf die zerebrale venöse drainage. Eine duplexsonographische untersuchung der vena jugularis interna und vena vertebralis*, in *Medizinischen Fakultät Charité*. 2002 Humboldt Universität Berlin, last accessed in March 2010 on http://edoc.hu-berlin.de/.

126. BLEASDALE R.A., PARKER K.H., and JONES C.J., Chasing the wave. Unfashionable but important new concepts in arterial wave travel. Am J Physiol Heart Circ Physiol, **284**(6): p. H1879-85,*2003*.

127. MUELLER H., AYRES S.M., GIANNELLI S., JR., CONKLIN E.F., MAZZARA J.T., and GRACE W.J., Effect of isoproterenol,l-norepinephrine, and intraaortic counterpulsation on hemodynamics and myocardial metabolism in shock following acute myocardial infarction. Circulation, **45**(2): p. 335-51,*1972*.

128. BLEIFELD W., MEYER-HARTWIG K., IRNICH W., BUSSMANN W.D., and MEYER J., Dynamics of balloons in intraaortic counterpulsation. Am J Roentgenol Radium Ther Nucl Med, **116**(1): p. 155-64,*1972*.

129. MCMAHON T.A., MURTHY V.S., CLARK C., JAFFRIN M.Y., and SHAPIRO A.H., The dynamics and the fluid mechanics of the intra-aortic balloon heart assist device, publ. #69-11. Fluid Mechanics Laboratory, Massachussets Institute of Technology *1969*.

130. SKALAK R., Synthesis of a complete circulation (chapter 19), in Cardiovascular fluid dynamics, D.H. Bergel, London: Academic Press. *1972*.

131. FRANK O., Die gerndform des arteriellen pulses. Z Biol, **37**: p. 483-526,*1899*.

132. JONES R.T., PETSCHEK H.E., and KANTROWITZ A.R., Elementary theory of synchronous arterio-arterial blood pumps. Med Biol Eng, **6**(3): p. 303-8,*1968*.

133. MCMAHON T.A., CLARK C., MURTHY V.S., and SHAPIRO A.H., Intra-aortic balloon experiments in a lumped-element hydraulic model of the circulation. J Biomech, **4**(5): p. 335-50,*1971*.

134. WOLF L., JR. and CLINCH J.M., Mock circulatory system for intra-aortic balloon testing. IEEE Trans Biomed Eng, **19**(1): p. 38-46,*1972*.

135. BOWLES C.T., SHAH S.S., NISHIMURA K., CLARK C., CUMMING D.V., PATTISON C.W., PEPPER J.R., and YACOUB M.H., Development of mock circulation models for the assessment of counterpulsation systems. Cardiovasc Res, **25**(11): p. 901-8,*1991*.

136. PANTALOS G.M., KOENIG S.C., GILLARS K.J., GIRIDHARAN G.A., and EWERT D.L., Characterization of an adult mock circulation for testing cardiac support devices. Asaio J, **50**(1): p. 37-46,*2004*.

137. KOENIG S.C., PANTALOS G.M., LITWAK K.N., GILLARS K.J., GIRIDHARAN G.A., MAGUIRE M., and SPENCE P.A., Hemodynamic and left ventricular pressure-volume responses to counterpulsation in mock circulation and acute large animal models. Conf Proc IEEE Eng Med Biol Soc, **5**: p. 3761-4,*2004*.

138. VANDENBERGHE S., SEGERS P., JOSEMANS H., VAN LOON J.P., RAKHORST G., and VERDONCK P., In vitro assessment of the unloading and perfusion capacities of the puca ii and the iabp. Perfusion, **19**(1): p. 25-32,*2004*.

139. FERRARI G., DE LAZZARI C., KOZARSKI M., CLEMENTE F., GORCZYNSKA K., MIMMO R., MONNANNI E., TOSTI G., and GUARAGNO M., A hybrid mock circulatory system: Testing a prototype under physiologic and pathological conditions. Asaio J, **48**(5): p. 487-94,*2002*.

140. FERRARI G., NICOLETTI A., DE LAZZARI C., CLEMENTE F., TOSTI G., GUARAGNO M., MIMMO R., AMBROSI D., and GORCZYNSKA K., A physical model of the human systemic arterial tree. Int J Artif Organs, **23**(9): p. 647-57,*2000*.

141. DE LAZZARI C. and DAROWSKI M., Cardiopulmonary mechanical interaction- modelling and simulation. Warsaw: Polish Academy of Sciences. *2002*.

142. STERGIOPULOS N., YOUNG D.F., and ROGGE T.R., Computer simulation of arterial flow with applications to arterial and aortic stenoses. J Biomech, **25**(12): p. 1477-88,*1992*.

143. WESTERHOF N., BOSMAN F., DE VRIES C.J., and NOORDERGRAAF A., Analog studies of the human systemic arterial tree. J Biomech, **2**(2): p. 121-43,*1969*.

144. SCHAAF B.W. and ABBRECHT P.H., Digital computer simulation of human systemic arterial pulse wave transmission: A nonlinear model. J Biomech, **5**(4): p. 345-64,*1972*.

145. VERHOEFF B.-J., SIEBES M., MEUWISSEN M., ATASEVER B., VOSKUIL M., DE WINTER R.J., KOCH K.T., TIJSSEN J.G.P., SPAAN J.A.E., and PIEK J.J., Influence of percutaneous coronary intervention on coronary microvascular resistance index. Circulation, **111**(1): p. 76-82,*2005*.

146. SEGERS P., DUBOIS F., DE WACHTER D., and VERDONCK P., Role and relevancy of a cardiovascular simulator. Cardiovascular Engineering, **3**(1): p. 48-56,*1998*.

147. WESTERHOF N., ELZINGA G., and SIPKEMA P., An artificial arterial system for pumping hearts. J Appl Physiol, **31**(5): p. 776-81,*1971*.

148. ABIOMED®, Bvs 5000 ® bi-ventricular support system blood pump: Instructions for use. Abiomed Inc,*1999*.

149. CASTRO P., BARAONA F., BAEZA C., MC-NAB P., BERLIN A., ZALAQUETT R., MORAN S., BECKER P., IRARRAZABAL M., GARAYAR B., CARVAJAL M., and CISTERNAS S., [ventricular assist device as a bridge to transplant in patients with cardiogenic shock. Preliminary experience in chile with abiomed bvs 5000]. Rev Med Chil, **134**(8): p. 1019-23,*2006*.

150. NICHOLS W.W. and O'ROURKE M.F., Mcdonald's blood flow in arteries. 3rd ed. London: Edward Arnold. *1990*.

151. KHUNATORN Y., SHANDAS R., DEGROFF C., and MAHALINGAM S., Comparison of in vitro velocity measurements in a scaled total cavopulmonary connection with computational predictions. Ann Biomed Eng, **31**(7): p. 810-22,*2003*.

152. TIMMS D., HAYNE M., MCNEIL K., and GALBRAITH A., A complete mock circulation loop for the evaluation of left, right, and biventricular assist devices. Artif Organs, **29**(7): p. 564-72,*2005*.

153. LIU Y., ALLAIRE P., WOOD H., and OLSEN D., Design and initial testing of a mock human circulatory loop for left ventricular assist device performance testing. Artif Organs, **29**(4): p. 341-5,*2005*.

154. DOW.COM/GLYCERINE/RESOURCES/TABLE18.HTM,*last accessed on 1/3/2010*.

155. DUR O., LARA M., ARNOLD D., VANDENBERGHE S., KELLER B.B., DEGROFF C., and PEKKAN K., Pulsatile in vitro simulation of the pediatric univentricular circulation for evaluation of cardiopulmonary assist scenarios. Artif Organs, **33**(11): p. 967-76,*2009*.

156. WATANABE K., ICHIKAWA S., ASAI T., MOTOMURA T., HATA A., ITO S., SHINOHARA T., TSUJIMURA S., GLUECK J.A., OESTMANN D.J., and NOSE Y., Centrifugal blood pump with a hydraulically-levitated impeller for a permanently implantable biventricular assist device. Artif Organs, **28**(6): p. 556-63,*2004*.

157. VOIGT O., BENKOWSKI R.J., and MORELLO G.F., Suction detection for the micromed debakey left ventricular assist device. Asaio J, **51**(4): p. 321-8,*2005*.

158. TIMMS D., HAYNE M., TAN A., and PEARCY M., Evaluation of left ventricular assist device performance and hydraulic force in a complete mock circulation loop. Artif Organs, **29**(7): p. 573-80,*2005*.

159. GREGORY S., TIMMS D., PEARCY M.J., and TANSLEY G., A naturally shaped silicone ventricle evaluated in a mock circulation loop: A preliminary study. J Med Eng Technol, **33**(3): p. 185-91,*2009*.

160. TSUJIMURA S., KUWABARA T., KOGUCHI H., YAMANE T., TSUTSUI T., and SANKAI Y., Development of failure detection system based on vibration

signal for smart artificial heart: In vitro study. Conf Proc IEEE Eng Med Biol Soc, **2008**: p. 697-702,*2008*.

161. DOHMEN G., SCHMITZ C., LANGEBARTELS G., STEINSEIFER U., SCHMITZ-RODE T., and AUTSCHBACH R., Impact of pressure recovery in the evaluation of the omnicarbon tilting disc valve. Thorac Cardiovasc Surg, **54**(3): p. 173-7,*2006*.

162. VERDONCK P.R., DUMONT K., SEGERS P., VANDENBERGHE S., and VAN NOOTEN G., Mock loop testing of on-x prosthetic mitral valve with doppler echocardiography. Artif Organs, **26**(10): p. 872-8,*2002*.

163. MEDVITZ R.B., KREIDER J.W., MANNING K.B., FONTAINE A.A., DEUTSCH S., and PATERSON E.G., Development and validation of a computational fluid dynamics methodology for simulation of pulsatile left ventricular assist devices. Asaio J, **53**(2): p. 122-31,*2007*.

164. MATTHYS K.S., ALASTRUEY J., PEIRO J., KHIR A.W., SEGERS P., VERDONCK P.R., PARKER K.H., and SHERWIN S.J., Pulse wave propagation in a model human arterial network: Assessment of 1-d numerical simulations against in vitro measurements. J Biomech, **40**(15): p. 3476-86,*2007*.

165. ZANNOLI R., CORAZZA I., and BRANZI A., Mechanical simulator of the cardiovascular system. Phys Med, **25**(2): p. 94-100,*2009*.

166. JARON D., MOORE T.W., and HE P., Theoretical considerations regarding the optimization of cardiac assistance by intraaortic balloon pumping. IEEE Trans Biomed Eng, **30**(3): p. 177-85,*1983*.

167. YOSHITANI H., AKASAKA T., KAJI S., KAWAMOTO T., KUME T., NEISHI Y., KOYAMA Y., and YOSHIDA K., Effects of intra-aortic balloon counterpulsation on coronary pressure in patients with stenotic coronary arteries. Am Heart J, **154**(4): p. 725-31,*2007*.

168. MIGLIORATO A., ANDO G., MICARI A., BALDARI S., and ARRIGO F., Coronary-subclavian steal phenomenon late after coronary artery bypass grafting: An underappreciated cause of myocardial ischemia? J Cardiovasc Med (Hagerstown), **10**(7): p. 578-80,*2009*.

169. FUCHS R.M., BRIN K.P., BRINKER J.A., GUZMAN P.A., HEUSER R.R., and YIN F.C., Augmentation of regional coronary blood flow by intra-aortic balloon counterpulsation in patients with unstable angina. Circulation, **68**(1): p. 117-23,*1983*.

170. YOUNG D.F., CHOLVIN N.R., and ROTH A.C., Pressure drop across artificially induced stenoses in the femoral arteries of dogs. Circ Res, **36**(6): p. 735-43,*1975*.

171. BIA D., ZOCALO Y., ARMENTANO R., CAMUS J., FORTEZA E., and CABRERA-FISCHER E., Increased reversal and oscillatory shear stress cause smooth muscle contraction-dependent changes in sheep aortic dynamics: Role in aortic balloon pump circulatory support. Acta Physiol (Oxf), **192**(4): p. 487-503,*2008*.

172. RAFFEL M., WILLERT C.E., WERELEY S.T., and KOMPENHANS J., Particle image velocimetry: A practical guide. 2nd ed.: Springer. *2007*.